INFORMATION TO USERS

This manuscript has been reproduced from the microfilm master. UMI films the text directly from the original or copy submitted. Thus, some thesis and dissertation copies are in typewriter face, while others may be from any type of computer printer.

The quality of this reproduction is dependent upon the quality of the copy submitted. Broken or indistinct print, colored or poor quality illustrations and photographs, print bleedthrough, substandard margins, and improper alignment can adversely affect reproduction.

In the unlikely event that the author did not send UMI a complete manuscript and there are missing pages, these will be noted. Also, if unauthorized copyright material had to be removed, a note will indicate the deletion.

Oversize materials (e.g., maps, drawings, charts) are reproduced by sectioning the original, beginning at the upper left-hand corner and continuing from left to right in equal sections with small overlaps.

Photographs included in the original manuscript have been reproduced xerographically in this copy. Higher quality 6" x 9" black and white photographic prints are available for any photographs or illustrations appearing in this copy for an additional charge. Contact UMI directly to order.

Bell & Howell Information and Learning
300 North Zeeb Road, Ann Arbor, MI 48106-1346 USA
800-521-0600

Optimal Discretization-Based Adaptive Finite Element Analysis for Electromagnetics

by

Dennis Giannacopoulos, B.Eng. (Electrical)

A thesis submitted to the Faculty of Graduate Studies and
Research in partial fulfillment of the requirements
for the degree of Doctor of Philosophy

Computational Analysis and Design Laboratory
Department of Electrical and Computer Engineering
McGill University
Montreal, Canada

October 1998

Abstract

One of the primary objectives of adaptive finite element analysis research is to determine how to effectively discretize a problem in order to obtain a sufficiently accurate solution efficiently. Consequently, a major research issue in adaptive finite element analysis is the feedback control system used to guide the adaption; essentially, one needs to resolve which error data to feed back after each iteration, and how to use it to initialize the next adaptive step. Currently, there exists substantial evidence suggesting that the optimality of a finite element discretization plays a significant role in the accuracy of computed solutions at given levels of problem refinement. Therefore, in order to exploit the potential benefits in adaptive finite element methods, the characterization of optimal finite element discretizations has been investigated extensively. However, valid criteria for characterizing optimal finite element discretizations for a sufficiently wide range of problem applications have not been reported. A theoretical formulation for the numerical study of optimal finite element solutions to partial differential equations of macroscopic electromagnetics is presented. The formulation is based on variational aspects of optimal discretizations for Helmholtz systems that are closely related to the underlying stationarity principle used in computing finite element solutions to continuum problems. The optimal characteristics of approximate finite element solutions, as predicted by the theory and observed numerically, have been employed to develop new optimal discretization-based feedback refinement criteria for use with advanced strategy adaption models in finite element electromagnetics. Numerical tests indicate that they are effective and economical for efficiently and reliably guiding practical h-, p- and hp-type adaption models towards accurate solutions.

In addition, a series of important benchmark adaption problems are introduced to examine the validity of the theoretical concepts and the practical value of the new refinement criteria. Moreover, many of the computational and theoretical difficulties inherent in the currently available characterizations of optimal finite element discretizations are explained and illustrated with numerical results computed for the same benchmark problems.

Résumé

Un des objectifs principaux de recherche d'analyse des éléments finis adaptifs est de déterminer comment discrétiser un problème afin d'obtenir une solution efficiente et en même temps suffisamment précise. Par conséquent, une question de recherche majeure dans l'analyse des éléments finis adaptifs est le système de contrôle de rétroactions utilisé pour diriger l'adaption: essentiellement, il est nécessaire de résoudre quelles données d'erreur à calculer après chaque itération, et comment les utiliser afin d'initialiser l'étape adaptive subséquente. Il existe présentement des évidences substantielles dans la revue de la documentation qui suggèrent que l'optimalité d'une discrétisation des éléments finis joue un rôle significatif dans la précision des solutions calculées à différents niveaux de raffinement de problèmes. Donc, la caractérisation des discrétisations optimales des éléments finis a été vastement examiné, afin d'exploiter les profits potentiels dans les méthodes des éléments finis adaptifs. Cependant, les critères valides pour caractériser les discretisations optimales des éléments finis n'a pas été rapporté pour une portée suffisament large d'applications de problèmes. Une formulation théorique est présentée pour l'étude numérique des solutions optimales des éléments finis aux équations différentielles partielles de "macroscopic" électromagnétique. La formulation est basée sur les aspects variationaux des discrétisations optimales pour les systèmes de Helmholtz, qui ressemblent au principe fondamental de "stationarity" utilisé afin de calculer les solutions des éléments finis aux problèmes de continuum. Les caractéristiques optimales des solutions des éléments finis approximatives, comme prédit par la théorie et observé numériquement, a été employé pour développer de nouveaux critères de raffinement de rétroactions basés sur les discrétisations optimales pour l'usage avec les modèles d'adaption de stratégies avancées dans les éléments finis électromagnétiques. Les résultats numériques indiquent qu'ils sont efficaces et économiques pour fiablement diriger les modèles d'adaption pratique *h*-, *p*- et *hp*-type vers des solutions précises.

En plus, une serie de problèmes importants d'adaption de référence est introduite pour examiner la validité des concepts théoriques et la valeur pratique des nouveaux critères de raffinement. De plus, des difficultés computationnelles ainsi que théoriques inhérentes aux caractérisations actuellement disponibles des discrétisations optimales des éléments finis sont expliquées et sont illustrées avec des résultats numériques.

Acknowledgements

I would like to express my sincere gratitude to Dr. J. S. McFee, my thesis advisor, for the invaluable guidance, support and patience he has provided throughout this research. His enthusiasm, helpfulness and interest have been important factors in making this work both enjoyable and meaningful. Furthermore, I am grateful to Drs. J. S. McFee, D. A. Lowther and J. P. Webb for the use of hardware and research software, without which some components of this work would not have been possible.

I would also like to thank my family, friends and colleagues for their kindness and generosity during my studies. Most of all, I wish to thank Ms. Fabianne Philippoussis and my mother, Ms. Ioanna Gioura, for their loving support and encouragement.

Finally, the financial support of NSERC (Natural Sciences and Engineering Research Council of Canada), CRIM (Centre Reserche Informatique de Montreal) and McGill University are also gratefully acknowledged.

Table of Contents

Chapter 1

Introduction

The science of electromagnetism, from its origins in classical antiquity to its contemporary study, has played a vital role in the intellectual development and the technological progress of mankind [1–9]. The ancients, who were familiar with the attractive power of loadstone and rubbed amber, contemplated the curious properties of these two substances and speculated about their nature. Some of the earliest observations of such magnetic and electric phenomena are attributed to Thales of Miletus, who lived in the sixth century B.C. and reasoned that "the magnet has a soul in it, because it moves the iron" [2]. One of the first practical applications of magnetic phenomena was the use of the compass for navigation, with the earliest written reference to it being by Alexander Neckam in A.D. 1186 [3]: undoubtedly, the use of the earth's magnetic field for guiding explorers and voyagers has had some of the most significant consequences for mankind since the Middle Ages. With the advent of the compass there also came further insight into the nature of the magnetic properties of materials. For example, in A.D. 1269 Pierre de Maricourt announced the discovery of the poles of a magnet; thus, giving rise to the theory of polarisation, which has since played a role of fundamental importance in natural philosophy [4]. The modern history of electricity and magnetism has its beginnings in the Renaissance, for it was in A.D. 1600 that William Gilbert published *De Magnete*, a work highly regarded not only for the significant findings presented therein, but also for the progress achieved by its clear statement of the scientific method [5]. Of foremost importance were Gilbert's discoveries that (i) the earth itself is a great magnet; thus, explaining the action of a compass, and (ii) that quite a large class of bodies could be induced by friction to display effects similar to the attractive power of rubbed amber. Gilbert's work helped

inspire a succession of experimental and theoretical investigations, culminating in the formulation of Maxwell's equations during the second half of the nineteenth century [6]. The solid mathematical foundation formulated by Maxwell provided a unified electromagnetic field theory, which has endured and has had profound implications in areas ranging from communications technology to relativity theory [7, 8]. Today, the study of electromagnetism continues to be at the forefront of scientific inquiry, where the electromagnetic field is considered one of the four fundamental force fields essential for describing and understanding the nature of our universe [9].

1.1 Finite Element Methods in Computational Electromagnetics

Our ability to understand electromagnetic phenomena and to analyze and design electric and magnetic devices, through the use of analytical and numerical methods, plays a vital role in modern society. It is only necessary to consider that electromagnetics encompasses, in part, the generation, storage, transmission, reception, transformation, and interpretation of electric and magnetic information and energy, to realize just how expansive the range of areas involving electromagnetism is. For instance, communications systems incorporating microwave and optical components, biomedical applications such as nuclear magnetic resonance (NMR) devices, direct- and alternating-current machines, high-voltage power distribution systems, and electronic computing systems represent only a fraction of the types of areas in which electromagnetics analysis and design are essential, but illustrate clearly the potential need to solve a diverse assortment of sophisticated engineering electromagnetics problems [10–13]. Mathematical models, such as Maxwell's differential or integral equations, which describe physical electromagnetic phenomena macroscopically, can be used to obtain closed-form or quasi-analytical solutions to certain electrical engineering problems in terms of their electromagnetic fields [14–17]. However, there are many practical and important instances where only approximate solutions can be obtained through the use of numerical methods. For example, consider the problem

of the scattering of radio waves by a metallic circular cylinder, which has a closed-form solution in terms of trigonometric and Bessel functions. In contrast, the similar problem involving a metallic rectangular cylinder necessitates the use of numerical analysis methods for its solution [18].

The finite element method (FEM) is a powerful numerical analysis technique which is well-suited to and appropriate for solving a large class of electromagnetics problems computationally [19–27]. Essentially, in order to solve the differential or integral equations that mathematically describe a physical electromagnetic system by using the FEM, the problem region is first divided into a finite number of geometric sub-regions, or *elements*. A model of the solution is then constructed over each individual element by an approximating function, which is uniquely defined by the numerical values of a set of parameters associated with it. These numerical values are subsequently computed based on satisfying global constraints which are mathematically equivalent to solving the original differential or integral equation describing the system. Amongst the many methods used within computational electromagnetics [26–35], the FEM's ability to handle problems with complex geometries, as well as its applicability to static, quasi-static, wave and transient problems and to problems containing material regions that are nonlinear, inhomogeneous, and anisotropic make it one of the most versatile and powerful computational techniques available today [23–27]. Moreover, the solid theoretical foundations upon which the FEM is based, as well as the rigorous mathematical analyses concerning the existence, convergence, and uniqueness of finite element solutions that have been established, further justify its use in electromagnetics research and design [36–47]. Currently, finite element analysis (FEA) is widely used in electromagnetics design and research — typically, FEA tools are used to numerically simulate and evaluate the performance of a new device design before building a prototype, or to computationally investigate the electromagnetic characteristics of natural and man-made systems and their interaction with, or impact on, their surrounding environments [13, 48–51].

1.2 Adaptive Finite Element Methods

While finite element methods (FEMs) are presently employed extensively for electromagnetics analysis and design [52, 53], the use of *adaptive* finite element methods (AFEMs) has gained considerable attention in recent years from numerical analysts for solving problems more efficiently than standard FEMs allow for [54]. In general, finite element solutions are inherently approximate: fundamentally, FEMs are based upon the principle of representing solutions to continuum problems by finite-dimensional approximations computed over finitely discretized domains [55]. Therefore, the accuracy of a finite element solution is directly dependent on both the number of free parameters used to mathematically model the problem, and on how effectively those parameters, or mathematical degrees of freedom (DOF), are distributed throughout the problem space. Furthermore, the computational cost associated with obtaining a finite element solution is related to the number of DOF used in the discretization of the problem. Consequently, the most efficient distribution of degrees of freedom for a problem is that which yields a sufficiently accurate solution for the lowest number of free parameters. Currently, the only practical way to achieve this objective is by using adaptive solution strategies which are capable of intelligently evolving and improving an efficient distribution of DOF over the problem domain by establishing solution error distributions, and then adjusting or adding DOF to the discretization to correct them [56–58].

Standard FEMs increase the number of DOF throughout the problem domain in a uniform fashion by augmenting the existing level of discretization in each subregion (element) equally. Generally, this can result in an inefficient solution process, since most field solutions rarely conform to the initial distribution of DOF over the entire problem domain for electromagnetics problems with complicated geometries and material properties, and uniform refinements do not allow for this distribution to be changed. In other words, the rate of solution variation may vary over the problem

domain: therefore, for a given level of relatively uniform discretization, the error in a finite element solution may also vary throughout the problem domain. Thus, by increasing the number of DOF in the regions of higher solution error only, it is possible to make the most significant improvement in the global accuracy of the finite-element solution for the least additional computational cost. In contrast, uniformly increasing the number of free parameters throughout the problem domain could provide an even greater overall improvement in the computed solution accuracy; however, the per capita increase in accuracy for each new DOF may not be as high, since new DOF added to regions which were already sufficiently well refined would not necessarily contribute to a significant improvement in the solution accuracy [56,57].

One of the primary objectives of AFEMs is to compute the solution to an engineering problem to within pre-specified accuracy tolerances for the lowest possible computational cost. In order to achieve this objective, the fundamental approach underlying the majority of AFEMs involves the efficient, iterative improvement, of a convergent sequence of increasingly accurate approximations of the true solution to a given engineering problem. A simple conceptual framework which is meaningful for the study of AFEMs is shown within the context of the general finite element solution scheme in Figure 1.1, where the individual steps of an adaptive method are constituents of one or the other of two major, procedural components: namely, the adaption model and the feedback control system used to guide the adaptive finite element process. Simply put, the adaption model includes those steps involved with updating a discretization, while the feedback control system is concerned with procedures related to resolving *how* to increase the level of discretization for a problem. Consequently, the specification of an adaption model and a feedback control strategy defines an adaptive method within this paradigm. More specifically, the procedure followed by most adaptive solution schemes, as outlined in Figure 1.2 along the lines described in [59], is to first create an initial discretization for the problem (A), and then solve the finite element problem based on this initial discretization (B). Once a

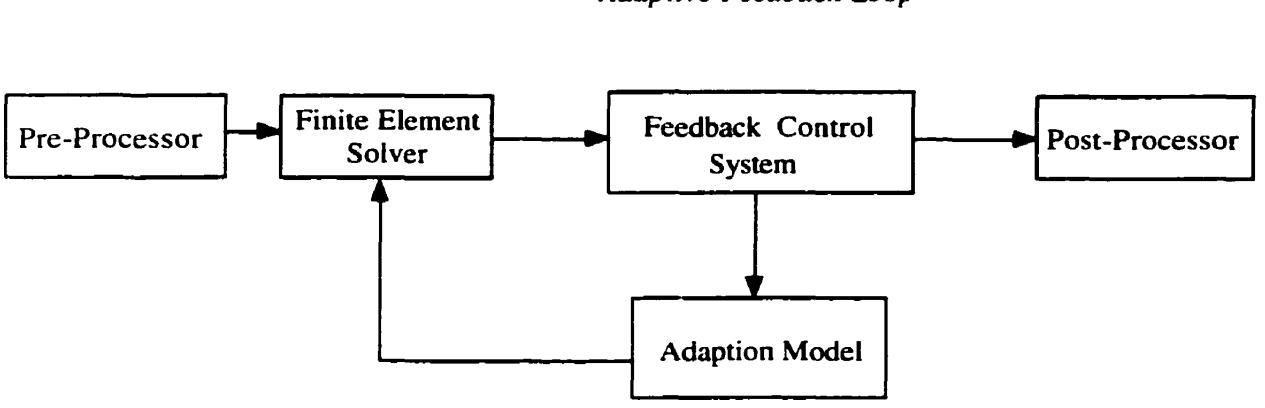

Figure 1.1: The adaption model and feedback control system framework for the study of AFEMs, within the context of the general finite element solution scheme. The general finite element solution process, usually, involves: (i) a pre-processing unit for building a computational model of the problem, (ii) a finite element solver for computing solutions to the discretized problems, and (iii) a post-processing unit for analyzing the computed solutions.

solution has been obtained, an estimate of by how much it is in error from the true solution with respect to a specific measure of error, will determine if a more accurate solution is required (C). If the error is within acceptable limits, the computed solution may then be utilized for its intended purposes. If the accuracy of the solution is unacceptable, however, the next steps in the adaptive scheme involve first, trying to estimate in what parts of the problem domain the solution is most in error (D), then determining the required refinement to most effectively improve the solution accuracy (E), and subsequently, appropriately adding DOF in the inaccurate regions (F). The finite element problem is then re-solved (B) to see whether the updated discretization leads to a sufficiently accurate solution (C), or if further refinement is required (D–F).

AFEMs are especially useful for solving complex problems efficiently, since the computer resources required can increase at a significant rate with respect to the problem size; for example, in some finite element implementations the approximate computational cost can be $\mathcal{O}(n^3)$, where n is proportional to the number of DOF used

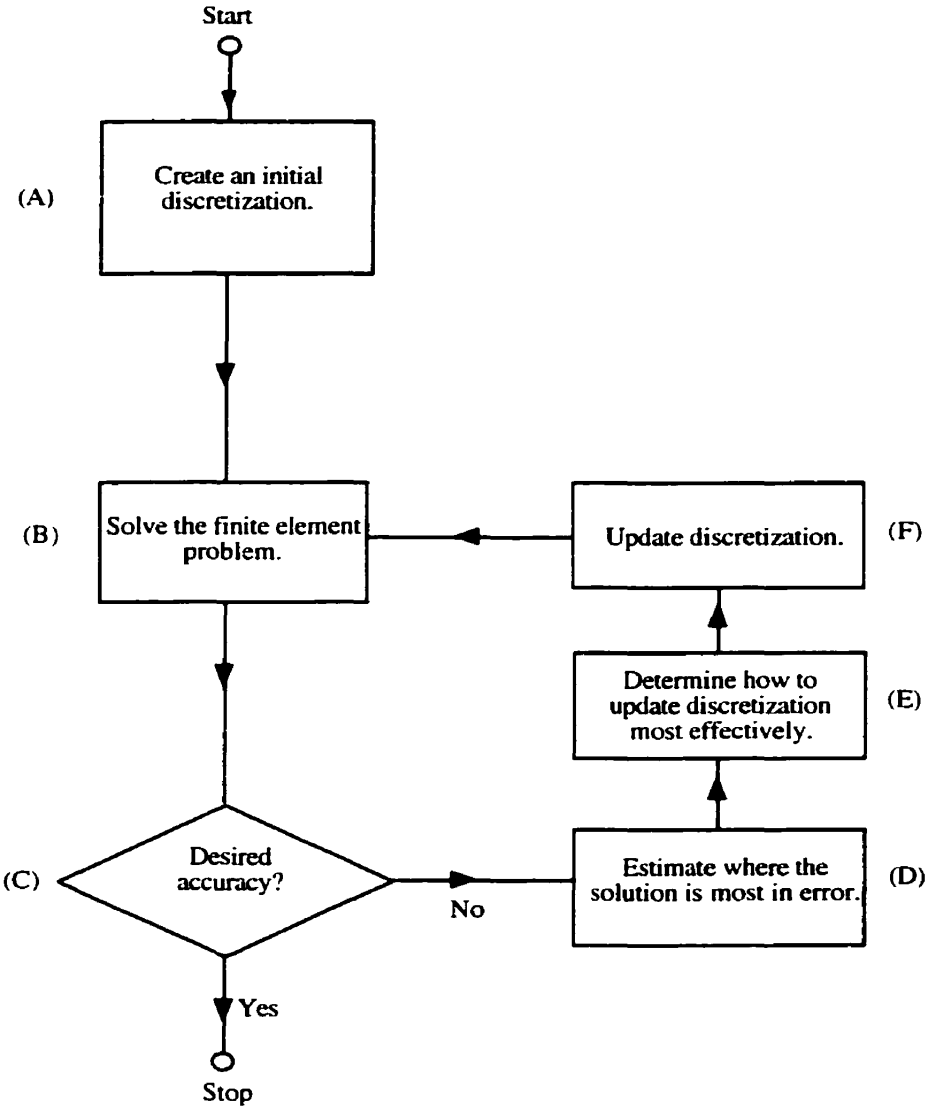

Figure 1.2: The general solution procedure for an adaptive finite element method, with six of the fundamental steps labeled as (A - F).

in the numerical model of the problem [23]. Today, many realistic problems require a large number of free, or unconstrained, modeling parameters in order to compute their solutions with sufficient accuracy. This has made the effective discretization of the physical problem a tacit requirement of efficient modern finite element packages. The need for such computational efficiency in finite element electromagnetics methods has led to an increased demand for advanced adaptive solver technologies. Thus, the research and development of *optimized* AFEMs proven to be effective, reliable, and versatile enough for general application in electromagnetics analysis and design, is considered to be a critical component of the state-of-the-art in FEA research.

As noted, an essential part of efficient FEMs is the effective discretization of the continuum problem, which involves the construction of (i) a *mesh* consisting of a finite number of geometric sub-domains, or elements, used to model the physical problem region under study, and (ii) a set of finite-dimensional approximating functions defined over the elements in order to compute the solution to the discretized problem. An *adaption model* is a set of well-defined procedures used in AFEMs for updating a finite element discretization. Presently, four basic types of adaption models are under study in the mainstream literature: (i) h-type, (ii) p-type, (iii) *combined* hp-type, and (iv) r-type. Essentially, these models differ only in the techniques used to update the finite element discretization within the adaptive feedback loop [57]. Briefly stated, h-type adaption models add elements to the mesh to improve a discretization; p-type adaption models increase the degree of approximation over elements within the mesh to improve a discretization; hp-type adaption models employ a combination of both procedures; and r-type adaption models reposition element vertices in the mesh to improve the solution accuracy. Each of these basic models have strong positive attributes and disadvantages, which make their use in AFEMs highly effective under different conditions, and all four are considered in this work. The basic adaption models are described and discussed in greater detail in the following four sections, in order to illustrate their importance in developing effective practical AFEMs.

1.2.1 The h-type Adaption Model

In h-type adaption models refinement of the finite element discretization is accomplished by adapting the size (h) of elements in the mesh, while keeping the order (p) of the approximating functions over the elements constant. Consequently, in order to improve the accuracy of a finite element solution using an h-type adaption model, the number of free parameters used to compute the solution is increased by increasing the total number of elements in the mesh; thereby, decreasing the overall average size, h_{avg}, of elements in the mesh:

$$h_{avg} = \frac{1}{N} \sum_{i=1}^{N} h_i, \tag{1.1}$$

where h_i is the size of the i^{th} element in a mesh comprised of a total of N elements. For example, Figure 1.3 shows a sample representation of four levels of uniform finite element h-refinement, using triangular elements, corresponding to four different relative average element sizes.

It has been proposed that the the point-wise error in a finite-element solution is, approximately, $\mathcal{O}(h^{min[p+1,\varsigma]})$ for an element of size h and polynomial order p, and where ς is a number proportional to the intensity of any local singularities[1] that may be present in the exact solution of the problem [55, 65]. This estimate is based on the argument that if a p^{th}-order approximating function is used to model the solution over an element of size h, then the dominant term in the difference between the Taylor series expansions, about a point within that element, of the finite-element and true solutions will be $\mathcal{O}(h^{p+1})$ if no singularities[2] in the exact solution exist nearby [44, 65].

[1] Solution singularities are primarily associated with sharp material edges and corners [60, 61]. The intensity of such singularities has been characterized mathematically as $\varsigma \equiv \frac{\pi}{\alpha}$, where α is the interior angle (in radians) of a vertex where two line segments composing part of the boundary $\partial\Omega$ of a problem domain Ω meet [62]. Using this approach, the intensity of a singularity associated with a 270° reentrant corner is given by $\varsigma = 0.67$; however, experimental results suggest that such a corner would result in a singularity intensity closer to $\varsigma = 0.71$ in terms of its effect on the solution error convergence rate [63]. Despite this particular discrepancy, it is generally agreed that $0.5 < \varsigma < 1$ for interior angles of the boundary $\partial\Omega$ that lie within the range $\pi < \alpha < 2\pi$ radians [55, 64].

[2] The local rate of solution error convergence for all values of p used in elements in the vicinity of any singularity that may be present is dominated by the intensity (ς) of the singularity. This behavior has been explained, by some authors, to be caused by the presence of infinite coefficients associated

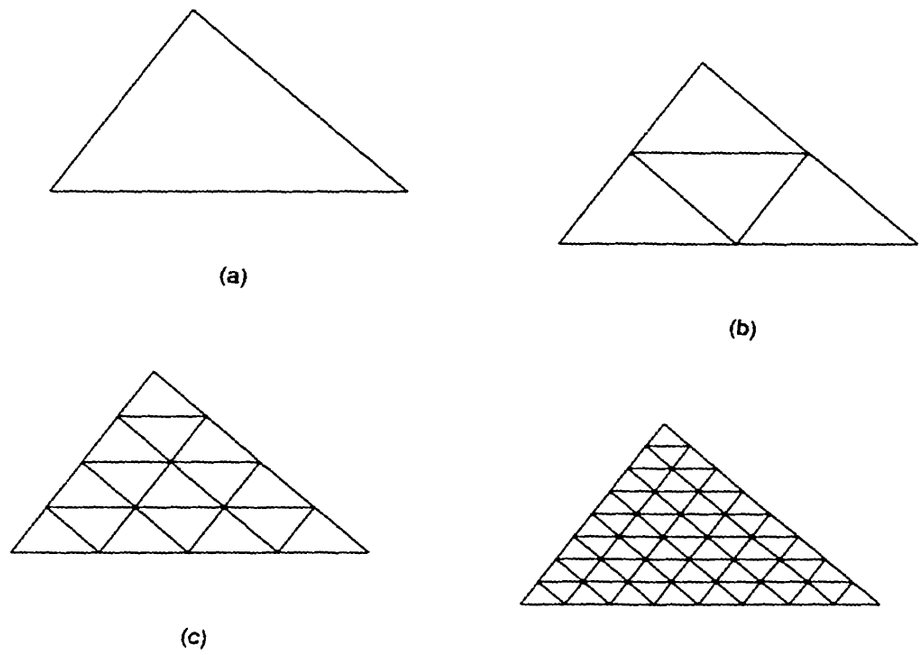

Figure 1.3: An example of four levels of uniform finite element h-refinement, using triangular elements, corresponding to four relative average element sizes is illustrated: (a) $h_{avg} = 1$, (b) $h_{avg} = 1/4$, (c) $h_{avg} = 1/16$, and (d) $h_{avg} = 1/64$.

For example, based on this estimate, the error in a finite element solution at a given point in the problem domain will be reduced by a factor of four for a halving of the element size, in a region where no singularities are present and first-order polynomial approximating functions are used. Although this argument, based on concepts from interpolation theory, is not completely theoretically justified in the context of finite-element approximations, estimates of solution error convergence rates based on it can be achieved asymptotically in practice as element sizes tend to zero [55]: therefore, such estimates are useful for understanding approximate error behavior in finite-element solutions [66].

Based on the above estimates for the error in finite-element solutions, it is evident that h-type adaption models may be used advantageously in AFEMs. For example, by increasing the number of DOF in the regions of high solution error, through the use of a larger number of smaller elements in those regions, it is possible to achieve significant improvements in the global accuracy of the finite-element solution at lower computational cost in comparison with uniformly increasing the number of free parameters throughout the entire problem domain. Conceptually, h-type adaptive refinement is uncomplicated; however, the practical implementation of h-adaption models involves certain complex issues that are addressed in the extensive literature on AFEMs. For example, h-adaption models typically increase the level of discretization in a finite element mesh by, first, introducing new vertices, which are then used to define additional elements. Consequently, the manner in which these new vertices are introduced to the discretization and how new elements are subsequently defined, can affect the quality of the resulting mesh; therefore, considerable attention has been given to these issues over the past several years [67–76].

Line segments, triangles, and tetrahedra are types of elements that are commonly used in one-, two-, and three-dimensional electromagnetic finite element analyses,

with higher order terms in the Taylor series expansion of the difference between the computed finite element solution and the true solution to the problem [55]. Furthermore, such infinite coefficients are argued to result from the presence of singularities in the true solution [55].

respectively. While the meshing of vertices into line segments for one-dimensional finite-element models is straightforward, the formation of meshes in two and three space dimensions can be more complicated [67, 77–79]. One difficulty is that there is usually more than one triangulation or tetrahedral subdivision possible for a given set of vertices over a two- or three-dimensional domain, respectively; therefore, Delaunay-type algorithms are frequently implemented in order to produce acceptable finite element meshes comprised of simplexes [67, 69, 70, 75]. Accordingly, some of the most successful h-type adaption models are those that employ a Delaunay-type algorithm to re-mesh a set of vertices each time the discretization is updated within the adaptive feedback loop [69, 70]; however, these types of h-adaption models also incur the added computational expense of incorporating a Delaunay algorithm at each adaptive iteration.

Although a Delaunay-type algorithm will produce the best possible mesh of simplexes for a given set of vertices, the quality of the mesh produced may still not be acceptable due to a poor set of vertices [70]. For example, Delaunay-based meshing algorithms help prevent, but do not guarantee avoiding the formation of long, thin elements that can lead to poorly conditioned matrices in finite element formulations, which, in turn, can compromise the accuracy of the computed solution [80]. Therefore, it is also important that a good set of vertices be defined before a finite element mesh is created. An effective approach for achieving this objective is described in [70], where the authors develop a new method for adding vertices to the problem domain. The method for positioning new vertices uses a combination of: (i) criteria based on the field solution accuracy; and (ii) a geometric criterion so that the quality of the mesh that will result from a Delaunay triangulation of the complete set of vertices is more likely to be acceptable than if only the field criteria had been used to decide where to add the new vertices. When element shapes other than simplexes are used to construct finite element meshes, approaches other than Delaunay-based algorithms must be considered for ensuring good quality h-adapted meshes. For ex-

ample, a "one-level" rule is described in [72] for obtaining smoothly graded meshes by subdividing quadrilateral and hexahedral elements. However, the process results in "one-irregular" meshes where adjacent elements can differ by up to one level of mesh refinement: therefore, the computed solution must be properly constrained so that continuity of the solution is maintained at the interfaces of such elements [61, 72, 81].

Adaptive finite element methods incorporating h-adaption models have been used successfully for various types of electrical engineering applications [56, 69, 76, 82–93]. In particular, for problems where singularities in the mathematical field solutions exist, such as those at sharp material edges and corners [64], h-type adaption models have proven to be quite effective, where a large number of smaller elements are needed close to the singularities, but fewer, larger elements of the same order suffice further away [57, 59, 60, 85, 94]. Given that the approximate error in a finite element solution is $\mathcal{O}(h^{min[p+1,\varsigma]})$, and that $\varsigma < 1$ in the vicinity of most singularities, it is evident that reducing the element sizes (h) near a singularity may be more advantageous than increasing the degree of approximation (p). Numerical studies have also shown that h-type refinement near singularities in finite element electromagnetics may result in near optimal rates of convergence for certain levels of discretization [57].

1.2.2 The p-type Adaption Model

In p-type adaption models refinement of the finite element discretization is accomplished by adapting the order (p) of approximating functions over elements, while keeping the size (h) of the elements in the mesh constant. Standard Lagrangian elements require the same order of approximating functions throughout the entire mesh to ensure a continuous finite element solution [23]; however, hierarchal elements permit increasing the order of only certain elements in the mesh, while still ensuring C^0 continuity of the computed solution. Thus, it is possible to evolve efficient distributions of DOF by raising the polynomial order of the elements only in the inaccurate parts of the mesh. Based on the interpolation theory error model described in the

previous section, the point-wise error in a finite element solution is approximately $\mathcal{O}(h^{p+1})$ over regions of a problem domain where no singularities are present. Therefore, if the finite element mesh is such that the element sizes are sufficiently small in regions away from singularities, then the improvement in the accuracy of the computed solution will be greater for an increase in the polynomial order (p) of the approximating functions rather than a decrease in the element size (h), according to the interpolation theory error model. Numerical studies have also shown that under certain conditions, p-type refinement may result in better rates of solution error convergence than those that can be achieved using h-adaption models [57].

In finite element electromagnetics, p-type adaption models incorporating hierarchal elements have been shown especially useful in high frequency problems, where the fields have a wave-like variation, and are better modeled in certain parts of the mesh by high-order elements, whereas lower order elements provide a sufficiently accurate approximation in other regions of the mesh [95]. As in low-frequency applications, the objective in high-frequency problems is to obtain a distribution of degrees of freedom such that they are more densely concentrated where the field is varying rapidly, and less so where the variation is slower. The meshes produced by automatic mesh generators typically have larger elements away from complex material boundaries. This type of mesh grading is usually satisfactory for static problems, where the fields tend to become increasingly uniform further away from boundaries. In high frequency devices, however, the wave-like fields away from material boundaries are particularly well represented by high-order polynomial approximating functions, and p-type refinement can be an attractive alternative to h-type refinement since it avoids the cost of re-meshing [55,59,95,96]. Finally, it is worth noting that the use of hierarchal finite elements in p-type adaption models has also been shown effective for low-frequency finite element electromagnetics [97].

The practical implementation of p-type adaption models involves key issues which

must be addressed. For example, the choice of basis functions[3] used to form hierarchal elements can play an important role in the effectiveness of a practical p-type adaption model. Although different alternatives exist for the set of hierarchal basis functions that can be used for a specific element shape and space dimension [55], attention must be paid to the linear independence of the basis functions. If the basis functions that are used to form the approximating function over a given element are not linearly independent, or are nearly linearly dependent, the resulting finite element matrices used to compute the numerical solution to the discretized problem will be ill-conditioned. Depending on whether a direct or an iterative method is used to solve the matrix problem that results from a finite element formulation, ill-conditioned matrices can lead to inaccurate solutions and slow convergence rates, respectively [80]; therefore, research on hierarchal basis functions has constituted an important component of the literature related to p-type adaption models over recent years [95]. One successful approach that has been adopted in order to develop hierarchal elements that preserve a reasonable degree of linear independence between their basis functions, has been to use orthogonal polynomials in the formulation of the basis functions [98]. Finally, it is interesting to note that, although Lagrangian elements can not be used as hierarchal elements in two- and higher-dimensional formulations, they tend to result in finite element matrices that have better condition numbers than those resulting from non-Lagrangian elements. This is primarily due to the high degree of linear independence that is inherent in the Lagrangian basis functions [98].

Adaptive finite element methods incorporating p-type adaption models are particularly valuable in the computational analysis and design of three-dimensional electromagnetic systems [58]. For example, the formation of a well-structured mesh consisting of tetrahedral elements based on Delaunay or other types of algorithms, is a complicated and relatively expensive task [67,73,99,100]; therefore, p-type adaptive

[3]Approximating functions (U) used in numerical methods can, usually, be described as a series of basis functions (N_i) weighted by coefficients (a_i), so that $U = \sum_{i=0}^{p} a_i N_i$. The number of terms in the series (p) is related to the polynomial order of the approximating function.

refinement using hierarchal tetrahedra is often considered more favorable than h-type adaption for three-dimensional problems [58]. However, it may not be possible to obtain a sufficiently accurate solution by increasing only the polynomial order of the approximating functions defined over the elements in a mesh, if the mesh contains too few elements or if the highest degree of approximation order available is too low; thus, a sufficiently h-refined mesh is often a prerequisite for p-type adaption models to be effective [59, 70].

1.2.3 The hp-type Adaption Model

In hp-type adaption models refinement of the finite-element discretization is achieved by adapting both the size (h) and the order (p) of elements in the mesh. In general, hybrid hp-adaptive approaches combine h- and p-type refinements in order to exploit the advantages of both these fundamental adaption models. Numerical results and theoretical work indicate that the ability to independently vary the two basic discretization parameters, h and p, should afford adaptive methods which employ combined hp-type adaption models the possibility of realizing superior rates of solution error convergence compared with those of methods that utilize pure h- or p-type adaption models [62, 94, 101–103]. The putative enhanced performance of combined hp-type adaption-based systems derives from the fact that the solution accuracy may be more greatly improved by decreasing the element size in certain parts of the problem domain, whereas, increasing the order of approximating functions over other parts of the solution realm may have the most significant effect on the solution accuracy. Therefore, a hybrid adaption model capable of both types of refinements should, theoretically, yield optimal rates of solution error convergence.

The theoretical analysis and practical performance of combined hp-type adaptive methods have received a considerable amount of attention within the literature on AFEMs during the last decade, since, in theory, optimal rates of solution error convergence can be obtained by combining h- and p-type adaption models [94, 101, 104];

however, the implementation and control of a hybrid *hp*-type system are inherently more complex than that of its simpler *h*- or *p*-type counterparts. Accordingly, in addition to the issues that are relevant to the design and implementation of *h*- and *p*-type adaption models, further concerns arise, related to the coupling of the *h*- and *p*-type refinement procedures, when dealing with combined *hp*-type adaption models. For example, the increased generality of hybrid *hp*-systems has practical implications from a programming perspective; essentially, sufficiently sophisticated data-structures and data management routines are required which can cope with arbitrary distributions of discretization parameters and the evolutionary interrelationships of these parameters as the finite-element discretization is iteratively refined during the adaptive process [105]. Although these issues have been addressed, to a certain extent, in the literature, the focus has been primarily on structured meshes, where the relationships between the discretization parameters associated with consecutive iterations are well-defined [72, 81, 101, 102, 106].

One major research problem that has emerged, associated with the implementation of hybrid *hp*-type adaption models, has been the development of systematic approaches for generating discretizations with optimized relative distributions of *h* and *p* [57, 61, 104, 107, 108]. For example, in fully-coupled *hp*-type adaption models, where *h* and *p* can be adapted simultaneously within any given iteration of the adaptive process, one of the primary difficulties is determining which parts of the discretization to enhance using *h*-refinement and where to employ *p*-refinement in such a way that the greatest improvement in solution accuracy is attained for the given increase in the total number of DOF used to compute the approximate solution [57,61]. Similarly, in decoupled *hp*-adaption models, where only one or the other of the two basic types of refinements are exploited during a given iteration within the adaptive feedback loop, the dilemma of which discretization parameter, *h* or *p*, to adapt at a given iteration so as to achieve the maximal decrease in solution error per unit new DOF exists [62,108–110]. These problems are tantamount to determining the optimal

trajectory through the abstract space of admissible *hp*-distributions, starting from an initial discretization and given a final, desired solution accuracy; where, the set of permissible trajectories is dependent upon the constraints of the specific adaptive method under consideration, that is, the combination of a particular adaption model and feedback control system. The optimal trajectory will be that which involves the lowest cumulative computational cost [111].

Although some theoretical approaches have been suggested for determining optimal *hp*-trajectories, the resulting discrete optimization problems are not readily solvable in a rigorous, analytical manner, if at all, for systems of realistic complexity [61, 107, 112]; therefore, numerical experiments have also been relied upon to glean insight on these problems [57, 104, 113]. Based, in part, on theoretical and numerical investigations, practical techniques have been developed which can, although not necessarily optimally, evolve distributions of the discretization parameters in such a way that hybrid *hp*-based adaptive methods out-perform pure *h*- or *p*-type systems. In general, such methods rely upon distribution criteria that are rooted in the principles fundamental to the development of effective *h*- and *p*-type adaption models [102, 114]. For example, a technique is described in [115] that uses *h*-refinements in regions of the problem domain that contain strong discontinuities of the solution, and *p*-type adaption over relatively smooth parts of the solution. Another approach which has recently been developed and applied successfully to electromagnetic AFEA is described in [116], and is based on using parallel processing to assess different discretization strategies at each *hp*-refinement step to help guide the evolution of the adaption. Finally, numerical studies have shown that despite the advantages of *hp*-type adaption models, simpler adaption models may give superior results under certain conditions. For example, a Helmholtz benchmark problem is described in [56], and examined later in this work, for which *hp*-adaption is inferior to the *p*-adaptive methods investigated for that system. This occurrence is an artifact of the constraints of the particular *hp*-adaptive method employed in that instance. Since the initial distribution of DOF

was reasonably compatible with the spatial variation of the wave solution to the system, an almost uniform p-type refinement was closer to the optimal hp-trajectory than one involving significant modification of the initial distribution of h. However, the hp-adaptive method considered for this case performed h-adaption initially, by design, and, therefore, did not result in optimal rates of solution error convergence.

1.2.4 The r-type Adaption Model

In r-type adaption models the finite-element discretization is refined by adapting the position (r) of element vertices in the mesh, in order to improve the accuracy of the computed solution [117]. As noted earlier, the solution error distribution for a given finite-element discretization will, in general, vary throughout the problem domain according to the relative rate of solution variation and the corresponding concentration of degrees of freedom (DOF). Therefore, r-type adaption models can evolve efficient finite-element discretizations by repositioning element vertices such that there is a sharper focus of DOF in regions where the solution variation is most rapid. The r-type adaption model is most often employed when maximal solution accuracy is required from discretizations with a given number of DOF [57, 72, 101, 118, 119]. Hence, r-adaption has been primarily investigated in the context adaptive systems that are based on evolving optimal finite element discretizations [56, 57, 117, 120–137]. These types of adaptive systems are discussed in greater depth in subsequent sections of this chapter, along with the inherent advantages and related costs of using r-type adaption models for their implementation.

1.3 Motivation for the Research

Typically, electromagnetic field problems can be cast in the form of a general operator equation such as

$$\mathcal{L}u = g, \tag{1.2}$$

where, for example, $\mathcal{L}$ is a linear operator which may be defined so that Eq. (1.2) can represent any of Maxwell's integral or differential equations of macroscopic electromagnetics, and u and g are symbolic representations of corresponding scalar or vector fields [138]. In general, g may be a given source of electromagnetic energy, and u is the unknown electromagnetic field, or a related auxiliary potential field, which satisfies Eq. (1.2) subject to appropriate boundary conditions for a specific problem under consideration. When solving electromagnetic field problems numerically by FEMs, the underlying approach is to define a space of admissible approximating functions, say V_h, from which the *closest* function, say u_h, to the true solution u, is eventually computed. The notion of *closeness* of an approximation, ultimately, depends upon the chosen measure of error in any given numerical formulation of the problem. Regardless of the specific numerical technique and error measure employed, the problem of finding the closest or *best* approximation to the true solution u can be pictured geometrically as shown in Figure 1.4 (a).

The procedures for obtaining the best approximate solution u_h from a given space of admissible approximating functions V_h are well established methods rooted in functional and numerical analysis [38, 41]. However, many of the prescriptions for obtaining such solutions usually place certain restrictions on the spaces of admissible approximating functions they employ, which can limit the potential accuracy of the computed solutions. For example, some numerical methods, such as the FEM, use a finite number of *fixed-position* geometric sub-domains (elements), over which interpolation functions are used to approximate the unknown field u. One of the restrictions, in these cases, is the imposed, *a priori* distribution of some of the mathematical DOF

used in numerically modeling the physical problem, due to the pre-assigned fixed topology of the geometric sub-domains. Without this restriction, a higher level of accuracy in the approximation could, possibly, be achieved by allowing for optimal distributions of DOF through the optimal discretization of the problem domain. In other words, if the specification of the geometric sub-domains were left unknown, and solved for simultaneously along with the underlying field solution, then it might be possible to model the true solution more accurately.

The increase in accuracy that may be possible by allowing for optimal discretization of the problem domain can also be pictured geometrically, as shown in Figure 1.4 (b). Here, the space of admissible approximating functions, V_h', is larger than the space associated with the pre-assigned, fixed-position subdomains, therefore, allowing for the possibility of an approximate solution u_h' to exist which is closer to the true solution u. However, the computational cost associated with determining optimal discretizations of the problem domain can be prohibitive, since the problem then becomes a geometrically nonlinear one: the approximating functions are, generally, dependent on the spatial coordinates defining the geometric sub-domains [129]. Therefore, rather than solving a system of simultaneous linear equations that would otherwise result from a FEM formulation,[4] the optimization of the discretization would lead to a system of simultaneous nonlinear equations to be solved. In theory, such systems of equations can be solved, despite the added computational complexity and cost; however, one complication which can arise in the context of computing optimal discretizations is that the solutions may not have valid physical meaning [129]. Most often, this can occur due to a phenomenon referred to as "mesh tangling", which, essentially, results from the overlapping of elements, in turn, leading to negative element areas or an undefined solution in the overlap regions [126]. Another example of

[4] Assuming no other nonlinearities exist in the problem formulation, e.g., nonlinear magnetic material regions in the problem domain. If the original problem already involves nonlinear components, then the incorporation of optimizing the discretization will increase the degree of nonlinearity of the resulting system of simultaneous equations to be solved.

how incorporating the optimization of the problem discretization into the finite element formulation can lead to non-physical solution characteristics, is when complex material parameters are used to model lossy materials. In this instance, as well as the previous one, unless preventive measures are built into the problem formulation, non-physical or imaginary discretizations can ensue. Therefore, the additional mathematical freedom and, thus, potential accuracy that is possible by allowing for a finite element discretization to be optimized, can also, unfortunately, lead to pathological cases.

Solutions that are normally computed using standard FEMs are only *optimal* under the given set of restrictions, i.e., the pre-assigned element topology. Nonetheless, this restricted approach seems to be very successful in terms of implementing practical computational methods. Yet, if certain characteristics of *truly optimal* approximate solutions, that is, the approximate solutions obtained with the restrictions lifted, were known *a priori*, then practical algorithms could be employed to *adaptively* compute solutions with similar optimal properties, but at a significantly lower cost than a non-adaptive, geometrically nonlinear formulation, and without the complications mentioned previously. This would ensure that the computed solutions were of maximal accuracy for a given level of problem discretization, while simultaneously benefiting from the efficiency of AFEMs. Although AFEMs are well-suited to the task of evolving finite element approximations with optimal-discretization solution properties, this can only be achieved through the effective use of appropriate feedback refinement criteria for guiding the adaption process towards optimal discretizations. Therefore, the characterization of solution properties associated with optimal finite element discretizations is an essential first step towards this objective.

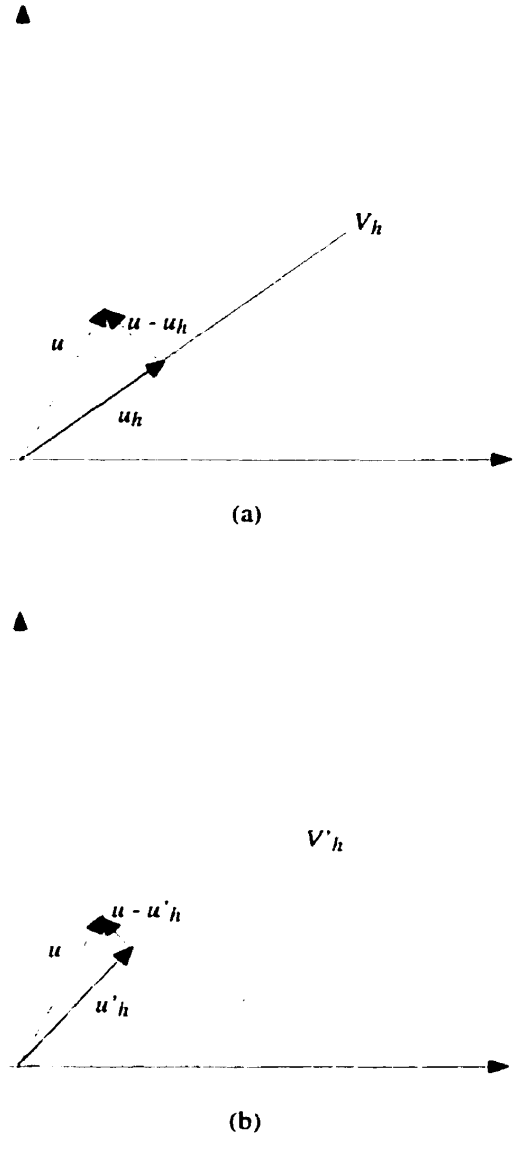

Figure 1.4: Geometric interpretations of best approximate solutions: (a) standard FEM, and (b) optimal discretization FEM. In (a), the space of admissible approximating functions is symbolically represented by a line, whereas in (b) the representation is by a planar region. The exact and approximate solutions are represented as vectors from some common origin, while the difference between them is drawn as a vector from the approximate to the exact solution.

1.4 Classical Origins and Review of Recent Work

Recently, in the mathematics and engineering communities, there has been considerable interest in the subject of optimal discretizations for numerical methods [56, 57, 117, 120–137]. Much of the work on this topic has been directly concerned with, or relevant to, numerical methods for solving equations of mathematical physics, such as the finite element method (FEM). The most prominent and enduring contributions to emerge in the literature on optimal discretizations for numerical methods have been based on the so called *equidistribution principle* (EP), and are discussed in section 1.4.2. Some of the preliminary developments and earlier work that have also played significant roles in this research area are first described, briefly, in the following section.

1.4.1 Preliminary Developments and Earlier Work

The concept of improving the accuracy of an approximate solution by optimizing a discretization has origins in the relatively early stages of the evolution of numerical methods during this century. For example, in 1903 L. V. Kantorovitch suggested a variation of the classical full-domain Rayleigh-Ritz and Galerkin methods[5] in which the coefficients of the basis functions were taken to be functions of the space-variables rather than simply undetermined constants [139]. The formulation resulted in a system of simultaneous differential equations from which the unknown coefficient functions could be determined. In contrast with the simpler system of simultaneous algebraic equations that occur in the standard full-domain Rayleigh-Ritz and Galerkin methods, Kantorovitch's variation could produce approximations of higher accuracy, but with the trade-off of added complexity in obtaining the solution. His idea was published again in 1942 [140], however, as pointed-out in [141], the method could be very sensitive to the choice of the first approximation. If this were carefully chosen,

[5]The classical full-domain Rayleigh-Ritz and Galerkin methods were the early precursors of FEMs.

a high degree of accuracy could often be attained with comparatively little numerical calculation, but for a less fortunate choice a considerable amount of computational labour could ensue. In fact, the method of finite differences (FD) was developed, partially, in order to overcome the undesirable consequences caused by an unsuitable choice of the approximating functions for full-domain Rayleigh-Ritz and Galerkin methods, in general, as explained in [142].

During the early 1970's, there was a resurgence of interest in optimal discretizations for numerical methods. Interestingly, one of the first works to be published in the mainstream literature on the topic dealt with the concept of optimal node[6] spacings for FD methods [120]. It was recognized that improved solution accuracy could, potentially, be obtained by optimizing the node point distribution for a problem. Given an initial nodal distribution $\{y_i^1\}$ with associated truncation error distribution $\{T_i^1\}$, the problem was formulated as one of obtaining successive nodal distributions $\{y_i^k\}$ for which $\{T_i^k\} \rightarrow \{0\}$, that is, the optimal node distribution. An explicit difference formula was developed for computing the successive nodal distributions. The superscript (k) denotes the iterate number; iteration being required because the formula is nonlinear. To illustrate the method, the equation $u'' + P(u, y)u' + Q(u, y) = 0$ subject to the boundary conditions $u(0) = 0$ and $u(1) = 1$, was solved for three sets of P and Q, corresponding to test examples from fluid dynamics. As evident from the boundary conditions, the test problems were confined to one dimension. Nonetheless, it was found that, indeed, maximal solution accuracy could be achieved by optimizing the node point distribution. One of the major implications of this finding was that it would now be possible to extract more accurate expressions for derivatives of the underlying field solution. Consequently, an important feature of optimizing the FD discretization was that more accurate post-processing could be performed, since many important engineering quantities are often computed from derivatives of the

[6] In FD methods, the problem domain is discretized by a set of *nodes*, where difference formulae are used to approximate derivatives of the unknown being solved for.

field solutions.

The significance of characterizing solution properties associated with optimal discretizations for modern FEMs received a considerable amount of theoretical and experimental attention in a series of independent works published during the 1970's [121–124]. The first of these publications, put forth the basic hypothesis that the computation of an optimal finite element solution must consider the problem discretization as a primary parameter in its formulation [121]. By using a simple one-dimensional model, an inductive argument was presented, based on the monotonic convergence property for the finite element method [143] and the extreme value theorem of calculus, for the existence of an optimum sub-division of the problem domain. One limitation of the argument was that it relied on the assumption that a single parameter could be used to characterize a discretization, and that proving that an optimal value of the parameter exists would, thus, also prove that an optimal discretization exists. Essentially, this assumption limited the argument to being useful for proving the existence of optimal one-dimensional meshes of only two elements. However, it was argued, by induction, that the concept should extend to meshes of any number of elements. The idea was applied to a practical problem of elastic displacement consisting of a cantilevered beam under different loading conditions. Due to the inherent symmetry of the problem under investigation, no optimization was considered in the y-direction, therefore, a one-dimensional analysis was possible although a two-dimensional problem was being modeled. The solution of the optimization equations could not be carried out explicitly due to the nonlinear manner in which the discretization parameters appeared in these equations; therefore, the authors adopted an iterative solution technique. This rendered the cost of solving problems with fine, or highly-discretized meshes, impractical for the added accuracy that could be achieved under such conditions. Given this high cost, it was concluded that what might be more important is what could be gleaned about the characteristics of optimal discretizations, rather than an actual technique for obtaining optimal

discretizations for practical problems. It was found that the optimum geometry discretization for the problem considered was characterized by a uniform (equidistant) mesh whenever a first-order mismatch occurred; for example, when the exact solution was of order x^2 and the finite element representation was piecewise linear. It should be noted, however, that this type of characterization is of little practical value for approximation methods such as the FEM, where the exact solution is not known. Although the results were specific to the problem being considered and the type of elements employed,[7] the work did establish the existence, if not uniqueness, of optimal finite element discretizations, and thus set the stage for subsequent investigations into the characterization of optimal finite element meshes.

One of the first analytical results to be published for characterizing optimal finite element discretizations was based on investigating an example consisting of a linearly tapered elastic rod that is fixed at one end and carries an axial load at the other [122]. Once again, a one-dimensional treatment was possible due to the symmetry of the problem. By assuming a piecewise linear finite element approximation, and by establishing a formula for the average cross-sectional area of an element given its location along the elastic rod, it was possible to derive an analytical expression characterizing an optimal mesh. It was found that the condition that must be satisfied by the optimal discretization is that the element boundaries should be defined such that the cross-sectional area at a given element boundary is equivalent to the square-root of the product of the cross-sectional areas at the adjacent element boundaries. This result was shown to correspond to each element containing the same amount of strain energy. This was a rather remarkable finding, since it suggested a very intuitive method for designing optimal finite element discretizations, simply by equidistributing the potential energy of the system throughout all of the elements. However, it was conjectured that this result may be confined to the specific example of a linearly tapered rod, and unfortunately, later studies would prove this to be the case [123, 124]. One of the

[7] Bilinear and biquadratic rectangular elements were used in computing the results.

most significant consequences of the finding was that it was the first successful practical characterization of optimal finite element discretizations, albeit only for a certain class of problems, since it did not require *a priori* knowledge of the exact solution, and prompted other researchers to probe further. For example, a more general characterization for optimal meshes was developed for elastic rods of any taper in [123]. The result was basically an extension of that presented in [122], and, therefore, included the same mesh optimality criteria for a linearly tapered elastic rod. Although it was now apparent that the equidistribution of potential energy amongst elements was no longer a valid characterization of optimal discretization-based solutions, another interesting characteristic of such solutions did emerge. Namely, it was found that the first derivative of the solution computed at the element boundaries (vertices) as the average of the derivative values in adjacent elements was exact for all tapers. Aside from being a more general characterization, this latest finding also added support to the notion that incorporating the optimization of the problem discretization into the solution process could result in more accurate post-processing. Subsequently, another study dealing with elastic rods under various loading conditions also concluded that a universally valid optimality criterion in terms of the average potential energy per element may not exist [124]. Noteworthy, the theoretical analyses developed in [122–124] for characterizing optimal finite element discretizations were based on linear finite element formulations. Restricting the approximations to first-order functions, allowed for critical simplifications in the derivations which would not have otherwise been possible. More importantly, however, these analytically oriented early works demonstrated the possibility of mathematically characterizing properties of optimal finite element solutions, which in turn held great promise for practical applications in terms of achieving improved solution accuracy and efficiency through adaptive refinements guided by optimal solution characteristics.

1.4.2 Equidistribution Principles

One of the most prominent and enduring trends that eventually emerged in the literature, in terms of analytically characterizing optimal discretizations for numerical methods, centered around the so called *equidistribution principle* (EP) [117, 125–127, 129–135, 137]. Although it had been shown earlier that the equidistribution of energy amongst elements in FEM discretizations was not a universally valid mesh optimality criterion, there was a strong conviction amongst various analysts that there must exist a universally valid mesh optimality criterion of some sort. One of the most general and powerful formulations to be published in this area was given in [127], and introduced the concept of the *grading function*, which would, subsequently, become a fundamental component of many of the future works to be published on the topic. In fact, a primary form of the grading function approach had been developed and published earlier in [125], however, in a less general format which was valid under far fewer conditions. By definition, a grading function is a function whose value changes by a constant amount over each element in a discretization. It may be noted, that by virtue of this basic definition, grading functions have most commonly been developed in a one-dimensional setting, although some attempts have been made to extend their application into higher-dimensional analyses [132, 134, 136].

Mathematically, a grading function is a convenient means by which to describe, or characterize, the placement of element vertices in a one-dimensional mesh. For a mesh with N elements, a grading function $\xi(x)$ must satisfy the following condition:

$$\xi(x_i) - \xi(x_{i-1}) = \int_{\Omega_i} \xi' \, dx = \frac{1}{N}, \tag{1.3}$$

where x_{i-1} and x_i are the coordinates of adjacent element vertices defining the i^{th} element over the sub-region Ω_i of the discretized problem domain. The general approach taken in [127] is to derive such a grading function that will minimize the approximation error in a computed finite element solution for a given problem. In other words, the optimal discretization will be that which has element vertices positioned such that

Eq. (1.3) is satisfied for the derived grading function. The first step in the derivation involves the definition of a general class of error measures appropriate for interpolation and approximation problems. The error is defined as the difference between the exact solution, u, and approximate solution u_h:

$$e = u - u_h, \tag{1.4}$$

and is measured in terms of the H^m-seminorm, $|e|_m$, over some interval $[a, b]$ for the one-dimensional case:

$$|e|_m^2 = \int_a^b (e^{(m)})^2 \, dx, \tag{1.5}$$

where m is the order of differentiation involved. The objective is to then find the grading function $\xi(x)$ in terms of the approximate solution u_h, such that Eq. (1.5) is minimized with respect to variations in the mesh coordinates. The authors proceed by representing the error in Eq. (1.4) and its m^{th}-order derivative as a Fourier sine series expansion over the sub-region Ω_i spanning the i^{th} element. Parseval's identity is then used to write the H^m-seminorm, $|e|_m$, as well as the H^{k+1}-seminorm, $|e|_{k+1}$, of the error in terms of the Fourier series coefficients and the element length, h_i, where:

$$h_i = x_i - x_{i-1}. \tag{1.6}$$

and where k represents the polynomial order of the approximate solution u_h. By doing so, it is possible to derive an inequality between the two different seminorms $|e|_m$ and $|e|_{k+1}$:

$$\int_{\Omega_i} [e^{(m)}]^2 dx \leq \frac{h_i}{\pi}^{2(k+1-m)} \int_{\Omega_i} [e^{(k+1)}]^2 \, dx. \tag{1.7}$$

which is valid so long as the polynomial degree of the approximation is greater than the order of differentiation in the H^m-seminorm of the error, that is, for $k > m$. Since the approximate solution u_h is only of polynomial order k, it is then possible to write the $(k+1)^{th}$-derivative of the error in Eq. (1.4) solely in terms of the $(k+1)^{th}$-derivative of the true solution u:

$$e^{(k+1)} = u^{(k+1)}. \tag{1.8}$$

This allows the H^m-seminorm of the error over the entire discretization to be expressed as the following inequality:

$$|e|_m^2 \leq \sum_{i=1}^{N} \frac{h_i}{\pi}^{2(k+1-m)} \int_{\Omega_i} [u^{(k+1)}]^2 \, dx. \tag{1.9}$$

It is worthwhile to note that the approximate solution u_h does not appear on the right hand side of the inequality (1.9), nor do any of its derivatives: this has key implications for the final result from the derivation of the grading function being sought. The basic condition in Eq. (1.3) which defines a grading function, is next used to derive an expression for the length of the i^{th} element, h_i, in terms of the number of elements in the mesh, N, and the first derivative of the unknown grading function, ξ'. This is possible by using the mid-point quadrature rule to approximate the integral of ξ' over the i^{th} element, which appears in Eq. (1.3). Similarly, the mid-point rule is used to approximate the integral of $[u^{(k+1)}]^2$ in the inequality (1.9). These two approximations are then substituted into the right hand side of the inequality (1.9), which results in:

$$|e|_m^2 \leq \frac{1}{(\pi N)^{2(k+1-m)}} \sum_{i=1}^{N} \frac{[u^{(k+1)}(x_{i-1/2})]^2}{[\xi'(x_{i-1/2})]^{2(k+1-m)}} h_i, \tag{1.10}$$

where $x_{i-1/2}$ represents the midpoint of the i^{th} element. By interpreting the expression on the right in the above inequality as a Riemann sum, the summation is replaced by definite integration, so that:

$$|e|_m^2 \leq \frac{1}{(\pi N)^{2(k+1-m)}} \int_a^b \frac{[u^{(k+1)}(x_{i-1/2})]^2}{[\xi'(x_{i-1/2})]^{2(k+1-m)}} \, dx. \tag{1.11}$$

Finally, to determine the grading function ξ that minimizes the integral in the above inequality, the solution to the corresponding Euler equation,

$$\frac{d}{dx} \frac{[u^{(k+1)}]^2}{[\xi']^{2(k+1-m)+1}} = 0, \tag{1.12}$$

is found to be:

$$\xi = \frac{\int_a^x [u^{(k+1)}]^{2/[2(k+1-m)+1]} \, dx}{\int_a^b [u^{(k+1)}]^{2/[2(k+1-m)+1]} \, dx}. \tag{1.13}$$

The above result can be used to iteratively generate optimal discretizations by adjusting element vertices until the grading function ξ in Eq. (1.13) changes by the constant amount $1/N$ over each element, as required by Eq. (1.3). It should be noted, however, that an explicit knowledge of the exact solution, u, is required; whereas, no knowledge of the approximate solution, u_h, is assumed. Thus, the grading function in Eq. (1.13) may be well suited to determining optimal discretizations for interpolation problems, but it is not appropriate for approximation problems where the exact solution is not known in advance. Although the authors acknowledge this limitation of their derivation, they, nonetheless, present an argument for the use of the grading function of Eq. (1.13) in approximation methods such as the FEM. Their argument asserts that finite element solutions computed to high levels of accuracy are close to the true solution, and, therefore, may be considered as interpolatory on the true solution. Although this may be true, under certain conditions, it is clearly not the case for low accuracy finite element solutions computed from crude discretizations. Furthermore, it will be shown later, that for certain finite element approximations it is possible to compute solutions that are interpolatory at all levels of discretization, but for which the above grading function in Eq. (1.13) does not correspond to the optimal discretization. Moreover, it will be demonstrated that these interpolatory finite element solutions do correspond to the optimal discretization of the problem domain, and thus, ironically, there is no need to use the grading function approach to optimize the finite element meshes under the exact conditions when it would be most appropriate to do so.

In evaluating the performance of the grading function approach developed in [127] for an interpolation test problem, it was found that discretizations which were iteratively computed based on grading functions produced solutions of higher accuracy than those computed on uniform meshes. However, it was found that the results were highly dependent upon the specific error measure used. In other words, meshes that were graded based on a specific norm or seminorm resulted in solution errors which

differed significantly from those of meshes graded based on other measures of the error.

It may be worthwhile to note, that although the derivation given in [127] is in terms of the H^m-seminorm of the error, it is possible to derive other grading functions for the error in the full H^m-norm. While such a derivation is not given in [127], it is a valuable observation since many approximation problems are based on formulations which involve the minimization of the error in terms of full norms. However, the approximation test problems presented in [127] were chosen such that H^m-seminorm based grading functions could be used. Also, the test problems selected had known analytical solutions, thus, it was possible to compare the relative performance of grading functions based on both approximate and exact solutions. It was found that the errors, measured in terms of the H^1-seminorm, in the solutions computed from meshes graded based on both approximate and exact solutions were lower than the errors resulting from uniform meshes, as would be expected. However, it was also shown that the meshes generated by using grading functions based on the exact solution were, in fact, the optimal meshes for the given formulation of the approximation problems considered. This is significant since discretizations that were evolved using grading functions based on the approximate solutions differed from the optimal discretizations. The reasons for this may lie in certain approximations that were made in the derivation. Namely, the midpoint quadrature rule was used to approximate integrals of derivatives of the unknown grading function, ξ, and the solution, u, during the formulation. Although this type of approximation can be quite accurate for linear or low order functions, it is not exact for higher order functions. This implies that if the exact solution, u, is of sufficiently high order relative to the polynomial degree, k, of the approximate solution, u_h, the quadrature rule used in approximating certain integrals in the formulation may be a source of error, since the $k+1$-derivative of the exact solution is involved. In addition, the interpretation of the summation in Eq. (1.10) as a definite integral in Eq. (1.11) is based on the assumption that the

element length, h_i, is sufficiently small. Thus, the general grading function, ξ, given in Eq. (1.13) will produce discretizations that are only asymptotically optimal in terms of minimizing the solution error, in the sense that they should converge to the truly optimal discretizations once the meshes contain a sufficiently large number of elements. However, the numerical results given for the approximation test problems in [127], indicate that for the solutions computed with the largest number of elements used, the meshes had still not converged to the optimal discretizations.

The grading function in Eq. (1.13) is general in the sense that it may be tailored to different norms and seminorms used in interpolation and approximation methods. However, there are certain restrictions and drawbacks to its use which have not yet been mentioned. For example, in finite element electromagnetics the H^1-seminorm and H^1-norm are often the measures of solution error that must be minimized in order to solve problems appropriately. Since these two error measures involve the first derivative of the underlying field solution, the approximation functions used must, therefore, be of at least second-order or higher in order to apply the result in Eq. (1.13). This follows from the condition $k > m$, that must hold, as described previously, since $m = 1$ in these cases. Additionally, it is evident from Eq. (1.13) that the order of differentiation of the solution, u, involved in the definition of the grading function which is appropriate for use over a given element is dependent on the polynomial degree, k, of the approximating functions employed over that element. This order of differentiation is always equal to $k + 1$, and, therefore, always results identically to zero since the approximation is of order k, which, in turn results in a grading function equal to zero. To overcome this difficulty, the authors used extrapolation to increase the degree of the approximation for the test problems considered in [127]. In particular, superconvergence theory was employed in order to compute the higher-order derivatives necessary for evaluation of the grading functions. Recent studies have shown, however, that superconvergence based derivatives of the underlying field solution, can give results with large errors for the values of the desired

derivatives in finite element electromagnetics applications [144].

The approach defined in [127] is representative of a larger body of work in the area of analytically characterizing optimal discretizations, as mentioned previously. In particular, the principle of equidistributing some quantity related to the problem solution amongst all the elements in a mesh is embodied by the grading function approach developed in [127], and has been investigated in numerous other publications including [117, 125, 126, 129–135, 137]. In fact, the formulation given in [125] was a primary form of that developed in [127], as mentioned earlier, but was based strictly on the assumption that optimal discretizations for only first-order finite element approximations were being sought. Thus, the resulting grading function used in [125] is consistent with that presented in [127] for $k = 1$ and $m = 1$. Consequently, the results of the computational tests presented in [125] for the one-dimensional approximation test problems considered there, are consistent with the analogous results in [127], in that the optimally graded meshes do not correspond exactly to the actual optimal discretizations for low numbers of elements, but, rather, tend to them asymptotically as the element sizes decrease. It was also noted in [125] that the computation of the optimally graded meshes was not stable under small perturbations in the corresponding approximate solutions. Thus, the relative accuracy of an approximate solution computed at a given level of discretization could affect the optimality of tne mesh determined from the grading function derived to compute the the optimal mesh.

In another publication dealing with optimal discretizations for first-order finite element methods, the authors adopted the approach of equidistributing the residual of the governing partial differential equation for one-dimensional test problems [126]. Although no theoretical justification was given for the use of this equidistribution principle, equidistribution criteria are often chosen heuristically, as pointed out in the review of equidistribution methods given in [129]. The original intention in [126] was to compute one-dimensional first-order finite element solutions based on the EP mentioned above; however, the system of nonlinear equations resulting from the si-

multaneous computation of the solution values and element vertex positions could not be solved directly, due to the occurrence of mesh tangling. Instead, the authors introduced fictitious "internodal viscosity" and "internodal spring forces" to keep element vertices at least slightly separated. In order to do so, the values of certain parameters associated with these fictitious terms had to be set empirically based on preliminary trial runs. Subsequently, it was found that the ability of the method to produce valid finite element meshes varied for different problem types if the same empirical values were used for these parameters. Also, it was observed that if these values were changed for a given problem, the resulting accuracy of the computed solutions varied, since the values of the parameters played a role in determining the problem discretization. Aside from these computational concerns related to the method proposed in [126], it is also important to note that without any theoretical basis for the choice of the mesh optimality criterion employed, it would be difficult to justify its use in AFEMs as a means of evolving optimal discretizations. Furthermore, counterexamples will be given later in this work for which the residual of the governing partial differential equation is not equidistributed amongst all of the elements in optimal discretizations computed for simple one-dimensional electromagnetic systems.

The equidistribution of error principle was also investigated in [131] to study the potential improvements in accuracy that could be realized by optimizing the problem discretization. The equidistribution criteria used in [131] to determine the ideal meshes is based on interpolation theory error estimates analogous to those used in superconvergence theory for finite element approximations [144]. Although these estimates are not strictly applicable to approximation methods such as the FEM, the numerical results indicate that the solution accuracy was improved by using meshes that equidistribute the $(1/k)^{th}$ power of the H^k-seminorm of the approximate solution when k^{th}-order approximation functions were used, compared with the results for uniform meshes. It is interesting to note that while the equivalent grading function used in [131] is similar to that developed in [127], there are slight differences between the

two results. This is worthy of mention, since both formulations rely upon assumptions based on interpolation theory, yet reach different conclusions.

More recently, the application of the grading function approach developed in [127] to higher-dimensional problems has been considered in [132, 134–136]. Specifically, it is claimed in [132] that the grading function derived in [127] should extend to two- and three-dimensional interpolation problems for determining optimal discretizations in terms of minimizing the interpolation error. However, the claim was based on the results from one-dimensional test problems given in [132, 133], and the preliminary test results for two-dimensional interpolation problems, admittedly, suffer significantly from mesh tangling. Furthermore, the techniques employed by the authors in [132, 133] to overcome mesh-tangling for one-dimensional problems, only partially work for the two-dimensional cases examined.

The use of a grading function similar to that in [127] was considered for use in two-dimensional approximation problems in [134]. The meshes employed consisted of quadrilaterals, rather than triangles, and although mesh tangling does not occur, it was found that the resulting optimal discretizations are not always unique. More importantly, it should be noted that the two-dimensional test problems examined in [134] were treated in a one-dimensional fashion: the optimization of the discretizations in the x- and y-directions were carried out independently. However, the use of standard, non-orthogonal basis functions employed in [134], would seem to not justify the independent optimization in the two space coordinates. Moreover, it was found that the approach was ineffective in terms of improving solution accuracy for the two-dimensional test problems considered. In light of these findings, the authors derived a modified version of their grading function which was based on including higher-order terms of the truncation errors involved in the approximations used in the original derivation. Overall, the results were found to be inconclusive, in that under certain conditions the new grading function gave better results, whereas, for other conditions the performance of the original grading function was superior.

Similarly, the grading function approach and EP were explored for use in two-dimensional interpolation problems in [135, 136]. It was found, however, that when solving problems with large solution gradients, the meshes generated via equidistribution could be very sensitive to small perturbations in the values of parameters used to compute the discretizations. Furthermore, it was observed that the occurrence of mesh tangling was quite sensitive to the initial mesh used to evolve an optimal discretization. The idea of using "nodal forces", as described earlier, to overcome the negative consequences of mesh tangling is alluded to by the authors in [135], but is not pursued because of uncertainty as to how to apply this approach to higher space dimensions than the one-dimensional context in which it had previously been used in. Finally, as stated in [136], the efficiency of the proposed method relative to standard, uniform methods was not considered due to the computational difficulties encountered.

A slightly different EP approach is developed in [117, 137] for finite element formulations, which involves the use of Lagrange multiplier methods in analytically characterizing optimal finite element discretizations. Although the basic idea in [117, 137] is the same as that in [127], in the sense that the optimal discretization which will minimize a measure of the error in the approximate solution is the objective, the formulation and results given in [117, 137] are directly in terms of equidistribution of the error measure itself, and not an auxiliary grading function. Specifically, it is shown in [117] that the optimal finite element discretization for any problem will be that which equidistributes the integral of the square of the solution error over each element in the mesh, regardless of how the solution error is defined. This is a rather impressive claim, but seems to suggest that for a given finite element formulation, say one based on minimizing the global potential energy of the system, different error criteria would lead to different optimal discretizations. However, for such a formulation, there can only be one true minimum of the potential energy, which should be associated with the true optimal discretization for a given problem. It may be

noted, that in the derivation of the optimality criterion given in [117], there was no consideration given to the interdependence of elemental errors. In other words, the derivation was based on the assumption that the error in each individual element in a mesh could be minimized without influence from the minimization of the error in other elements in the discretization. In general, such an assumption is not valid for approximation problems, where it is essential that the approximate solution over a given element is somehow related to that of, at least, adjacent elements; thus, in general, there is interdependence amongst elemental errors.

A mathematical formulation is given in [137] which is aimed at providing theoretical justification for the use of an EP published earlier in [130] based on equidistributing the energy norm of the error in finite element approximations. There are key features of the formulation that may be worthwhile to note. First, error estimates based on interpolation theory are used as the fundamental basis of the derivation. As mentioned earlier, such estimates are not, in general, valid for finite element approximations. Nonetheless, based on these estimates, it is shown that given a finite element discretization consisting of square elements, uniformly subdividing those elements which will result in the energy norm of the error being equally distributed amongst all the elements in the mesh, will produce the optimal finite element discretization for the problem. However, this result is to be expected, given that one of the critical simplifications that occurs early in the formulation, implicitly constrains the error to be equally distributed amongst the elements in subsequent refinements of the mesh. Although, no numerical results are provided in [137] to support the theoretical findings, it was shown in [130] that while the approach of equidistributing the energy norm of the solution error can provide benefits in terms of improved solution accuracy under certain conditions, this criterion was unable to concentrate elements in regions of high solution gradients for the problems examined. Unfortunately, it is in just such regions that high concentrations of DOF are needed in order to compute accurate finite element solutions to electromagnetics problems efficiently [57].

As noted in the comprehensive review given in [129] of adaptive finite element methods that involve the optimization of the problem discretization, most methods move element vertices to equidistribute some quantity related to the computed solution or the approximation error associated with it. However, there has yet to be found a universal equidistribution criterion appropriate for characterizing optimal finite element discretizations for a sufficiently wide range of problem applications. Since the simultaneous computation of the problem discretization and the solution values converts a linear problem into a nonlinear one, or usually makes a nonlinear problem all the more difficult to solve, it is valid to question the value of expending the additional effort required to solve such problems. Furthermore, given the considerable amount of work that has been done to date, and the key issues which still remain to be resolved, it is useful to recall the potential benefits of continued research in this area. As pointed out in [129], the field holds great promise for developing improved adaptive methods, and, hence, the reduction of computational costs in many areas in which the numerical solution of problems plays a vital role in modern day engineering analysis and design.

1.5 Thesis Objective

Currently, there exists substantial evidence suggesting that the optimality of a finite element discretization plays a significant role in the accuracy of computed solutions at given levels of problem refinement. To date, the characterization of mesh optimality criteria in order to exploit the potential benefits most advantageously in AFEMs have been investigated extensively. However, the approaches that have been used have either, been inappropriate for finite element applications, or have not produced sufficiently conclusive findings. The objective of this work is to develop an adequately general theoretical framework appropriate for the qualitative and numerical study of optimal finite element discretizations for electromagnetic systems, and to, ultimately, produce effective refinement criteria for reliably and efficiently guiding adaptive finite element solvers towards optimal solutions.

1.6 Thesis Outline

The first step towards achieving the objective of the thesis will be to formulate the problem of simultaneously solving for the electromagnetic field solution values along with the optimal discretization parameters as a well-posed nonlinear optimization problem. In Chapter 2, a general formulation, valid for the three common orthogonal coordinate reference systems, will be given for one-dimensional finite element analysis of electromagnetic systems possessing appropriate symmetry. Similarly, a derivation for the optimization of two-dimensional finite element triangular discretizations and the extension to tetrahedral meshes for three-dimensional problems will also be presented in Chapter 2. In all cases, the formulations will allow for the polynomial order of the approximation to vary over a given mesh, so that the advantages of optimal discretizations for h-, p- and hp-type adaption models may be explored. Subsequently, the formulations will be used to compute truly optimal finite element solutions for a series of important benchmark electromagnetic systems. In Chapter 3, the optimal so-

lutions for one-dimensional finite element analysis of electromagnetic systems will be used to investigate the validity and usefulness of currently available optimality criteria; to propose a new set of characterizations for optimal finite element discretizations; and to evaluate the potential performance advantages of the new characterizations for the primary adaption models. In Chapter 4, the optimal solutions will be used to extend the new concepts to two- and three-dimensional analyses of electromagnetic systems, and the value of the new characterizations for practical AFEMs will be assessed. Next, a formulation will be developed for second-order functional derivatives which will be used to enhance the new characterizations for optimal finite element discretizations, and the numerical performance of the enhanced characterizations will be examined and evaluated in Chapter 5. Finally, the theoretical and practical value of the new optimal discretization-based approach for AFEA will be concluded in Chapter 6.

Chapter 2

Formulations for Optimal Finite Element Solutions

The review of the methods used for characterizing optimal finite element discretizations given in the previous chapter has revealed that the most reliable approaches for determining optimality criteria are those based on the principle of, first, computing optimal solutions and, subsequently, analyzing the characteristics of such solutions. The aim of this chapter is to present a set of nonlinear systems of equations which can be used to simultaneously compute optimal field solution values along with optimal geometric discretization parameters corresponding to finite element formulations for one-, two-, and three-dimensional scalar boundary value problems in macroscopic electromagnetics. In order to derive such systems of equations which can yield optimal finite element solutions, a mathematical formulation will be developed based on well-established variational principles. Moreover, the formulation will be sufficiently general to allow for the consideration of a range of electromagnetics problems including static and time-harmonic phenomena. In addition, finite element discretizations with arbitrary distributions of element sizes and degrees of approximating functions will be assumed, so that there will be no restrictions imposed on the possible distribution of DOF throughout the problem space, other than those inherent in the types of elements and specific approximating functions used to discretize the continuum problem.

Although several different choices exist for the shape of the elements to be used in a finite element mesh, the most basic types of elements employed in finite element electromagnetics are simplexes. For example, line segments, triangles, and tetrahedra are commonly used in one-, two-, and three-dimensional electromagnetics finite element applications, respectively. The algebraic completeness property of the approximat-

ing functions that can be defined over simplexes make such elements geometrically isotropic, and therefore appropriate for modeling solutions of arbitrary variation over different parts of problem domains [23, 145]. Furthermore, any polygonal or polyhedral problem domain can be exactly decomposed into a set of simplexes, but not necessarily into any other standard element shape [138]. For this work, simplex elements will be employed exclusively, however, the formulation will not be restricted to specific approximating functions.

Ultimately, the equations derived from the mathematical formulation developed in this chapter will be solved, using standard optimization methods, in order to compute truly optimal finite element solutions to a series of benchmark electromagnetic systems. That is, the solutions computed in this manner will be of the highest accuracy possible for a given level of problem refinement for the variational approach used, as will be shown later, since the fundamental variational principle underlying the problem formulation is itself used as the basis for deriving the optimization equations. Therefore, these solutions will permit for the reliable determination of theoretically valid discretization optimality criteria for finite element electromagnetics applications.

2.1 Abstract Variational Problem

One of the standard approaches that is used for solving electromagnetic field problems numerically by FEMs is to reformulate the original continuum problem, cast in terms of Maxwell's field equations, using a variational principle that leads to a system of algebraic equations, for the discretized problem, whose solution represents that of the underlying continuum problem [138]. Although such variational reformulations of electromagnetics problems are based on well established mathematical theory, a brief description of some of the fundamental principles involved will be given here in order to develop certain concepts that are necessary for the derivation of the optimization equations to follow later in this chapter.

The mathematical formulation developed in this chapter for deriving the systems

of nonlinear algebraic equations that will eventually be solved in order to compute optimal finite element solutions for electromagnetic problems that can be cast in the form of general operator equations such as Eq. (1.2), as explained in section 1.3, is based upon the variational principle of finding the function $u(x, y, z)$ which renders the functional $F(u)$ stationary, where:

$$F(u) = \frac{1}{2} \langle \mathcal{L}u, u \rangle - \langle u, g \rangle . \tag{2.1}$$

In Eq. (2.1) above, the notation $\langle \cdot, \cdot \rangle$ denotes the symmetric product defined over the problem region Ω as:

$$\langle \phi, \psi \rangle = \int_{\Omega} \phi \psi \, d\Omega, \tag{2.2}$$

where ϕ and ψ represent real or complex valued scalar functions.[1] Assuming that $\mathcal{L}$, together with its associated boundary conditions, represents a self-adjoint complex operator, that is,

$$\langle \mathcal{L}\phi, \psi \rangle = \langle \phi, \mathcal{L}\psi \rangle , \tag{2.3}$$

then it can be shown [25] that for an arbitrary variation, δu, in the function $u(x, y, z)$, the functional $F(u + \delta u)$ will be stationary about u if:

$$\delta F = 0, \tag{2.4}$$

where δF is the first variation of F, and is given by:

$$\delta F = \langle \delta u, \mathcal{L}u - g \rangle . \tag{2.5}$$

Thus, in order for the condition in (2.4) to hold, the following equation must be satisfied:

$$\mathcal{L}u - g = 0, \tag{2.6}$$

[1] The variational principle described in this section is also applicable to vector problems, for which the inner product is defined as $\langle \mathbf{a}, \mathbf{b} \rangle = \int_{\Omega} \mathbf{a} \cdot \mathbf{b} \, d\Omega$. However, only problems that can be expressed in terms of scalar unknowns will be considered in this work.

since the first variation of F must vanish for an arbitrary variation,[2] δu, from Eq. (2.5). Therefore, finding the function $u(x, y, z)$ that renders the functional $F(u)$, as defined in Eq. (2.1), stationary, is equivalent to solving the original electromagnetics problem in the form of an operator equation such as Eq. (1.2). Furthermore, it should be noted, that for a given problem, the function $u(x, y, z)$ for which $F(u)$ is stationary, may be determined uniquely since it must satisfy Maxwell's equations subject to the specific boundary conditions associated with the original electromagnetics problem [12].

In FEMs that employ the variational principle described above, the functional F is uniquely defined by the numerical values of a finite set of parameters that are, in general, associated with the approximating functions used to model the solution over the discretized problem domain. Thus, for the discretized finite element problem, the stationarity requirement of Eq. (2.4) amounts to finding the stationary point of F with respect to variations in these parameters. This can be achieved by the usual methods of the differential calculus, namely, by setting to zero the first derivative of F with respect to each of the parameters, and solving the resulting system of algebraic equations [141]. It is a direct consequence of the fact that this type of stationarity principle is required for the solution of finite element problems formulated using the above variational approach, that such formulations can lead to theoretically justified methods which are intrinsically suited to optimizing finite element discretizations [56].

2.2 Generalized Functional for Electromagnetic Systems

In the following, a generalized functional is presented which will be shown to be appropriate for the variational finite element formulation of a range of one-, two-, and three-dimensional scalar boundary value problems in macroscopic electromagnetics.

[2] In the discussion above, it is assumed that only admissible functions, i.e., functions which comply with the boundary conditions and continuity requirements of the given electromagnetics problem, and that are sufficiently differentiable to the degree required to evaluate the functional F as defined in Eq. (2.1), are considered for determining the stationary point of the functional F. Thus, the arbitrary variation δu referred to above, must vanish on any boundaries of the problem domain for which u is constrained, so that $u + \delta u$ may also be a member of the set of admissible functions [138].

The approach taken is to begin with a sufficiently general differential equation, together with associated boundary conditions, and to apply the variational principle described earlier in this chapter in order to derive the corresponding functional. A merit of this type of approach is its generality, since such a formulation, which is valid for the general differential equation considered here, allows problems in Laplace's equation, Poisson's equation, the Helmholtz equation, and a diffusion equation to be solved by simply dropping terms from the general equation. Thus, problems involving static, quasi-static, and wave-like phenomena may all be investigated with the resulting formulation.

Consider the following general, second-order, scalar, partial differential equation:

$$\nabla \cdot (p \nabla u) + (k^2 + D)u = g, \tag{2.7}$$

in the enclosed region Ω bounded by the surface S, for which the solution u must satisfy the boundary conditions:

$$\begin{aligned} u|_{S_d} &= u_d, \text{ and.} \\ \left.\frac{\partial u}{\partial n}\right|_{S_n} &= 0. \end{aligned} \tag{2.8}$$

The symbols appearing in (2.7) and (2.8) have the following meaning:

u is the electromagnetic field unknown to be solved for;

p is a material-related parameter equal to ε, μ^{-1}, or 1;

ε is the permittivity;

μ is the permeability;

k is the free space wave number equal to $\omega\sqrt{\mu\varepsilon}$ or 0;

ω is the frequency in radians/s;

D is a parameter equal to $-j\omega\sigma\xi$;

j is equal to $\sqrt{-1}$;

σ is the conductivity;

ξ is equal to μ, 1, or 0;

g is a source function;

S_d represents Dirichlet surfaces; and,

S_n represents Neumann surfaces;

where, Dirichlet surfaces are those parts of the problem domain boundary on which the solution u must take on a prescribed value u_d. Similarly, on Neumann surfaces the component of the gradient of the solution in the direction normal to the surface, $\partial u/\partial n$, must take on a prescribed value, zero in this instance. In addition, it may be noted that the surface bounding the entire problem region Ω, is comprised of the union of the Dirichlet and Neumann surfaces, i.e., $S = S_d + S_n$.

The differential equation (2.7) above may be written in the form of the operator equation (1.2), if the operator $\mathcal{L}$ is defined as:

$$\mathcal{L} = \nabla\cdot(p\nabla)\cdot + (k^2 + D)\cdot \tag{2.9}$$

However, due to the inhomogeneous Dirichlet boundary condition expressed in (2.8), this operator is not self-adjoint for the unknown function u. It can be readily shown, by introducing a new unknown function u_o:

$$u_o = u - o, \tag{2.10}$$

where o is any function that satisfies the given inhomogeneous boundary condition, that the operator $\mathcal{L}$ is self-adjoint for this new unknown function. Therefore, if u is substituted by $u_o + \phi$ in the original operator equation (1.2), then the variational principle described earlier in this chapter may be applied to the resulting equation for u_o. Consequently, the corresponding functional, when expanded in terms of Eq. (2.10) above, may be written as:

$$F(u) = \frac{1}{2}\langle \mathcal{L}u, u\rangle - \frac{1}{2}\langle \mathcal{L}u, \phi\rangle + \frac{1}{2}\langle u, \mathcal{L}\phi\rangle - \langle u, g\rangle\,. \tag{2.11}$$

where terms that do not contain u have been discarded, since stationarity of F is sought with respect to variations only in the unknown function u. It may be verified,

by using the self-adjoint property of $\mathcal{L}$ for $u_o = u - \phi$, that the first variation of F with respect to u is given by Eq. (2.5). Therefore, the function u which is the solution to the electromagnetics boundary value problem defined by the differential equation (2.7) and the boundary conditions (2.8), will render the functional $F(u)$ of Eq. (2.11) stationary.

The functional given above may be simplified, so that it can be expressed solely in terms of the electromagnetic field solution required, u, by substituting the expanded form of the operator $\mathcal{L}$ of Eq. (2.9) into Eq. (2.11), which after some cancellation of terms renders:

$$\begin{aligned} F(u) &= \frac{1}{2}\int_\Omega \left\{\nabla\cdot(p\nabla u) + (k^2 + D)u\right\} u \, d\Omega \\ &\quad + \frac{1}{2}\int_\Omega \{u\nabla\cdot(p\nabla\phi) - \phi\nabla\cdot(p\nabla u)\} \, d\Omega \\ &\quad - \int_\Omega ug \, d\Omega, \end{aligned} \tag{2.12}$$

Upon applying Green's second integral identity to the middle term above, there results:

$$\begin{aligned} F(u) &= \frac{1}{2}\int_\Omega \left\{\nabla\cdot(p\nabla u) + (k^2 + D)u\right\} u \, d\Omega \\ &\quad + \frac{1}{2}\oint_S p\left(u\frac{\partial\phi}{\partial n} - \phi\frac{\partial u}{\partial n}\right) dS - \int_\Omega ug \, d\Omega, \end{aligned} \tag{2.13}$$

and, since both u and ϕ satisfy the boundary conditions of Eq.(2.8), their application to the above expression leads to:

$$\begin{aligned} F(u) &= \frac{1}{2}\int_\Omega \left\{\nabla\cdot(p\nabla u) + (k^2 + D)u\right\} u \, d\Omega \\ &\quad + \frac{1}{2}\oint_{S_d} p\left(u_d\frac{\partial\phi}{\partial n} - u_d\frac{\partial u}{\partial n}\right) dS - \int_\Omega ug \, d\Omega. \end{aligned} \tag{2.14}$$

However, terms that do not contain the unknown function u may be discarded, since they will not appear in the first variation equation (2.4) which must be satisfied in

order to determine the stationary point of the functional, whence it follows that:

$$F(u) = \frac{1}{2}\int_{\Omega}\left\{\nabla\cdot(p\nabla u) + (k^2 + D)u\right\} u\, d\Omega - \frac{1}{2}\oint_{S_d} p\left(u_d\frac{\partial u}{\partial n}\right) dS - \int_{\Omega} ug\, d\Omega. \quad (2.15)$$

Next, applying Green's first integral identity to the first term of the left-most integral above, it may be written as the difference between a surface and a volume integration, namely:

$$\frac{1}{2}\int_{\Omega}\left[\nabla\cdot(p\nabla u)\right] u\, d\Omega = \frac{1}{2}\oint_{S} u\left(p\frac{\partial u}{\partial n}\right) dS - \frac{1}{2}\int_{\Omega}\nabla u\cdot(p\nabla u)\, d\Omega. \quad (2.16)$$

Subsequently, the surface integral in (2.16) may be separated into two separate components, one corresponding to the Dirichlet and the other to the Neumann surfaces of the problem domain. Upon applying the appropriate boundary conditions of Eq. (2.8) to each of the resulting surface integrals, it is readily seen that integration over Neumann surfaces will result in zero. However, the remaining integral over Dirichlet surfaces is identical, but opposite in sign, to that in Eq. (2.15) above. Thus, the true solution to Eq. (2.7) over the problem domain Ω is the admissible function u for which the following functional F is stationary.

$$F(u) = -\frac{1}{2}\int_{\Omega}\left\{p\nabla u\cdot\nabla u - \left(k^2 + D\right)u^2 + 2gu\right\} d\Omega. \quad (2.17)$$

or equivalently,

$$F(u) = \frac{1}{2}\int_{\Omega}\left\{p\nabla u\cdot\nabla u - \left(k^2 + D\right)u^2 + 2gu\right\} d\Omega. \quad (2.18)$$

since the leading minus sign does not play a role in the first variation equation (2.4) which must be satisfied for stationarity to hold.

2.3 Nonlinear System Formulation for the Finite Element Equations

As alluded to earlier in this chapter, discretized forms of the functional defined by (2.18) may be used to compute finite element solutions to electromagnetics problems cast in terms of the general differential equation (2.7) and its associated boundary

conditions (2.8). Furthermore, such discretized functionals are uniquely defined by the numerical values of a finite set of unknowns, or solution parameters. The approach followed in this study, is to, first, develop a nonlinear system of optimization equations from a variational finite element formulation, which can then be solved using standard optimization methods in order to compute optimal values of the solution unknowns. The fundamental stationarity condition of the variational principle presented earlier, is used as the basis of deriving the optimization equations.

The optimization equations which will be used to compute optimal finite element solutions to the general differential equation (2.7) are derived from the first variation expressions (2.4) for the functional F in (2.18). Conceptually, the dependence of the functional F, for which a stationary point is required, on the solution unknowns may be expressed as:

$$F = F(\mathbf{u}(\mathbf{x}), \mathbf{x}), \tag{2.19}$$

where the field solution is symbolically represented by the vector of field solution parameters $\mathbf{u}$, while $\mathbf{x}$ represents a vector whose elements correspond to the unconstrained geometric discretization parameters for a given problem. Moreover, any dependence of the field solution parameters on the discretization parameters is expressed by:

$$\mathbf{u} = \mathbf{u}(\mathbf{x}). \tag{2.20}$$

Consequently, stationarity of the functional F with respect to variations in $\mathbf{u}$, with the geometric discretization held fixed, is achieved by satisfying the following condition:

$$\left.\frac{\partial F}{\partial \mathbf{u}}\right|_{\mathbf{x}} = 0, \tag{2.21}$$

which is equivalent to the usual variational finite element formulation for fixed-position geometric sub-domains. In addition, for finite element formulations in which the geometric discretization for a problem can also vary, stationarity of the functional

with respect to variations in the geometric discretization implies:

$$\frac{\partial F}{\partial \mathbf{x}} = \left.\frac{\partial F}{\partial \mathbf{u}}\right|_{\mathbf{x}} \frac{\partial \mathbf{u}}{\partial \mathbf{x}} + \left.\frac{\partial F}{\partial \mathbf{x}}\right|_{\mathbf{u}} = 0. \tag{2.22}$$

Thus, from (2.21) it follows that:

$$\left.\frac{\partial F}{\partial \mathbf{x}}\right|_{\mathbf{u}} = 0, \tag{2.23}$$

represents the first variation equations corresponding to variations in the geometric discretization of a problem.

The optimization equations which can be used to simultaneously compute optimal field solution values along with optimal geometric discretization parameters for finite element formulations, i.e. (2.21) and (2.23) may be expressed as a nonlinear system of equations:

$$\mathbf{F}(\mathbf{U}) = \mathbf{0}. \tag{2.24}$$

where the individual elements of the vector $\mathbf{F}$ represent first-variation expressions of the functional F with respect to the corresponding elements of the unknown vector $\mathbf{U}$. For example, in a problem where $\mathcal{N}$ is the number of unknowns to be optimized, then:

$$\mathbf{F} = [\mathcal{F}_1, \mathcal{F}_2, \ldots, \mathcal{F}_{\mathcal{N}}], \tag{2.25}$$

$$\mathbf{U} = [\mathcal{U}_1, \mathcal{U}_2, \ldots, \mathcal{U}_{\mathcal{N}}], \tag{2.26}$$

and,

$$\mathcal{F}_i = \frac{\partial F}{\partial \mathcal{U}_i}. \tag{2.27}$$

Thus, the nonlinear system (2.24) will have the form:

$$\begin{aligned} \mathcal{F}_1(\mathcal{U}_1, \mathcal{U}_2, \ldots, \mathcal{U}_{\mathcal{N}}) &= 0 \\ \mathcal{F}_2(\mathcal{U}_1, \mathcal{U}_2, \ldots, \mathcal{U}_{\mathcal{N}}) &= 0 \\ &\vdots \\ \mathcal{F}_{\mathcal{N}}(\mathcal{U}_1, \mathcal{U}_2, \ldots, \mathcal{U}_{\mathcal{N}}) &= 0. \end{aligned} \tag{2.28}$$

and may be solved using standard optimization methods. The solution $\mathbf{U}$ of (2.28) is the characterization of the *best* approximation, from the space of admissible approximations, to the true solution u of (2.7).

2.4 Finite Element Optimization Equations

Discretized forms of the functional (2.18) given earlier in this chapter, and the finite element optimization equations derived from them, based on the first variation expressions described above, are presented in the following. The discretized functionals are developed using conventional approaches found in standard finite element references; therefore, only the key steps and results are mentioned here. However, details differing from the usual treatments, or that are of significance in the derivation of the finite element optimization equations, will be considered in greater depth.

2.4.1 One-Dimensional Systems

Electromagnetic systems which possess the appropriate type of geometric symmetry may be analyzed using one-dimensional (1-D) finite element formulations. Consider the 1-D element with vertex positions x_e and x_{e+1} such that $(x_{e+1} > x_e)$, as shown in Fig. 2.1. The location of a point $P(x)$ within the element may be expressed in terms of the simplex coordinates, ζ_1 and ζ_2, which are defined as follows:

$$\zeta_1 = \frac{x - x_e}{x_{e+1} - x_e}; \quad \zeta_2 = \frac{x_{e+1} - x}{x_{e+1} - x_e}. \tag{2.29}$$

and which satisfy the relationship,

$$\zeta_1 + \zeta_2 = 1. \tag{2.30}$$

The purely local nature of the simplex coordinates defined above, allows for the development of certain parts of the finite element formulation that follows to be accomplished in a manner independent of the global coordinate system. Thus, the results developed for any given element can then be applied to any other element by means of simple coordinate transformation rules. Furthermore, it may be noted that although only one coordinate is needed, from Eq. (2.30), various quantities arising in some stages of the formulation may be more conveniently defined in terms of both ζ_1 and ζ_2.

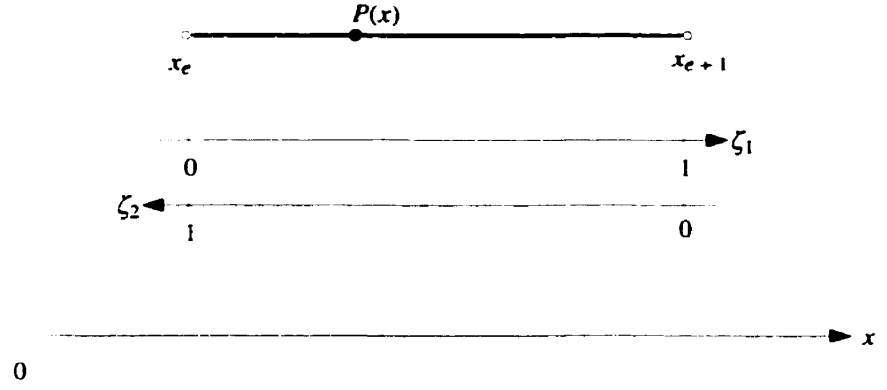

Figure 2.1: Simplex coordinates for a 1-D finite element.

The required field solution u to the differential equation (2.7) may be approximated, over an individual 1-D element, e, using a linear combination of basis functions, $\alpha_i(\zeta_1, \zeta_2)$, such as:

$$u \approx \sum_{i=0}^{n_e} U_i \alpha_i(\zeta_1, \zeta_2), \tag{2.31}$$

where the U_i are real or complex, constant coefficients, that represent the $n_e + 1$ field solution unknowns associated with the element. The basis functions in Eq.(2.31) are left general for the moment, however, explicit forms are specified in the next chapter where numerical results are computed for the benchmark systems considered there. Substituting the above approximation for u into the functional (2.18) yields:

$$F^{(e)} = \frac{1}{2} \sum_{i=0}^{n_e} \sum_{j=0}^{n_e} U_i U_j \int_{\Omega_e} \left\{ p \nabla \alpha_i \cdot \nabla \alpha_j - (k^2 + D) \alpha_i \alpha_j \right\} d\Omega$$

$$+ \sum_{i=0}^{n_e} U_i \int_{\Omega_e} g \alpha_i \, d\Omega, \tag{2.32}$$

where Ω_e represents the portion of the problem domain associated with a single element, e, and $F^{(e)}$ represents the corresponding portion of the functional.

For one-dimensional systems where x represents the independent coordinate variable over which the solution $u(x)$ may vary, the following identity applies:

$$\nabla \alpha_i \cdot \nabla \alpha_j = \frac{\partial \alpha_i}{\partial x} \frac{\partial \alpha_j}{\partial x}. \tag{2.33}$$

Each of the partial derivatives of the basis functions with respect to the independent coordinate variable in the above identity may be expanded in terms of partial derivatives with respect to the simplex coordinates, by applying the chain rule of differentiation as follows:

$$\frac{\partial \alpha_i}{\partial x} = \frac{\partial \alpha_i}{\partial \zeta_1}\frac{\partial \zeta_1}{\partial x} + \frac{\partial \alpha_i}{\partial \zeta_2}\frac{\partial \zeta_2}{\partial x}, \tag{2.34}$$

where, from Eq. (2.29):

$$\frac{\partial \zeta_1}{\partial x} = \frac{1}{h_e}; \quad \frac{\partial \zeta_2}{\partial x} = -\frac{1}{h_e}, \tag{2.35}$$

in which h_e represents the size of the one-dimensional element e, i.e.,

$$h_e = x_{e+1} - x_e. \tag{2.36}$$

Hence, the identity (2.33) may be rewritten as:

$$\nabla \alpha_i \cdot \nabla \alpha_j = \frac{1}{h_e^2}\left(\frac{\partial \alpha_i}{\partial \zeta_1} - \frac{\partial \alpha_i}{\partial \zeta_2}\right)\left(\frac{\partial \alpha_j}{\partial \zeta_1} - \frac{\partial \alpha_j}{\partial \zeta_2}\right), \tag{2.37}$$

and if the basis functions, $\alpha_i(\zeta_1, \zeta_2)$, are expressed only in terms of one of the simplex coordinates, say ζ_1, by using the relationship (2.30), the above expression simplifies to:

$$\nabla \alpha_i \cdot \nabla \alpha_j = \frac{1}{h_e^2}\frac{\partial \alpha_i}{\partial \zeta_1}\frac{\partial \alpha_j}{\partial \zeta_1}. \tag{2.38}$$

Furthermore, for one-dimensional systems in which the independent coordinate variable is represented by x, the following coordinate transformation is applicable:

$$d\zeta_1 = \frac{\partial \zeta_1}{\partial x}\,dx = \frac{1}{h_e}\,dx. \tag{2.39}$$

Now, let

$$d\Omega = x^r\,dx, \quad (r = 0, 1, 2), \tag{2.40}$$

where the parameter r will be defined shortly. However, from the definition of ζ_1 given in (2.29), and using (2.36), it is evident that,

$$x = \zeta_1 h_e + x_e. \tag{2.41}$$

Thus, from Eqs.(2.39) through (2.41), it follows that

$$d\Omega = (\zeta_1 h_e + x_e)^r h_e \, d\zeta_1, \quad (r = 0, 1, 2). \tag{2.42}$$

Therefore, upon substituting Eqs. (2.38) and (2.42) into Eq. (2.32), the general form of the discretized functional over a typical element e, for which a stationary point is sought within the finite-dimensional space of admissible approximation functions, is given by:

$$\begin{aligned} F^{(e)} &= \frac{1}{2} \sum_{i=0}^{n_e} \sum_{j=0}^{n_e} U_i U_j \int_{\zeta_1=0}^{1} \frac{p_e}{h_e^2} \frac{\partial \alpha_i}{\partial \zeta_1} \frac{\partial \alpha_j}{\partial \zeta_1} [\zeta_1 h_e + x_e]^r h_e \, d\zeta_1 \\ &\quad - \frac{1}{2} \sum_{i=0}^{n_e} \sum_{j=0}^{n_e} U_i U_j \int_{\zeta_1=0}^{1} (k_e^2 + D_e) \, \alpha_i \alpha_j [\zeta_1 h_e + x_e]^r h_e \, d\zeta_1 \\ &\quad + \sum_{i=0}^{n_e} U_i \int_{\zeta_1=0}^{1} g_e \, \alpha_i [\zeta_1 h_e + x_e]^r h_e \, d\zeta_1. \end{aligned} \tag{2.43}$$

where p_e, k_e, D_e, and g_e represent the specific forms of p, k, D, and g in Ω_e, respectively. Moreover, these quantities are assumed to be expressed purely in terms of the single simplex coordinate ζ_1. In addition, the dependency of the functional on the underlying coordinate reference system is determined by the value of the parameter r as follows:

$r = 0$ corresponds to a Cartesian coordinate system: (x, y, z);

$r = 1$ corresponds to a circular cylindrical coordinate system: (ρ, ϕ, z); and,

$r = 2$ corresponds to a spherical coordinate system: (R, θ, ϕ).

Although the functional $F^{(e)}$ defined above corresponds to a one-dimensional finite element formulation, the relative contribution from each element in a discretization to the functional over the entire three-dimensional volume associated with a given problem, must be included in $F^{(e)}$ in order to correctly apply the variational principle

described earlier in this chapter. Hence, the Jacobian, $(\zeta_1 h_e + x_e)^r h_e$, in (2.43) corresponds to transformations from the more familiar forms of the differential elements of volume associated with the three common coordinate systems as defined above by the value of the parameter r. However, it should be noted that any factors which do not differ in the unit volume from one element to the next, for a particular coordinate system, have not been included in the expression above for the elemental functional $F^{(e)}$. Specifically, when considering one-dimensional problems defined with respect to the three reference coordinate systems discussed above, the independent coordinate variable will be taken to be either x, ρ, or R in each case, respectively, for the problems considered in this study. However, the independent coordinate variable in all three cases will be consistently represented by the symbol x. Thus, the volume corresponding to each element in a given one-dimensional discretization is determined, to within a common multiplicative factor, by considering the differential volume element defined in (2.40), or alternatively, in (2.42).

The functional corresponding to a typical element, e, given in (2.43) may be expressed more concisely by first defining the following quantities:

$$\begin{aligned} V_{ij}^{(e)} &= \int_{\zeta_1=0}^{1} \frac{p_e}{h_e^2} \frac{\partial \alpha_i}{\partial \zeta_1} \frac{\partial \alpha_j}{\partial \zeta_1} [\zeta_1 h_e + x_e]^r h_e \, d\zeta_1 . \\ B_{ij}^{(e)} &= \int_{\zeta_1=0}^{1} (k_e^2 + D_e) \, \alpha_i \alpha_j [\zeta_1 h_e + x_e]^r h_e \, d\zeta_1 , \text{ and} \\ f_i^{(e)} &= \int_{\zeta_1=0}^{1} g_e \, \alpha_i [\zeta_1 h_e + x_e]^r h_e \, d\zeta_1 . \end{aligned} \tag{2.44}$$

Equation (2.43) may then be written as:

$$F^{(e)} = \frac{1}{2} \sum_{i=0}^{n_e} \sum_{j=0}^{n_e} U_i U_j V_{ij}^{(e)} - \frac{1}{2} \sum_{i=0}^{n_e} \sum_{j=0}^{n_e} U_i U_j B_{ij}^{(e)} + \sum_{i=0}^{n_e} U_i f_i^{(e)}, \tag{2.45}$$

or, in matrix form as:

$$F^{(e)} = \frac{1}{2} \mathbf{u}^{(e)T} \mathbf{V}^{(e)} \mathbf{u}^{(e)} - \frac{1}{2} \mathbf{u}^{(e)T} \mathbf{B}^{(e)} \mathbf{u}^{(e)} + \mathbf{u}^{(e)T} \mathbf{f}^{(e)}, \tag{2.46}$$

where, the vector $\mathbf{u}^{(e)}$ consists of the field solution unknowns, U_i, associated with a specific element, e, of a one-dimensional finite element discretization comprised of N elements in total, as shown in Fig. (2.2). Thus, the functional corresponding to the entire discretization is given by:

$$F = \sum_{e=1}^{N} F^{(e)}. \tag{2.47}$$

The optimization equations for the field solution parameters, $\mathbf{u}^{(e)}$, associated with a typical element, e, may be derived by considering the first variation equations defined by:

$$\frac{\partial F^{(e)}}{\partial U_i} = 0, \quad (i = 0, 1, \ldots, n_e), \tag{2.48}$$

or, equivalently by:

$$\frac{\partial F^{(e)}}{\partial \mathbf{u}^{(e)}} = \mathbf{0}. \tag{2.49}$$

Applying the following result:

$$\begin{aligned} \frac{\partial}{\partial \mathbf{u}}(\mathbf{u}^T\mathbf{w}) &= \left(\frac{\partial \mathbf{u}^T}{\partial \mathbf{u}}\right)\mathbf{w} + \left(\frac{\partial \mathbf{w}^T}{\partial \mathbf{u}}\right)\mathbf{u} \\ &= \mathbf{w} + \left(\frac{\partial \mathbf{w}^T}{\partial \mathbf{u}}\right)\mathbf{u}, \end{aligned} \tag{2.50}$$

and from the symmetry of the matrices $\mathbf{V}^{(e)}$ and $\mathbf{B}^{(e)}$, it can be readily shown that Eq. (2.49) yields:

$$\mathbf{V}^{(e)}\mathbf{u}^{(e)} - \mathbf{B}^{(e)}\mathbf{u}^{(e)} + \mathbf{f}^{(e)} = \mathbf{0}. \tag{2.51}$$

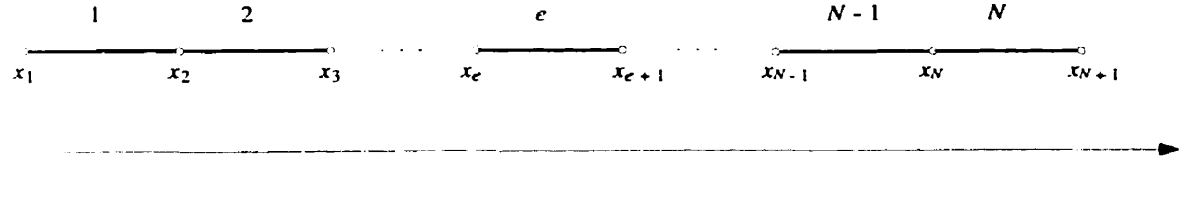

Figure 2.2: A 1-D finite element mesh of N elements.

Thus, similar treatment of all the elements in a discretization results in the set of equations:

$$\mathbf{V}^{(e)}\mathbf{u}^{(e)} - \mathbf{B}^{(e)}\mathbf{u}^{(e)} = -\mathbf{f}^{(e)}, \quad (e = 1, 2, \ldots, N). \tag{2.52}$$

which may be solved for optimizing the values of the entire set of field solution parameters, $\mathbf{u}$, for a given problem. It may be noted, that in practical finite element implementations some of the field solution parameters may be common to more than one element. The optimization equations corresponding to any such parameters may be consolidated into a single equation by, first, consolidating any field solution parameter common to more than one element into a single unknown (see [138] for example).

The optimization equations for the geometric discretization parameters may be derived by considering the first variation equations defined by:

$$\frac{\partial F}{\partial x_e} = 0, \quad (e = 2, 3, \ldots, N), \tag{2.53}$$

where the positions of the end vertices, x_1 and x_{N+1}, are constrained to the boundaries of the problem domain, and, therefore, are not permitted to vary. It may be useful to recall that,

$$F = \sum_{e=1}^{N} F^{(e)}, \tag{2.54}$$

where the dependence of $F^{(e)}$ on the discretization parameters is such that:

$$F^{(e)} = F^{(e)}(x_e, h_e(x_e, x_{e+1})). \tag{2.55}$$

Therefore, (2.55) implies:

$$F^{(e-1)} = F^{(e-1)}(x_{e-1}, h_{e-1}(x_{e-1}, x_e)). \tag{2.56}$$

and, thus:

$$\frac{\partial F}{\partial x_e} = \frac{\partial F^{(e-1)}}{\partial x_e} + \frac{\partial F^{(e)}}{\partial x_e}, \tag{2.57}$$

where,

$$\frac{\partial F^{(e-1)}}{\partial x_e} = \frac{\partial F^{(e-1)}}{\partial x_e} + \frac{\partial F^{(e-1)}}{\partial h_{e-1}} \frac{\partial h_{e-1}}{\partial x_e}. \tag{2.58}$$

However, the first term on the right in Eq. (2.58) is equal to zero since x_e does not appear explicitly in $F^{(e-1)}$, and from (2.36), we have:

$$\frac{\partial h_{e-1}}{\partial x_e} = 1. \tag{2.59}$$

Hence,

$$\frac{\partial F^{(e-1)}}{\partial x_e} = \frac{\partial F^{(e-1)}}{\partial h_{e-1}}. \tag{2.60}$$

Similarly,

$$\frac{\partial F^{(e)}}{\partial x_e} = \frac{\partial F^{(e)}}{\partial x_e} + \frac{\partial F^{(e)}}{\partial h_e}\frac{\partial h_e}{\partial x_e}. \tag{2.61}$$

but, from Eq. (2.36):

$$\frac{\partial h_e}{\partial x_e} = -1. \tag{2.62}$$

Hence,

$$\frac{\partial F^{(e)}}{\partial x_e} = \frac{\partial F^{(e)}}{\partial x_e} - \frac{\partial F^{(e)}}{\partial h_e}. \tag{2.63}$$

Finally, substituting (2.60) and (2.63) in (2.57) yields:

$$\frac{\partial F}{\partial x_e} = \frac{\partial F^{(e-1)}}{\partial h_{e-1}} + \frac{\partial F^{(e)}}{\partial x_e} - \frac{\partial F^{(e)}}{\partial h_e}. \tag{2.64}$$

Thus, the set of optimization equations corresponding to the entire set of geometric discretization parameters for a given problem is defined by:

$$\frac{\partial F^{(e-1)}}{\partial h_{e-1}} + \frac{\partial F^{(e)}}{\partial x_e} - \frac{\partial F^{(e)}}{\partial h_e} = 0. \quad (e = 2, 3, \ldots, N). \tag{2.65}$$

which may also be expressed in matrix form as:

$$\frac{1}{2}\left(\mathbf{u}^{(e-1)T}\mathbf{P}^{(e-1)}\mathbf{u}^{(e-1)} + \mathbf{u}^{(e)T}\mathbf{S}^{(e)}\mathbf{u}^{(e)}\right)$$

$$-\frac{1}{2}\left(\mathbf{u}^{(e-1)T}\mathbf{Q}^{(e-1)}\mathbf{u}^{(e-1)} + \mathbf{u}^{(e)T}\mathbf{T}^{(e)}\mathbf{u}^{(e)}\right)$$

$$+\mathbf{u}^{(e-1)T}\mathbf{d}^{(e-1)} + \mathbf{u}^{(e)T}\mathbf{r}^{(e)} = 0, \quad (e = 2, 3, \ldots, N), \tag{2.66}$$

where, the matrices and vectors in the above equation are defined as follows:

$$
\begin{aligned}
P_{ij}^{(e-1)} &= \frac{\partial}{\partial h_{e-1}} V_{ij}^{(e-1)}; \\
S_{ij}^{(e)} &= \left[\frac{\partial}{\partial x_e} - \frac{\partial}{\partial h_e}\right] V_{ij}^{(e)}; \\
Q_{ij}^{(e-1)} &= \frac{\partial}{\partial h_{e-1}} B_{ij}^{(e-1)}; \\
T_{ij}^{(e)} &= \left[\frac{\partial}{\partial x_e} - \frac{\partial}{\partial h_e}\right] B_{ij}^{(e)}; \\
d_i^{(e-1)} &= \frac{\partial}{\partial h_{e-1}} f_i^{(e-1)}; \text{ and,} \\
r_i^{(e)} &= \left[\frac{\partial}{\partial x_e} - \frac{\partial}{\partial h_e}\right] f_i^{(e)}.
\end{aligned}
\tag{2.67}
$$

Solving the combined set of equations (2.52) and (2.66) simultaneously for the field solution unknowns, $\mathbf{u}$, and the discretization parameters, $\mathbf{x}$, will yield the optimal finite element solution for a given problem within the space of admissible solutions which can be defined by the chosen sets of basis functions used to model the solution over the problem domain. It may be noted that (2.52) is equivalent to the set of equations that can be solved for only the field solution unknowns in conventional finite element formulations which have fixed-position elements. Furthermore, it should be noted that (2.66) may not be solved independently of (2.52) for the discretization parameters, since the former have been derived based on the condition of stationarity of the functional with respect to the field solution parameters. In general, stationarity of the functional with respect to the field solution parameters is dependent on the values of the discretization parameters, i.e., the element vertex positions. This dependence is due to the fact that the approximating functions defined over individual elements are defined uniquely by the values of both their associated field solution parameters and the element vertex positions.

2.4.2 Two-Dimensional Systems

Electromagnetic systems that possess translational or rotational symmetries may be analyzed using two-dimensional (2-D) finite element formulations. For example, in Cartesian problems where the field solution variation is independent of the coordinate variable z, i.e., $u = u(x, y)$, a finite element discretization may be constructed in the xy-plane. Consider the 2-D triangular element with vertex positions (x_i, y_i), $i = 1, 2, 3$, as shown in Fig. (2.3). The location of a point $P(x, y)$ within the element may be expressed in terms of the simplex coordinates, ζ_1, ζ_2, and ζ_3, which are defined as follows:

$$\zeta_1 = \frac{\text{Area}(P23)}{\text{Area}(123)}; \quad \zeta_2 = \frac{\text{Area}(1P3)}{\text{Area}(123)}; \quad \zeta_3 = \frac{\text{Area}(12P)}{\text{Area}(123)}. \tag{2.68}$$

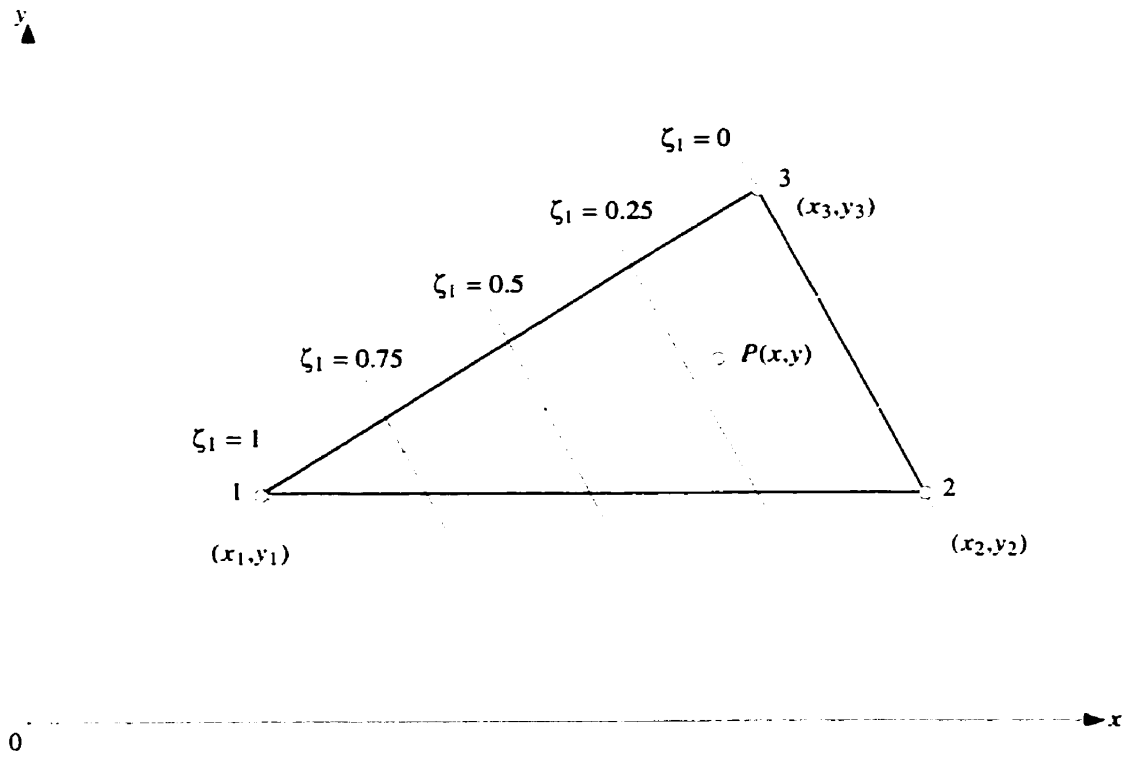

Figure 2.3: A triangular element with lines of constant ζ_1 shown, and the three sub-simplexes $P23$, $1P2$, and $12P$ used in the definition of ζ_1, ζ_2, and ζ_3.

and satisfy the relationship:

$$\zeta_1 + \zeta_2 + \zeta_3 = 1. \tag{2.69}$$

Just as in the 1-D case, the required field solution, u, to the differential equation (2.7) may be approximated over each triangular element in a 2-D discretization. For example, the following approximation may be used in element e:

$$u \approx \sum_{i=0}^{n_e} U_i \alpha_i(\zeta_1, \zeta_2, \zeta_3), \tag{2.70}$$

where, now, the $\alpha_i(\zeta_1, \zeta_2, \zeta_3)$ are two-dimensional basis functions. Once again, the U_i are real or complex, constant coefficients, that represent the $n_e + 1$ field solution unknowns associated with the element e. Similarly, the source function, g, in Eq. (2.7) may be approximated by

$$g \approx \sum_{i=0}^{n_e} G_i \alpha_i(\zeta_1, \zeta_2, \zeta_3), \tag{2.71}$$

where, in this case, the G_i are known real or complex, constant coefficients. Following a similar line of derivation as in the 1-D case, substitution of the above approximations for u and g in the functional (2.18) yields:

$$\begin{aligned} F^{(e)} &= \frac{1}{2} \sum_{i=0}^{n_e} \sum_{j=0}^{n_e} U_i U_j \int_{\Omega_e} \left\{ p \nabla \alpha_i \cdot \nabla \alpha_j - (k^2 + D) \alpha_i \alpha_j \right\} d\Omega \\ &+ \sum_{i=0}^{n_e} \sum_{j=0}^{n_e} U_i G_j \int_{\Omega_e} \alpha_i \alpha_j \, d\Omega. \end{aligned} \tag{2.72}$$

where Ω_e represents the portion of the problem domain associated with a single element, e, and $F^{(e)}$ represents the corresponding portion of the functional.

For two-dimensional systems where x and y represent the independent coordinate variables, it follows that:

$$\nabla \alpha_i \cdot \nabla \alpha_j = \frac{\partial \alpha_i}{\partial x} \frac{\partial \alpha_j}{\partial x} + \frac{\partial \alpha_i}{\partial y} \frac{\partial \alpha_j}{\partial y}. \tag{2.73}$$

The partial derivatives of the basis functions with respect to the independent coordinate variables in the above identity may be expanded in terms of partial derivatives

with respect to the simplex coordinates, as follows:

$$\frac{\partial \alpha_i}{\partial x} = \sum_{m=1}^{3} \frac{\partial \alpha_i}{\partial \zeta_m} \frac{\partial \zeta_m}{\partial x}. \tag{2.74}$$

and,

$$\frac{\partial \alpha_i}{\partial y} = \sum_{m=1}^{3} \frac{\partial \alpha_i}{\partial \zeta_m} \frac{\partial \zeta_m}{\partial y}. \tag{2.75}$$

Furthermore, the partial derivatives of the simplex coordinates with respect to the independent coordinate variables may be determined explicitly by, first, noting that the area of a triangle, for example, the 2-D element depicted in Fig. (2.3), may be expressed in determinant form as:

$$\mathcal{A} = \text{Area}(123) = \frac{1}{2} \begin{vmatrix} 1 & x_1 & y_1 \\ 1 & x_2 & y_2 \\ 1 & x_3 & y_3 \end{vmatrix}. \tag{2.76}$$

Similarly, the remaining sub-triangle areas in (2.68) which define the simplex coordinates may be expressed as:

$$\begin{aligned} \text{Area}(P23) &= \frac{1}{2} \begin{vmatrix} 1 & x & y \\ 1 & x_2 & y_2 \\ 1 & x_3 & y_3 \end{vmatrix}; \\ \text{Area}(1P3) &= \frac{1}{2} \begin{vmatrix} 1 & x_1 & y_1 \\ 1 & x & y \\ 1 & x_3 & y_3 \end{vmatrix}; \text{ and,} \\ \text{Area}(12P) &= \frac{1}{2} \begin{vmatrix} 1 & x_1 & y_1 \\ 1 & x_2 & y_2 \\ 1 & x & y \end{vmatrix}. \end{aligned} \tag{2.77}$$

Expanding the determinants in (2.76) and (2.77), and after some rearranging, it follows from (2.68) that:

$$\begin{aligned} \zeta_1 &= [(x_2y_3 - x_3y_2) + (y_2 - y_3)x + (x_3 - x_2)y] \,/\, 2\mathcal{A}; \\ \zeta_2 &= [(x_3y_1 - x_1y_3) + (y_3 - y_1)x + (x_1 - x_3)y] \,/\, 2\mathcal{A}; \\ \zeta_3 &= [(x_1y_2 - x_2y_1) + (y_1 - y_2)x + (x_2 - x_1)y] \,/\, 2\mathcal{A}; \end{aligned} \tag{2.78}$$

Therefore, it may be readily confirmed that:

$$\frac{\partial \zeta_i}{\partial x} = \frac{y_{i+1} - y_{i-1}}{2\mathcal{A}}; \quad \frac{\partial \zeta_i}{\partial y} = \frac{x_{i-1} - x_{i+1}}{2\mathcal{A}}. \tag{2.79}$$

where the subscripts progress modulo 3, i.e., cyclically around the three vertices of the triangular element in Fig. (2.3). Thus, (2.74) and (2.75) may be rewritten as:

$$\frac{\partial \alpha_i}{\partial x} = \frac{1}{2\mathcal{A}} \sum_{m=1}^{3} b_m \frac{\partial \alpha_i}{\partial \zeta_m}. \tag{2.80}$$

and,

$$\frac{\partial \alpha_i}{\partial y} = \frac{1}{2\mathcal{A}} \sum_{m=1}^{3} c_m \frac{\partial \alpha_i}{\partial \zeta_m}, \tag{2.81}$$

where b_i and c_i are defined, again in modulo 3 notation, as:

$$b_i = y_{i+1} - y_{i-1}; \quad c_i = x_{i-1} - x_{i+1}. \tag{2.82}$$

In addition, it may be shown that the coordinate transformation:

$$d\zeta_1 \, d\zeta_2 = \frac{\partial(\zeta_1, \zeta_2)}{\partial(x, y)} \, dx \, dy. \tag{2.83}$$

yields the following differential element of area, $d\Omega$, for integration in simplex coordinates over a triangular element with area $\mathcal{A}_e$:

$$d\Omega = 2\mathcal{A}_e \, d\zeta_1 \, d\zeta_2. \tag{2.84}$$

Hence, by substitution of (2.80) and (2.81) in (2.73), the general form of the discretized functional over a typical element, e, for which a stationary point is sought within the space of admissible approximation functions, may be written as:

$$\begin{aligned} F^{(e)} &= \frac{1}{2} \sum_{i=0}^{n_e} \sum_{j=0}^{n_e} U_i U_j \left[\frac{1}{2\mathcal{A}_e} \sum_{m=1}^{3} \sum_{n=1}^{3} (b_m b_n + c_m c_n) \, I_{ijmn}^{(e)} \right] \\ &\quad - \frac{1}{2} \sum_{i=0}^{n_e} \sum_{j=0}^{n_e} U_i U_j 2\mathcal{A}_e \, B_{ij}^{(e)} + \sum_{i=0}^{n_e} \sum_{j=0}^{n_e} U_i G_j 2\mathcal{A}_e \, H_{ij}^{(e)}. \end{aligned} \tag{2.85}$$

where,

$$\begin{aligned} I_{ijmn}^{(e)} &= \int_{\zeta_1=0}^{1} \int_{\zeta_2=0}^{1-\zeta_1} p_e \frac{\partial \alpha_i}{\partial \zeta_m} \frac{\partial \alpha_j}{\partial \zeta_n} \, d\zeta_1 \, d\zeta_2; \\ B_{ij}^{(e)} &= \int_{\zeta_1=0}^{1} \int_{\zeta_2=0}^{1-\zeta_1} (k_e^2 + D_e) \, \alpha_i \alpha_j \, d\zeta_1 \, d\zeta_2 \text{ and,} \\ H_{ij}^{(e)} &= \int_{\zeta_1=0}^{1} \int_{\zeta_2=0}^{1-\zeta_1} \alpha_i \alpha_j \, d\zeta_1 \, d\zeta_2. \end{aligned} \tag{2.86}$$

It should be noted, that p_e, k_e, and D_e represent the specific forms of p, k, and D, in Ω_e, respectively. Moreover, it is assumed that p_e, k_e, D_e, as well as the basis functions α_i, may all be expressed entirely in terms of the two simplex coordinates (ζ_1, ζ_2) by using the relationship (2.69). Although such an assumption implies that the third terms in the summations over m and n in (2.80), (2.81), and (2.85) need not be included, they are left intact since, in some instances, it may be more convenient to first express derivatives of the basis functions in terms of all three simplex coordinates.

The functional corresponding to a typical element, e, given in (2.85) may be written in matrix form as:

$$F^{(e)} = \frac{1}{2}\mathbf{u}^{(e)T}\mathbf{V}^{(e)}\mathbf{u}^{(e)} - \frac{1}{2}\mathbf{u}^{(e)T}(2\mathcal{A}_e\,\mathbf{B}^{(e)})\mathbf{u}^{(e)} + \mathbf{u}^{(e)T}(2\mathcal{A}_e\,\mathbf{H}^{(e)})\mathbf{g}^{(e)}, \tag{2.87}$$

where, $\mathbf{u}^{(e)}$ and $\mathbf{g}^{(e)}$ are the vectors of the field solution and source term parameters, respectively, associated with a specific element, e, of a two-dimensional discretization; and the entries of the matrix $\mathbf{V}^{(e)}$ are defined by:

$$V_{ij}^{(e)} = \frac{1}{2\mathcal{A}_e}\sum_{m=1}^{3}\sum_{n=1}^{3}(b_m b_n + c_m c_n)\, I_{ijmn}^{(e)}. \tag{2.88}$$

Thus, the functional corresponding to a discretization over the entire problem domain comprising N elements is given by:

$$F = \sum_{e=1}^{N} F^{(e)}. \tag{2.89}$$

The optimization equations for the field solution parameters, $\mathbf{u}^{(e)}$, associated with a typical element, e, may be derived in an analogous manner to that presented earlier for one-dimensional systems: namely, by considering the first variation equations:

$$\frac{\partial F^{(e)}}{\partial \mathbf{u}^{(e)}} = \mathbf{0}. \tag{2.90}$$

By applying the result (2.50), and from the symmetry of the matrices $\mathbf{V}^{(e)}$ and $\mathbf{B}^{(e)}$, it can be readily shown that that Eq. (2.90) yields:

$$\mathbf{V}^{(e)}\mathbf{u}^{(e)} - (2\mathcal{A}_e\,\mathbf{B}^{(e)})\mathbf{u}^{(e)} + (2\mathcal{A}_e\,\mathbf{H}^{(e)})\mathbf{g}^{(e)} = \mathbf{0}. \tag{2.91}$$

Thus, similar treatment of all the elements in a discretization results in the set of equations:

$$\mathbf{V}^{(e)}\mathbf{u}^{(e)} - (2\mathcal{A}_e\,\mathbf{B}^{(e)})\mathbf{u}^{(e)} = -(2\mathcal{A}_e\,\mathbf{H}^{(e)})\mathbf{g}^{(e)}, \quad (e = 1, 2, \ldots, N). \tag{2.92}$$

which may be solved for optimizing the values of the entire set of field solution parameters, $\mathbf{u}$, for a given problem, if the geometric discretization is held fixed. It may be noted that, any optimization equations corresponding to field solution unknowns which are common to more than one element, may be consolidated into a single optimization equation by, first, consolidating the common unknowns into a single unknown parameter.

The optimization equations for the geometric discretization parameters, i.e., the element vertex positions, associated with an element, say e, may be derived by considering the first variation equations defined by:

$$\frac{\partial F^{(e)}}{\partial x_l^{(e)}} = 0, \quad (l = 1, 2, 3), \tag{2.93}$$

and,

$$\frac{\partial F^{(e)}}{\partial y_l^{(e)}} = 0, \quad (l = 1, 2, 3), \tag{2.94}$$

where, $x_l^{(e)}$ and $y_l^{(e)}$ represent the x and y coordinate values of the position of vertex l ($l = 1, 2, 3$) for element e, respectively. In the 1-D formulation presented earlier, where the mesh topology was known *a priori*, it was possible to show that only that portion of the discretized functional for the entire problem corresponding to the two elements sharing a common vertex were functions of the position of their common vertex. This *a priori* knowledge allowed the first variation equations for the geometric discretization parameters to be derived in a global fashion over the entire problem discretization. However, in two-dimensional meshes composed of triangular elements, several elements may share a common vertex. In general, it is not possible to predetermine the topology of a 2-D mesh; therefore, it is necessary to derive the first variation equations for the 2-D geometric discretization parameters in a local manner,

i.e., element-wise, just as for the field solution parameters. It should be noted, that for a specific 2-D system, the first variation expressions corresponding to a discretization parameter common to more than a single element may also be consolidated into a single optimization equation.

More explicit forms of (2.93) and (2.94) may be derived as follows. First, consider:

$$\frac{\partial F^{(e)}}{\partial x_l^{(e)}} = \frac{\partial}{\partial x_l^{(e)}} \left[\frac{1}{2} \mathbf{u}^{(e)T} \mathbf{V}^{(e)} \mathbf{u}^{(e)} - \frac{1}{2} \mathbf{u}^{(e)T} (2\mathcal{A}_e \, \mathbf{B}^{(e)}) \mathbf{u}^{(e)} + \mathbf{u}^{(e)T} (2\mathcal{A}_e \, \mathbf{H}^{(e)}) \mathbf{g}^{(e)} \right]. \quad (2.95)$$

Since $\mathbf{u}^{(e)}$, $\mathbf{g}^{(e)}$, $\mathbf{B}^{(e)}$, and $\mathbf{H}^{(e)}$ are independent of the geometric discretization parameters, the above identity may be rewritten as:

$$\frac{\partial F^{(e)}}{\partial x_l^{(e)}} = \frac{1}{2} \mathbf{u}^{(e)T} \left(\frac{\partial}{\partial x_l^{(e)}} \mathbf{V}^{(e)} \right) \mathbf{u}^{(e)} - \frac{1}{2} \mathbf{u}^{(e)T} \frac{\partial (2\mathcal{A}_e)}{\partial x_l^{(e)}} \mathbf{B}^{(e)} \mathbf{u}^{(e)} + \mathbf{u}^{(e)T} \frac{\partial (2\mathcal{A}_e)}{\partial x_l^{(e)}} \mathbf{H}^{(e)} \mathbf{g}^{(e)}. \quad (2.96)$$

Furthermore, it follows from (2.88) that the component-wise partial derivatives of $\mathbf{V}^{(e)}$ with respect to $x_l^{(e)}$ are given by:

$$\frac{\partial V_{ij}^{(e)}}{\partial x_l^{(e)}} = \frac{1}{4\mathcal{A}_e^2} \sum_{m=1}^{3} \sum_{n=1}^{3} \left[2\mathcal{A}_e \left(\frac{\partial (b_m b_n)}{\partial x_l^{(e)}} + \frac{\partial (c_m c_n)}{\partial x_l^{(e)}} \right) - (b_m b_n + c_m c_n) \frac{\partial (2\mathcal{A}_e)}{\partial x_l^{(e)}} \right] I_{ijmn}^{(e)} \quad (2.97)$$

which may be simplified upon noting from (2.82) that:

$$\frac{\partial (b_m b_n)}{\partial x_l^{(e)}} = 0, \quad (m, n, l = 1, 2, 3). \quad (2.98)$$

In addition, it may be confirmed from (2.76) and (2.82) that:

$$\frac{\partial (2\mathcal{A}_e)}{\partial x_l^{(e)}} = b_l, \quad (l = 1, 2, 3). \quad (2.99)$$

Thus, applying the simplifications (2.98) and (2.99) to (2.97) yields:

$$\frac{\partial V_{ij}^{(e)}}{\partial x_l^{(e)}} = \frac{1}{4\mathcal{A}_e^2} \sum_{m=1}^{3} \sum_{n=1}^{3} \left[2\mathcal{A}_e \frac{\partial (c_m c_n)}{\partial x_l^{(e)}} - (b_m b_n + c_m c_n) \, b_l \right] I_{ijmn}^{(e)}. \quad (2.100)$$

Similarly, it can be readily shown that:

$$\frac{\partial V_{ij}^{(e)}}{\partial y_l^{(e)}} = \frac{1}{4\mathcal{A}_e^2} \sum_{m=1}^{3} \sum_{n=1}^{3} \left[2\mathcal{A}_e \frac{\partial (b_m b_n)}{\partial y_l^{(e)}} - (b_m b_n + c_m c_n) \, c_l \right] I_{ijmn}^{(e)} \quad (2.101)$$

after noting from (2.82) that:

$$\frac{\partial(c_m c_n)}{\partial y_l^{(e)}} = 0, \quad (m, n, l = 1, 2, 3), \tag{2.102}$$

and from (2.76) and (2.82) that:

$$\frac{\partial(2\mathcal{A}_e)}{\partial y_l^{(e)}} = c_l, \quad (l = 1, 2, 3). \tag{2.103}$$

Therefore, the set of optimization equations for the geometric discretization parameters associated with a given triangular element, e, in a two-dimensional finite element mesh is given by:

$$\frac{1}{2}\mathbf{u}^{(e)T}\mathbf{S}^{(e)}\mathbf{u}^{(e)} - \frac{b_l}{2}\mathbf{u}^{(e)T}\mathbf{B}^{(e)}\mathbf{u}^{(e)} + b_l\,\mathbf{u}^{(e)T}\mathbf{H}^{(e)}\mathbf{g}^{(e)} = 0, \quad (l = 1, 2, 3) \tag{2.104}$$

and,

$$\frac{1}{2}\mathbf{u}^{(e)T}\mathbf{T}^{(e)}\mathbf{u}^{(e)} - \frac{c_l}{2}\mathbf{u}^{(e)T}\mathbf{B}^{(e)}\mathbf{u}^{(e)} + c_l\,\mathbf{u}^{(e)T}\mathbf{H}^{(e)}\mathbf{g}^{(e)} = 0, \quad (l = 1, 2, 3), \tag{2.105}$$

where the entries of the matrices $\mathbf{S}^{(e)}$ and $\mathbf{T}^{(e)}$ are defined as follows:

$$S_{ij}^{(e)} = \frac{\partial V_{ij}^{(e)}}{\partial x_l^{(e)}}; \text{ and,}$$

$$T_{ij}^{(e)} = \frac{\partial V_{ij}^{(e)}}{\partial y_l^{(e)}}. \tag{2.106}$$

It may be noted that the partial derivatives of $(b_m b_n)$ and of $(c_m c_n)$ with respect to the element vertex positions, which appear in (2.100) and in (2.101), can be determined directly from (2.82) and are given in Table 2.1 and Table 2.2 for reference, where they are expressed in terms of b_i and c_i.

The combined set of equations (2.92), (2.104), and (2.105) may be solved simultaneously for the optimal values of all the unconstrained field solution and geometric discretization parameters in a given problem. Once again, it may be noted that the optimization equations for the geometric discretization parameters may not be solved independently of those for the field solution parameters, for the same reasons

as those given for the 1-D case. Furthermore, the formulation for two-dimensional systems presented above, has been developed independently of specific basis functions and, therefore, is valid for any choice of legitimate finite element basis functions.

Table 2.1: Explicit forms of $\partial(b_m b_n)/\partial y_l^{(e)}$ in terms of b_i for $m, n, l = 1, 2, 3$.

$(m,n)/l$	1	2	3
(1,1)	0	$2b_1$	$-2b_1$
(1,2), (2,1)	$-b_1$	b_2	$b_1 - b_2$
(2,2)	$-2b_2$	0	$2b_2$
(1,3), (3,1)	b_1	$b_3 - b_1$	$-b_3$
(2,3), (3,2)	$b_2 - b_3$	$-b_2$	b_3
(3,3)	$2b_3$	$-2b_3$	0

Table 2.2: Explicit forms of $\partial(c_m c_n)/\partial x_l^{(e)}$ in terms of c_i for $m, n, l = 1, 2, 3$.

$(m,n)/l$	1	2	3
(1,1)	0	$-2c_1$	$2c_1$
(1,2), (2,1)	c_1	$-c_2$	$c_2 - c_1$
(2,2)	$2c_2$	0	$-2c_2$
(1,3), (3,1)	$-c_1$	$c_1 - c_3$	c_3
(2,3), (3,2)	$c_3 - c_2$	c_2	$-c_3$
(3,3)	$-2c_3$	$2c_3$	0

2.4.3 Three-Dimensional Systems

Many practical electromagnetic systems do not possess the appropriate symmetry to allow for one- or two-dimensional treatments, and, therefore, must be analyzed using full three-dimensional (3-D) formulations. For example, in problems where the field solution variation is described in terms of the coordinate variables, x, y, and z, i.e., $u = u(x, y, z)$, the 3-D counterparts of the optimization equations given above for 2-D systems may be derived following an exactly analogous procedure in three dimensions. Consider the tetrahedral element with vertex positions (x_i, y_i, z_i), $i = 1, 2, 3, 4$, as shown in Fig. (2.4). The location of a point $P(x, y, z)$ within the element may be expressed in terms of the simplex coordinates ζ_1, ζ_2, ζ_3, and ζ_4, which are defined as follows:

$$\zeta_1 = \frac{\text{Volume}(P234)}{\text{Volume}(1234)}; \quad \zeta_2 = \frac{\text{Volume}(1P34)}{\text{Volume}(1234)};$$
$$\zeta_3 = \frac{\text{Volume}(12P4)}{\text{Volume}(1234)}; \quad \zeta_4 = \frac{\text{Volume}(123P)}{\text{Volume}(1234)}; \tag{2.107}$$

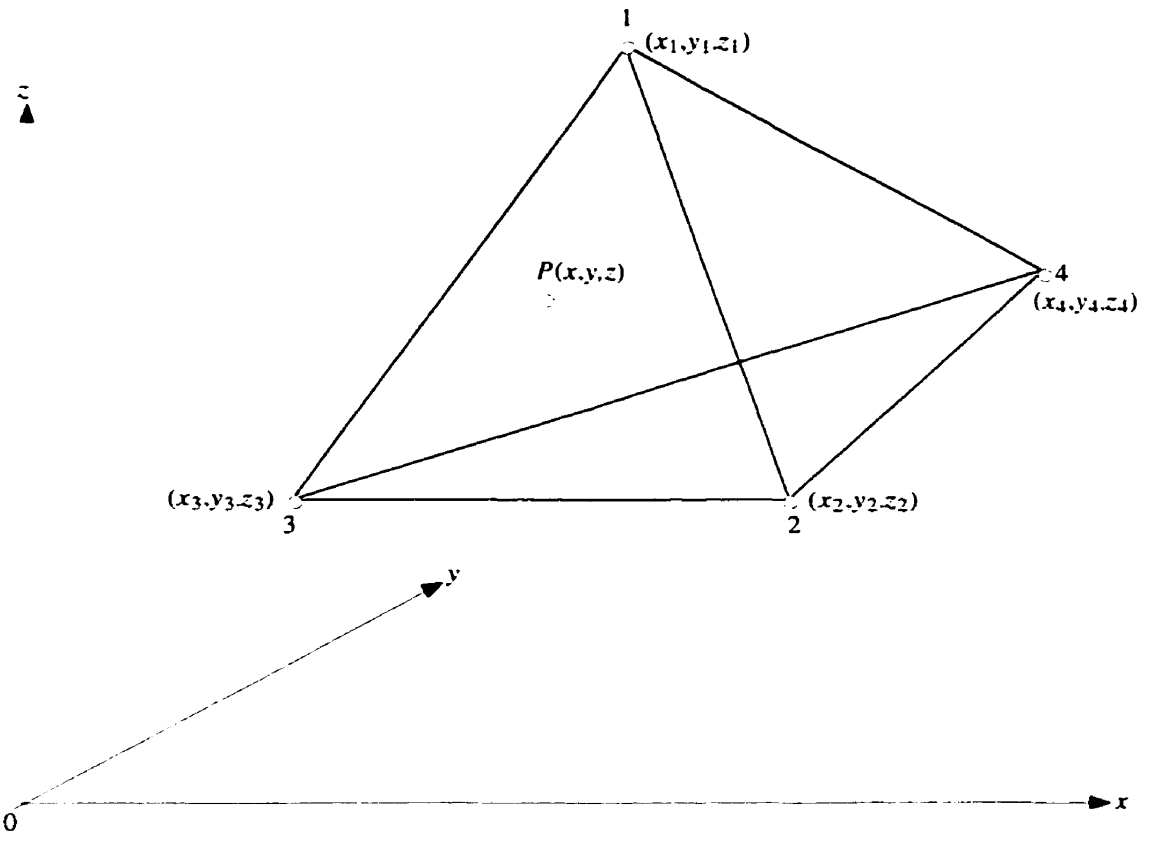

Figure 2.4: A tetrahedral element and the sub-simplex $P234$ used in the definition of ζ_1.

and satisfy the relationship:

$$\zeta_1 + \zeta_2 + \zeta_3 + \zeta_4 = 1. \tag{2.108}$$

Furthermore, the volume of a tetrahedron, for example, the 3-D element depicted in Fig. (2.4), may be expressed in determinant form as:

$$\mathcal{V} = \text{Volume}(1234) = \frac{1}{6}\begin{vmatrix} 1 & x_1 & y_1 & z_1 \\ 1 & x_2 & y_2 & z_2 \\ 1 & x_3 & y_3 & z_3 \\ 1 & x_4 & y_4 & z_4 \end{vmatrix}. \tag{2.109}$$

Similarly, the remaining sub-volumes in (2.107) which define the simplex coordinates

may be expressed as:

$$\text{Volume}(P234) = \frac{1}{6}\begin{vmatrix} 1 & x & y & z \\ 1 & x_2 & y_2 & z_2 \\ 1 & x_3 & y_3 & z_3 \\ 1 & x_4 & y_4 & z_4 \end{vmatrix};$$

$$\text{Volume}(1P34) = \frac{1}{6}\begin{vmatrix} 1 & x_1 & y_1 & z_1 \\ 1 & x & y & z \\ 1 & x_3 & y_3 & z_3 \\ 1 & x_4 & y_4 & z_4 \end{vmatrix};$$

$$\text{Volume}(12P4) = \frac{1}{6}\begin{vmatrix} 1 & x_1 & y_1 & z_1 \\ 1 & x_2 & y_2 & z_2 \\ 1 & x & y & z \\ 1 & x_4 & y_4 & z_4 \end{vmatrix}; \text{ and,}$$

$$\text{Volume}(123P) = \frac{1}{6}\begin{vmatrix} 1 & x_1 & y_1 & z_1 \\ 1 & x_2 & y_2 & z_2 \\ 1 & x_3 & y_3 & z_3 \\ 1 & x & y & z \end{vmatrix}. \tag{2.110}$$

Expanding the determinants in (2.109) and (2.110), and after some rearranging, it follows from (2.107) that:

$$6\mathcal{V} = \sum_{i=1}^{4} a_i, \tag{2.111}$$

and,

$$\zeta_i = [a_i + b_i x + c_i y + d_i z] / 6\mathcal{V}, \quad \text{for } i = 1, 2, 3, 4, \tag{2.112}$$

where, a_i, b_i, c_i, and d_i can be defined as follows with the subscripts progressing modulo 4:

$$a_i = (-1)^{i+1}\begin{vmatrix} x_{i+1} & y_{i+1} & z_{i+1} \\ x_{i+2} & y_{i+2} & z_{i+2} \\ x_{i-1} & y_{i-1} & z_{i-1} \end{vmatrix}, \tag{2.113}$$

$$b_i = (-1)^{i}\begin{vmatrix} 1 & y_{i+1} & z_{i+1} \\ 1 & y_{i+2} & z_{i+2} \\ 1 & y_{i-1} & z_{i-1} \end{vmatrix}, \tag{2.114}$$

$$c_i = (-1)^{i+1}\begin{vmatrix} 1 & x_{i+1} & z_{i+1} \\ 1 & x_{i+2} & z_{i+2} \\ 1 & x_{i-1} & z_{i-1} \end{vmatrix}, \text{ and,} \tag{2.115}$$

$$d_i = (-1)^i \begin{vmatrix} 1 & x_{i+1} & y_{i+1} \\ 1 & x_{i+2} & y_{i+2} \\ 1 & x_{i-1} & y_{i-1} \end{vmatrix}. \tag{2.116}$$

In addition, it may be shown that the coordinate transformation:

$$d\zeta_1\, d\zeta_2\, d\zeta_3 = \frac{\partial(\zeta_1, \zeta_2, \zeta_3)}{\partial(x, y, z)}\, dx\, dy\, dz, \tag{2.117}$$

yields the following differential element of volume, $d\Omega$, for integration in simplex coordinates over a tetrahedral element with volume $\mathcal{V}_e$:

$$d\Omega = 6\mathcal{V}_e\, d\zeta_1\, d\zeta_2\, d\zeta_3. \tag{2.118}$$

Subsequently, if the required field solution, u, to the differential equation (2.7) and the source function, g, therein, are approximated over each tetrahedral element analogously to the 2-D case, it may be shown that the general form of the discretized functional over a typical element, e, for which a stationary point is sought within the space of admissible approximation functions, may be written as:

$$\begin{aligned} F^{(e)} &= \frac{1}{2}\sum_{i=0}^{n_e}\sum_{j=0}^{n_e} U_i U_j \left[\frac{1}{6\mathcal{V}_e}\sum_{m=1}^{4}\sum_{n=1}^{4}(b_m b_n + c_m c_n + d_m d_n)\, I_{ijmn}^{(e)}\right] \\ &\quad - \frac{1}{2}\sum_{i=0}^{n_e}\sum_{j=0}^{n_e} U_i U_j 6\mathcal{V}_e\, B_{ij}^{(e)} + \sum_{i=0}^{n_e}\sum_{j=0}^{n_e} U_i G_j 6\mathcal{V}_e\, H_{ij}^{(e)}, \end{aligned} \tag{2.119}$$

where,

$$I_{ijmn}^{(e)} = \int_{\zeta_1=0}^{1}\int_{\zeta_2=0}^{1-\zeta_1}\int_{\zeta_3=0}^{1-\zeta_1-\zeta_2} p_e \frac{\partial\alpha_i}{\partial\zeta_m}\frac{\partial\alpha_j}{\partial\zeta_n}\, d\zeta_1\, d\zeta_2\, d\zeta_3;$$

$$B_{ij}^{(e)} = \int_{\zeta_1=0}^{1}\int_{\zeta_2=0}^{1-\zeta_1}\int_{\zeta_3=0}^{1-\zeta_1-\zeta_2} (k_e^2 + D_e)\,\alpha_i\alpha_j\, d\zeta_1\, d\zeta_2\, d\zeta_3; \text{ and,}$$

$$H_{ij}^{(e)} = \int_{\zeta_1=0}^{1}\int_{\zeta_2=0}^{1-\zeta_1}\int_{\zeta_3=0}^{1-\zeta_1-\zeta_2} \alpha_i\alpha_j\, d\zeta_1\, d\zeta_2\, d\zeta_3. \tag{2.120}$$

It should be noted that the integrands in (2.120) are assumed to be expressed purely in terms of the three simplex coordinates $(\zeta_1, \zeta_2, \zeta_3)$. Therefore, $I_{ijmn}^{(e)}$, $B_{ij}^{(e)}$, and $H_{ij}^{(e)}$

are all quantities that are independent of both the size and shape of a specific tetrahedral element, in that they do not involve the geometric discretization parameters associated with an element, i.e., the element vertex positions.

The functional corresponding to a typical element, e, given in (2.119) may be written in matrix form similar to that for the 2-D case, i.e.,

$$F^{(e)} = \frac{1}{2}\mathbf{u}^{(e)T}\mathbf{V}^{(e)}\mathbf{u}^{(e)} - \frac{1}{2}\mathbf{u}^{(e)T}(6\mathcal{V}_e\,\mathbf{B}^{(e)})\mathbf{u}^{(e)} + \mathbf{u}^{(e)T}(6\mathcal{V}_e\,\mathbf{H}^{(e)})\mathbf{g}^{(e)}. \tag{2.121}$$

where, $\mathbf{u}^{(e)}$ and $\mathbf{g}^{(e)}$ are the vectors of the field solution and source term parameters, respectively, associated with a specific element, e, of a three-dimensional discretization; and the entries of the matrix $\mathbf{V}^{(e)}$ are defined by:

$$V_{ij}^{(e)} = \frac{1}{6\mathcal{V}_e}\sum_{m=1}^{4}\sum_{n=1}^{4}(b_m b_n + c_m c_n + d_m d_n)\, I_{ijmn}^{(e)}. \tag{2.122}$$

As before, the functional corresponding to a discretization over the entire problem domain comprising N elements is given by:

$$F = \sum_{e=1}^{N} F^{(e)}. \tag{2.123}$$

The optimization equations for the field solution parameters, $\mathbf{u}^{(e)}$, associated with a typical element, e, may be derived by, once again, considering the first variation equations:

$$\frac{\partial F^{(e)}}{\partial \mathbf{u}^{(e)}} = \mathbf{0}. \tag{2.124}$$

Applying the result (2.50), and by the symmetry of the matrices $\mathbf{V}^{(e)}$ and $\mathbf{B}^{(e)}$, it is readily seen that Eq. (2.124) yields:

$$\mathbf{V}^{(e)}\mathbf{u}^{(e)} - (6\mathcal{V}_e\,\mathbf{B}^{(e)})\mathbf{u}^{(e)} + (6\mathcal{V}_e\,\mathbf{H}^{(e)})\mathbf{g}^{(e)} = \mathbf{0}. \tag{2.125}$$

Thus, similar treatment of all the elements in a discretization results in the set of equations:

$$\mathbf{V}^{(e)}\mathbf{u}^{(e)} - (6\mathcal{V}_e\,\mathbf{B}^{(e)})\mathbf{u}^{(e)} = -(6\mathcal{V}_e\,\mathbf{H}^{(e)})\mathbf{g}^{(e)}, \quad (e = 1, 2, \ldots, N), \tag{2.126}$$

which may be solved for optimizing the values of the entire set of field solution parameters, $\mathbf{u}$, for a given problem, if the geometric discretization is held fixed. Of course, any optimization equations corresponding to field solution unknowns which are common to more than one element, may be consolidated into a single optimization equation by, first, consolidating the common unknowns into a single unknown parameter.

The optimization equations for the geometric discretization parameters, i.e., the element vertex positions, associated with a tetrahedral element, e, may be derived by considering the first variation equations defined by:

$$\frac{\partial F^{(e)}}{\partial x_l^{(e)}} = 0, \quad (l = 1, 2, 3, 4), \tag{2.127}$$

$$\frac{\partial F^{(e)}}{\partial y_l^{(e)}} = 0, \quad (l = 1, 2, 3, 4), \tag{2.128}$$

and,

$$\frac{\partial F^{(e)}}{\partial z_l^{(e)}} = 0, \quad (l = 1, 2, 3, 4), \tag{2.129}$$

where, $x_l^{(e)}$, $y_l^{(e)}$, and $z_l^{(e)}$ represent the x, y, and z coordinate values of the position of vertex l ($l = 1, 2, 3, 4$) for element e, respectively. In three-dimensional meshes composed of tetrahedral elements, several elements may share a common vertex. In general, it is not possible to pre-determine the topology of a 3-D mesh: therefore, it is necessary to derive the first variation equations for the 3-D geometric discretization parameters in a local manner, i.e., element-wise, just as for the field solution parameters. It should be noted, that for a specific 3-D system, the first variation expressions corresponding to a discretization parameter common to more than a single element may be consolidated into a single optimization equation.

To derive more explicit forms of (2.127), (2.128), and (2.129), first consider:

$$\frac{\partial F^{(e)}}{\partial x_l^{(e)}} = \frac{\partial}{\partial x_l^{(e)}} \left[\frac{1}{2} \mathbf{u}^{(e)T} \mathbf{V}^{(e)} \mathbf{u}^{(e)} - \frac{1}{2} \mathbf{u}^{(e)T} (6\mathcal{V}_e \mathbf{B}^{(e)}) \mathbf{u}^{(e)} + \mathbf{u}^{(e)T} (6\mathcal{V}_e \mathbf{H}^{(e)}) \mathbf{g}^{(e)} \right]. \tag{2.130}$$

Since $\mathbf{u}^{(e)}$, $\mathbf{g}^{(e)}$, $\mathbf{B}^{(e)}$, and $\mathbf{H}^{(e)}$ are independent of the geometric discretization parameters, the above identity may be rewritten as:

$$\frac{\partial F^{(e)}}{\partial x_l^{(e)}} = \frac{1}{2}\mathbf{u}^{(e)T}\left(\frac{\partial}{\partial x_l^{(e)}}\mathbf{V}^{(e)}\right)\mathbf{u}^{(e)} - \frac{1}{2}\mathbf{u}^{(e)T}\frac{\partial(6\mathcal{V}_e)}{\partial x_l^{(e)}}\mathbf{B}^{(e)}\mathbf{u}^{(e)} + \mathbf{u}^{(e)T}\frac{\partial(6\mathcal{V}_e)}{\partial x_l^{(e)}}\mathbf{H}^{(e)}\mathbf{g}^{(e)}. \tag{2.131}$$

Moreover, it may be seen from (2.122) that the component-wise partial derivatives of $\mathbf{V}^{(e)}$ with respect to $x_l^{(e)}$ are given by:

$$\frac{\partial V_{ij}^{(e)}}{\partial x_l^{(e)}} = \frac{1}{36\mathcal{V}_e^2}\sum_{m=1}^{4}\sum_{n=1}^{4}\left[6\mathcal{V}_e\left(\frac{\partial(b_m b_n)}{\partial x_l^{(e)}} + \frac{\partial(c_m c_n)}{\partial x_l^{(e)}} + \frac{\partial(d_m d_n)}{\partial x_l^{(e)}}\right)\right.$$

$$\left. -(b_m b_n + c_m c_n + d_m d_n)\frac{\partial(6\mathcal{V}_e)}{\partial x_l^{(e)}}\right] I_{ijmn}^{(e)} \tag{2.132}$$

which may be simplified upon noting from (2.114) that:

$$\frac{\partial(b_m b_n)}{\partial x_l^{(e)}} = 0, \quad (m, n, l = 1, 2, 3, 4). \tag{2.133}$$

In addition, it may be confirmed from (2.109) and (2.114) that:

$$\frac{\partial(6\mathcal{V}_e)}{\partial x_l^{(e)}} = b_l, \quad (l = 1, 2, 3, 4). \tag{2.134}$$

Thus, applying the simplifications (2.133) and (2.134) to (2.132) yields:

$$\frac{\partial V_{ij}^{(e)}}{\partial x_l^{(e)}} = \frac{1}{36\mathcal{V}_e^2}\sum_{m=1}^{4}\sum_{n=1}^{4}\left[6\mathcal{V}_e\left(\frac{\partial(c_m c_n)}{\partial x_l^{(e)}} + \frac{\partial(d_m d_n)}{\partial x_l^{(e)}}\right) - (b_m b_n + c_m c_n + d_m d_n)b_l\right] I_{ijmn}^{(e)}. \tag{2.135}$$

Similarly, it can be readily shown that:

$$\frac{\partial V_{ij}^{(e)}}{\partial y_l^{(e)}} = \frac{1}{36\mathcal{V}_e^2}\sum_{m=1}^{4}\sum_{n=1}^{4}\left[6\mathcal{V}_e\left(\frac{\partial(b_m b_n)}{\partial y_l^{(e)}} + \frac{\partial(d_m d_n)}{\partial y_l^{(e)}}\right) - (b_m b_n + c_m c_n + d_m d_n)c_l\right] I_{ijmn}^{(e)} \tag{2.136}$$

after noting from (2.115) that:

$$\frac{\partial(c_m c_n)}{\partial y_l^{(e)}} = 0, \quad (m, n, l = 1, 2, 3, 4), \tag{2.137}$$

and from (2.109) and (2.115) that:

$$\frac{\partial(6\mathcal{V}_e)}{\partial y_l^{(e)}} = c_l, \quad (l = 1, 2, 3, 4). \tag{2.138}$$

Also, it may be confirmed that:

$$\frac{\partial V_{ij}^{(e)}}{\partial z_l^{(e)}} = \frac{1}{36\mathcal{V}_e^2} \sum_{m=1}^{4} \sum_{n=1}^{4} \left[6\mathcal{V}_e \left(\frac{\partial (b_m b_n)}{\partial z_l^{(e)}} + \frac{\partial (c_m c_n)}{\partial z_l^{(e)}} \right) - (b_m b_n + c_m c_n + d_m d_n) d_l \right] I_{ijmn}^{(e)} \tag{2.139}$$

since, from (2.116), it may be noted that:

$$\frac{\partial (d_m d_n)}{\partial z_l^{(e)}} = 0, \quad (m, n, l = 1, 2, 3, 4). \tag{2.140}$$

and from (2.109) and (2.116), it may be shown that:

$$\frac{\partial (6\mathcal{V}_e)}{\partial z_l^{(e)}} = d_l, \quad (l = 1, 2, 3, 4). \tag{2.141}$$

Therefore, the set of optimization equations for the geometric discretization parameters associated with a given tetrahedral element, e, in a three-dimensional finite element mesh is given by the following three equations:

$$\frac{1}{2} \mathbf{u}^{(e)T} \mathbf{S}^{(e)} \mathbf{u}^{(e)} - \frac{b_l}{2} \mathbf{u}^{(e)T} \mathbf{B}^{(e)} \mathbf{u}^{(e)} + b_l \, \mathbf{u}^{(e)T} \mathbf{H}^{(e)} \mathbf{g}^{(e)} = 0, \quad (l = 1, 2, 3, 4). \tag{2.142}$$

$$\frac{1}{2} \mathbf{u}^{(e)T} \mathbf{T}^{(e)} \mathbf{u}^{(e)} - \frac{c_l}{2} \mathbf{u}^{(e)T} \mathbf{B}^{(e)} \mathbf{u}^{(e)} + c_l \, \mathbf{u}^{(e)T} \mathbf{H}^{(e)} \mathbf{g}^{(e)} = 0, \quad (l = 1, 2, 3, 4), \tag{2.143}$$

and,

$$\frac{1}{2} \mathbf{u}^{(e)T} \mathbf{W}^{(e)} \mathbf{u}^{(e)} - \frac{d_l}{2} \mathbf{u}^{(e)T} \mathbf{B}^{(e)} \mathbf{u}^{(e)} + d_l \, \mathbf{u}^{(e)T} \mathbf{H}^{(e)} \mathbf{g}^{(e)} = 0, \quad (l = 1, 2, 3, 4). \tag{2.144}$$

where the entries of the matrices $\mathbf{S}^{(e)}$, $\mathbf{T}^{(e)}$, and $\mathbf{W}^{(e)}$ are defined as follows:

$$S_{ij}^{(e)} = \frac{\partial V_{ij}^{(e)}}{\partial x_l^{(e)}};$$

$$T_{ij}^{(e)} = \frac{\partial V_{ij}^{(e)}}{\partial y_l^{(e)}}; \text{ and,}$$

$$W_{ij}^{(e)} = \frac{\partial V_{ij}^{(e)}}{\partial z_l^{(e)}}. \tag{2.145}$$

It may be noted that the partial derivatives of $(b_m b_n)$, $(c_m c_n)$, and $(d_m d_n)$ with respect to the element vertex positions, which appear in (2.135), (2.136), and (2.139), can be determined directly from (2.114) through (2.116), and are given for reference in Table 2.3 through Table 2.8, where the quantities $\mathcal{X}_{ij}$, $\mathcal{Y}_{ij}$, and $\mathcal{Z}_{ij}$ are defined as follows:

$$\mathcal{X}_{ij} = x_i - x_j \tag{2.146}$$

$$\mathcal{Y}_{ij} = y_i - y_j \tag{2.147}$$

$$\mathcal{Z}_{ij} = z_i - z_j \tag{2.148}$$

Finally, the combined set of optimization equations (2.126), and (2.142) through (2.144), for all ϵ, may be solved simultaneously for the optimal values of the field solution and geometric discretization parameters that are not constrained for a given problem. As in the 1-D, and 2-D cases, the formulation presented above is valid for any choice of legitimate finite element basis functions.

Table 2.3: Explicit forms of $\partial(b_m b_n)/\partial y_l^{(c)}$ in terms of b_i and $\mathcal{Z}_{ij}$ for $m, n, l = 1, 2, 3, 4$.

$(m,n)/l$	1	2	3	4
(1,1)	0	$2b_1\mathcal{Z}_{43}$	$2b_1\mathcal{Z}_{24}$	$2b_1\mathcal{Z}_{32}$
(1,2), (2,1)	$b_1\mathcal{Z}_{34}$	$b_2\mathcal{Z}_{43}$	$b_2\mathcal{Z}_{24} + b_1\mathcal{Z}_{41}$	$b_2\mathcal{Z}_{32} + b_1\mathcal{Z}_{13}$
(1,3), (3,1)	$b_1\mathcal{Z}_{42}$	$b_3\mathcal{Z}_{43} + b_1\mathcal{Z}_{14}$	$b_3\mathcal{Z}_{24}$	$b_3\mathcal{Z}_{32} + b_1\mathcal{Z}_{21}$
(1,4), (4,1)	$b_1\mathcal{Z}_{23}$	$b_4\mathcal{Z}_{43} + b_1\mathcal{Z}_{31}$	$b_4\mathcal{Z}_{24} + b_1\mathcal{Z}_{12}$	$b_4\mathcal{Z}_{32}$
(2,2)	$2b_2\mathcal{Z}_{34}$	0	$2b_2\mathcal{Z}_{41}$	$2b_2\mathcal{Z}_{13}$
(2,3), (3,2)	$b_3\mathcal{Z}_{34} + b_2\mathcal{Z}_{42}$	$b_2\mathcal{Z}_{14}$	$b_3\mathcal{Z}_{41}$	$b_3\mathcal{Z}_{13} + b_2\mathcal{Z}_{21}$
(2,4), (4,2)	$b_4\mathcal{Z}_{34} + b_2\mathcal{Z}_{23}$	$b_2\mathcal{Z}_{31}$	$b_4\mathcal{Z}_{41} + b_2\mathcal{Z}_{12}$	$b_4\mathcal{Z}_{13}$
(3,3)	$2b_3\mathcal{Z}_{42}$	$2b_3\mathcal{Z}_{14}$	0	$2b_3\mathcal{Z}_{21}$
(3,4), (4,3)	$b_4\mathcal{Z}_{42} + b_3\mathcal{Z}_{23}$	$b_4\mathcal{Z}_{14} + b_3\mathcal{Z}_{31}$	$b_3\mathcal{Z}_{12}$	$b_4\mathcal{Z}_{21}$
(4,4)	$2b_4\mathcal{Z}_{23}$	$2b_4\mathcal{Z}_{31}$	$2b_4\mathcal{Z}_{12}$	0

Table 2.4: Explicit forms of $\partial(b_m b_n)/\partial z_l^{(e)}$ in terms of b_i and $\mathcal{Y}_{ij}$ for $m, n, l = 1, 2, 3, 4$.

$(m,n)/l$	1	2	3	4
(1,1)	0	$2b_1\mathcal{Y}_{34}$	$2b_1\mathcal{Y}_{42}$	$2b_1\mathcal{Y}_{23}$
(1,2), (2,1)	$b_1\mathcal{Y}_{43}$	$b_2\mathcal{Y}_{34}$	$b_2\mathcal{Y}_{42} + b_1\mathcal{Y}_{14}$	$b_2\mathcal{Y}_{23} + b_1\mathcal{Y}_{31}$
(1,3), (3,1)	$b_1\mathcal{Y}_{24}$	$b_3\mathcal{Y}_{34} + b_1\mathcal{Y}_{41}$	$b_3\mathcal{Y}_{42}$	$b_3\mathcal{Y}_{23} + b_1\mathcal{Y}_{12}$
(1,4), (4,1)	$b_1\mathcal{Y}_{32}$	$b_4\mathcal{Y}_{34} + b_1\mathcal{Y}_{13}$	$b_4\mathcal{Y}_{42} + b_1\mathcal{Y}_{21}$	$b_4\mathcal{Y}_{23}$
(2,2)	$2b_2\mathcal{Y}_{43}$	0	$2b_2\mathcal{Y}_{14}$	$2b_2\mathcal{Y}_{31}$
(2,3), (3,2)	$b_3\mathcal{Y}_{43} + b_2\mathcal{Y}_{24}$	$b_2\mathcal{Y}_{41}$	$b_3\mathcal{Y}_{14}$	$b_3\mathcal{Y}_{31} + b_2\mathcal{Y}_{12}$
(2,4), (4,2)	$b_4\mathcal{Y}_{43} + b_2\mathcal{Y}_{32}$	$b_2\mathcal{Y}_{13}$	$b_4\mathcal{Y}_{14} + b_2\mathcal{Y}_{21}$	$b_4\mathcal{Y}_{31}$
(3,3)	$2b_3\mathcal{Y}_{24}$	$2b_3\mathcal{Y}_{41}$	0	$2b_3\mathcal{Y}_{12}$
(3,4), (4,3)	$b_4\mathcal{Y}_{24} + b_3\mathcal{Y}_{32}$	$b_4\mathcal{Y}_{41} + b_3\mathcal{Y}_{13}$	$b_3\mathcal{Y}_{21}$	$b_4\mathcal{Y}_{12}$
(4,4)	$2b_4\mathcal{Y}_{32}$	$2b_4\mathcal{Y}_{13}$	$2b_4\mathcal{Y}_{21}$	0

Table 2.5: Explicit forms of $\partial(c_m c_n)/\partial x_l^{(e)}$ in terms of c_i and $\mathcal{Z}_{ij}$ for $m, n, l = 1, 2, 3, 4$.

$(m,n)/l$	1	2	3	4
(1,1)	0	$2c_1\mathcal{Z}_{34}$	$2c_1\mathcal{Z}_{42}$	$2c_1\mathcal{Z}_{23}$
(1,2), (2,1)	$c_1\mathcal{Z}_{43}$	$c_2\mathcal{Z}_{34}$	$c_2\mathcal{Z}_{42}+c_1\mathcal{Z}_{14}$	$c_2\mathcal{Z}_{23}+c_1\mathcal{Z}_{31}$
(1,3), (3,1)	$c_1\mathcal{Z}_{24}$	$c_3\mathcal{Z}_{34}+c_1\mathcal{Z}_{41}$	$c_3\mathcal{Z}_{42}$	$c_3\mathcal{Z}_{23}+c_1\mathcal{Z}_{12}$
(1,4), (4,1)	$c_1\mathcal{Z}_{32}$	$c_4\mathcal{Z}_{34}+c_1\mathcal{Z}_{13}$	$c_4\mathcal{Z}_{42}+c_1\mathcal{Z}_{21}$	$c_4\mathcal{Z}_{23}$
(2,2)	$2c_2\mathcal{Z}_{43}$	0	$2c_2\mathcal{Z}_{14}$	$2c_2\mathcal{Z}_{31}$
(2,3), (3,2)	$c_3\mathcal{Z}_{43}+c_2\mathcal{Z}_{24}$	$c_2\mathcal{Z}_{41}$	$c_3\mathcal{Z}_{14}$	$c_3\mathcal{Z}_{31}+c_2\mathcal{Z}_{12}$
(2,4), (4,2)	$c_4\mathcal{Z}_{43}+c_2\mathcal{Z}_{32}$	$c_2\mathcal{Z}_{13}$	$c_4\mathcal{Z}_{14}+c_2\mathcal{Z}_{21}$	$c_4\mathcal{Z}_{31}$
(3,3)	$2c_3\mathcal{Z}_{24}$	$2c_3\mathcal{Z}_{41}$	0	$2c_3\mathcal{Z}_{12}$
(3,4), (4,3)	$c_4\mathcal{Z}_{24}+c_3\mathcal{Z}_{32}$	$c_4\mathcal{Z}_{41}+c_3\mathcal{Z}_{13}$	$c_3\mathcal{Z}_{21}$	$c_4\mathcal{Z}_{12}$
(4,4)	$2c_4\mathcal{Z}_{32}$	$2c_4\mathcal{Z}_{13}$	$2c_4\mathcal{Z}_{21}$	0

Table 2.6: Explicit forms of $\partial(c_m c_n)/\partial z_l^{(e)}$ in terms of c_i and $\mathcal{X}_{ij}$ for $m, n, l = 1, 2, 3, 4$.

$(m.n)/l$	1	2	3	4
(1.1)	0	$2c_1\mathcal{X}_{43}$	$2c_1\mathcal{X}_{24}$	$2c_1\mathcal{X}_{32}$
(1.2), (2.1)	$c_1\mathcal{X}_{34}$	$c_2\mathcal{X}_{43}$	$c_2\mathcal{X}_{24} + c_1\mathcal{X}_{41}$	$c_2\mathcal{X}_{32} + c_1\mathcal{X}_{13}$
(1.3), (3.1)	$c_1\mathcal{X}_{42}$	$c_3\mathcal{X}_{43} + c_1\mathcal{X}_{14}$	$c_3\mathcal{X}_{24}$	$c_3\mathcal{X}_{32} + c_1\mathcal{X}_{21}$
(1.4), (4.1)	$c_1\mathcal{X}_{23}$	$c_4\mathcal{X}_{43} + c_1\mathcal{X}_{31}$	$c_4\mathcal{X}_{24} + c_1\mathcal{X}_{12}$	$c_4\mathcal{X}_{32}$
(2.2)	$2c_2\mathcal{X}_{34}$	0	$2c_2\mathcal{X}_{41}$	$2c_2\mathcal{X}_{13}$
(2.3), (3.2)	$c_3\mathcal{X}_{34} + c_2\mathcal{X}_{42}$	$c_2\mathcal{X}_{14}$	$c_3\mathcal{X}_{41}$	$c_3\mathcal{X}_{13} + c_2\mathcal{X}_{21}$
(2.4), (4.2)	$c_4\mathcal{X}_{34} + c_2\mathcal{X}_{23}$	$c_2\mathcal{X}_{31}$	$c_4\mathcal{X}_{41} + c_2\mathcal{X}_{12}$	$c_4\mathcal{X}_{13}$
(3.3)	$2c_3\mathcal{X}_{42}$	$2c_3\mathcal{X}_{14}$	0	$2c_3\mathcal{X}_{21}$
(3.4), (4.3)	$c_4\mathcal{X}_{42} + c_3\mathcal{X}_{23}$	$c_4\mathcal{X}_{14} + c_3\mathcal{X}_{31}$	$c_3\mathcal{X}_{12}$	$c_4\mathcal{X}_{21}$
(4.4)	$2c_4\mathcal{X}_{23}$	$2c_4\mathcal{X}_{31}$	$2c_4\mathcal{X}_{12}$	0

Table 2.7: Explicit forms of $\partial(d_m d_n)/\partial x_l^{(e)}$ in terms of d_i and $\mathcal{Y}_{ij}$ for $m,\ n,\ l = 1, 2, 3, 4$.

$(m,n)/l$	1	2	3	4
(1,1)	0	$2d_1\mathcal{Y}_{43}$	$2d_1\mathcal{Y}_{24}$	$2d_1\mathcal{Y}_{32}$
(1,2), (2,1)	$d_1\mathcal{Y}_{34}$	$d_2\mathcal{Y}_{43}$	$d_2\mathcal{Y}_{24} + d_1\mathcal{Y}_{41}$	$d_2\mathcal{Y}_{32} + d_1\mathcal{Y}_{13}$
(1,3), (3,1)	$d_1\mathcal{Y}_{42}$	$d_3\mathcal{Y}_{43} + d_1\mathcal{Y}_{14}$	$d_3\mathcal{Y}_{24}$	$d_3\mathcal{Y}_{32} + d_1\mathcal{Y}_{21}$
(1,4), (4,1)	$d_1\mathcal{Y}_{23}$	$d_4\mathcal{Y}_{43} + d_1\mathcal{Y}_{31}$	$d_4\mathcal{Y}_{24} + d_1\mathcal{Y}_{12}$	$d_4\mathcal{Y}_{32}$
(2,2)	$2d_2\mathcal{Y}_{34}$	0	$2d_2\mathcal{Y}_{41}$	$2d_2\mathcal{Y}_{13}$
(2,3), (3,2)	$d_3\mathcal{Y}_{34} + d_2\mathcal{Y}_{42}$	$d_2\mathcal{Y}_{14}$	$d_3\mathcal{Y}_{41}$	$d_3\mathcal{Y}_{13} + d_2\mathcal{Y}_{21}$
(2,4), (4,2)	$d_4\mathcal{Y}_{34} + d_2\mathcal{Y}_{23}$	$d_2\mathcal{Y}_{31}$	$d_4\mathcal{Y}_{41} + d_2\mathcal{Y}_{12}$	$d_4\mathcal{Y}_{13}$
(3,3)	$2d_3\mathcal{Y}_{42}$	$2d_3\mathcal{Y}_{14}$	0	$2d_3\mathcal{Y}_{21}$
(3,4), (4,3)	$d_4\mathcal{Y}_{42} + d_3\mathcal{Y}_{23}$	$d_4\mathcal{Y}_{14} + d_3\mathcal{Y}_{31}$	$d_3\mathcal{Y}_{12}$	$d_4\mathcal{Y}_{21}$
(4,4)	$2d_4\mathcal{Y}_{23}$	$2d_4\mathcal{Y}_{31}$	$2d_4\mathcal{Y}_{12}$	0

Table 2.8: Explicit forms of $\partial(d_m d_n)/\partial y_l^{(c)}$ in terms of d_i and $\mathcal{X}_{ij}$ for $m, n, l = 1, 2, 3, 4$.

$(m,n)/l$	1	2	3	4
(1,1)	0	$2d_1\mathcal{X}_{34}$	$2d_1\mathcal{X}_{42}$	$2d_1\mathcal{X}_{23}$
(1,2), (2,1)	$d_1\mathcal{X}_{43}$	$d_2\mathcal{X}_{34}$	$d_2\mathcal{X}_{42} + d_1\mathcal{X}_{14}$	$d_2\mathcal{X}_{23} + d_1\mathcal{X}_{31}$
(1,3), (3,1)	$d_1\mathcal{X}_{24}$	$d_3\mathcal{X}_{34} + d_1\mathcal{X}_{41}$	$d_3\mathcal{X}_{42}$	$d_3\mathcal{X}_{23} + d_1\mathcal{X}_{12}$
(1,4), (4,1)	$d_1\mathcal{X}_{32}$	$d_4\mathcal{X}_{34} + d_1\mathcal{X}_{13}$	$d_4\mathcal{X}_{42} + d_1\mathcal{X}_{21}$	$d_4\mathcal{X}_{23}$
(2,2)	$2d_2\mathcal{X}_{43}$	0	$2d_2\mathcal{X}_{14}$	$2d_2\mathcal{X}_{31}$
(2,3), (3,2)	$d_3\mathcal{X}_{43} + d_2\mathcal{X}_{24}$	$d_2\mathcal{X}_{41}$	$d_3\mathcal{X}_{14}$	$d_3\mathcal{X}_{31} + d_2\mathcal{X}_{12}$
(2,4), (4,2)	$d_4\mathcal{X}_{43} + d_2\mathcal{X}_{32}$	$d_2\mathcal{X}_{13}$	$d_4\mathcal{X}_{14} + d_2\mathcal{X}_{21}$	$d_4\mathcal{X}_{31}$
(3,3)	$2d_3\mathcal{X}_{24}$	$2d_3\mathcal{X}_{41}$	0	$2d_3\mathcal{X}_{12}$
(3,4), (4,3)	$d_4\mathcal{X}_{24} + d_3\mathcal{X}_{32}$	$d_4\mathcal{X}_{41} + d_3\mathcal{X}_{13}$	$d_3\mathcal{X}_{21}$	$d_4\mathcal{X}_{12}$
(4,4)	$2d_4\mathcal{X}_{32}$	$2d_4\mathcal{X}_{13}$	$2d_4\mathcal{X}_{21}$	0

Chapter 3

Numerical Evaluation of the One-Dimensional Finite Element Optimization Equations

As previously noted, there exists substantial evidence suggesting that the optimality of a finite element discretization plays a significant role in the accuracy of computed solutions at given levels of problem refinement. Furthermore, it is believed that characterizations of optimal finite element solutions which are known *a priori*, can be used in adaptive finite element methods to compute solutions with similar optimal properties in a cost-efficient and reliable manner. The major goal of the thesis is to develop effective optimal discretization-based refinement criteria for efficiently and reliably guiding practical adaptive finite element solvers towards accurate solutions. Unfortunately, very little research on the optimality of finite element discretizations for electromagnetic systems is available, and, therefore, a very limited amount of insight on how to achieve the main thesis goal is available. Moreover, the review of currently available characterizations of optimal finite element discretizations presented in section 1.4 has revealed that there are serious shortcomings with these characterizations. It was concluded that some of the most commonly used approaches are derived based on principles and using assumptions which are not completely theoretically justified. In addition, while some of the other optimality criteria reported in the literature appear to work well for very specific types of problems, they have not been found to be appropriate for characterizing optimal finite element discretizations for a sufficiently wide range of problem applications to be of practical value. Furthermore, many of the investigations in this area which report theoretical characterizations of optimal finite element discretizations with confidence, fail to support their claims with sufficiently conclusive numerical results.

In this chapter, important benchmark electromagnetic problems are introduced in order to achieve a threefold objective. First, the validity and the fundamental value of the nonlinear system of one-dimensional finite element optimization equations, derived in the previous chapter, are confirmed numerically. In order to achieve this objective, the equations are used to compute a series of optimal finite element solutions, that is, solutions with both optimal field solution values and optimal geometric discretization parameters, for the benchmark problems considered. The results are confirmed using techniques which are described in subsequent sections of this chapter. The second objective of this chapter is to use the computed optimal discretization benchmarks to investigate the validity of the reported difficulties with the currently available characterizations of optimal finite element discretizations, to determine to what extent these problems are present in electromagnetic applications, and to decide the usefulness of the existing optimality criteria for electromagnetic systems. The final objective of this chapter is to provide practical support for the hypothesis that the optimality of a discretization is strongly related to the solution accuracy that can be achieved for a fixed number of free modeling parameters used at a given iteration within an adaptive finite element solution process. This last objective is directly related to the main goal of the thesis, and is achieved by using the finite element optimization equations and the analysis of the benchmark results computed to develop a theoretically justified, efficient, reliable and practical optimal discretization-based refinement criterion for one-dimensional AFEA. Finally, the performance of the new refinement criterion is evaluated with a series of studies involving the primary adaption models in order to investigate the potential benefits of using the finite element optimization equations, derived in section 2.4, for practical electromagnetic AFEA.

The primary motivation for this chapter is that the optimization equations for one-dimensional electromagnetic systems can be directly solved more readily, and with fewer obstacles, than the corresponding two- and three-dimensional equations. Consequently, the more comprehensive investigations of one-dimensional systems that

are possible may, potentially, provide more useful insight into the practical value of optimal discretization-based AFEA for electromagnetics than may be gleaned from the necessarily less exhaustive analyses of two- and three-dimensional systems that are possible.

3.1 Optimal Discretization Benchmark Systems

In order to confirm the validity of reported problems with existing optimality criteria, to examine the basic value optimal finite element discretizations for electromagnetic analysis, and to evaluate the potential value of developing practical optimal discretization based refinement criteria for AFEMs, two informative numerical benchmark systems are examined comprehensively. Specifically, the fundamental electromagnetic point and line singularity models are used to compute a series of finite element solutions with both optimal field solution and optimal geometric discretization parameter values. Subsequently, these optimal benchmark solutions are used in section 3.2 to examine the optimality criteria reported in the literature and discussed earlier in this work. As stated in Chapter 2, it is generally accepted that the most reliable approaches for evaluating the usefulness of optimality criteria are those based on the principle of, first, computing optimal solutions and, subsequently, analyzing the characteristics of such solutions. Accordingly, the approach used in this work to conduct these types of investigations is based on this principle.

Although there are several possible choices for one-dimensional benchmark systems which can be used in the principal investigations of this chapter, the point and line singularity models where chosen for the following important reasons. First, these two fundamental electromagnetic systems are sufficiently simple to be amenable to solution by the optimization techniques appropriate for solving the corresponding nonlinear systems of finite element optimization equations derived in section 2.4.1. Second, as with many one-dimensional electromagnetic systems, analytical expressions for the field solutions and other relevant quantities associated with the point

and line singularity models can be used to assess the accuracy, efficiency, validity, or reliability of the key optimality criteria or related procedures considered in this work. Third, the field solutions associated with the point and line singularity models contain singularities characteristic of those associated with the sharp material edges and corners which are present in many practical systems [64, 138]. Typically, the presence of sharp material edges and corners can drastically decrease the convergence rate of the finite element method if appropriate measures are not taken [55, 138]; therefore, the accurate and efficient resolution of the singularities associated with sharp material edges and corners is an important challenge for all types of finite element analyses and has been addressed by various researchers. One approach has been to develop specialized finite element approximating functions which incorporate appropriate singular basis functions [146–148]. This type of approach has been shown to work well for certain test problems, but can also suffer from some disadvantages related to its use as described in [138]. The reduced convergence rate of the finite element method when field singularities are present may also be improved by using discretizations which have strongly focussed distributions of DOF close to the singularities. This second approach can be achieved by AFEMs which can recognize and refine the regions of rapid solution variation near singularities [57, 59]. However, before AFEA can be developed and applied effectively and reliably to practical problems in which singular field behavior is a significant factor, it is important to first study the characteristics of optimal finite element discretizations of electromagnetic systems where this type of behavior is prevalent and its effects on the convergence of the finite element method can be isolated from other possible contributing factors. To this end, the point and line singularity models are ideal choices for computing the one-dimensional benchmark results described and discussed in the following two sections.

3.1.1 Benchmark System 1

The first benchmark system is based on the classical free-space point charge model. The objective for this benchmark system is to compute the functional value based on the resolution of a radial neighborhood close to the point charge and spanning a 100-fold decay in electric scalar potential: the point charge, of magnitude $10^{-9}/9$ (C), is located at the origin, and the two boundaries of the problem domain are set at radial distances of 0.1 (m) and 10 (m) away from the charge. The primary feature of this system is the rapid field solution variation close to the singularity. This feature is common to many practical devices that contain sharp material corners, and has been shown to drastically reduce the convergence rate of the finite element method.

The electrostatic system used to establish the optimal discretization benchmark results of this section was analyzed for electric scalar potential using the one-dimensional finite element formulation and the corresponding finite element optimization equations derived in section 2.4.1. Standard Lagrangian basis functions were employed to approximate the unknown field solution over the elements [23]. Specifically, first-, second-, fourth- and eighth-order finite element approximations were considered. The optimal values of the field solution parameters and geometric discretization parameters were computed by solving the nonlinear system of optimization equations with a Gauss-Newton method [149] using double-precision arithmetic. The solutions were computed using termination criteria of 10^{-10} for both the unknown equation variables and the residuals of the nonlinear equations. Finally, the functional values were calculated from the computed scalar potentials using exact differentiation and integration.

The optimal discretization benchmark results for this electrostatic system were computed and confirmed using two independent approaches. First, the results were obtained using explicitly derived analytical expressions for the entries of all the element matrices required to form the complete system of one-dimensional nonlinear

finite element optimization equations. It should be noted that these matrix entries are not independent of the placement of an element relative to the global coordinate system; therefore, they can only be evaluated numerically once the element vertex positions are specified numerically. Furthermore, the specific matrices required for the optimal discretization-based analysis of the point-charge model have not previously been published. Thus, the correctness of the explicit analytical matrix entries could not be guaranteed. Hence, the computed optimal discretization benchmark results were confirmed with additional independent calculations of the unknown variables. Specifically, a symbolic mathematics software package [150] was used to express the finite element optimization equations symbolically, and these were evaluated numerically at each iteration of the solution optimization process. The optimal discretization results computed by this second method were in complete agreement with those computed using the first approach.

The simplifications arising from the physical symmetry of the benchmark system considered here, namely, that its field solution behavior can be characterized mathematically by one space variable, is of definite value in computing the desired numerical results. Nevertheless, an immense amount of computational effort can still be required to solve for the optimal solution parameters due to the nonlinearities associated with incorporating the optimization of the finite element geometric discretizations. Moreover, the required computational effort increases rapidly with both the number of elements and the order of the finite element approximation used. Consequently, the maximum numbers of unconstrained parameters used in each of the investigations described and discussed in this section were determined, primarily, by the following two important considerations. First, a sufficient range of accuracy in the computed functional values was required in order to objectively and reliably assess the convergence of the FEM when used with optimal discretizations. Second, as relatively high solution accuracy levels are achieved with increasingly refined discretizations, the incremental improvement in functional value accuracy versus the corresponding

incremental computational effort required can become extremely expensive. Hence, the range of optimal discretization benchmark results reported next were computed in order to satisfy the above requirement subject to this computational cost constraint.

A series of 20 optimal first-order finite element solutions were computed for the first benchmark system by solving the appropriate systems of nonlinear optimization equations derived in section 2.4.1. The optimal values of the geometric discretization parameters, x_i, and the field solution parameters, U_i, for each of the optimal solutions computed for meshes ranging from 1 to 20 elements are reported in Tables 3.1–3.3. It should be noted, that each first-order element used in these meshes has two geometric discretization parameters associated with it which define the element's vertex positions, and two field solution parameters which correspond to the electric scalar potential multiplicative coefficients of the first-order basis functions defined over the element. Furthermore, the boundary conditions were enforced by fixing the positions of the first and last vertices in the mesh to the corresponding geometric boundaries of the problem domain, and by setting the the values of the field solution parameters at the problem boundaries to correspond to the analytical values of the electric scalar potential there.

The percent error in the functional values computed from the 20 first-order optimal discretizations specified by Tables 3.1–3.3 is shown in Figure 3.1. Also shown, for comparison, is the percent error in functional values computed from a series of 20 solutions corresponding to uniform first-order finite element discretizations. For both cases, the percent errors were calculated using the analytical functional value of 9.9000 (Jm/F) for this benchmark system. This functional value is, simply, twice the electrostatic potential energy of the system divided by $4\pi\varepsilon_o$, where $\varepsilon_o = 8.854187817 \times 10^{-12}$(F/m) is the permittivity of free space. The superior accuracy in the functional values computed from the first-order optimal discretization solutions relative to the uniform results for this benchmark system is directly related to the relative distribution of DOF over the problem domain: the optimal discretization-based formulation fo-

Table 3.1: Optimal computed values of the geometric discretization parameters, x_i, and field solution parameters, U_i, for first-order finite element solutions for Benchmark System 1 using N elements, where $N = 1, 2, \ldots, 8$.

i/N	1		2		3		4	
	x_i	U_i	x_i	U_i	x_i	U_i	x_i	U_i
1	0.1000	10.0000	0.1000	10.0000	0.1000	10.0000	0.1000	10.0000
2	10.0000	0.1000	0.2725	0.6707	0.2028	3.7814	0.1740	5.1705
3	N/A	N/A	10.0000	0.1000	0.5485	0.4860	0.3502	2.0713
4	N/A	N/A	N/A	N/A	10.0000	0.1000	0.9306	0.4098
5	N/A	N/A	N/A	N/A	N/A	N/A	10.0000	0.1000

i/N	5		6		7		8	
	x_i	U_i	x_i	U_i	x_i	U_i	x_i	U_i
1	0.1000	10.0000	0.1000	10.0000	0.1000	10.0000	0.1000	10.0000
2	0.1578	6.0080	0.1473	6.5862	0.1398	7.0155	0.1344	7.3486
3	0.2724	3.1863	0.2305	4.0209	0.2044	4.6746	0.1866	5.2018
4	0.5404	1.3595	0.3930	2.1938	0.3166	2.9041	0.2704	3.5087
5	1.3926	0.3600	0.7643	0.9958	0.5318	1.6312	0.4141	2.2189
6	10.0000	0.1000	1.8884	0.3221	1.0097	0.7838	0.6842	1.2820
7	N/A	N/A	10.0000	0.1000	2.3772	0.2921	1.2657	0.6480
8	N/A	N/A	N/A	N/A	10.0000	0.1000	2.8358	0.2681
9	N/A	N/A	N/A	N/A	N/A	N/A	10.0000	0.1000

Note: The table entries represent radial distance from the origin values for x_i with units (m), and electrostatic scalar potential values for U_i with units (V).

Table 3.2: Optimal computed values of the geometric discretization parameters, x_i, and field solution parameters, U_i, for first-order finite element solutions for Benchmark System 1 using N elements, where $N = 9, 10, \ldots, 16$.

i/N	9		10		11		12	
	x_i	U_i	x_i	U_i	x_i	U_i	x_i	U_i
1	0.1000	10.0000	0.1000	10.0000	0.1000	10.0000	0.1000	10.0000
2	0.1302	7.6150	0.1268	7.8330	0.1242	8.0147	0.1220	8.1683
3	0.1739	5.6359	0.1643	5.9994	0.1568	6.3079	0.1509	6.5728
4	0.2398	4.0262	0.2182	4.4720	0.2022	4.8591	0.1898	5.1976
5	0.3443	2.7494	0.2987	3.2241	0.2669	3.6478	0.2435	4.0265
6	0.5209	1.7694	0.4250	2.2285	0.3627	2.6535	0.3195	3.0438
7	0.8461	1.0498	0.6350	1.4583	0.5112	1.8556	0.4311	2.2334
8	1.5244	0.5547	1.0140	0.8868	0.7547	1.2337	0.6021	1.5793
9	3.2559	0.2489	1.7805	0.4872	1.1851	0.7673	0.8784	1.0658
10	10.0000	0.1000	3.6367	0.2331	2.0306	0.4362	1.3574	0.6768
11	N/A	N/A	10.0000	0.1000	3.9807	0.2202	2.2726	0.3965
12	N/A	N/A	N/A	N/A	10.0000	0.1000	4.2916	0.2094
13	N/A	N/A	N/A	N/A	N/A	N/A	10.0000	0.1000

i/N	13		14		15		16	
	x_i	U_i	x_i	U_i	x_i	U_i	x_i	U_i
1	0.1000	10.0000	0.1000	10.0000	0.1000	10.0000	0.1000	10.0000
2	0.1201	8.3000	0.1186	8.4141	0.1172	8.5139	0.1161	8.6019
3	0.1461	6.8028	0.1421	7.0041	0.1387	7.1818	0.1358	7.3398
4	0.1801	5.4956	0.1722	5.7598	0.1657	5.9955	0.1603	6.2068
5	0.2256	4.3659	0.2116	4.6711	0.2003	4.9466	0.1910	5.1961
6	0.2879	3.4010	0.2639	3.7277	0.2452	4.0267	0.2301	4.3008
7	0.3756	2.5883	0.3352	2.9195	0.3046	3.2277	0.2808	3.5139
8	0.5033	1.9150	0.4349	2.2363	0.3851	2.5411	0.3475	2.8287
9	0.6966	1.3687	0.5786	1.6679	0.4968	1.9586	0.4373	2.2382
10	1.0048	0.9366	0.7941	1.2041	0.6566	1.4720	0.5612	1.7355
11	1.5293	0.6062	1.1329	0.8348	0.8937	1.0728	0.7369	1.3139
12	2.5053	0.3649	1.6995	0.5498	1.2618	0.7529	0.9950	0.9663
13	4.5733	0.2002	2.7282	0.3390	1.8671	0.5040	1.3908	0.6860
14	10.0000	0.1000	4.8293	0.1924	2.9413	0.3176	2.0315	0.4660
15	N/A	N/A	10.0000	0.1000	5.0628	0.1857	3.1445	0.2996
16	N/A	N/A	N/A	N/A	10.0000	0.1000	5.2763	0.1798
17	N/A	N/A	N/A	N/A	N/A	N/A	10.0000	0.1000

Note: The table entries represent radial distance from the origin values for x_i with units (m), and electrostatic scalar potential values for U_i with units (V).

Table 3.3: Optimal computed values of the geometric discretization parameters, x_i, and field solution parameters, U_i, for first-order finite element solutions for Benchmark System 1 using N elements, where $N = 17, 18, 19, 20$.

i/N	17		18		19		20	
	x_i	U_i	x_i	U_i	x_i	U_i	x_i	U_i
1	0.1000	10.0000	0.1000	10.0000	0.1000	10.0000	0.1000	10.0000
2	0.1151	8.6801	0.1142	8.7500	0.1134	8.8129	0.1127	8.8698
3	0.1333	7.4811	0.1311	7.6083	0.1292	7.7233	0.1275	7.8278
4	0.1556	6.3974	0.1517	6.5700	0.1482	6.7270	0.1452	6.8705
5	0.1832	5.4231	0.1767	5.6302	0.1711	5.8199	0.1662	5.9942
6	0.2178	4.5525	0.2076	4.7841	0.1989	4.9978	0.1915	5.1955
7	0.2617	3.7798	0.2461	4.0269	0.2332	4.2567	0.2223	4.4708
8	0.3182	3.0993	0.2949	3.3536	0.2758	3.5923	0.2600	3.8164
9	0.3924	2.5053	0.3574	2.7594	0.3295	3.0005	0.3068	3.2290
10	0.4916	1.9920	0.4390	2.2395	0.3981	2.4773	0.3655	2.7048
11	0.6275	1.5535	0.5477	1.7890	0.4873	2.0183	0.4403	2.2404
12	0.8188	1.1843	0.6956	1.4030	0.6054	1.6196	0.5370	1.8322
13	1.0973	0.8785	0.9022	1.0766	0.7650	1.2769	0.6644	1.4766
14	1.5193	0.6303	1.2002	0.8051	0.9866	0.9861	0.8357	1.1701
15	2.1923	0.4341	1.6469	0.5835	1.3034	0.7431	1.0717	0.9091
16	3.3382	0.2842	2.3490	0.4071	1.7731	0.5437	1.4064	0.6901
17	5.4723	0.1747	3.5227	0.2709	2.5017	0.3838	1.8977	0.5094
18	10.0000	0.1000	5.6528	0.1701	3.6985	0.2593	2.6501	0.3637
19	N/A	N/A	10.0000	0.1000	5.8196	0.1661	3.8660	0.2492
20	N/A	N/A	N/A	N/A	10.0000	0.1000	5.9740	0.1625
21	N/A	N/A	N/A	N/A	N/A	N/A	10.0000	0.1000

Note: The table entries represent radial distance from the origin values for x_i with units (m), and electrostatic scalar potential values for U_i with units (V).

cuses DOF close to the point charge where the field solution variation is very rapid; whereas, the DOF are equally distributed over the entire problem domain in the uniform case. For example, Figure 3.2 illustrates the placement of the element vertices for corresponding optimal and uniform meshes with two, three and four elements. The comparison of optimal and uniform meshes ranging from five elements to eight elements is shown in Figure 3.3. Furthermore, it may be noted from the numerical values reported Table 3.2 and Table 3.3 that the balance of the optimal first-order discretizations computed for Benchmark System 1 also have element vertex positions effectively distributed for efficiently resolving the rapid field solution variation close to the singularity.

Figure 3.4 shows the results of a basic computational experiment designed to confirm the validity of the one-dimensional finite element optimization equations used to compute the optimal first-order finite element discretization results in this section. This simple numerical experiment was based on resolving the electrostatic benchmark system using the most fundamental discretization. Specifically, a series of 100,000 two-element first-order meshes were used to compute individual functional values corresponding to fixing the unconstrained element vertex common to both of the elements in the mesh at 100,000 regularly spaced positions between the two end vertices defining the boundaries of the problem domain. It should be noted that for each of the meshes defined by this method, the single unknown scalar electric potential value at the common vertex was computed using the standard finite element formulation with the geometric discretization held fixed. The results confirmed those obtained by solving the finite element optimization equations directly: the position of the free vertex which yielded the smallest possible functional value was the same as that obtained by direct optimization, with an error tolerance of $\pm 4.95 \times 10^{-5}$ (m). Furthermore, the functional value corresponding to the mesh defined by this optimal vertex position represents the minimum electrostatic potential energy configuration of the two-element first-order finite element model for this benchmark system, as il-

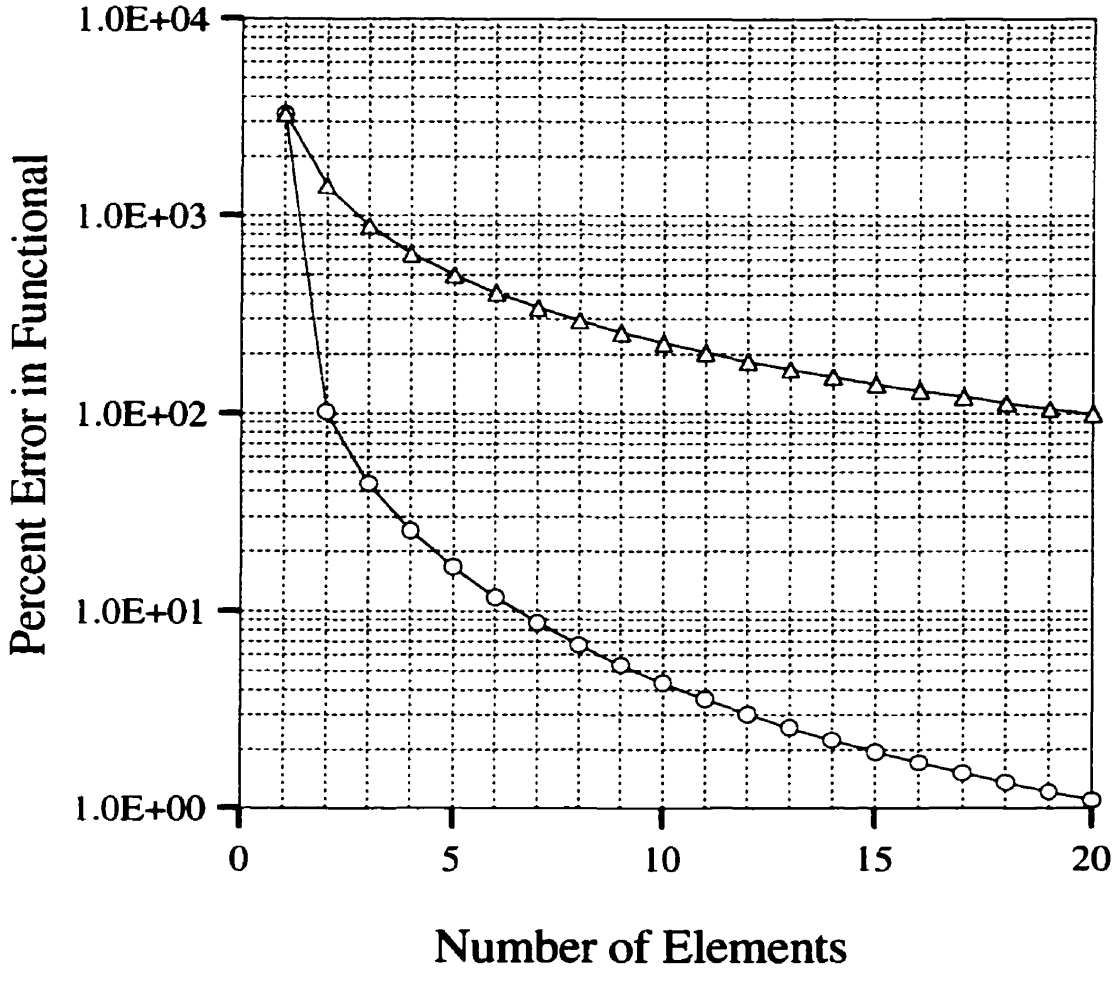

Figure 3.1: The variation of percent error in functional value with discretization level for first-order finite element solutions for Benchmark System 1 is illustrated. The triangle knot results correspond to percent error in functional values computed from solutions based on uniform discretizations. The circle knot results correspond to percent error in functional values computed from solutions based on optimal discretizations.

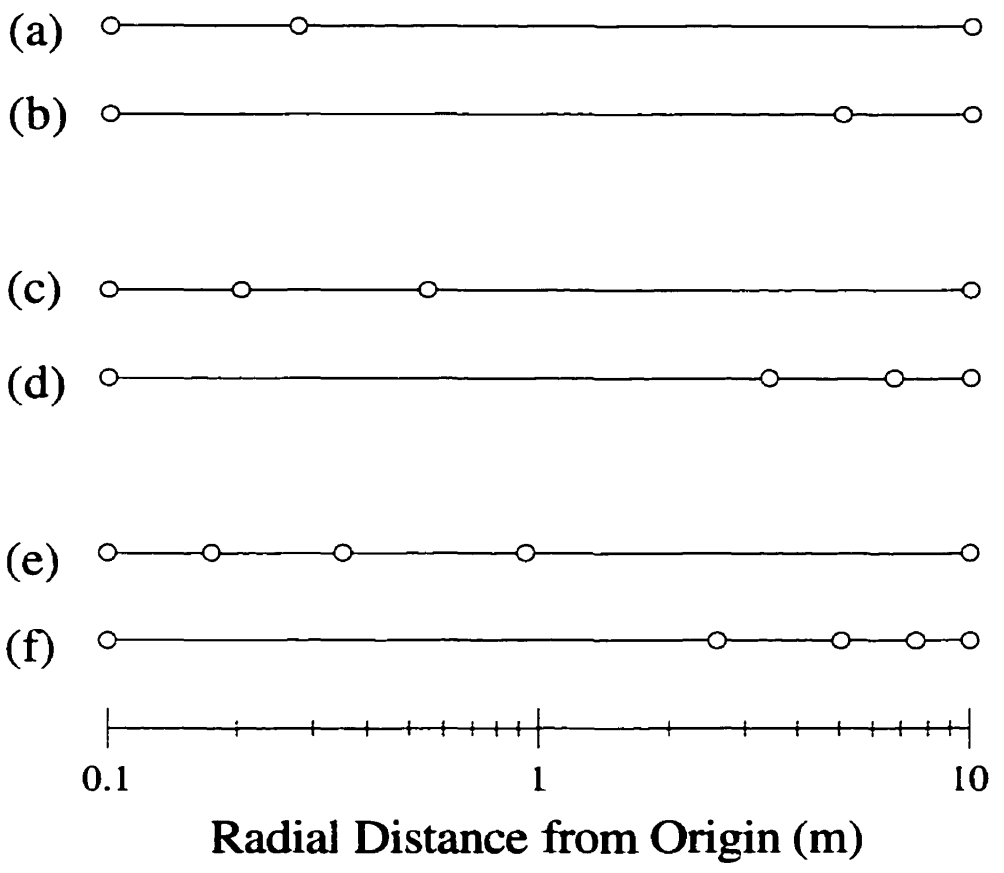

Figure 3.2: First-order optimal and uniform radial discretizations for the one-dimensional electrostatic potential analysis of Benchmark System 1 are illustrated: (a) 2 element optimal mesh; (b) 2 element uniform mesh; (c) 3 element optimal mesh; (d) 3 element uniform mesh; (e) 4 element optimal mesh; (f) 4 element uniform mesh. The radial discretizations are plotted on a logarithmic scale because of the proximity of the element vertices to each other near the singularity in the optimal meshes. Note: the positions of the element vertices in the optimal meshes are specified in Table 3.1.

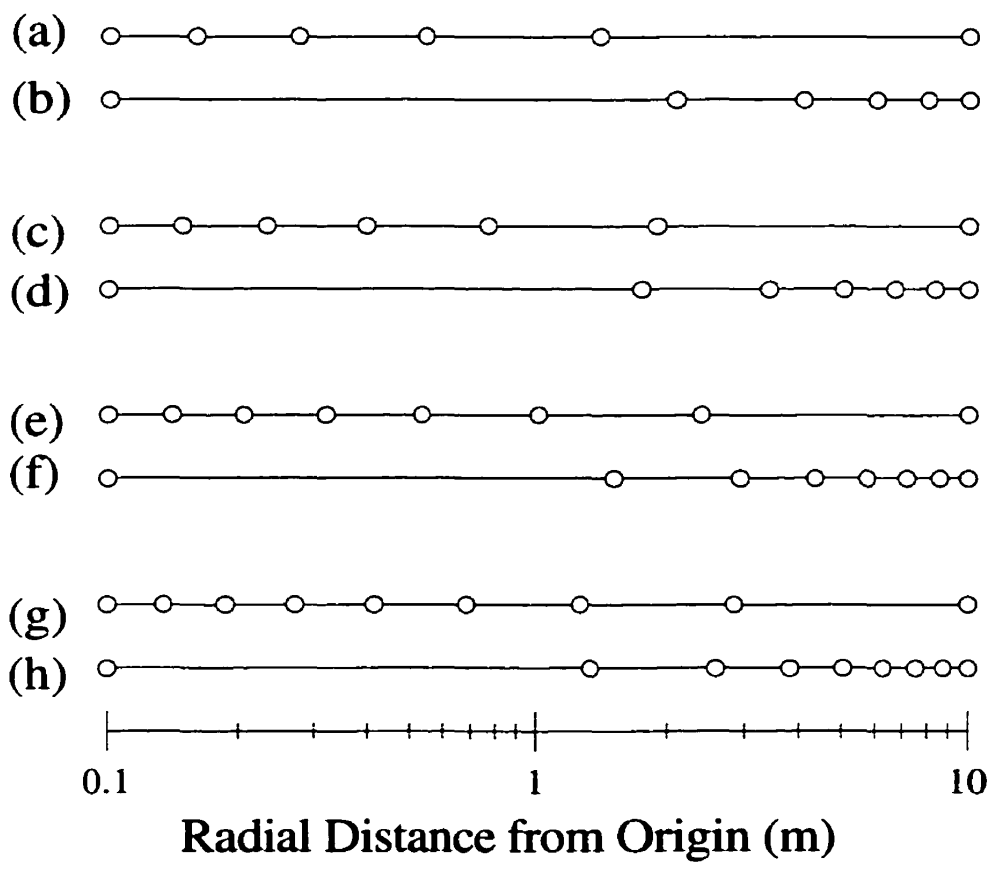

Figure 3.3: First-order optimal and uniform radial discretizations for the one-dimensional electrostatic potential analysis of Benchmark System 1 are illustrated: (a) 5 element optimal mesh; (b) 5 element uniform mesh: (c) 6 element optimal mesh; (d) 6 element uniform mesh; (e) 7 element optimal mesh; (f) 7 element uniform mesh; (g) 8 element optimal mesh; (h) 8 element uniform mesh. The radial discretizations are plotted on a logarithmic scale because of the proximity of the element vertices to each other near the singularity in the optimal meshes. Note: the positions of the element vertices in the optimal meshes are specified in Table 3.1.

lustrated by Figure 3.4. This is wholly consistent with the underlying stationarity principle fundamental to the variational finite element formulation used throughout this work. Finally, the error tolerance stated above is, simply, one-half of the interval used to define successive vertex positions for computing the range of functional values used to confirm the results obtained by solving the finite element optimization equations directly.

A series of 16 optimal second-order finite element solutions were computed for Benchmark System 1 using the same techniques described for the first-order results. The optimal values of the geometric discretization parameters, x_i, and the field solution parameters, U_i, for each of the optimal solutions computed for meshes ranging from 1 to 16 elements are reported in Tables 3.4–3.6. It should be noted, that each second-order element used in these meshes has two geometric discretization parameters associated with it which define the element's vertex positions, and three field solution parameters which correspond to the electric scalar potential multiplicative coefficients of the second-order basis functions defined over the element. The boundary conditions used to compute the second-order results were enforced in the same manner as in the first-order case. Furthermore, the second-order optimal discretization benchmark results for this electrostatic system were computed twice, using the same approach described for confirming the accuracy of the first-order results.

The percent error in the functional values computed from the 16 second-order optimal discretizations specified by Tables 3.4–3.6 is shown in Figure 3.5. Also shown in Figure 3.5, is the percent error in functional values computed from a series of 16 solutions corresponding to uniform second-order finite element discretizations. The superior accuracy in the functional values computed from the second-order optimal discretization solutions relative to the uniform results is, again, directly related to the more efficient relative distribution of DOF over the problem domain. For example, the placement of the element vertices for corresponding optimal and uniform second-order meshes with two, three and four elements is illustrated by Figure 3.6. The

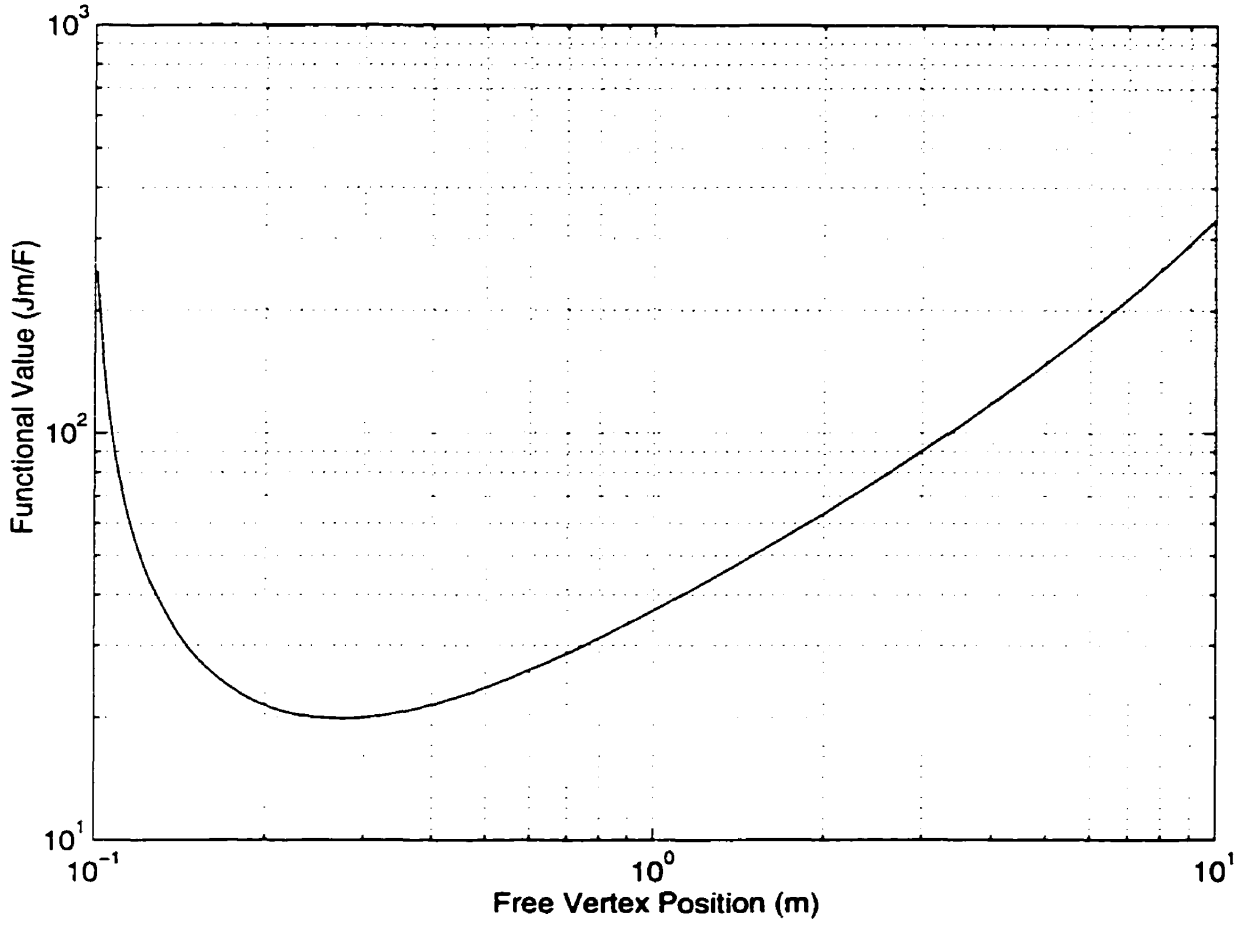

Figure 3.4: The variation in functional value with choice of free vertex position for a first-order two-element mesh is illustrated for Benchmark System 1. The plot is based on 100,000 functional values computed by fixing the unconstrained element vertex at 100,000 uniformly spaced positions between the two geometric boundaries of the problem domain. Logarithmic axes are used for the plot in order to adequately resolve the variation in the functional value near the optimal vertex position corresponding to the true minimum in the electrostatic potential energy of the discretized, first-order, two-element finite element model. Note: the optimal vertex position is specified in Table 3.1.

Table 3.4: Optimal computed values of the geometric discretization parameters, x_i, and field solution parameters, U_i, for second-order finite element solutions for Benchmark System 1 using N elements, where $N = 1, 2, \ldots, 8$.

i/N	1		2		3		4	
	x_i	U_i	x_i	U_i	x_i	U_i	x_i	U_i
1	0.1000	10.0000	0.1000	10.0000	0.1000	10.0000	0.1000	10.0000
2	10.0000	1.9723	0.4072	3.2685	0.2717	5.2942	0.2155	6.3345
3	N/A	0.1000	10.0000	1.0033	1.0153	3.3226	0.5427	4.5240
4	N/A	N/A	N/A	0.2759	10.0000	1.3463	1.7622	2.5685
5	N/A	N/A	N/A	0.1000	N/A	0.6544	10.0000	1.7067
6	N/A	N/A	N/A	N/A	N/A	0.2156	N/A	0.8122
7	N/A	N/A	N/A	N/A	N/A	0.1000	N/A	0.4754
8	N/A	N/A	N/A	N/A	N/A	N/A	N/A	0.1861
9	N/A	N/A	N/A	N/A	N/A	N/A	N/A	0.1000

i/N	5		6		7		8	
	x_i	U_i	x_i	U_i	x_i	U_i	x_i	U_i
1	0.1000	10.0000	0.1000	10.0000	0.1000	10.0000	0.1000	10.0000
2	0.1855	7.0098	0.1675	7.4833	0.1555	7.8316	0.1471	8.0974
3	0.3779	5.3434	0.2984	5.9504	0.2528	6.4196	0.2236	6.7930
4	0.8762	3.5246	0.5757	4.2837	0.4337	4.8946	0.3536	5.3937
5	2.4742	2.5857	1.2369	3.3220	0.7970	3.9406	0.5864	4.4633
6	10.0000	1.5649	3.1026	2.2731	1.6025	2.9057	1.0321	3.4610
7	N/A	1.0878	10.0000	1.7074	3.6475	2.2888	1.9599	2.8183
8	N/A	0.5798	N/A	1.0903	10.0000	1.6169	4.1194	2.1228
9	N/A	0.3721	N/A	0.7849	N/A	1.2394	10.0000	1.6955
10	N/A	0.1687	N/A	0.4548	N/A	0.8274	N/A	1.2313
11	N/A	0.1000	N/A	0.3090	N/A	0.6125	N/A	0.9606
12	N/A	N/A	N/A	0.1573	N/A	0.3787	N/A	0.6654
13	N/A	N/A	N/A	0.1000	N/A	0.2679	N/A	0.5041
14	N/A	N/A	N/A	N/A	N/A	0.1494	N/A	0.3281
15	N/A	N/A	N/A	N/A	N/A	0.1000	N/A	0.2395
16	N/A	N/A	N/A	N/A	N/A	N/A	N/A	0.1434
17	N/A	N/A	N/A	N/A	N/A	N/A	N/A	0.1000

Note: The table entries represent radial distance from the origin values for x_i with units (m), and electrostatic scalar potential values for U_i with units (V).

Table 3.5: Optimal computed values of the geometric discretization parameters, x_i, and field solution parameters, U_i, for second-order finite element solutions for Benchmark System 1 using N elements, where $N = 9, 10, 11, 12$.

i/N	9		10		11		12	
	x_i	U_i	x_i	U_i	x_i	U_i	x_i	U_i
1	0.1000	10.0000	0.1000	10.0000	0.1000	10.0000	0.1000	10.0000
2	0.1408	8.3064	0.1360	8.4748	0.1322	8.6132	0.1292	8.7288
3	0.2035	7.0969	0.1889	7.3488	0.1778	7.5610	0.1691	7.7421
4	0.3030	5.8074	0.2685	6.1550	0.2436	6.4508	0.2250	6.7051
5	0.4672	4.9084	0.3921	5.2908	0.3411	5.6219	0.3045	5.9110
6	0.7517	3.9465	0.5911	4.3714	0.4895	4.7448	0.4204	5.0744
7	1.2735	3.2944	0.9253	3.7205	0.7229	4.1017	0.5936	4.4433
8	2.3025	2.5937	1.5159	3.0256	1.1041	3.4191	0.8603	3.7766
9	4.5300	2.1339	2.6269	2.5460	1.7557	2.9287	1.2853	3.2820
10	10.0000	1.6378	4.8894	2.0320	2.9322	2.4065	1.9904	2.7581
11	N/A	1.3246	10.0000	1.6876	5.2060	2.0401	3.2182	2.3767
12	N/A	0.9851	N/A	1.3170	10.0000	1.6483	5.4867	1.9714
13	N/A	0.7804	N/A	1.0771	N/A	1.3807	10.0000	1.6826
14	N/A	0.5577	N/A	0.8178	N/A	1.0935	N/A	1.3747
15	N/A	0.4308	N/A	0.6567	N/A	0.9034	N/A	1.1606
16	N/A	0.2924	N/A	0.4819	N/A	0.6985	N/A	0.9314
17	N/A	0.2189	N/A	0.3786	N/A	0.5677	N/A	0.7765
18	N/A	0.1388	N/A	0.2660	N/A	0.4262	N/A	0.6100
19	N/A	0.1000	N/A	0.2034	N/A	0.3397	N/A	0.5012
20	N/A	N/A	N/A	0.1351	N/A	0.2458	N/A	0.3837
21	N/A	N/A	N/A	0.1000	N/A	0.1914	N/A	0.3099
22	N/A	N/A	N/A	N/A	N/A	0.1321	N/A	0.2298
23	N/A	N/A	N/A	N/A	N/A	0.1000	N/A	0.1818
24	N/A	N/A	N/A	N/A	N/A	N/A	N/A	0.1296
25	N/A	N/A	N/A	N/A	N/A	N/A	N/A	0.1000

Note: The table entries represent radial distance from the origin values for x_i with units (m), and electrostatic scalar potential values for U_i with units (V).

Table 3.6: Optimal computed values of the geometric discretization parameters, x_i, and field solution parameters, U_i, for second-order finite element solutions for Benchmark System 1 using N elements, where $N = 13, 14, 15, 16$.

i/N	13		14		15		16	
	x_i	U_i	x_i	U_i	x_i	U_i	x_i	U_i
1	0.1000	10.0000	0.1000	10.0000	0.1000	10.0000	0.1000	10.0000
2	0.1266	8.8268	0.1245	8.9108	0.1226	8.9839	0.1211	9.0477
3	0.1622	7.8982	0.1565	8.0342	0.1517	8.1542	0.1477	8.2603
4	0.2105	6.9259	0.1989	7.1193	0.1895	7.2905	0.1816	7.4425
5	0.2771	6.1651	0.2559	6.3902	0.2391	6.5913	0.2254	6.7713
6	0.3708	5.3668	0.3338	5.6277	0.3052	5.8622	0.2825	6.0733
7	0.5054	4.7501	0.4420	5.0266	0.3945	5.2775	0.3579	5.5050
8	0.7031	4.1013	0.5951	4.3967	0.5172	4.6667	0.4589	4.9131
9	1.0017	3.6071	0.8168	3.9061	0.6887	4.1818	0.5960	4.4354
10	1.4669	3.0860	1.1456	3.3908	0.9334	3.6743	0.7855	3.9371
11	2.2184	2.6952	1.6475	2.9946	1.2906	3.2758	1.0523	3.5387
12	3.4858	2.2819	2.4388	2.5775	1.8254	2.8579	1.4358	3.1224
13	5.7371	1.9773	3.7359	2.2615	2.6508	2.5339	2.0004	2.7931
14	10.0000	1.6543	5.9617	1.9279	3.9694	2.1933	2.8545	2.4482
15	N/A	1.4208	10.0000	1.6792	6.1640	1.9327	4.1879	2.1786
16	N/A	1.1725	N/A	1.4160	10.0000	1.6581	6.3473	1.8956
17	N/A	0.9970	N/A	1.2233	N/A	1.4512	10.0000	1.6772
18	N/A	0.8096	N/A	1.0187	N/A	1.2326	N/A	1.4474
19	N/A	0.6806	N/A	0.8720	N/A	1.0706	N/A	1.2725
20	N/A	0.5423	N/A	0.7157	N/A	0.8990	N/A	1.0880
21	N/A	0.4499	N/A	0.6063	N/A	0.7742	N/A	0.9498
22	N/A	0.3505	N/A	0.4892	N/A	0.6416	N/A	0.8036
23	N/A	0.2863	N/A	0.4094	N/A	0.5473	N/A	0.6960
24	N/A	0.2169	N/A	0.3238	N/A	0.4467	N/A	0.5819
25	N/A	0.1740	N/A	0.2673	N/A	0.3768	N/A	0.4995
26	N/A	0.1274	N/A	0.2063	N/A	0.3021	N/A	0.4119
27	N/A	0.1000	N/A	0.1675	N/A	0.2516	N/A	0.3500
28	N/A	N/A	N/A	0.1255	N/A	0.1974	N/A	0.2840
29	N/A	N/A	N/A	0.1000	N/A	0.1621	N/A	0.2386
30	N/A	N/A	N/A	N/A	N/A	0.1239	N/A	0.1899
31	N/A	N/A	N/A	N/A	N/A	0.1000	N/A	0.1574
32	N/A	N/A	N/A	N/A	N/A	N/A	N/A	0.1225
33	N/A	N/A	N/A	N/A	N/A	N/A	N/A	0.1000

Note: The table entries represent radial distance from the origin values for x_i with units (m), and electrostatic scalar potential values for U_i with units (V).

comparison of optimal and uniform second-order meshes ranging from five elements to eight elements is shown in Figure 3.7. Furthermore, it may be noted from the numerical values specified in Table 3.5 and Table 3.6 that the balance of the optimal second-order discretizations computed for Benchmark System 1 also have effectively distributed element vertices for efficiently resolving the rapid field solution variation close to the point charge.

The results of the same basic computational experiment used to confirm the validity of the optimal first-order discretization results are shown for the second-order case in Figure 3.8. It should be noted, however, that for each of the meshes used to compute the functional values for the second-order experiment, three unknown scalar electric potential values were computed using the standard finite element formulation with the geometric discretization held fixed: one potential value uniquely associated with each element; and one potential value defined at the common vertex. Finally, the position of the free vertex which yielded the smallest possible functional value was the same as that obtained by direct optimization, again with an error tolerance of $\pm 4.95 \times 10^{-5}$ (m) as defined for the first-order case.

In addition to the first- and second-order optimal discretization results presented for Benchmark System 1, a series of eight optimal fourth-order finite-element solutions were computed using the same techniques described above. The optimal values of the geometric discretization parameters, x_i, and the field solution parameters, U_i, for each of the optimal fourth-order solutions are reported in Table 3.7 and Table 3.8. It should be noted that each element in the fourth-order meshes has two geometric discretization parameters associated with it which define the element's vertex positions, and five field solution parameters which correspond to the electric scalar potential multiplicative coefficients of the fourth-order basis functions defined over the elements. The boundary conditions were enforced as in the previous cases, and the accuracy of the fourth-order optimal discretization benchmark results were confirmed with two independent calculations analogous to those used for the first- and

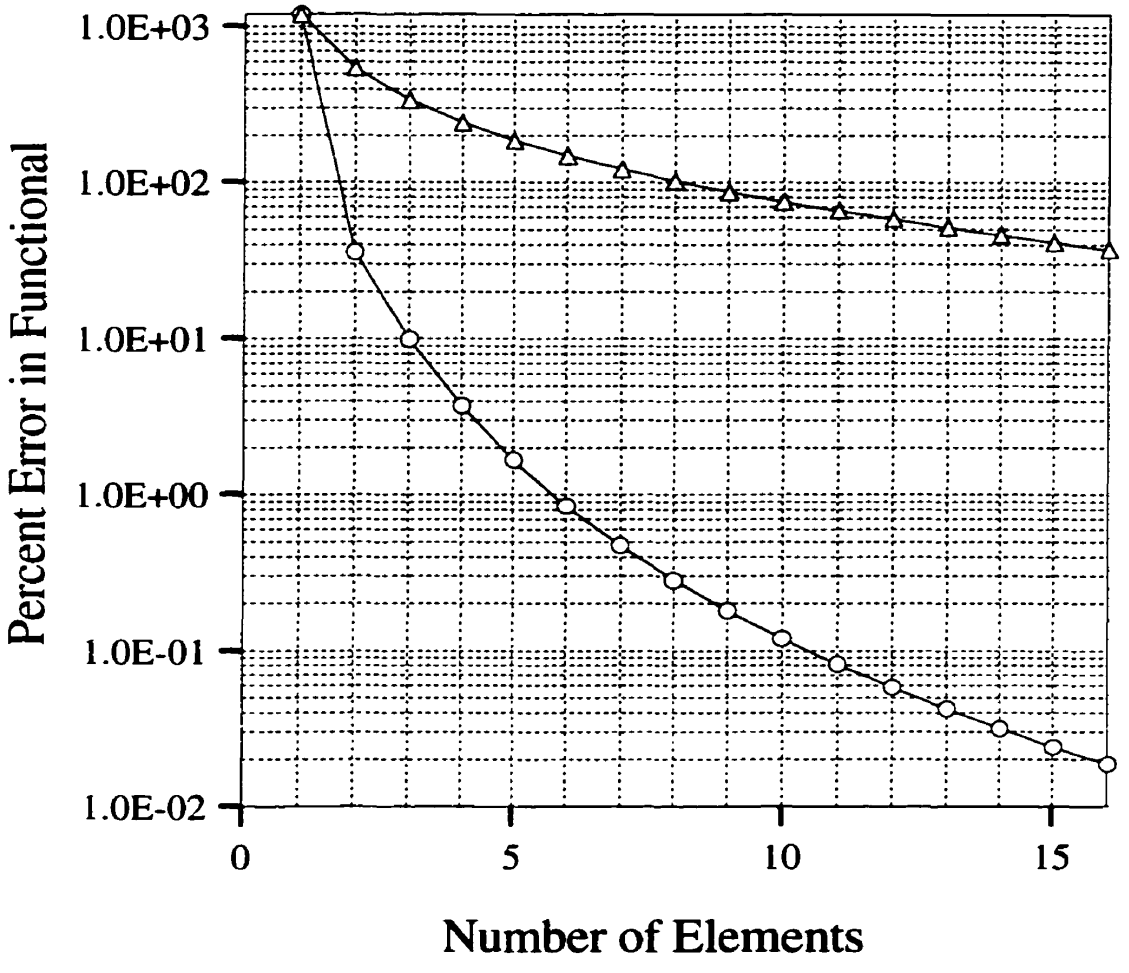

Figure 3.5: The variation of percent error in functional value with discretization level for second-order finite element solutions for Benchmark System 1 is illustrated. The triangle knot results correspond to percent error in functional values computed from solutions based on uniform discretizations. The circle knot results correspond to percent error in functional values computed from solutions based on optimal discretizations.

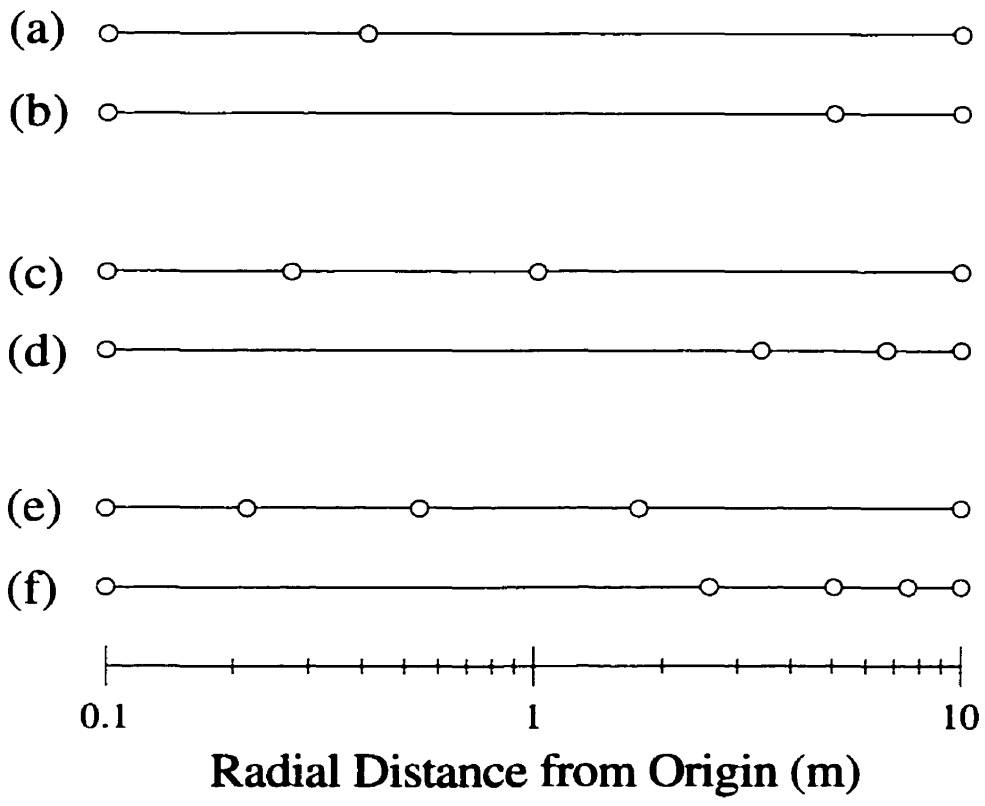

Figure 3.6: Second-order optimal and uniform radial discretizations for the one-dimensional electrostatic potential analysis of Benchmark System 1 are illustrated: (a) 2 element optimal mesh; (b) 2 element uniform mesh; (c) 3 element optimal mesh; (d) 3 element uniform mesh; (e) 4 element optimal mesh; (f) 4 element uniform mesh. The radial discretizations are plotted on a logarithmic scale because of the proximity of the element vertices to each other near the singularity in the optimal meshes. Note: the positions of the element vertices in the optimal meshes are specified in Table 3.4.

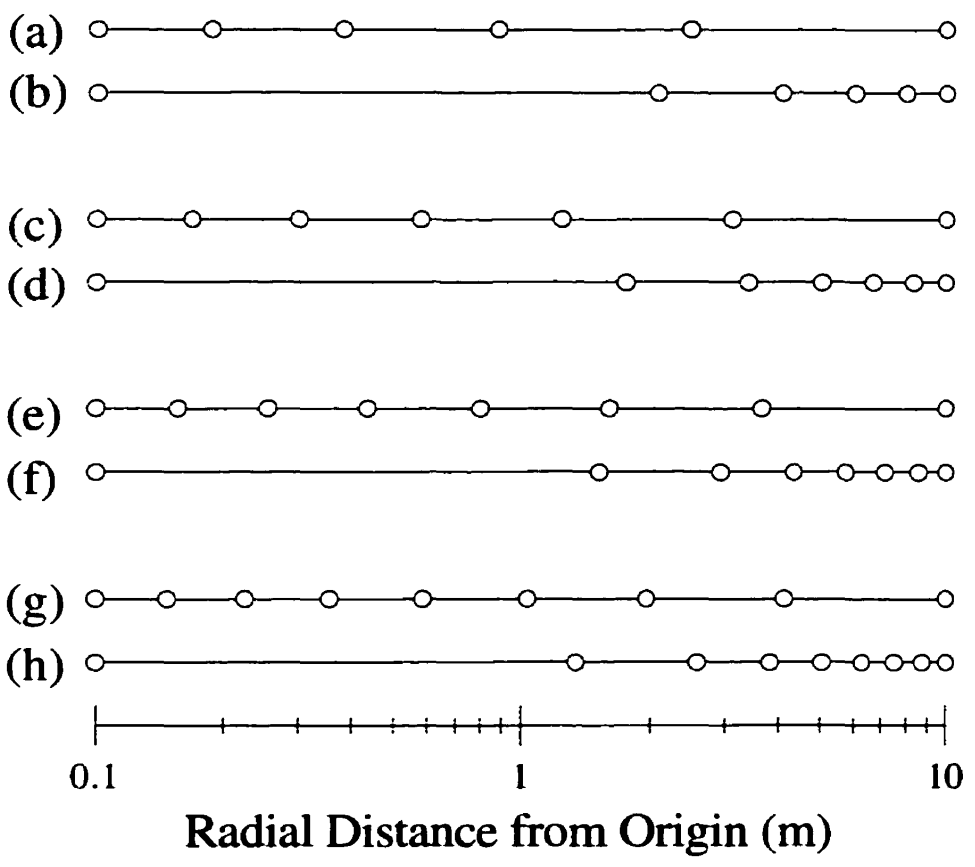

Figure 3.7: Second-order optimal and uniform radial discretizations for the one-dimensional electrostatic potential analysis of Benchmark System 1 are illustrated: (a) 5 element optimal mesh; (b) 5 element uniform mesh; (c) 6 element optimal mesh; (d) 6 element uniform mesh; (e) 7 element optimal mesh; (f) 7 element uniform mesh; (g) 8 element optimal mesh; (h) 8 element uniform mesh. The radial discretizations are plotted on a logarithmic scale because of the proximity of the element vertices to each other near the singularity in the optimal meshes. Note: the positions of the element vertices in the optimal meshes are specified in Table 3.4.

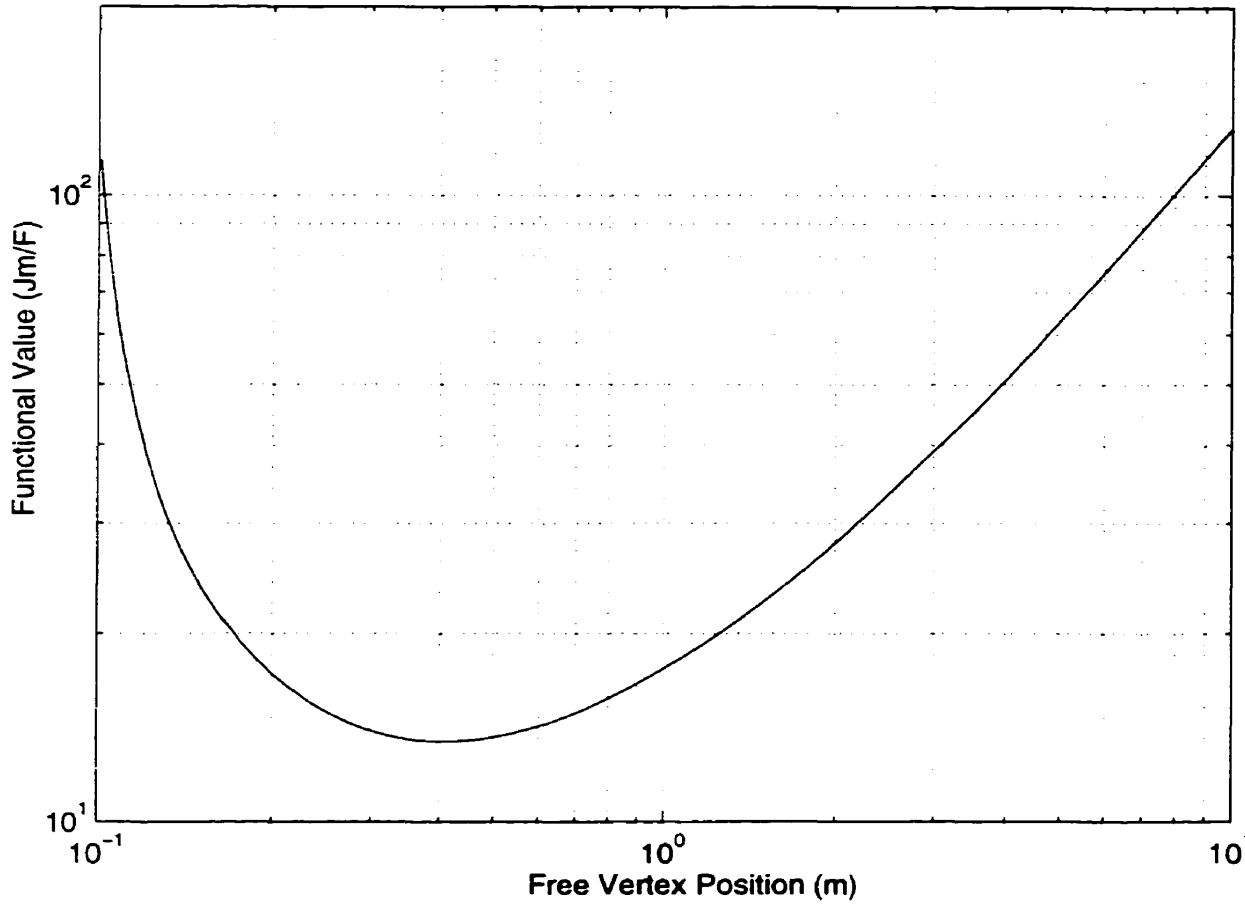

Figure 3.8: The variation in functional value with choice of free vertex position for a second-order two-element mesh is illustrated for Benchmark System 1. The plot is based on 100.000 functional values computed by fixing the unconstrained element vertex at 100.000 uniformly spaced positions between the two geometric boundaries of the problem domain. Logarithmic axes are used for the plot in order to adequately resolve the variation in the functional value near the optimal vertex position corresponding to the true minimum in the electrostatic potential energy of the discretized, second-order, two-element finite element model. Note: the optimal vertex position is specified in Table 3.4.

second-order cases.

The convergence in percent error of the functional values computed from the eight fourth-order optimal discretizations specified by Table 3.7 and Table 3.8 and the corresponding uniform discretizations is illustrated in Figure 3.9. The superior accuracy in the functional values computed from the fourth-order optimal discretizations relative to the uniform results is, once more, attributed to the more efficient relative placement of the element vertices illustrated in Figure 3.10 and Figure 3.11. Finally, Figure 3.12 shows the results of the two-element basic computational test used to confirm the validity of the fourth-order optimal discretization results. It should be noted that for each of the meshes used to compute the functional values for the fourth-order experiment, seven unknown scalar electric potential values were computed using the standard finite element formulation with the geometric discretization held fixed: three potential values uniquely associated with each element; and one potential value defined at the common vertex. The results of the experiment confirmed, with an error tolerance of $\pm 4.95 \times 10^{-5}$ (m), that the optimal position of the free vertex computed by direct solution of the finite element optimization equations correctly corresponds to the smallest possible functional value for a fourth-order two-element mesh.

The final set of optimal discretization results computed for Benchmark System 1 consists of a series of four optimal eighth-order solutions specified by the optimal values of the geometric discretization parameters, x_i, and the field solution parameters, U_i, reported in Table 3.9. The eighth-order optimal results were computed following completely analogous procedures used to compute the first-, second- and fourth-order results described in the preceding paragraphs. However, it may be noted that each element in the eighth-order meshes has two geometric discretization parameters associated with it which define the element's vertex positions, and nine field solution parameters which correspond to the electric scalar potential multiplicative coefficients of the eighth-order basis functions defined over the elements.

The convergence in percent error of the functional values computed from the

Table 3.7: Optimal computed values of the geometric discretization parameters, x_i, and field solution parameters, U_i, for fourth-order finite element solutions for Benchmark System 1 using N elements, where $N = 1, 2, 3, 4$.

i/N	1		2		3		4	
	x_i	U_i	x_i	U_i	x_i	U_i	x_i	U_i
1	0.1000	10.0000	0.1000	10.0000	0.1000	10.0000	0.1000	10.0000
2	10.0000	1.5845	0.6345	4.1645	0.3477	6.1571	0.2539	7.2153
3	N/A	0.4090	10.0000	2.4872	1.5341	4.4437	0.7246	5.6471
4	N/A	0.3567	N/A	1.8138	10.0000	3.4992	2.4142	4.6462
5	N/A	0.1000	N/A	1.3195	N/A	2.8568	10.0000	3.9365
6	N/A	N/A	N/A	0.3545	N/A	1.5358	N/A	2.6861
7	N/A	N/A	N/A	0.1796	N/A	1.0436	N/A	2.0398
8	N/A	N/A	N/A	0.1434	N/A	0.8022	N/A	1.6489
9	N/A	N/A	N/A	0.1000	N/A	0.6374	N/A	1.3777
10	N/A	N/A	N/A	N/A	N/A	0.2734	N/A	0.8688
11	N/A	N/A	N/A	N/A	N/A	0.1706	N/A	0.6345
12	N/A	N/A	N/A	N/A	N/A	0.1300	N/A	0.5027
13	N/A	N/A	N/A	N/A	N/A	0.1000	N/A	0.4128
14	N/A	N/A	N/A	N/A	N/A	N/A	N/A	0.2312
15	N/A	N/A	N/A	N/A	N/A	N/A	N/A	0.1603
16	N/A	N/A	N/A	N/A	N/A	N/A	N/A	0.1244
17	N/A	N/A	N/A	N/A	N/A	N/A	N/A	0.1000

Note: The table entries represent radial distance from the origin values for x_i with units (m), and electrostatic scalar potential values for U_i with units (V).

Table 3.8: Optimal computed values of the geometric discretization parameters, x_i, and field solution parameters, U_i, for fourth-order finite element solutions for Benchmark System 1 using N elements, where $N = 5, 6, 7, 8$.

i/N	5		6		7		8	
	x_i	U_i	x_i	U_i	x_i	U_i	x_i	U_i
1	0.1000	10.0000	0.1000	10.0000	0.1000	10.0000	0.1000	10.0000
2	0.2101	7.8391	0.1852	8.2420	0.1694	8.5213	0.1587	8.7196
3	0.4735	6.4484	0.3596	7.0110	0.2967	7.4243	0.2581	7.7303
4	1.1626	5.4794	0.7376	6.1009	0.5399	6.5779	0.4314	6.9428
5	3.1791	4.7594	1.6148	5.3980	1.0269	5.9039	0.7439	6.3004
6	10.0000	3.6219	3.8260	4.3688	2.0556	4.9695	1.3298	5.4474
7	N/A	2.9246	10.0000	3.6700	4.3719	4.2911	2.4770	4.7982
8	N/A	2.4544	N/A	3.1648	10.0000	3.7760	4.8396	4.2875
9	N/A	2.1115	N/A	2.7804	N/A	3.3705	10.0000	3.8745
10	N/A	1.5471	N/A	2.2013	N/A	2.7968	N/A	3.3175
11	N/A	1.2215	N/A	1.8224	N/A	2.3904	N/A	2.9008
12	N/A	1.0105	N/A	1.5554	N/A	2.0874	N/A	2.5772
13	N/A	0.8597	N/A	1.3556	N/A	1.8520	N/A	2.3183
14	N/A	0.5991	N/A	1.0445	N/A	1.5110	N/A	1.9626
15	N/A	0.4600	N/A	0.8499	N/A	1.2764	N/A	1.7017
16	N/A	0.3743	N/A	0.7169	N/A	1.1050	N/A	1.5022
17	N/A	0.3143	N/A	0.6192	N/A	0.9738	N/A	1.3443
18	N/A	0.2044	N/A	0.4610	N/A	0.7786	N/A	1.1230
19	N/A	0.1515	N/A	0.3674	N/A	0.6487	N/A	0.9644
20	N/A	0.1209	N/A	0.3057	N/A	0.5562	N/A	0.8452
21	N/A	0.1000	N/A	0.2613	N/A	0.4864	N/A	0.7520
22	N/A	N/A	N/A	0.1861	N/A	0.3794	N/A	0.6185
23	N/A	N/A	N/A	0.1446	N/A	0.3111	N/A	0.5253
24	N/A	N/A	N/A	0.1184	N/A	0.2638	N/A	0.4567
25	N/A	N/A	N/A	0.1000	N/A	0.2287	N/A	0.4037
26	N/A	N/A	N/A	N/A	N/A	0.1730	N/A	0.3259
27	N/A	N/A	N/A	N/A	N/A	0.1391	N/A	0.2733
28	N/A	N/A	N/A	N/A	N/A	0.1165	N/A	0.2354
29	N/A	N/A	N/A	N/A	N/A	0.1000	N/A	0.2066
30	N/A	N/A	N/A	N/A	N/A	N/A	N/A	0.1631
31	N/A	N/A	N/A	N/A	N/A	N/A	N/A	0.1348
32	N/A	N/A	N/A	N/A	N/A	N/A	N/A	0.1149
33	N/A	N/A	N/A	N/A	N/A	N/A	N/A	0.1000

Note: The table entries represent radial distance from the origin values for x_i with units (m), and electrostatic scalar potential values for U_i with units (V).

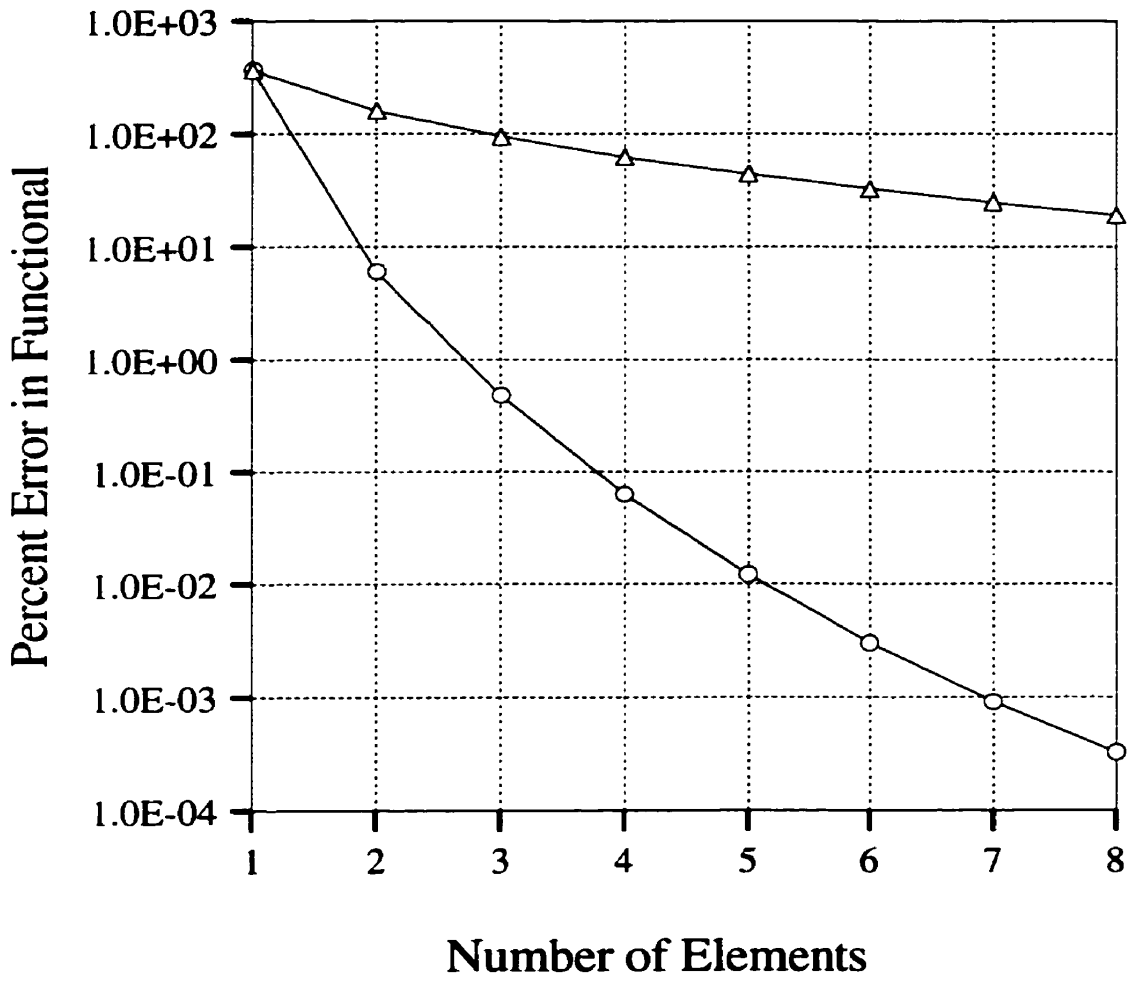

Figure 3.9: The variation of percent error in functional value with discretization level for fourth-order finite element solutions for Benchmark System 1 is illustrated. The triangle knot results correspond to percent error in functional values computed from solutions based on uniform discretizations. The circle knot results correspond to percent error in functional values computed from solutions based on optimal discretizations.

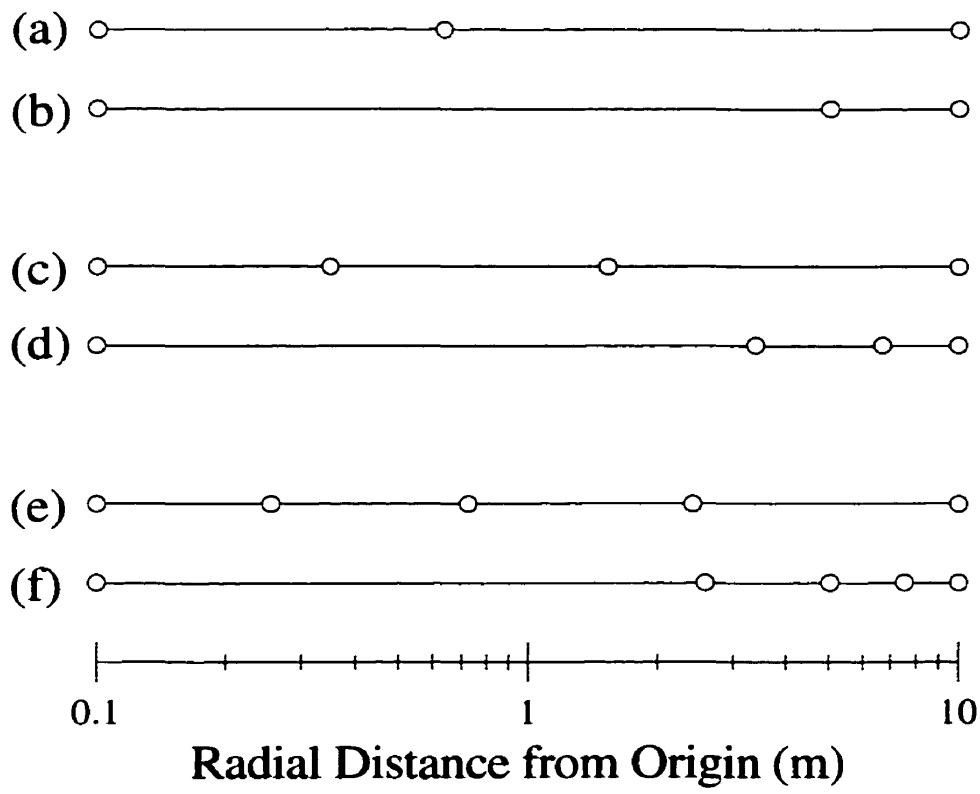

Figure 3.10: Fourth-order optimal and uniform radial discretizations for the one-dimensional electrostatic potential analysis of Benchmark System 1 are illustrated: (a) 2 element optimal mesh; (b) 2 element uniform mesh; (c) 3 element optimal mesh: (d) 3 element uniform mesh; (e) 4 element optimal mesh; (f) 4 element uniform mesh. The radial discretizations are plotted on a logarithmic scale because of the proximity of the element vertices to each other near the singularity in the optimal meshes. Note: the positions of the element vertices in the optimal meshes are specified in Table 3.7.

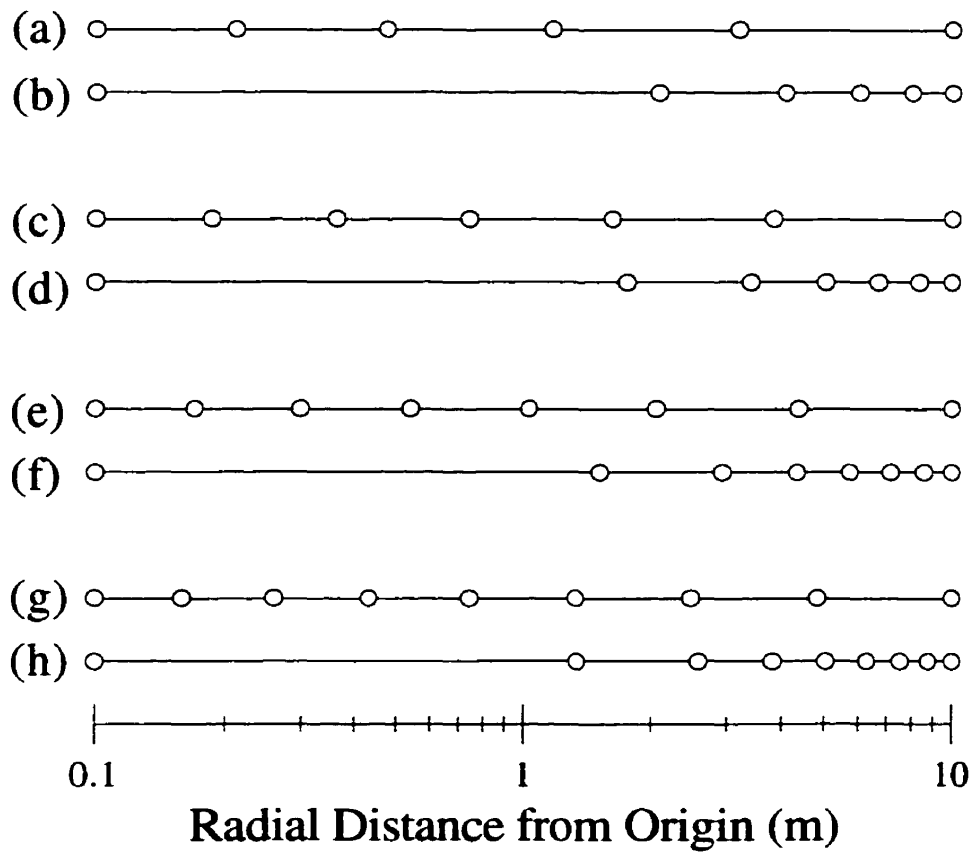

Figure 3.11: Fourth-order optimal and uniform radial discretizations for the one-dimensional electrostatic potential analysis of Benchmark System 1 are illustrated: (a) 5 element optimal mesh; (b) 5 element uniform mesh; (c) 6 element optimal mesh; (d) 6 element uniform mesh; (e) 7 element optimal mesh; (f) 7 element uniform mesh; (g) 8 element optimal mesh; (h) 8 element uniform mesh. The radial discretizations are plotted on a logarithmic scale because of the proximity of the element vertices to each other near the singularity in the optimal meshes. Note: the positions of the element vertices in the optimal meshes are specified in Table 3.8.

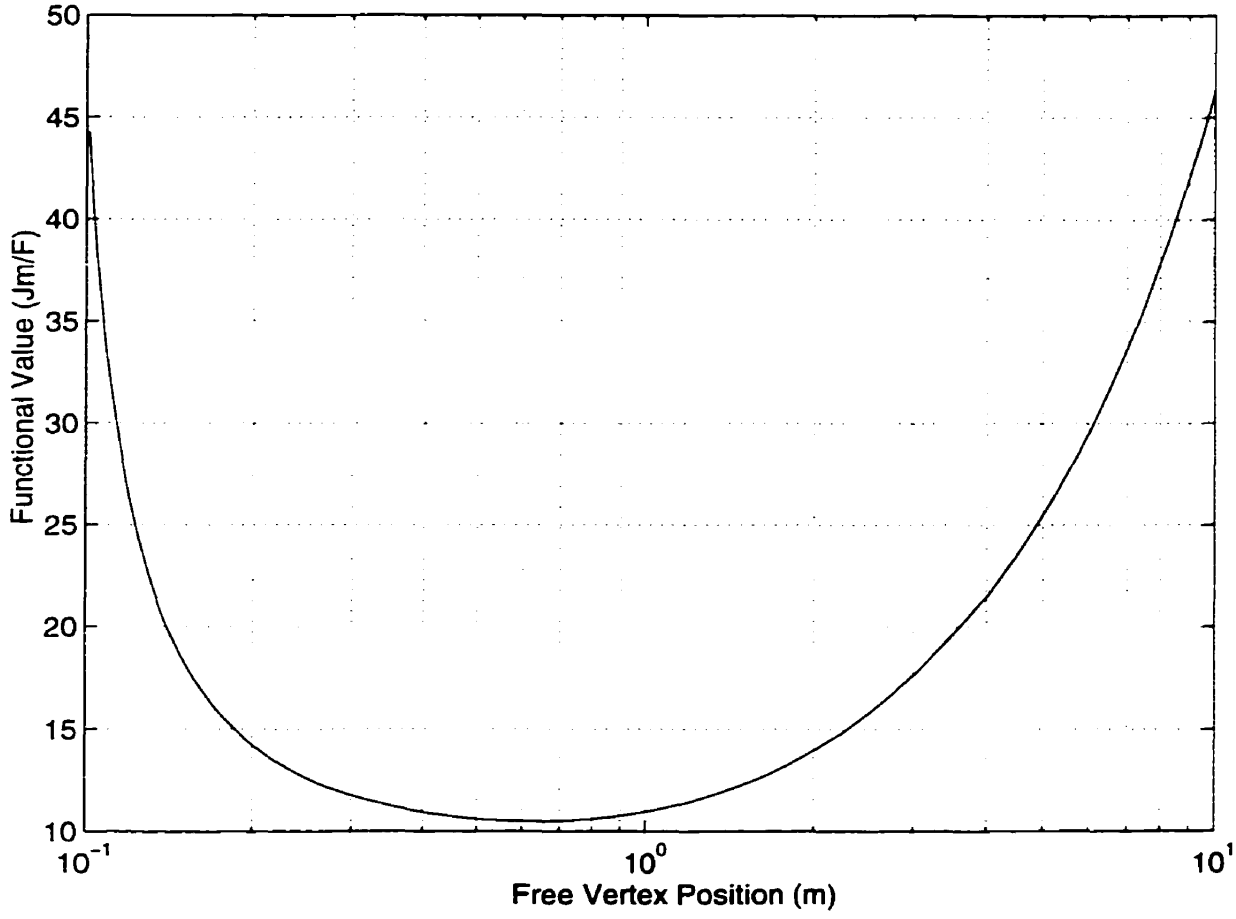

Figure 3.12: The variation in functional value with choice of free vertex position for a fourth-order two-element mesh is illustrated for Benchmark System 1. The plot is based on 100,000 functional values computed by fixing the unconstrained element vertex at 100,000 uniformly spaced positions between the two geometric boundaries of the problem domain. A logarithmic scale is used for the x-axis of the plot in order to adequately resolve the variation in the functional value near the optimal vertex position corresponding to the true minimum in the electrostatic potential energy of the discretized, fourth-order, two-element finite element model. Note: the optimal vertex position is specified in Table 3.7.

four eighth-order optimal discretizations specified by Table 3.9 and the corresponding uniform discretizations is illustrated in Figure 3.13. The efficient placement of the element vertices for the optimal discretizations is contrasted with the corresponding uniform discretizations in Figure 3.14. Finally, the results of the two-element basic computational test used to confirm the validity of the eighth-order optimal discretization results are shown in Figure 3.15. It should be noted that for each of the meshes used to compute the functional values for the eighth-order experiment, thirteen unknown scalar electric potential values were computed using the standard finite element formulation with the geometric discretization held fixed: six potential values uniquely associated with each element; and one potential value defined at the common vertex. The results of the experiment confirm the optimal position of the free vertex computed by direct solution of the finite element optimization equations, with an error tolerance of $\pm 4.95 \times 10^{-5}$ (m).

In summary, a total of 48 optimal finite element solutions were computed for Benchmark System 1 using first-, second-, fourth- and eighth-order standard Lagrangian basis functions. The accuracy of the computed optimal geometric discretization and field solution parameters was confirmed using two independent calculations, and the validity of the results was verified with basic computational experiments. These optimal discretization benchmark results will be employed in section 3.2 to analyze previously reported finite element optimality criteria and, subsequently, in section 3.3 to evaluate the performance of practical adaption models in resolving Benchmark System 1.

Table 3.9: Optimal computed values of the geometric discretization parameters, x_i, and field solution parameters, U_i, for eighth-order finite element solutions for Benchmark System 1 using N elements, where $N = 1, 2, 3, 4$.

i/N	1		2		3		4	
	x_i	U_i	x_i	U_i	x_i	U_i	x_i	U_i
1	0.1000	10.0000	0.1000	10.0000	0.1000	10.0000	0.1000	10.0000
2	10.0000	1.0430	0.8096	5.2785	0.4020	7.2585	0.2804	8.1600
3	N/A	0.7112	10.0000	3.6149	1.8374	5.6989	0.8490	6.8921
4	N/A	0.3891	N/A	2.7253	10.0000	4.6890	2.7919	5.9650
5	N/A	0.2479	N/A	2.1922	N/A	3.9839	10.0000	5.2578
6	N/A	0.2393	N/A	1.8408	N/A	3.4636	N/A	4.7006
7	N/A	0.1442	N/A	1.5750	N/A	3.0625	N/A	4.2501
8	N/A	0.1337	N/A	1.3844	N/A	2.7455	N/A	3.8784
9	N/A	0.1000	N/A	1.2308	N/A	2.4876	N/A	3.5665
10	N/A	N/A	N/A	0.5039	N/A	1.7194	N/A	2.8452
11	N/A	N/A	N/A	0.3255	N/A	1.3147	N/A	2.3667
12	N/A	N/A	N/A	0.2343	N/A	1.0633	N/A	2.0259
13	N/A	N/A	N/A	0.1841	N/A	0.8930	N/A	1.7709
14	N/A	N/A	N/A	0.1539	N/A	0.7699	N/A	1.5730
15	N/A	N/A	N/A	0.1291	N/A	0.6762	N/A	1.4148
16	N/A	N/A	N/A	0.1134	N/A	0.6032	N/A	1.2855
17	N/A	N/A	N/A	0.1000	N/A	0.5442	N/A	1.1779
18	N/A	N/A	N/A	N/A	N/A	0.3497	N/A	0.9159
19	N/A	N/A	N/A	N/A	N/A	0.2580	N/A	0.7493
20	N/A	N/A	N/A	N/A	N/A	0.2041	N/A	0.6339
21	N/A	N/A	N/A	N/A	N/A	0.1689	N/A	0.5493
22	N/A	N/A	N/A	N/A	N/A	0.1442	N/A	0.4847
23	N/A	N/A	N/A	N/A	N/A	0.1256	N/A	0.4336
24	N/A	N/A	N/A	N/A	N/A	0.1114	N/A	0.3923
25	N/A	N/A	N/A	N/A	N/A	0.1000	N/A	0.3582
26	N/A	N/A	N/A	N/A	N/A	N/A	N/A	0.2708
27	N/A	N/A	N/A	N/A	N/A	N/A	N/A	0.2177
28	N/A	N/A	N/A	N/A	N/A	N/A	N/A	0.1820
29	N/A	N/A	N/A	N/A	N/A	N/A	N/A	0.1563
30	N/A	N/A	N/A	N/A	N/A	N/A	N/A	0.1371
31	N/A	N/A	N/A	N/A	N/A	N/A	N/A	0.1220
32	N/A	N/A	N/A	N/A	N/A	N/A	N/A	0.1099
33	N/A	N/A	N/A	N/A	N/A	N/A	N/A	0.1000

Note: The table entries represent radial distance from the origin values for x_i with units (m), and electrostatic scalar potential values for U_i with units (V).

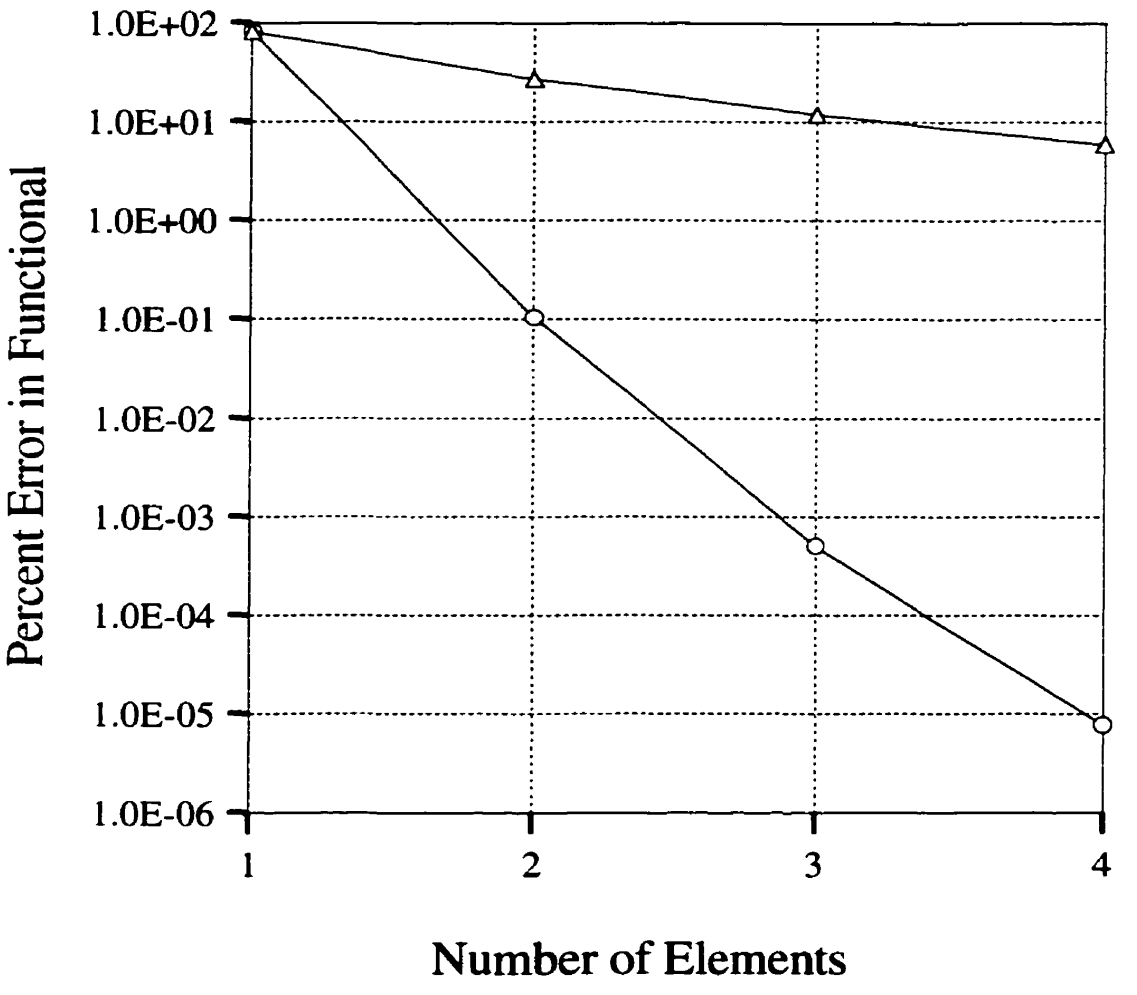

Figure 3.13: The variation of percent error in functional value with discretization level for eighth-order finite element solutions for Benchmark System 1 is illustrated. The triangle knot results correspond to percent error in functional values computed from solutions based on uniform discretizations. The circle knot results correspond to percent error in functional values computed from solutions based on optimal discretizations.

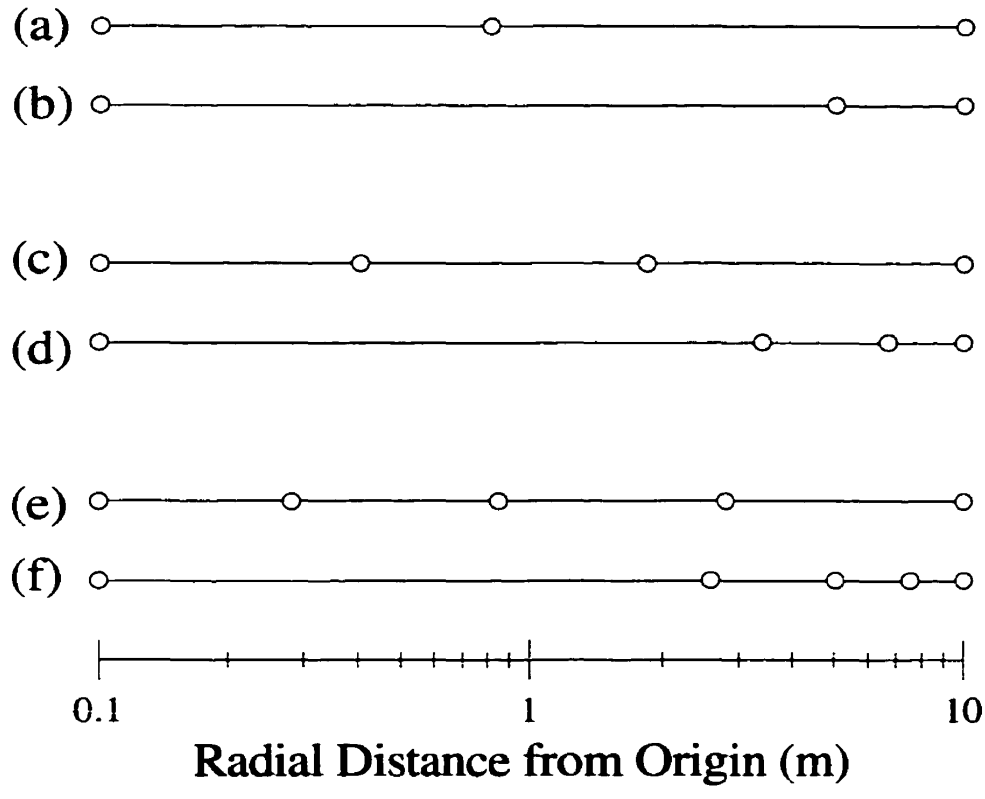

Figure 3.14: Eighth-order optimal and uniform radial discretizations for the one-dimensional electrostatic potential analysis of Benchmark System 1 are illustrated: (a) 2 element optimal mesh; (b) 2 element uniform mesh; (c) 3 element optimal mesh; (d) 3 element uniform mesh; (e) 4 element optimal mesh; (f) 4 element uniform mesh. The radial discretizations are plotted on a logarithmic scale because of the proximity of the element vertices to each other near the singularity in the optimal meshes. Note: the positions of the element vertices in the optimal meshes are specified in Table 3.9.

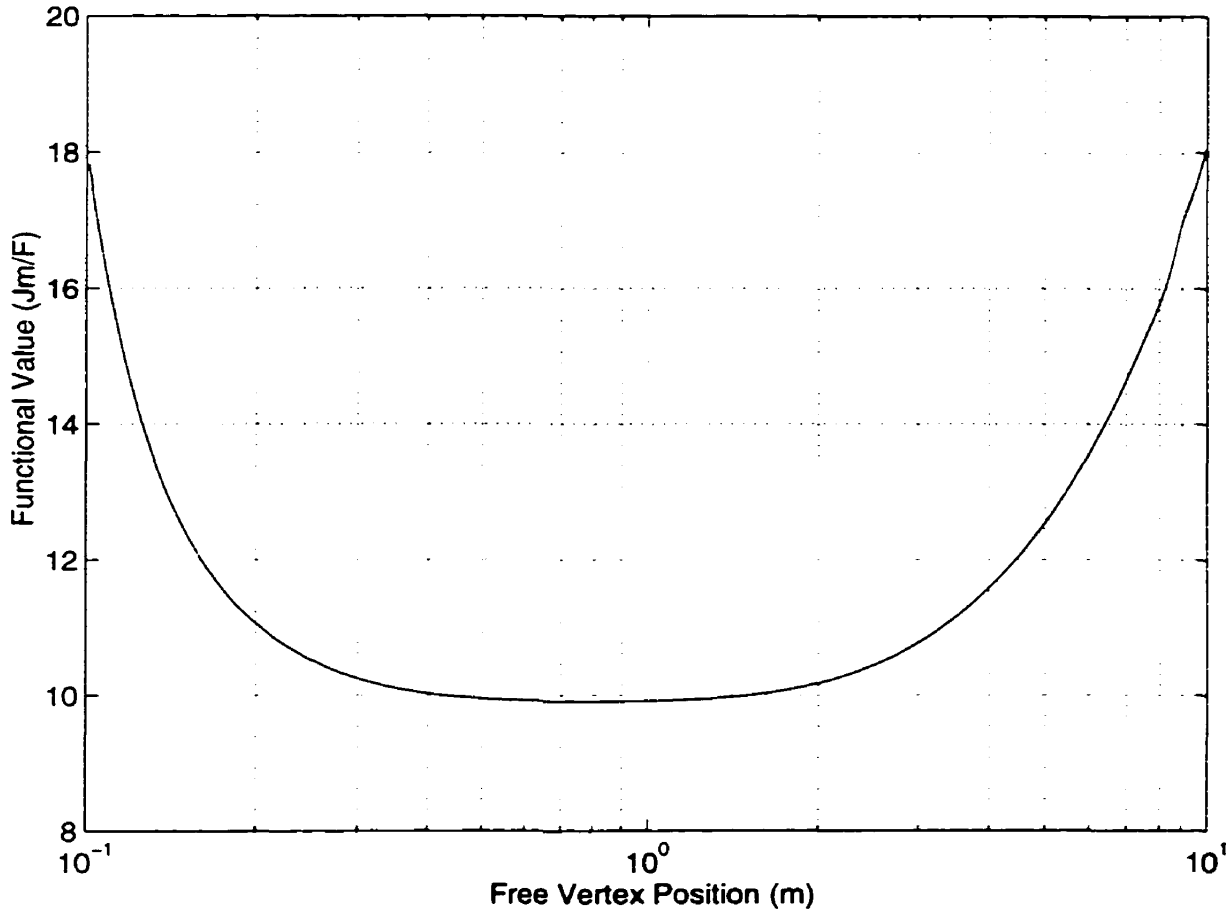

Figure 3.15: The variation in functional value with choice of free vertex position for an eighth-order two-element mesh is illustrated for Benchmark System 1. The plot is based on 100,000 functional values computed by fixing the unconstrained element vertex at 100,000 uniformly spaced positions between the two geometric boundaries of the problem domain. A logarithmic scale is used for the x-axis of the plot in order to adequately resolve the variation in the functional value near the optimal vertex position corresponding to the true minimum in the electrostatic potential energy of the discretized, eighth-order, two-element finite element model. Note: the optimal vertex position is specified in Table 3.9.

3.1.2 Benchmark System 2

The second benchmark system is based on a straight, infinitely long, uniform, static line current in free space. The objective for this benchmark system is to compute the functional value based on the resolution of a radial neighborhood close to the line current and spanning a 100-fold decay in magnetic vector potential magnitude: the line current, of magnitude 5×10^6 (A), is directed along the positive z-coordinate axis in a circular-cylindrical reference coordinate system, and the two boundaries of the problem domain are fixed at radial distances of 0.1 (m) and 10 (m) away from the current. The primary feature of this system is the rapid field solution variation close to the singular current source distribution. This feature is common to many devices that contain sharp material edges, and has been shown to drastically reduce the convergence rate of the finite element method.

The magnetostatic system used to establish the optimal discretization benchmark results of this section was analyzed for magnetic vector potential using the one-dimensional finite element formulation and the corresponding finite element optimization equations derived in section 2.4.1. The optimal discretization benchmark results for this magnetostatic system were computed using exactly the same procedures that were used for Benchmark System 1. Furthermore, the same range of results were computed, and the same measures were taken to confirm the accuracy of the numerical results that were computed and the validity of the formulation and the solution methods that were employed to compute these results. Unlike Benchmark System 1, the analytical magnetic vector potential field solution for Benchmark System 2 is, formally, a vector field. However, the physical symmetry inherent in the magnetostatic system results in a single, z-directed, field component for the magnetic vector potential corresponding to the system. Moreover, the field solution variation of the system can be characterized mathematically by one space variable. Therefore, the same scalar one-dimensional finite element formulation presented in section 2.4.1

and used in section 3.1.1 for the analysis of Benchmark System 1, was also used for the analysis of Benchmark System 2 in this section.

The optimal values of the geometric discretization parameters, x_i, and the field solution parameters, U_i, for the series of 20 optimal first-order finite element solutions that were computed for Benchmark System 2 are reported in Tables 3.10–3.12. The convergence in percent error of the functional values computed from these optimal discretizations and the corresponding uniform discretizations is illustrated in Figure 3.16. The results of the two-element basic computational test which was used to confirm the validity of the first-order optimal discretization results for Benchmark System 2 are shown in Figure 3.17. Similarly, the series of 16 optimal second-order finite element solutions computed for Benchmark System 2 are reported in Tables 3.13–3.15; the convergence in the percent errors of the optimal discretization-based and uniform discretization-based functional values are compared in Figure 3.18; and the results of the second-order two-element numerical validation experiment are shown in Figure 3.19. The analogous set of fourth-order results for Benchmark System 2 are presented in Tables 3.16–3.17, Figure 3.20 and Figure 3.21. In addition, the equivalent set of eighth-order results are given in Table 3.18, Figure 3.22 and Figure 3.23. The superior accuracy in the functional values computed from the optimal discretization solutions relative to the uniform results for this benchmark system may be noted for the first-, second-, fourth- and eighth-order cases in Figure 3.16, Figure 3.18, Figure 3.20 and Figure 3.22, respectively. Finally, all of the first-, second-, fourth-, and eighth-order numerical validation experiments confirmed, with the same error tolerance reported for Benchmark System 1, that the optimal position of the free vertex computed by direct solution of the finite element optimization equations correctly corresponds to the smallest possible functional value in each case, as illustrated by Figure 3.17, Figure 3.19, Figure 3.21 and Figure 3.23, respectively.

Although the analyses of Benchmark System 1 and Benchmark System 2 are very similar, there are some important differences which are discussed next. First, the

Table 3.10: Optimal computed values of the geometric discretization parameters, x_i, and field solution parameters, U_i, for first-order finite element solutions for Benchmark System 2 using N elements, where $N = 1, 2, \ldots, 8$.

i/N	1		2		3		4	
	x_i	U_i	x_i	U_i	x_i	U_i	x_i	U_i
1	0.1000	4.6517	0.1000	4.6517	0.1000	4.6517	0.1000	4.6517
2	10.0000	0.0465	1.0000	2.3491	0.4642	3.1166	0.3162	3.5004
3	N/A	N/A	10.0000	0.0465	2.1544	1.5816	1.0000	2.3491
4	N/A	N/A	N/A	N/A	10.0000	0.0465	3.1623	1.1978
5	N/A	N/A	N/A	N/A	N/A	N/A	10.0000	0.0465

i/N	5		6		7		8	
	x_i	U_i	x_i	U_i	x_i	U_i	x_i	U_i
1	0.1000	4.6517	0.1000	4.6517	0.1000	4.6517	0.1000	4.6517
2	0.2512	3.7306	0.2154	3.8842	0.1931	3.9938	0.1778	4.0760
3	0.6310	2.8096	0.4642	3.1166	0.3728	3.3359	0.3162	3.5004
4	1.5849	1.8886	1.0000	2.3491	0.7197	2.6780	0.5623	2.9247
5	3.9811	0.9675	2.1544	1.5816	1.3895	2.0202	1.0000	2.3491
6	10.0000	0.0465	4.6416	0.8140	2.6827	1.3623	1.7783	1.7735
7	N/A	N/A	10.0000	0.0465	5.1795	0.7044	3.1623	1.1978
8	N/A	N/A	N/A	N/A	10.0000	0.0465	5.6234	0.6222
9	N/A	N/A	N/A	N/A	N/A	N/A	10.0000	0.0465

Note: The table entries represent radial distance from the origin values for x_i with units (m), and vector magnetic potential values for U_i with units (Wb/m).

Table 3.11: Optimal computed values of the geometric discretization parameters, x_i, and field solution parameters, U_i, for first-order finite element solutions for Benchmark System 2 using N elements, where $N = 9, 10, \ldots, 16$.

i/N	9		10		11		12	
	x_i	U_i	x_i	U_i	x_i	U_i	x_i	U_i
1	0.1000	4.6517	0.1000	4.6517	0.1000	4.6517	0.1000	4.6517
2	0.1668	4.1400	0.1585	4.1912	0.1520	4.2330	0.1468	4.2679
3	0.2783	3.6283	0.2512	3.7307	0.2310	3.8144	0.2154	3.8842
4	0.4642	3.1166	0.3981	3.2701	0.3511	3.3957	0.3162	3.5004
5	0.7743	2.6049	0.6310	2.8096	0.5337	2.9771	0.4642	3.1166
6	1.2915	2.0933	1.0000	2.3491	0.8111	2.5584	0.6813	2.7329
7	2.1544	1.5816	1.5849	1.8886	1.2328	2.1398	1.0000	2.3491
8	3.5938	1.0699	2.5119	1.4281	1.8738	1.7211	1.4678	1.9653
9	5.9948	0.5582	3.9811	0.9676	2.8480	1.3025	2.1544	1.5816
10	10.0000	0.0465	6.3096	0.5070	4.3288	0.8838	3.1623	1.1978
11	N/A	N/A	10.0000	0.0465	6.5793	0.4652	4.6416	0.8140
12	N/A	N/A	N/A	N/A	10.0000	0.0465	6.8129	0.4303
13	N/A	N/A	N/A	N/A	N/A	N/A	10.0000	0.0465

i/N	13		14		15		16	
	x_i	U_i	x_i	U_i	x_i	U_i	x_i	U_i
1	0.1000	4.6517	0.1000	4.6517	0.1000	4.6517	0.1000	4.6517
2	0.1425	4.2974	0.1389	4.3227	0.1359	4.3447	0.1334	4.3639
3	0.2031	3.9432	0.1931	3.9938	0.1848	4.0377	0.1778	4.0760
4	0.2894	3.5890	0.2683	3.6649	0.2512	3.7307	0.2371	3.7882
5	0.4125	3.2347	0.3728	3.3359	0.3415	3.4236	0.3162	3.5004
6	0.5878	2.8805	0.5179	3.0070	0.4642	3.1166	0.4217	3.2126
7	0.8377	2.5262	0.7197	2.6780	0.6310	2.8096	0.5623	2.9247
8	1.1938	2.1720	1.0000	2.3491	0.8577	2.5026	0.7499	2.6369
9	1.7013	1.8177	1.3895	2.0202	1.1659	2.1956	1.0000	2.3491
10	2.4245	1.4635	1.9307	1.6912	1.5849	1.8886	1.3335	2.0613
11	3.4551	1.1092	2.6827	1.3623	2.1544	1.5816	1.7783	1.7735
12	4.9239	0.7550	3.7276	1.0333	2.9286	1.2746	2.3714	1.4856
13	7.0170	0.4008	5.1795	0.7044	3.9811	0.9676	3.1623	1.1978
14	10.0000	0.0465	7.1969	0.3755	5.4117	0.6605	4.2170	0.9100
15	N/A	N/A	10.0000	0.0465	7.3564	0.3535	5.6234	0.6222
16	N/A	N/A	N/A	N/A	10.0000	0.0465	7.4989	0.3343
17	N/A	N/A	N/A	N/A	N/A	N/A	10.0000	0.0465

Note: The table entries represent radial distance from the origin values for x_i with units (m), and vector magnetic potential values for U_i with units (Wb/m).

Table 3.12: Optimal computed values of the geometric discretization parameters, x_i, and field solution parameters, U_i, for first-order finite element solutions for Benchmark System 2 using N elements, where $N = 17, 18, 19, 20$.

i/N	17		18		19		20	
	x_i	U_i	x_i	U_i	x_i	U_i	x_i	U_i
1	0.1000	4.6517	0.1000	4.6517	0.1000	4.6517	0.1000	4.6517
2	0.1311	4.3808	0.1292	4.3958	0.1274	4.4093	0.1259	4.4214
3	0.1719	4.1099	0.1668	4.1400	0.1624	4.1669	0.1585	4.1912
4	0.2254	3.8390	0.2154	3.8842	0.2069	3.9246	0.1995	3.9609
5	0.2955	3.5681	0.2783	3.6283	0.2637	3.6822	0.2512	3.7307
6	0.3875	3.2972	0.3594	3.3725	0.3360	3.4398	0.3162	3.5004
7	0.5080	3.0263	0.4642	3.1166	0.4281	3.1974	0.3981	3.2701
8	0.6661	2.7554	0.5995	2.8608	0.5456	2.9550	0.5012	3.0399
9	0.8733	2.4845	0.7743	2.6049	0.6952	2.7127	0.6310	2.8096
10	1.1450	2.2137	1.0000	2.3491	0.8859	2.4703	0.7943	2.5794
11	1.5013	1.9428	1.2915	2.0933	1.1288	2.2279	1.0000	2.3491
12	1.9684	1.6719	1.6681	1.8374	1.4384	1.9855	1.2589	2.1188
13	2.5809	1.4010	2.1544	1.5816	1.8330	1.7432	1.5849	1.8886
14	3.3839	1.1301	2.7826	1.3275	2.3357	1.5008	1.9953	1.6583
15	4.4367	0.8592	3.5938	1.0699	2.9764	1.2584	2.5119	1.4281
16	5.8171	0.5883	4.6416	0.8140	3.7927	1.0160	3.1623	1.1978
17	7.6270	0.3174	5.9948	0.5582	4.8329	0.7736	3.9811	0.9676
18	10.0000	0.0465	7.7426	0.3024	6.1585	0.5313	5.0119	0.7373
19	N/A	N/A	10.0000	0.0465	7.8476	0.2889	6.3096	0.5070
20	N/A	N/A	N/A	N/A	10.0000	0.0465	7.9433	0.2768
21	N/A	N/A	N/A	N/A	N/A	N/A	10.0000	0.0465

Note: The table entries represent radial distance from the origin values for x_i with units (m), and vector magnetic potential values for U_i with units (Wb/m).

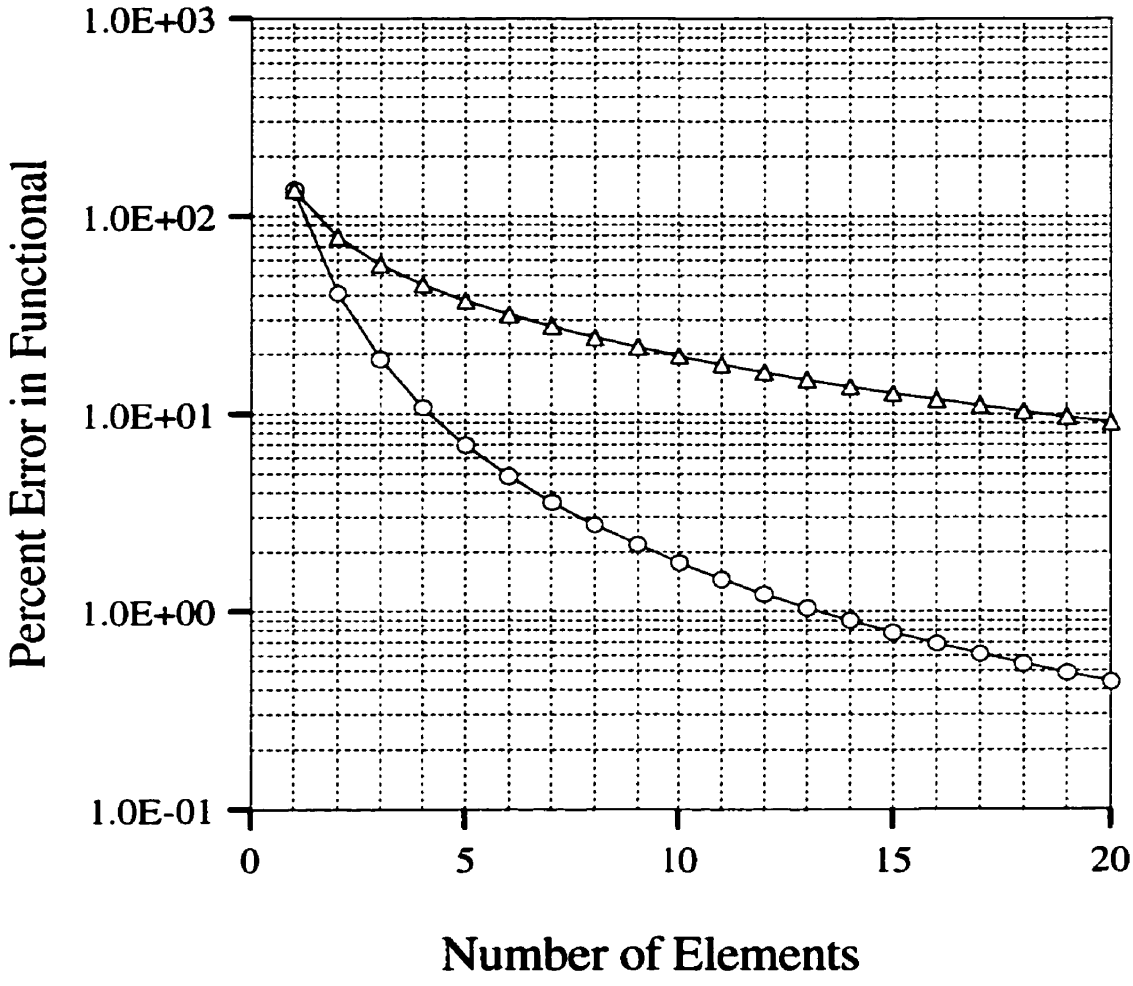

Figure 3.16: The variation of percent error in functional value with discretization level for first-order finite element solutions for Benchmark System 2 is illustrated. The triangle knot results correspond to percent error in functional values computed from solutions based on uniform discretizations. The circle knot results correspond to percent error in functional values computed from solutions based on optimal discretizations.

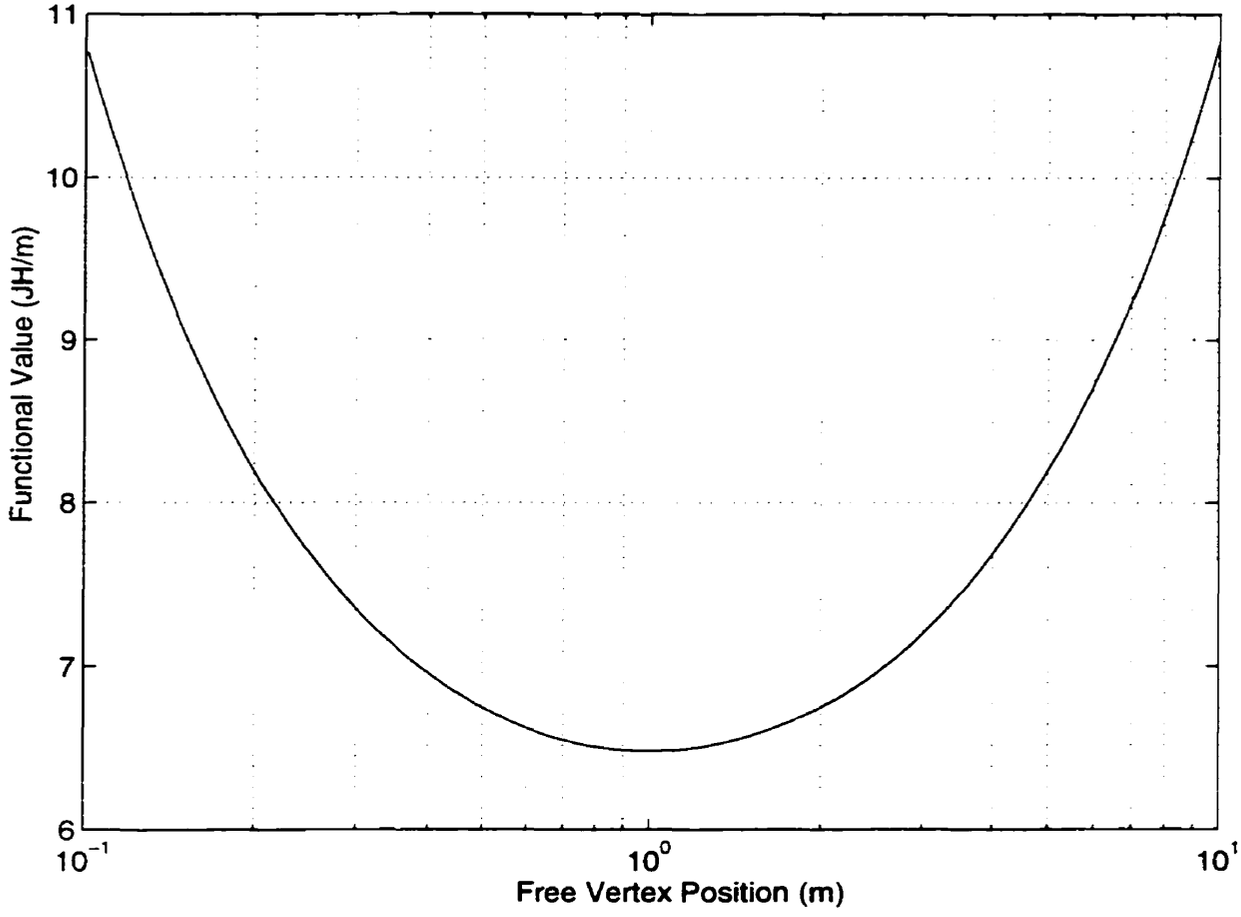

Figure 3.17: The variation in functional value with choice of free vertex position for a first-order two-element mesh is illustrated for Benchmark System 2. The plot is based on 100,000 functional values computed by fixing the unconstrained element vertex at 100,000 uniformly spaced positions between the two geometric boundaries of the problem domain. A logarithmic scale is used for the x-axis of the plot in order to adequately resolve the variation in the functional value near the optimal vertex position corresponding to the true minimum in the magnetostatic potential energy of the discretized, first-order, two-element finite element model. Note: the optimal vertex position is specified in Table 3.10.

Table 3.13: Optimal computed values of the geometric discretization parameters, x_i, and field solution parameters, U_i, for second-order finite element solutions for Benchmark System 2 using N elements, where $N = 1, 2, \ldots, 8$.

i/N	1		2		3		4	
	x_i	U_i	x_i	U_i	x_i	U_i	x_i	U_i
1	0.1000	4.6517	0.1000	4.6517	0.1000	4.6517	0.1000	4.6517
2	10.0000	1.2206	1.0000	3.0294	0.4642	3.6364	0.3162	3.9265
3	N/A	0.0465	10.0000	2.3491	2.1544	3.1166	1.0000	3.5004
4	N/A	N/A	N/A	0.7268	10.0000	2.1014	3.1623	2.7752
5	N/A	N/A	N/A	0.0465	N/A	1.5816	10.0000	2.3491
6	N/A	N/A	N/A	N/A	N/A	0.5663	N/A	1.6239
7	N/A	N/A	N/A	N/A	N/A	0.0465	N/A	1.1978
8	N/A	N/A	N/A	N/A	N/A	N/A	N/A	0.4726
9	N/A	N/A	N/A	N/A	N/A	N/A	N/A	0.0465

i/N	5		6		7		8	
	x_i	U_i	x_i	U_i	x_i	U_i	x_i	U_i
1	0.1000	4.6517	0.1000	4.6517	0.1000	4.6517	0.1000	4.6517
2	0.2512	4.0920	0.2154	4.1977	0.1931	4.2705	0.1778	4.3235
3	0.6310	3.7307	0.4642	3.8842	0.3728	3.9938	0.3162	4.0760
4	1.5849	3.1710	1.0000	3.4302	0.7197	3.6126	0.5623	3.7479
5	3.9811	2.8096	2.1544	3.1166	1.3895	3.3359	1.0000	3.5004
6	10.0000	2.2500	4.6416	2.6626	2.6827	2.9548	1.7783	3.1723
7	N/A	1.8886	10.0000	2.3491	5.1795	2.6780	3.1623	2.9247
8	N/A	1.3289	N/A	1.8951	10.0000	2.2969	5.6234	2.5966
9	N/A	0.9676	N/A	1.5816	N/A	2.0202	10.0000	2.3491
10	N/A	0.4079	N/A	1.1276	N/A	1.6390	N/A	2.0210
11	N/A	0.0465	N/A	0.8140	N/A	1.3623	N/A	1.7735
12	N/A	N/A	N/A	0.3601	N/A	0.9811	N/A	1.4453
13	N/A	N/A	N/A	0.0465	N/A	0.7044	N/A	1.1978
14	N/A	N/A	N/A	N/A	N/A	0.3232	N/A	0.8697
15	N/A	N/A	N/A	N/A	N/A	0.0465	N/A	0.6222
16	N/A	N/A	N/A	N/A	N/A	N/A	N/A	0.2940
17	N/A	N/A	N/A	N/A	N/A	N/A	N/A	0.0465

Note: The table entries represent radial distance from the origin values for x_i with units (m), and vector magnetic potential values for U_i with units (Wb/m).

Table 3.14: Optimal computed values of the geometric discretization parameters, x_i, and field solution parameters, U_i, for second-order finite element solutions for Benchmark System 2 using N elements, where $N = 9, 10, 11, 12$.

i/N	9		10		11		12	
	x_i	U_i	x_i	U_i	x_i	U_i	x_i	U_i
1	0.1000	4.6517	0.1000	4.6517	0.1000	4.6517	0.1000	4.6517
2	0.1668	4.3638	0.1585	4.3954	0.1520	4.4208	0.1468	4.4416
3	0.2783	4.1400	0.2512	4.1912	0.2310	4.2330	0.2154	4.2679
4	0.4642	3.8521	0.3981	3.9349	0.3511	4.0021	0.3162	4.0579
5	0.7743	3.6283	0.6310	3.7307	0.5337	3.8144	0.4642	3.8842
6	1.2915	3.3404	1.0000	3.4743	0.8111	3.5835	0.6813	3.6741
7	2.1544	3.1166	1.5849	3.2701	1.2328	3.3957	1.0000	3.5004
8	3.5938	2.8288	2.5119	3.0138	1.8738	3.1648	1.4678	3.2903
9	5.9948	2.6049	3.9811	2.8096	2.8480	2.9771	2.1544	3.1166
10	10.0000	2.3171	6.3096	2.5533	4.3288	2.7462	3.1623	2.9066
11	N/A	2.0933	10.0000	2.3491	6.5793	2.5584	4.6416	2.7329
12	N/A	1.8054	N/A	2.0928	10.0000	2.3275	6.8129	2.5228
13	N/A	1.5816	N/A	1.8886	N/A	2.1398	10.0000	2.3491
14	N/A	1.2937	N/A	1.6323	N/A	1.9089	N/A	2.1390
15	N/A	1.0699	N/A	1.4281	N/A	1.7211	N/A	1.9653
16	N/A	0.7820	N/A	1.1718	N/A	1.4902	N/A	1.7553
17	N/A	0.5582	N/A	0.9676	N/A	1.3025	N/A	1.5816
18	N/A	0.2703	N/A	0.7112	N/A	1.0716	N/A	1.3715
19	N/A	0.0465	N/A	0.5070	N/A	0.8838	N/A	1.1978
20	N/A	N/A	N/A	0.2507	N/A	0.6529	N/A	0.9877
21	N/A	N/A	N/A	0.0465	N/A	0.4652	N/A	0.8140
22	N/A	N/A	N/A	N/A	N/A	0.2342	N/A	0.6040
23	N/A	N/A	N/A	N/A	N/A	0.0465	N/A	0.4303
24	N/A	N/A	N/A	N/A	N/A	N/A	N/A	0.2202
25	N/A	N/A	N/A	N/A	N/A	N/A	N/A	0.0465

Note: The table entries represent radial distance from the origin values for x_i with units (m), and vector magnetic potential values for U_i with units (Wb/m).

Table 3.15: Optimal computed values of the geometric discretization parameters, x_i, and field solution parameters, U_i, for second-order finite element solutions for Benchmark System 2 using N elements, where $N = 13, 14, 15, 16$.

i/N	13		14		15		16	
	x_i	U_i	x_i	U_i	x_i	U_i	x_i	U_i
1	0.1000	4.6517	0.1000	4.6517	0.1000	4.6517	0.1000	4.6517
2	0.1425	4.4590	0.1389	4.4738	0.1359	4.4865	0.1334	4.4975
3	0.2031	4.2974	0.1931	4.3227	0.1848	4.3447	0.1778	4.3639
4	0.2894	4.1048	0.2683	4.1449	0.2512	4.1795	0.2371	4.2097
5	0.4125	3.9432	0.3728	3.9938	0.3415	4.0377	0.3162	4.0760
6	0.5878	3.7506	0.5179	3.8159	0.4642	3.8725	0.4217	3.9218
7	0.8377	3.5890	0.7197	3.6649	0.6310	3.7307	0.5623	3.7882
8	1.1938	3.3963	1.0000	3.4870	0.8577	3.5655	0.7499	3.6340
9	1.7013	3.2347	1.3895	3.3359	1.1659	3.4236	1.0000	3.5004
10	2.4245	3.0421	1.9307	3.1580	1.5849	3.2584	1.3335	3.3462
11	3.4551	2.8805	2.6827	3.0070	2.1544	3.1166	1.7783	3.2126
12	4.9239	2.6878	3.7276	2.8291	2.9286	2.9514	2.3714	3.0584
13	7.0170	2.5262	5.1795	2.6780	3.9811	2.8096	3.1623	2.9247
14	10.0000	2.3336	7.1969	2.5002	5.4117	2.6444	4.2170	2.7706
15	N/A	2.1720	10.0000	2.3491	7.3564	2.5026	5.6234	2.6369
16	N/A	1.9793	N/A	2.1712	10.0000	2.3374	7.4989	2.4827
17	N/A	1.8177	N/A	2.0202	N/A	2.1956	10.0000	2.3491
18	N/A	1.6251	N/A	1.8423	N/A	2.0304	N/A	2.1949
19	N/A	1.4635	N/A	1.6912	N/A	1.8886	N/A	2.0613
20	N/A	1.2708	N/A	1.5133	N/A	1.7234	N/A	1.9071
21	N/A	1.1092	N/A	1.3623	N/A	1.5816	N/A	1.7735
22	N/A	0.9166	N/A	1.1844	N/A	1.4164	N/A	1.6193
23	N/A	0.7550	N/A	1.0333	N/A	1.2746	N/A	1.4856
24	N/A	0.5624	N/A	0.8555	N/A	1.1094	N/A	1.3314
25	N/A	0.4008	N/A	0.7044	N/A	0.9676	N/A	1.1978
26	N/A	0.2081	N/A	0.5265	N/A	0.8024	N/A	1.0436
27	N/A	0.0465	N/A	0.3755	N/A	0.6605	N/A	0.9100
28	N/A	N/A	N/A	0.1976	N/A	0.4953	N/A	0.7558
29	N/A	N/A	N/A	0.0465	N/A	0.3535	N/A	0.6222
30	N/A	N/A	N/A	N/A	N/A	0.1883	N/A	0.4680
31	N/A	N/A	N/A	N/A	N/A	0.0465	N/A	0.3343
32	N/A	N/A	N/A	N/A	N/A	N/A	N/A	0.1801
33	N/A	N/A	N/A	N/A	N/A	N/A	N/A	0.0465

Note: The table entries represent radial distance from the origin values for x_i with units (m), and vector magnetic potential values for U_i with units (Wb/m).

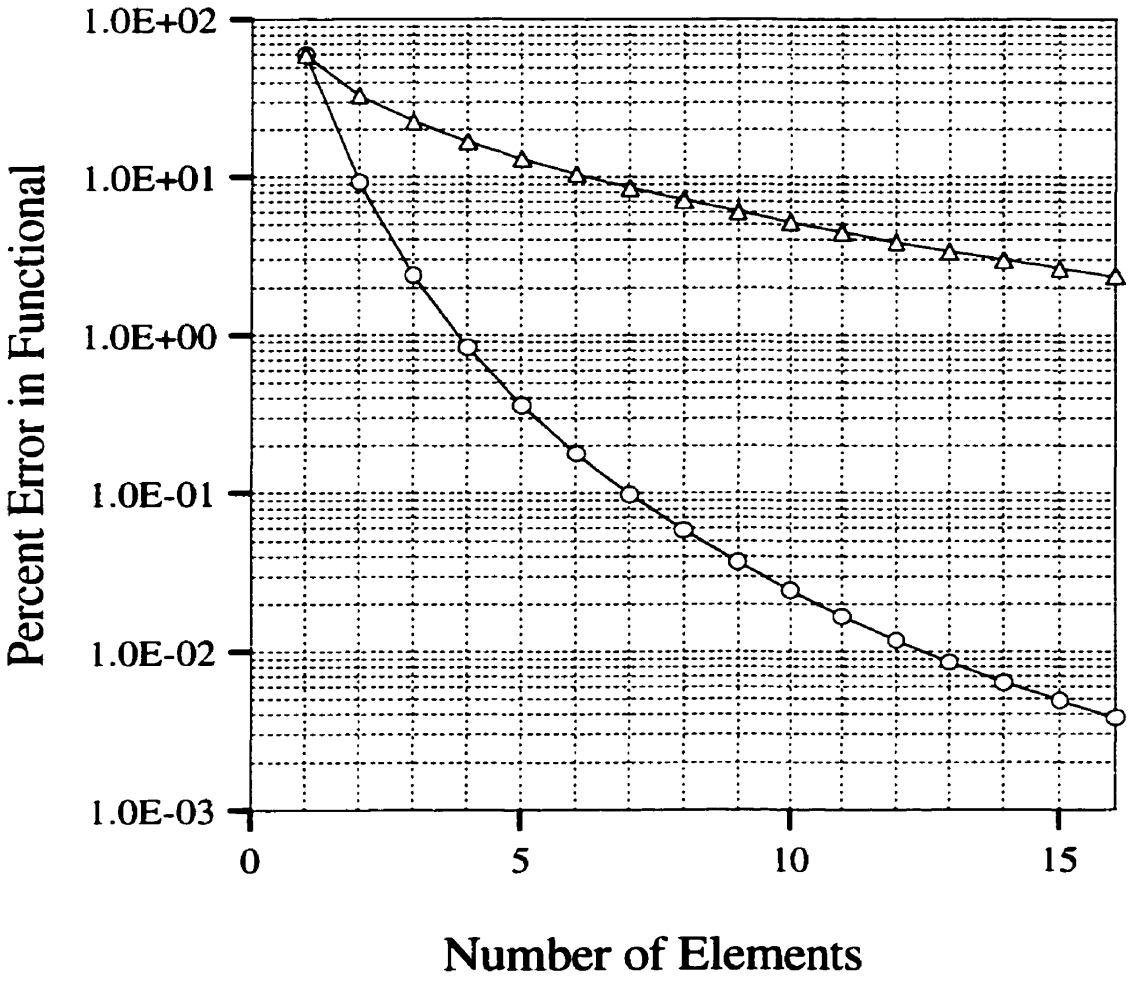

Figure 3.18: The variation of percent error in functional value with discretization level for second-order finite element solutions for Benchmark System 2 is illustrated. The triangle knot results correspond to percent error in functional values computed from solutions based on uniform discretizations. The circle knot results correspond to percent error in functional values computed from solutions based on optimal discretizations.

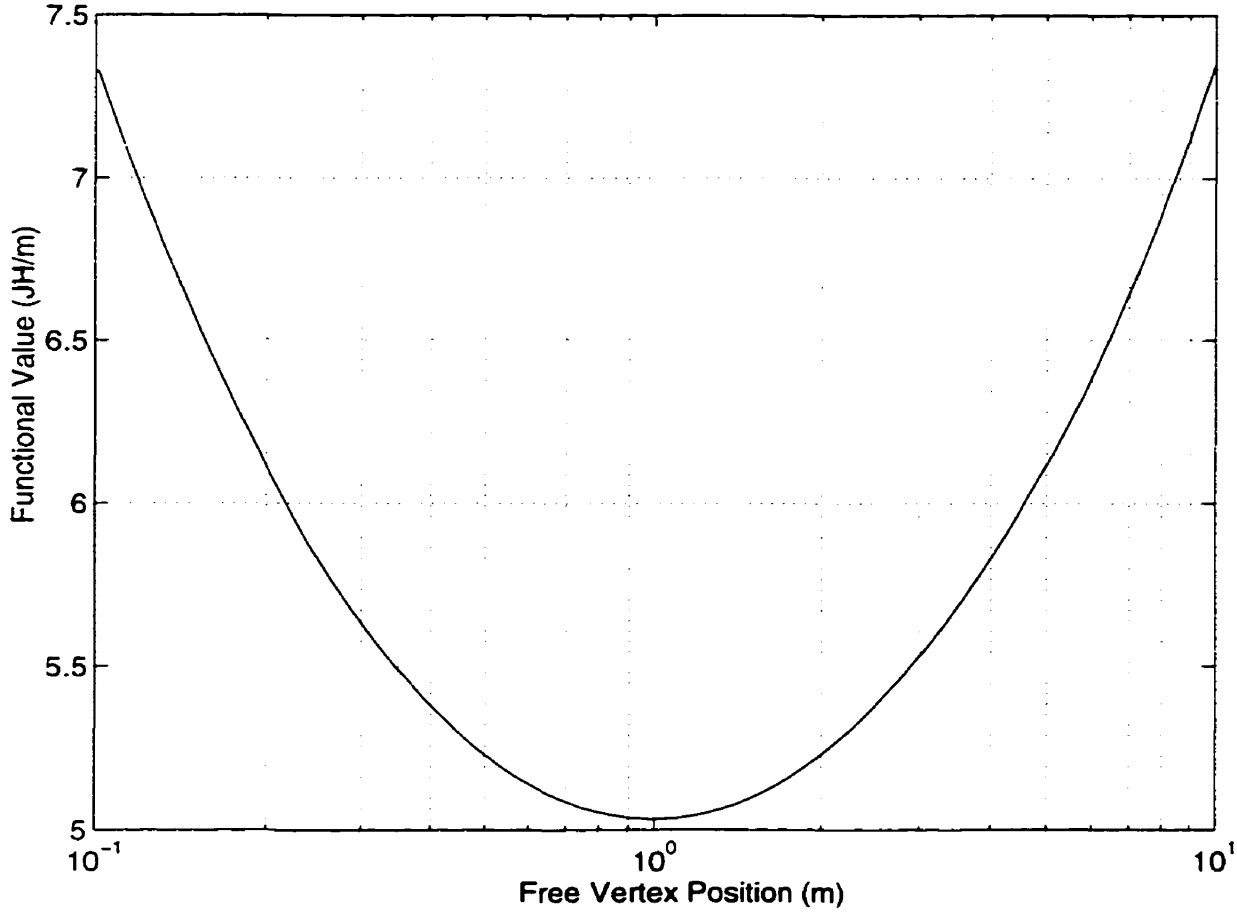

Figure 3.19: The variation in functional value with choice of free vertex position for a second-order two-element mesh is illustrated for Benchmark System 2. The plot is based on 100,000 functional values computed by fixing the unconstrained element vertex at 100,000 uniformly spaced positions between the two geometric boundaries of the problem domain. A logarithmic scale is used for the x-axis of the plot in order to adequately resolve the variation in the functional value near the optimal vertex position corresponding to the true minimum in the magnetostatic potential energy of the discretized, second-order, two-element finite element model. Note: the optimal vertex position is specified in Table 3.13.

Table 3.16: Optimal computed values of the geometric discretization parameters, x_i, and field solution parameters, U_i, for fourth-order finite element solutions for Benchmark System 2 using N elements, where $N = 1, 2, 3, 4$.

i/N	1		2		3		4	
	x_i	U_i	x_i	U_i	x_i	U_i	x_i	U_i
1	0.1000	4.6517	0.1000	4.6517	0.1000	4.6517	0.1000	4.6517
2	10.0000	1.6198	1.0000	3.4682	0.4642	4.0021	0.3162	4.2188
3	N/A	0.8568	10.0000	2.9485	2.1544	3.6144	1.0000	3.9187
4	N/A	0.4307	N/A	2.6137	10.0000	3.3369	3.1623	3.6884
5	N/A	0.0465	N/A	2.3491	N/A	3.1166	10.0000	3.5004
6	N/A	N/A	N/A	1.1656	N/A	2.4671	N/A	3.0675
7	N/A	N/A	N/A	0.6459	N/A	2.0794	N/A	2.7674
8	N/A	N/A	N/A	0.3111	N/A	1.8018	N/A	2.5371
9	N/A	N/A	N/A	0.0465	N/A	1.5816	N/A	2.3491
10	N/A	N/A	N/A	N/A	N/A	0.9320	N/A	1.9162
11	N/A	N/A	N/A	N/A	N/A	0.5443	N/A	1.6161
12	N/A	N/A	N/A	N/A	N/A	0.2667	N/A	1.3858
13	N/A	N/A	N/A	N/A	N/A	0.0465	N/A	1.1978
14	N/A	N/A	N/A	N/A	N/A	N/A	N/A	0.7649
15	N/A	N/A	N/A	N/A	N/A	N/A	N/A	0.4648
16	N/A	N/A	N/A	N/A	N/A	N/A	N/A	0.2345
17	N/A	N/A	N/A	N/A	N/A	N/A	N/A	0.0465

Note: The table entries represent radial distance from the origin values for x_i with units (m), and vector magnetic potential values for U_i with units (Wb/m).

Table 3.17: Optimal computed values of the geometric discretization parameters, x_i, and field solution parameters, U_i, for fourth-order finite element solutions for Benchmark System 2 using N elements, where $N = 5, 6, 7, 8$.

i/N	5		6		7		8	
	x_i	U_i	x_i	U_i	x_i	U_i	x_i	U_i
1	0.1000	4.6517	0.1000	4.6517	0.1000	4.6517	0.1000	4.6517
2	0.2512	4.3308	0.2154	4.3980	0.1931	4.4425	0.1778	4.4740
3	0.6310	4.0887	0.4642	4.1960	0.3728	4.2696	0.3162	4.3232
4	1.5849	3.8939	1.0000	4.0281	0.7197	4.1223	0.5623	4.1922
5	3.9811	3.7307	2.1544	3.8842	1.3895	3.9938	1.0000	4.0760
6	10.0000	3.4098	4.6416	3.6305	2.6827	3.7846	1.7783	3.8986
7	N/A	3.1676	10.0000	3.4285	5.1795	3.6117	3.1623	3.7478
8	N/A	2.9729	N/A	3.2605	10.0000	3.4644	5.6234	3.6168
9	N/A	2.8096	N/A	3.1166	N/A	3.3359	10.0000	3.5004
10	N/A	2.4887	N/A	2.8630	N/A	3.1267	N/A	3.3232
11	N/A	2.2466	N/A	2.6610	N/A	2.9538	N/A	3.1723
12	N/A	2.0519	N/A	2.4930	N/A	2.8065	N/A	3.0413
13	N/A	1.8886	N/A	2.3491	N/A	2.6780	N/A	2.9247
14	N/A	1.5677	N/A	2.0954	N/A	2.4688	N/A	2.7476
15	N/A	1.3255	N/A	1.8934	N/A	2.2959	N/A	2.5967
16	N/A	1.1308	N/A	1.7255	N/A	2.1486	N/A	2.4656
17	N/A	0.9676	N/A	1.5816	N/A	2.0202	N/A	2.3491
18	N/A	0.6467	N/A	1.3279	N/A	1.8108	N/A	2.1719
19	N/A	0.4045	N/A	1.1259	N/A	1.6380	N/A	2.0210
20	N/A	0.2098	N/A	0.9580	N/A	1.4906	N/A	1.8899
21	N/A	0.0465	N/A	0.8140	N/A	1.3623	N/A	1.7735
22	N/A	N/A	N/A	0.5604	N/A	1.1529	N/A	1.5961
23	N/A	N/A	N/A	0.3584	N/A	0.9800	N/A	1.4452
24	N/A	N/A	N/A	0.1904	N/A	0.8327	N/A	1.3141
25	N/A	N/A	N/A	0.0465	N/A	0.7044	N/A	1.1978
26	N/A	N/A	N/A	N/A	N/A	0.4951	N/A	1.0204
27	N/A	N/A	N/A	N/A	N/A	0.3222	N/A	0.8695
28	N/A	N/A	N/A	N/A	N/A	0.1750	N/A	0.7384
29	N/A	N/A	N/A	N/A	N/A	0.0465	N/A	0.6222
30	N/A	N/A	N/A	N/A	N/A	N/A	N/A	0.4446
31	N/A	N/A	N/A	N/A	N/A	N/A	N/A	0.2936
32	N/A	N/A	N/A	N/A	N/A	N/A	N/A	0.1625
33	N/A	N/A	N/A	N/A	N/A	N/A	N/A	0.0465

Note: The table entries represent radial distance from the origin values for x_i with units (m), and vector magnetic potential values for U_i with units (Wb/m).

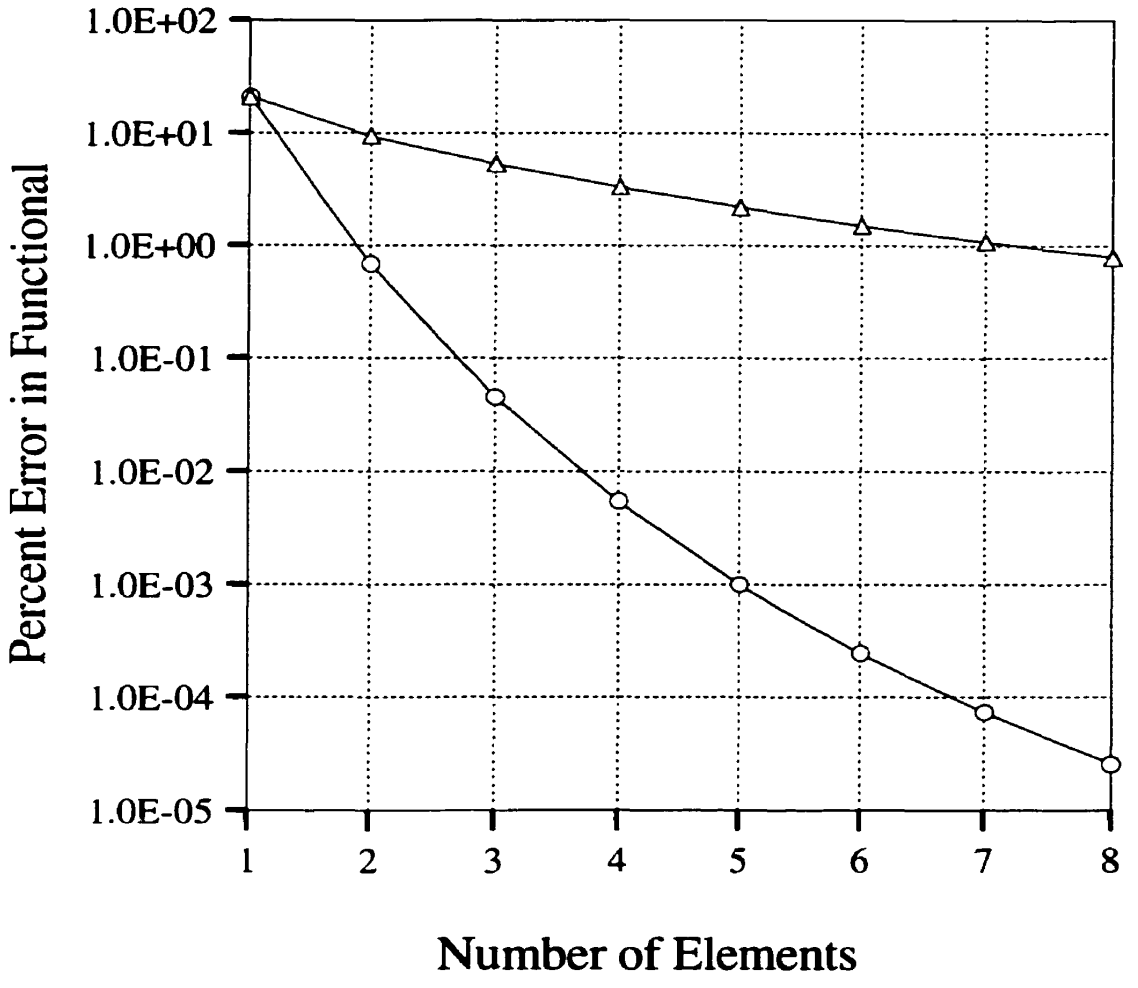

Figure 3.20: The variation of percent error in functional value with discretization level for fourth-order finite element solutions for Benchmark System 2 is illustrated. The triangle knot results correspond to percent error in functional values computed from solutions based on uniform discretizations. The circle knot results correspond to percent error in functional values computed from solutions based on optimal discretizations.

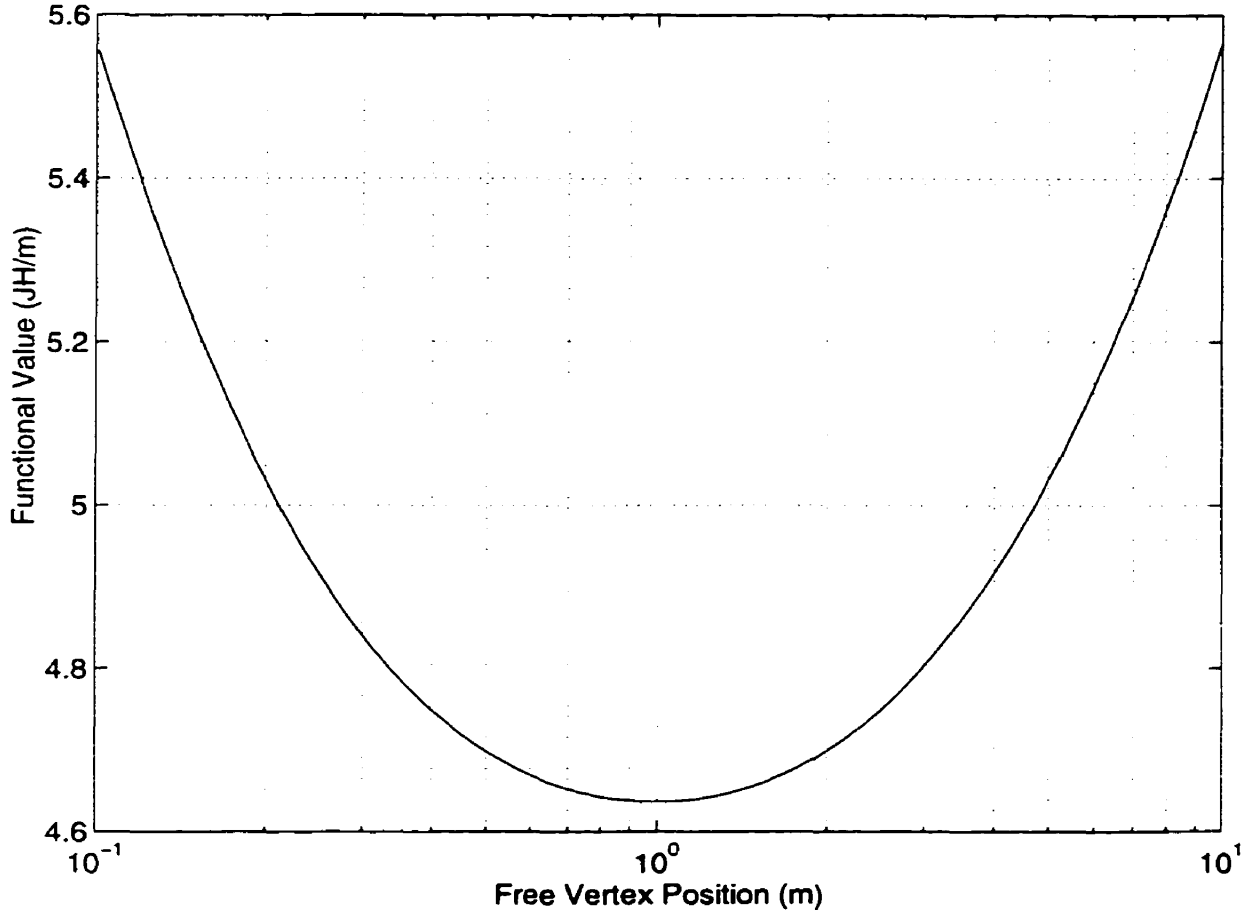

Figure 3.21: The variation in functional value with choice of free vertex position for a fourth-order two-element mesh is illustrated for Benchmark System 2. The plot is based on 100,000 functional values computed by fixing the unconstrained element vertex at 100,000 uniformly spaced positions between the two geometric boundaries of the problem domain. A logarithmic scale is used for the x-axis of the plot in order to adequately resolve the variation in the functional value near the optimal vertex position corresponding to the true minimum in the magnetostatic potential energy of the discretized, fourth-order, two-element finite element model. Note: the optimal vertex position is specified in Table 3.16.

Table 3.18: Optimal computed values of the geometric discretization parameters, x_i, and field solution parameters, U_i, for eighth-order finite element solutions for Benchmark System 2 using N elements, where $N = 1, 2, 3, 4$.

i/N	1		2		3		4	
	x_i	U_i	x_i	U_i	x_i	U_i	x_i	U_i
1	0.1000	4.6517	0.1000	4.6517	0.1000	4.6517	0.1000	4.6517
2	10.0000	2.0911	1.0000	3.8969	0.4642	4.2764	0.3162	4.4127
3	N/A	1.4880	10.0000	3.4740	2.1544	4.0043	1.0000	4.2199
4	N/A	1.0319	N/A	3.1752	10.0000	3.7905	3.1623	4.0584
5	N/A	0.7548	N/A	2.9469	N/A	3.6145	10.0000	3.9193
6	N/A	0.5411	N/A	2.7613	N/A	3.4650	N/A	3.7973
7	N/A	0.3319	N/A	2.6036	N/A	3.3348	N/A	3.6885
8	N/A	0.1899	N/A	2.4687	N/A	3.2197	N/A	3.5905
9	N/A	0.0465	N/A	2.3491	N/A	3.1166	N/A	3.5004
10	N/A	N/A	N/A	1.5943	N/A	2.7415	N/A	3.2612
11	N/A	N/A	N/A	1.1714	N/A	2.4695	N/A	3.0678
12	N/A	N/A	N/A	0.8727	N/A	2.2558	N/A	2.9058
13	N/A	N/A	N/A	0.6443	N/A	2.0799	N/A	2.7665
14	N/A	N/A	N/A	0.4587	N/A	1.9303	N/A	2.6442
15	N/A	N/A	N/A	0.3010	N/A	1.8002	N/A	2.5352
16	N/A	N/A	N/A	0.1661	N/A	1.6851	N/A	2.4370
17	N/A	N/A	N/A	0.0465	N/A	1.5816	N/A	2.3491
18	N/A	N/A	N/A	N/A	N/A	1.2066	N/A	2.1086
19	N/A	N/A	N/A	N/A	N/A	0.9344	N/A	1.9158
20	N/A	N/A	N/A	N/A	N/A	0.7206	N/A	1.7543
21	N/A	N/A	N/A	N/A	N/A	0.5446	N/A	1.6152
22	N/A	N/A	N/A	N/A	N/A	0.3950	N/A	1.4932
23	N/A	N/A	N/A	N/A	N/A	0.2648	N/A	1.3844
24	N/A	N/A	N/A	N/A	N/A	0.1498	N/A	1.2863
25	N/A	N/A	N/A	N/A	N/A	0.0465	N/A	1.1978
26	N/A	N/A	N/A	N/A	N/A	N/A	N/A	0.9580
27	N/A	N/A	N/A	N/A	N/A	N/A	N/A	0.7653
28	N/A	N/A	N/A	N/A	N/A	N/A	N/A	0.6037
29	N/A	N/A	N/A	N/A	N/A	N/A	N/A	0.4647
30	N/A	N/A	N/A	N/A	N/A	N/A	N/A	0.3427
31	N/A	N/A	N/A	N/A	N/A	N/A	N/A	0.2339
32	N/A	N/A	N/A	N/A	N/A	N/A	N/A	0.1358
33	N/A	N/A	N/A	N/A	N/A	N/A	N/A	0.0465

Note: The table entries represent radial distance from the origin values for x_i with units (m), and vector magnetic potential values for U_i with units (Wb/m).

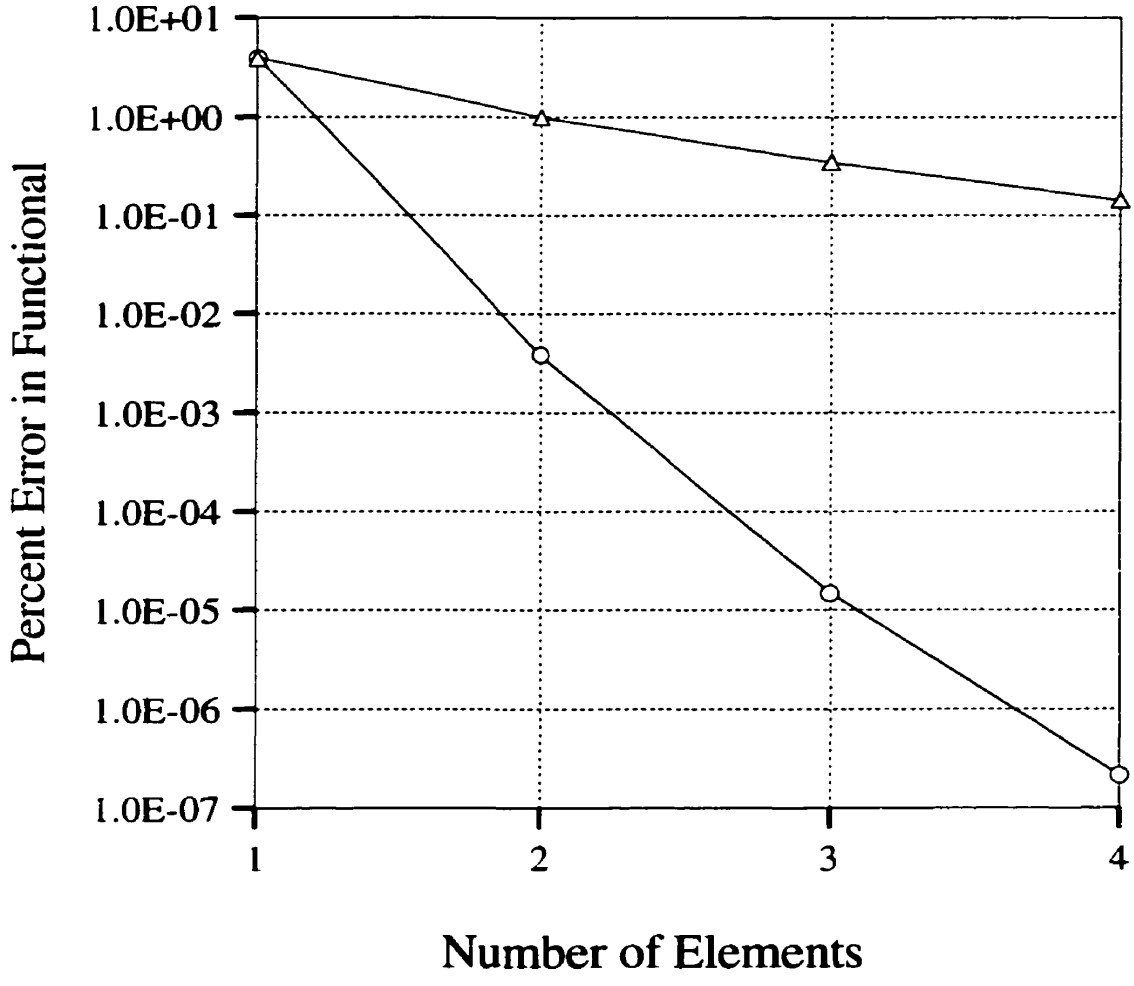

Figure 3.22: The variation of percent error in functional value with discretization level for eighth-order finite element solutions for Benchmark System 2 is illustrated. The triangle knot results correspond to percent error in functional values computed from solutions based on uniform discretizations. The circle knot results correspond to percent error in functional values computed from solutions based on optimal discretizations.

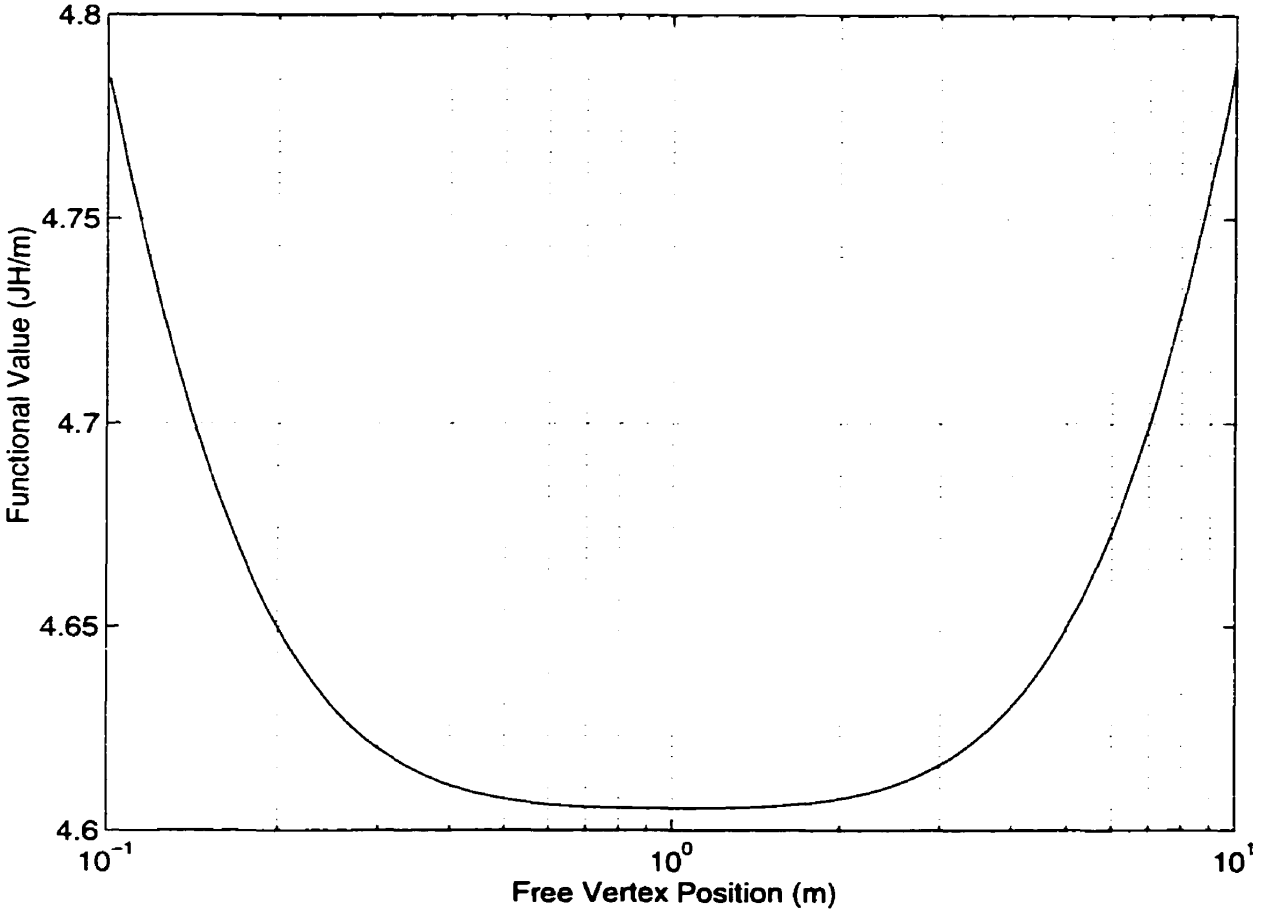

Figure 3.23: The variation in functional value with choice of free vertex position for an eighth-order two-element mesh is illustrated for Benchmark System 2. The plot is based on 100,000 functional values computed by fixing the unconstrained element vertex at 100,000 uniformly spaced positions between the two geometric boundaries of the problem domain. A logarithmic scale is used for the x-axis of the plot in order to adequately resolve the variation in the functional value near the optimal vertex position corresponding to the true minimum in the magnetostatic potential energy of the discretized, eighth-order, two-element finite element model. Note: the optimal vertex position is specified in Table 3.18.

boundary conditions used in Benchmark System 2 for the magnitude of the magnetic vector potential were 4.651687057 (Wb/m) at $x = 0.1$ (m) and $4.651687057 \times 10^{-2}$ at $x = 10.0$ (m), which correspond to the analytical values at the problem boundaries when the arbitrary zero reference potential is chosen to be at $x = 10.47615753$ (m). Second, the analytical functional value of 4.6052 (JH/m) was used to calculate the percent errors in functional values computed from the finite element solutions considered for Benchmark System 2. This functional value is, simply, twice the magnetostatic potential energy per unit length of the system multiplied by the factor $\mu_o/2\pi$, where $\mu_o = 4\pi \times 10^{-7}$ (H/m) is the permeability of free space. Third, the optimal discretizations for Benchmark System 2 have the interesting property that the optimal vertex positions for a mesh comprised of a given number of elements is independent of the order of the finite element approximation used (for the specific orders considered in this work). For example, the optimal two-element first-order mesh has exactly the same vertex positions as the optimal two-element second-, fourth- and eighth-order meshes. The optimal values of the geometric discretization parameters reported in Tables 3.10–3.18 may be examined to confirm that this interesting property holds not only for the two-element case, but also for the full range of optimal meshes with equivalent numbers of elements. Hence, the placement of the element vertices for corresponding optimal and uniform meshes with two, three and four elements in each of the first-, second-, fourth- and eighth-order cases is illustrated by Figure 3.24; and the comparison of optimal and uniform meshes ranging from five elements to eight elements for each of the first-, second- and fourth-order cases is shown in Figure 3.25. It may be noted that the superior accuracy in the functional values computed from the optimal discretization solutions relative to the uniform results for Benchmark System 2, is directly related to the more efficient relative distribution of DOF over the problem domain, as illustrated by Figure 3.24 and Figure 3.25 for the meshes represented therein. Furthermore, the numerical values specified in Tables 3.10–3.18 indicate that the balance of the optimal discretizations computed for

Benchmark System 2 also have effectively distributed element vertices for efficiently resolving the rapid field solution variation close to the line current. The fourth, and final, important distinction between the optimal discretization-based finite element solutions computed for the two benchmark systems is that the first-order optimal magnetic vector potential solutions computed for Benchmark System 2, and reported in Tables 3.10–3.12, are interpolatory on the true solution to the continuum problem. The value of this interesting feature of the first-order optimal results computed for the magnetostatic system will be discussed in Section 3.1.2. It may be noted from Tables 3.13–3.18 that the optimal second-, fourth-, and eighth-order solutions for Benchmark System 2 also have exact analytical values for the magnitude of the magnetic vector potential at the positions of the element vertices in any given mesh, but not at the interpolation points within the elements themselves; therefore, only the first-order optimal solutions are interpolatory on the true solution.

In summary, a total of 48 optimal finite element solutions were computed for Benchmark System 2 using first-, second-, fourth- and eighth-order standard Lagrangian basis functions. The accuracy and validity of the results were confirmed using exactly the same methods used for Benchmark System 1. The optimal discretization benchmark results presented in this section will be employed in section 3.2 to analyze previously reported finite element optimality criteria and, subsequently, in section 3.3 to evaluate the performance of practical adaption models in resolving Benchmark System 2.

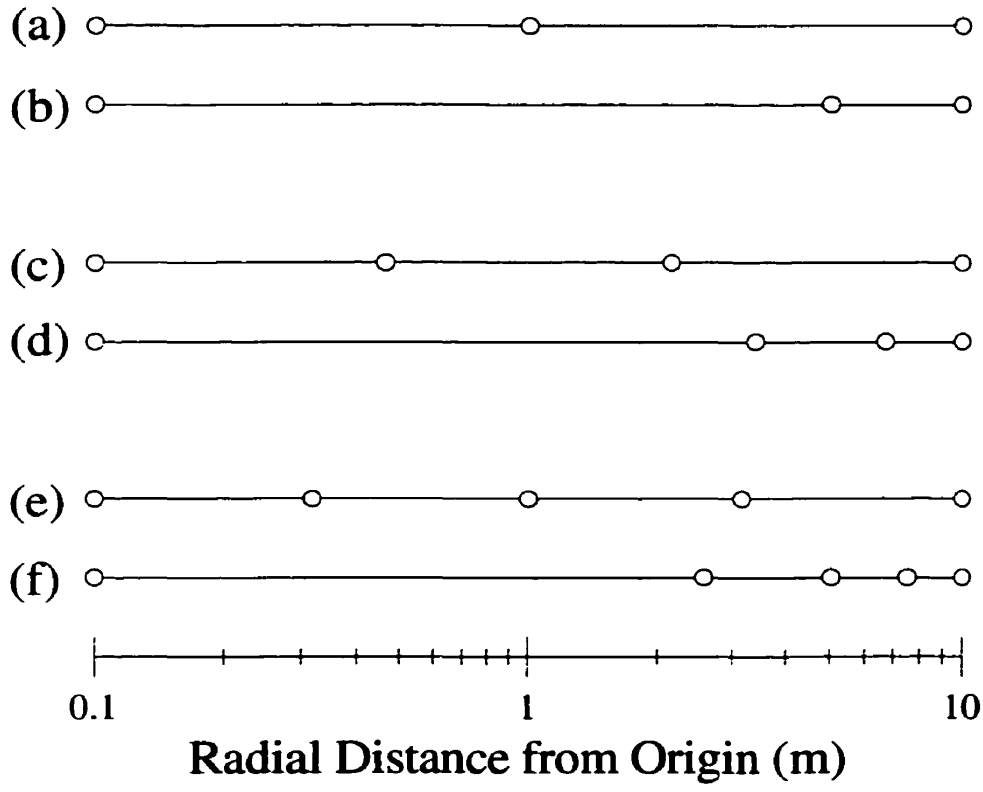

Figure 3.24: First-, second-, fourth-, and eighth-order optimal and uniform radial discretizations for the one-dimensional vector magnetic potential analysis of Benchmark System 2 are illustrated: (a) 2 element optimal mesh; (b) 2 element uniform mesh; (c) 3 element optimal mesh; (d) 3 element uniform mesh; (e) 4 element optimal mesh; (f) 4 element uniform mesh. The radial discretizations are plotted on a logarithmic scale because of the proximity of the element vertices to each other near the singularity in the optimal meshes. Note: the positions of the element vertices in the optimal meshes are specified in Table 3.10, 3.13, 3.16 and 3.18.

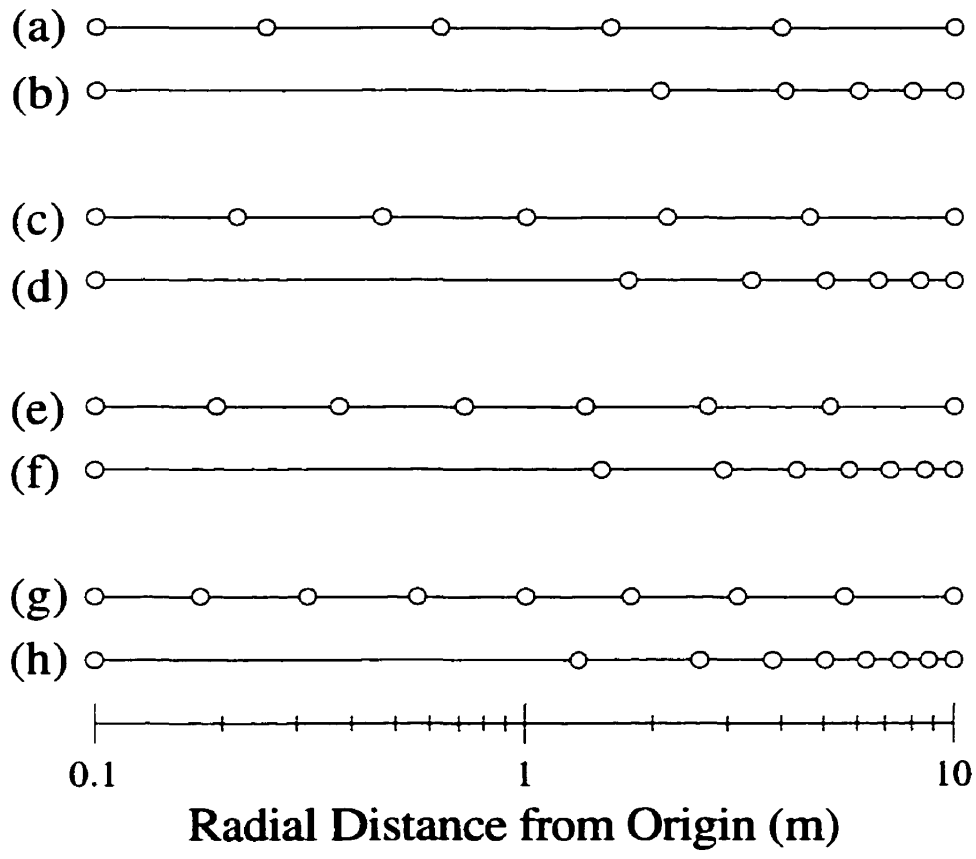

Figure 3.25: First-, second-, and fourth-order optimal and uniform radial discretizations for the one-dimensional vector magnetic potential analysis of Benchmark System 2 are illustrated: (a) 5 element optimal mesh; (b) 5 element uniform mesh; (c) 6 element optimal mesh; (d) 6 element uniform mesh; (e) 7 element optimal mesh; (f) 7 element uniform mesh; (g) 8 element optimal mesh; (h) 8 element uniform mesh. The radial discretizations are plotted on a logarithmic scale because of the proximity of the element vertices to each other near the singularity in the optimal meshes. Note: the positions of the element vertices in the optimal meshes are specified in Table 3.10, 3.13, and 3.17.

3.2 Finite Element Optimality Criteria Evaluations

In this section, reported problems with currently available finite element optimality criteria will be investigated with the optimal discretization results computed for the two benchmark systems considered above. The objective is to determine to what extent the problems are present in electromagnetic applications, and to evaluate the usefulness of the optimality criteria that are examined for AFEA of electromagnetic systems. The specific optimality criteria that are studied in this section were considered based on the following important reasons. First, optimality criteria which have, potentially, the most significant implications for AFEA of electromagnetic systems, but that have not been previously evaluated with optimal finite element solutions for electromagnetic benchmark systems are considered in this work. Second, optimality criteria which have previously been found to be ineffective based on conclusive numerical evidence are not considered in this work. Finally, many of the most commonly used optimality criteria rely on approximations based on superconvergence theory; therefore, the validity of certain relevant superconvergence concepts is evaluated in this section, in order to assess the implications for the broad range of optimality criteria which rely upon the correctness of those concepts.

3.2.1 Benchmark System 1

As noted in the review of currently available characterizations of optimal finite element discretizations presented in section 1.4, one of the most general and powerful formulations to be published in the mainstream literature is the grading function approach developed in [127]. In fact, this grading function approach has been used as the basis for developing and investigating numerous other optimality criteria [125, 132–136], also discussed in section 1.4. Its popularity has been attributed, mainly, to the rigorous mathematical analysis used in its derivation, and to the wide range of problem types to which it may be applied. However, as previously noted, there are certain key assumptions used in the derivation and specific approximations

that must be used when the grading function approach developed in [127] is applied to finite element approximate solutions of continuum problems, which may limit the effectiveness of related optimality criteria. In order to address this concern, the appropriate forms of the grading function reported in [127] were analyzed using the optimal discretization results computed for Benchmark System 1. Specifically, the grading function corresponding to the H^1-seminorm of the solution error was examined, which is consistent with the variational finite element formulation used in this work [125, 127]. Furthermore, the analytical field solution for Benchmark System 1 was used, as ideally prescribed in [127], to evaluate the grading functions suitable for the first-, second-, fourth- and eighth-order optimal finite element solutions computed for the electrostatic benchmark system. It may be noted that the use of the analytical field solution in evaluating the grading functions eliminates the reliance on superconvergence and extrapolation methods that would otherwise be required to compute the necessary derivatives of the finite element approximate field solutions. To this end, the existence of an analytical field solution for the electrostatic benchmark system extinguishes the adverse affects that these auxiliary procedures might introduce. The results of the numerical evaluation of the grading functions examined for Benchmark System 1 are discussed next.

The average percent errors in the grading function optimality criteria computed for the first-order optimal discretizations for Benchmark System 1 are shown in Figure 3.26. The percent errors were calculated based on satisfying the fundamental equidistribution principle of Eq. (1.3) in section 1.4.2, which is also the definition of a grading function: a function that must change by the same amount, $1/N$, over each element in a mesh comprised of N elements. Hence, for each of the optimal first-order solutions considered, the average percent error in the grading function optimality criteria was calculated as the mean of the percent error in satisfying this basic definition over each individual element. It should be noted that the general form of the grading function that was examined (given by Eq. (1.13) in section 1.4.2), will, by definition,

change by an average amount of $1/N$ over each element in *any* N-element mesh; however, for an *optimal* N-element mesh the grading function should change by the exact amount of $1/N$ over each element. As illustrated by Figure 3.26, the average error in equidistributing the change in the grading function over each element in a mesh ranged from approximately 28 to 57 percent for the optimal first-order solutions computed for meshes ranging from 2 to 20 elements. It should be noted that the H^1-seminorm form of the grading function developed in [127], and examined here, is not, strictly, applicable to the case of first-order approximations according to the derivation presented in [127]; however, since exactly the same form of the grading function was derived in [125] specifically for first-order finite element solutions, it is evaluated in this section for the first-order optimal discretization-based solutions computed for Benchmark System 1. The average percent errors in the grading function optimality criteria computed for the second-order optimal discretizations for Benchmark System 1 are shown in Figure 3.27. These percent errors were computed using exactly the same procedure that was used for the first-order case described above. The average error in equidistributing the change in the grading function over each element in a mesh is shown to lie in the range from approximately 22 to 41 percent for the optimal second-order solutions computed for meshes ranging from 2 to 16 elements. Similarly, a range of average errors from approximately 17 to 24 percent for the grading function optimality criteria corresponding to the fourth-order optimal solutions computed for Benchmark System 1 is shown in Figure 3.28. Finally, the analogous eighth-order results are shown in Figure 3.29, where the average error in equidistributing the change in the grading function over each element in a mesh is shown to be within the range of approximately 11 to 13 percent.

The relatively high percent errors reported above for the grading function optimality criteria evaluated for Benchmark System 1 confirm that there are serious problems associated with using these optimality criteria for electrostatic AFEA. Namely, for the optimal finite element discretizations considered, the corresponding grading functions

did not change by the same amount over each of the elements comprising the optimal meshes. Furthermore, it should be noted that the error in equidistributing the change in the grading functions over all of the elements in a mesh did not improve with increasing numbers of elements (i.e., with increasing finite element solution accuracy) in the optimal meshes over each of the first-, second-, fourth- and eighth-order series of optimal discretizations computed for Benchmark System 1. In fact, the grading functions appear to change more uniformly over the elements in the optimal meshes comprised of the smallest numbers of elements! This is in contrast with the findings reported in [125, 127], where the change in the grading functions over the elements in a mesh asymptotically approached a uniform distribution with increasing solution accuracy; however, the test cases examined in [125, 127] did not involve the same type of singular field solutions as those corresponding to Benchmark System 1. Therefore, the principle of equidistributing the change in the grading function, examined in this work, over each element in a mesh cannot be recommended for use as an optimal refinement criterion for adaptively evolving efficient distributions of DOF in order to effectively resolve regions of rapid field solution variation in electrostatic AFEA.

A second type of optimality criterion, which is based on the principle of equidistributing the residual of the governing partial differential equation (PDE) of a physical system, is considered next. Unlike the grading function optimality criteria discussed above, the approach of equidistributing the residual of the PDE governing the field solution behavior of a physical system has not been justified with rigorous theoretical analyses, but rather, has most often been employed heuristically, as pointed out in [129]. Nevertheless, PDE residual based optimality criteria have, potentially, significant implications for AFEA of electromagnetic systems for the following important reason. One of the strongest positive attributes of PDE residual based optimality criteria is the direct measure they can provide of how well the computed approximate solutions satisfy the equations used to mathematically model a physical system. This mathematically intuitive and simple approach is more often well understood and

readily accepted by finite element engineering communities than more mathematically abstract optimality criteria, for example, those based on the grading function approach described above. Thus, PDE residual based refinement criteria have been developed and investigated extensively for AFEA [151]; however, PDE residual based optimality criteria have not been previously evaluated with optimal finite element solutions for electromagnetic benchmark systems. The results of the numerical evaluation of the PDE residual optimality criteria examined for Benchmark System 1 are discussed next.

The average percent errors in the PDE residual optimality criteria computed for the first-order optimal discretizations for Benchmark System 1 are shown in Figure 3.26. The percent errors were calculated based on equidistributing the residual of the PDE corresponding to the electrostatic benchmark system (the approach developed and recommended in [126]). Hence, for each of the optimal first-order solutions considered, the average percent error in the PDE residual was calculated as the mean of the percent error in equidistributing the PDE residual over each individual element. As illustrated by Figure 3.26, the average error in equidistributing the PDE residual over each element in a mesh ranged from approximately 83 to 98 percent for the optimal first-order solutions computed for meshes ranging from 2 to 20 elements. The average percent errors computed for the second-order optimal discretizations for Benchmark System 1 are shown in Figure 3.27. These percent errors were computed using exactly the same procedure that was used for the first-order case described above. The average error in equidistributing the PDE residual over each element in a mesh is shown to lie in the range from approximately 90 to 96 percent for the optimal second-order solutions computed for meshes ranging from 2 to 16 elements. Similarly, a range of average errors from approximately 89 to 94 percent for equidistributing the PDE residual corresponding to the fourth-order optimal solutions computed for Benchmark System 1 is shown in Figure 3.28. Finally, the analogous eighth-order results are shown in Figure 3.29, where the average error is seen to be within the

range of approximately 85 to 95 percent.

In the course of evaluating the PDE residual optimality criteria described and discussed above, it was noted that a minor modification in how the optimality criteria are defined had interesting consequences. Specifically, when the PDE residual over an element scaled by the size of that element was evaluated for the optimal discretization-based solutions computed for Benchmark System 1, it was observed that, overall, the error in equidistributing this modified criterion was significantly reduced compared to the unscaled version considered above. Figure 3.26 shows that the average error in equidistributing the PDE residual scaled by the element size over each element in a mesh ranged from approximately 0.27 to 37 percent (compare with 83 to 98 percent for the unscaled version) for the optimal first-order solutions computed for meshes ranging from 2 to 20 elements. The corresponding second-order errors are shown by Figure 3.27 to lie in the range from approximately 0.05 to 17 percent (compare with 90 to 96 percent for the unscaled version); a range of average errors from approximately 0.31 to 0.94 percent (compare with 89 to 94 percent for the unscaled version) corresponding to the fourth-order case is shown in Figure 3.28; and the eighth-order results are shown in Figure 3.29, where the average error is seen to be within the range of approximately 1.6 to 3.0 percent (compare with 85 to 95 percent for the unscaled version).

The relatively high percent errors reported above for the PDE residual optimality criteria evaluated for Benchmark System 1 confirm that there are serious problems associated with using these optimality criteria for electrostatic AFEA. Namely, for the optimal finite element discretizations considered, the corresponding PDE residual was not equidistributed over each of the elements comprising the optimal meshes. Furthermore, it should be noted that the error in equidistributing the PDE residual over all of the elements in a mesh did not improve substantially with increasing numbers of elements (i.e., with increasing finite element solution accuracy) in the optimal meshes over each of the first-, second-, fourth- and eighth-order series of op-

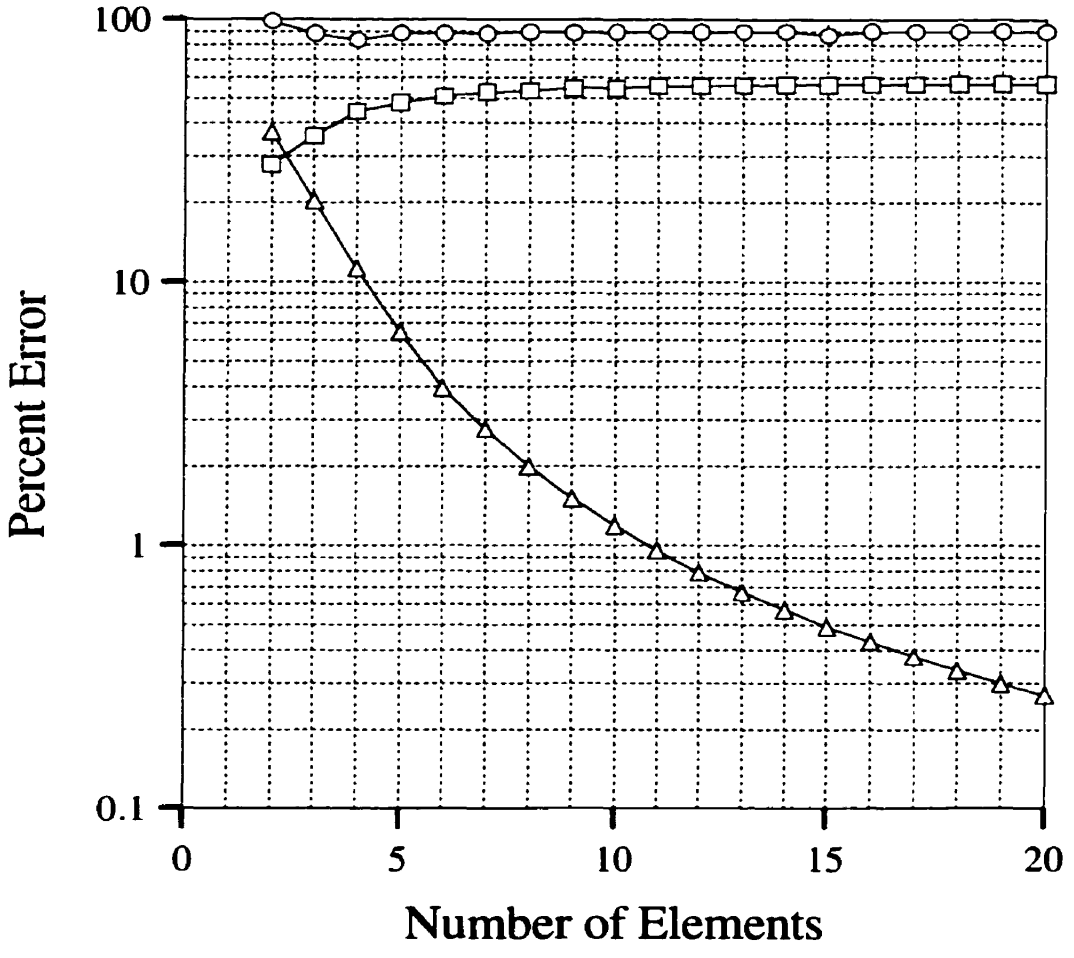

Figure 3.26: Evaluation of optimal discretization properties for optimal first-order discretizations for Benchmark System 1. The plot illustrates the variation of equidistribution error with the number of elements in a mesh. The square knot results correspond to the error in equidistributing the grading function over each element in a mesh. The circle knot results correspond to the error in equidistributing the residual of the partial differential equation over each element in a mesh. The triangle knot results correspond to the error in equidistributing the residual of the partial differential equation scaled by the element size.

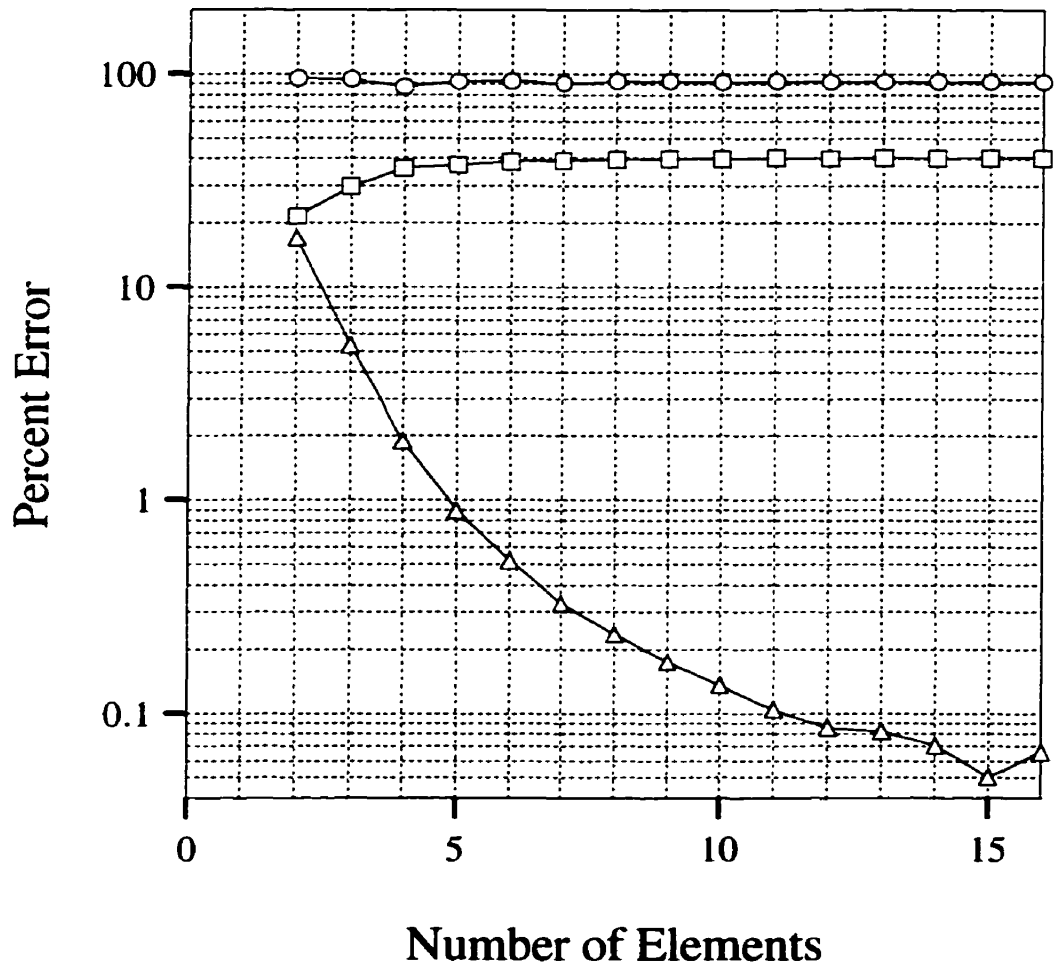

Figure 3.27: Evaluation of optimal discretization properties for optimal second-order discretizations for Benchmark System 1. The plot illustrates the variation of equidistribution error with the number of elements in a mesh. The square knot results correspond to the error in equidistributing the grading function over each element in a mesh. The circle knot results correspond to the error in equidistributing the residual of the partial differential equation over each element in a mesh. The triangle knot results correspond to the error in equidistributing the residual of the partial differential equation scaled by the element size.

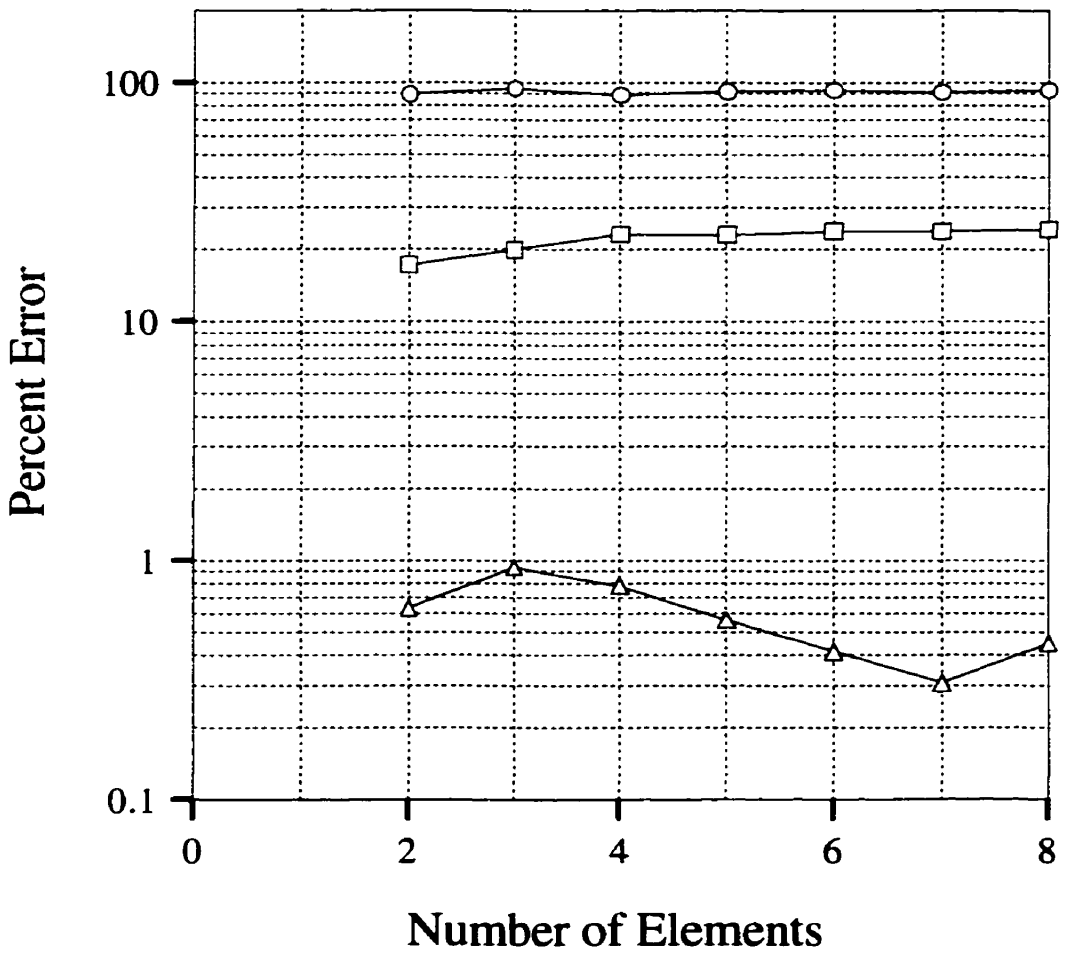

Figure 3.28: Evaluation of optimal discretization properties for optimal fourth-order discretizations for Benchmark System 1. The plot illustrates the variation of equidistribution error with the number of elements in a mesh. The square knot results correspond to the error in equidistributing the grading function over each element in a mesh. The circle knot results correspond to the error in equidistributing the residual of the partial differential equation over each element in a mesh. The triangle knot results correspond to the error in equidistributing the residual of the partial differential equation scaled by the element size.

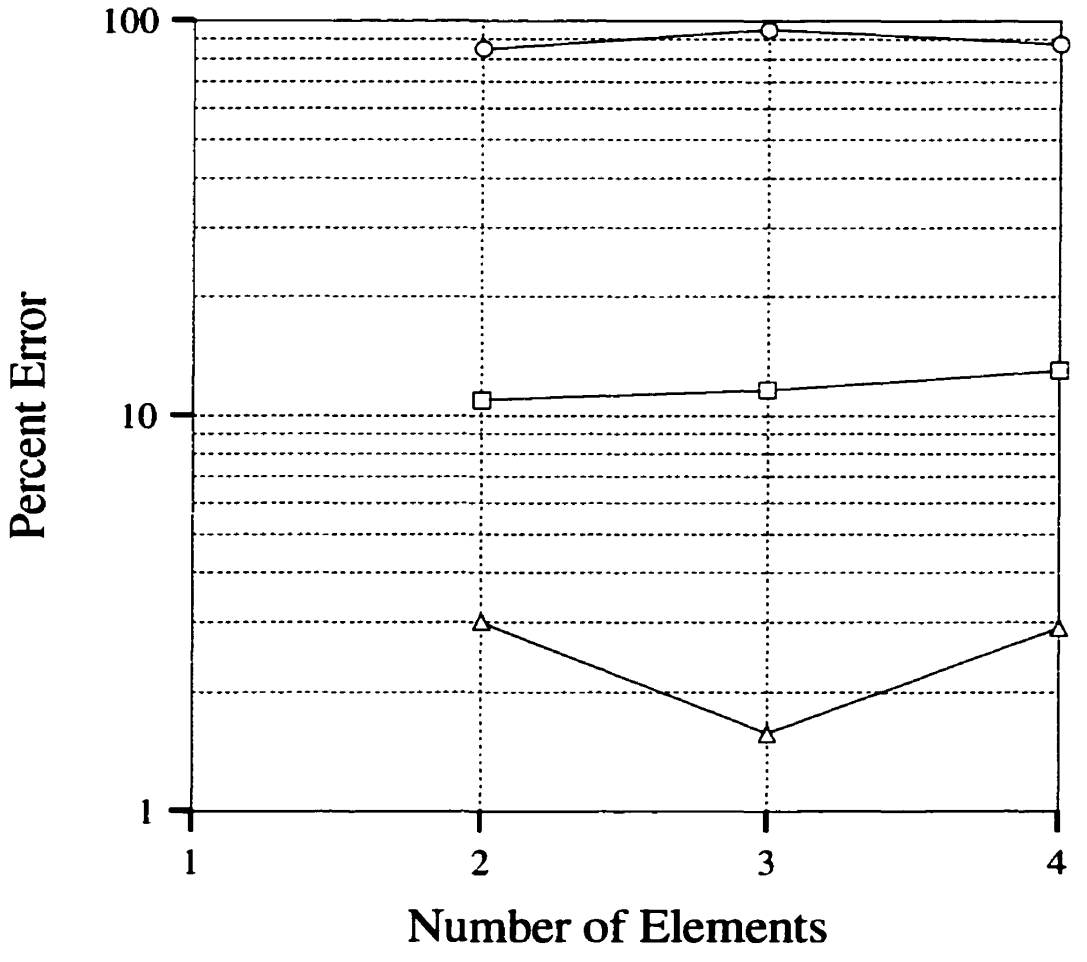

Figure 3.29: Evaluation of optimal discretization properties for optimal eighth-order discretizations for Benchmark System 1. The plot illustrates the variation of equidistribution error with the number of elements in a mesh. The square knot results correspond to the error in equidistributing the grading function over each element in a mesh. The circle knot results correspond to the error in equidistributing the residual of the partial differential equation over each element in a mesh. The triangle knot results correspond to the error in equidistributing the residual of the partial differential equation scaled by the element size.

timal discretizations computed for Benchmark System 1. However, it may be noted from Figure 3.26 and Figure 3.27, that the error in equidistributing the PDE residual scaled by the element size over all of the elements in a mesh did improve significantly with increasing numbers of elements in the optimal meshes over both of the first- and second-order series of optimal discretizations, respectively. Moreover, the average error in equidistributing this scaled version of the PDE residual was always less than 1 and 3 percent for the fourth- and eight-order optimal meshes, respectively. Therefore, the following may be concluded from the findings revealed by these investigations. First, the principle of equidistributing the PDE residual over each element in a mesh cannot be recommended for use as an optimal refinement criterion for adaptively evolving efficient distributions of DOF in order to effectively resolve regions of rapid field solution variation in electrostatic AFEA. Second, the principle of equidistributing the PDE residual scaled by the element size appears to be more effective for characterizing optimal finite element discretizations for Benchmark System 1; however, it would not be prudent to recommend this modified principle as the basis for developing refinement criteria without providing theoretical justification, and without further investigating its effectiveness for a wider range of problems.

3.2.2 Benchmark System 2

The grading function and PDE residual optimality criteria examined with the optimal discretization results for Benchmark System 1, are also evaluated in this section with the optimal finite element solutions computed for Benchmark System 2. In addition, the first-order optimal discretization results for Benchmark System 2 are used to evaluate derivative superconvergence properties employed in the derivation and application of many commonly used optimality and refinement criteria for AFEA. The significance of evaluating both the grading function and PDE residual optimality criteria has been addressed, in the preceding section, in terms of the implications that these optimality criteria hold for electromagnetic AFEA; therefore, the results from

the numerical evaluation of these criteria for Benchmark System 2 are presented in this section without further elaboration. However, the implications of the evaluation of derivative superconvergence properties will be explained, since they have not previously been discussed in sufficient detail. Moreover, the features of the optimal first-order finite element solutions corresponding to the magnetostatic benchmark system which provide the ideal experimental evidence required to rigorously examine the fundamental claims of superconvergence theory will be elucidated.

The average percent errors in the grading function optimality criteria computed for the first-order optimal discretizations for Benchmark System 2 are shown in Figure 3.30. The percent errors were calculated in exactly the same way as described for Benchmark System 1. As illustrated by Figure 3.30, the average error in equidistributing the change in the grading function over each element in a mesh ranged from approximately 35 to 37 percent for the optimal first-order solutions computed for meshes ranging from 2 to 20 elements. These first-order results are extremely interesting for the following important reason. As noted in section 3.1.2, the first-order optimal magnetic vector potential solutions computed for Benchmark System 2 are interpolatory on the true solution to the continuum problem; therefore, according to the arguments presented in [127], these first-order finite element approximate solutions are ideally suited for use with the approach of equidistributing the change in the grading function over each element in a mesh in order to determine the optimal discretization of the problem domain. However, since these interpolatory finite element solutions do correspond to the optimal discretization of the problem domain, there is, ironically, no need to use the grading function approach to optimize the finite element meshes under the exact conditions when it would be most appropriate to do so. The average percent errors in the grading function optimality criteria computed for the second-order optimal discretizations for Benchmark System 2 are shown by Figure 3.31 to lie in the range from approximately 21 to 23 percent for meshes ranging from 2 to 16 elements. Similarly, a range of average errors from approximately 12 to

13 percent for the grading function optimality criteria corresponding to the fourth-order optimal solutions computed for Benchmark System 2 is shown in Figure 3.32. Finally, the analogous eighth-order results are shown in Figure 3.33, where the average error in equidistributing the change in the grading function over each element in a mesh is shown to be within the range of 6 to 7 percent.

The relatively high percent errors reported above for the grading function optimality criteria evaluated for Benchmark System 2 confirm that there are serious reliability problems associated with using these optimality criteria for magnetostatic AFEA. Namely, for the optimal finite element discretizations considered, the corresponding grading functions did not change by the same amount over each element comprising the optimal meshes. Furthermore, it should be noted that the error in equidistributing the change in the grading functions over all of the elements in a mesh did not vary by more than approximately 2 percent with increasing numbers of elements (i.e., with increasing finite element solution accuracy) in the optimal meshes over each of the first-, second-, fourth- and eighth-order series of optimal discretizations computed for Benchmark System 2. This is in contrast with the findings reported in [125, 127], where the change in the grading functions over the elements in a mesh asymptotically approached a uniform distribution with increasing solution accuracy, as previously noted. Therefore, the principle of equidistributing the change in the grading functions examined in this work over each element in a mesh cannot be recommended for use as an optimal refinement criterion for adaptively evolving efficient distributions of DOF in order to effectively resolve regions of rapid field solution variation in magnetostatic AFEA.

The average percent errors in the PDE residual optimality criteria computed for the first-order optimal discretizations for Benchmark System 2 are shown in Figure 3.30. The percent errors were calculated based on equidistributing the residual of the PDE corresponding to the magnetostatic benchmark system over each element in a mesh. As illustrated by Figure 3.31, the average errors ranged from approximately

82 to 92 percent for the optimal first-order solutions computed for meshes ranging from 2 to 20 elements. The average error in equidistributing the PDE residual over each element in a mesh is shown to lie in the range from approximately 82 to 95 percent for the optimal second-order solutions computed for meshes ranging from 2 to 16 elements. Similarly, a range of average errors from approximately 88 to 92 percent for equidistributing the PDE residual corresponding to the fourth-order optimal solutions computed for Benchmark System 2 is shown in Figure 3.32. Finally, it should be noted that the analogous eighth-order results could not be computed for this benchmark system.[1]

Figure 3.30 shows that the average error in equidistributing the PDE residual scaled by the element size over each element in a mesh was identically zero for the optimal first-order solutions computed for meshes ranging from 2 to 20 elements (compare with 82 to 92 percent for the unscaled version). The corresponding second- and fourth-order errors are shown by Figure 3.31 and 3.32, respectively, to also be identically zero for all of the optimal discretizations considered (compare with 82 to 95 and 88 to 92 percent for the unscaled second- and fourth-order versions, respectively). Finally, it should be noted that the analogous eighth-order results could not be computed for this benchmark system, for the same reason stated above.

The relatively high percent errors reported above for the PDE residual optimality criteria evaluated for Benchmark System 2 confirm that there are significant reliability problems associated with using these optimality criteria for magnetostatic AFEA. Namely, for the optimal finite element discretizations considered, the corresponding PDE residual was not equidistributed over each of the elements comprising the optimal meshes. Furthermore it should be noted, that the error in equidistributing the PDE residual over all of the elements in a mesh did not improve with increasing numbers of elements (i.e., with increasing finite element solution accuracy) in the optimal meshes over each of the first-, second- and fourth-order series of optimal discretizations

[1] Due to a commercial software configuration dilemma not yet resolved by the manufacturer.

computed for Benchmark System 2. However, it may be noted from Figures 3.30–3.32 that the PDE residual scaled by the element size was exactly equidistributed over each of the elements in a mesh for all of the first-, second- and fourth-order optimal discretizations computed for Benchmark System 2. Therefore, the following may be concluded from the findings revealed by these investigations. First, the principle of equidistributing the PDE residual over each element in a mesh cannot be recommended for use an an optimal refinement criterion for adaptively evolving efficient distributions of DOF in order to effectively resolve regions of rapid field solution variation in magnetostatic AFEA. Second, the principle of equidistributing the PDE residual scaled by the element size appears to be entirely sufficient for characterizing the first-, second- and fourth-order optimal discretizations for Benchmark System 2. Finally, it would not be prudent to recommend developing refinement criteria based on this modified principle without providing theoretical justification for its use and without further examining its effectiveness for a wider range of magnetostatic problems.

In addition to the grading function and PDE residual optimality criteria evaluated for Benchmark System 2, the usefulness of superconvergence phenomena in finite element magnetics is investigated in this section. Specifically, reports on the superconvergent characteristics of potential-based derivatives at the Gauss-Legendre quadrature points of first-order elements are tested. In recent years, the development and application of superconvergence concepts for FEA error estimation and control has attracted a good deal of interest in the research community [152, 153]. In essence, superconvergence theory states that a finite element solution is inherently more accurate at certain points in the discretization than it is at others – and that these high accuracy locations are known *a priori* [154]. The computational analysis and design of magnetic devices frequently involves quantities related to derivatives of the underlying potential field solutions; therefore, superconvergence of derivative values of finite element potential solutions could have significant implications [155–157].

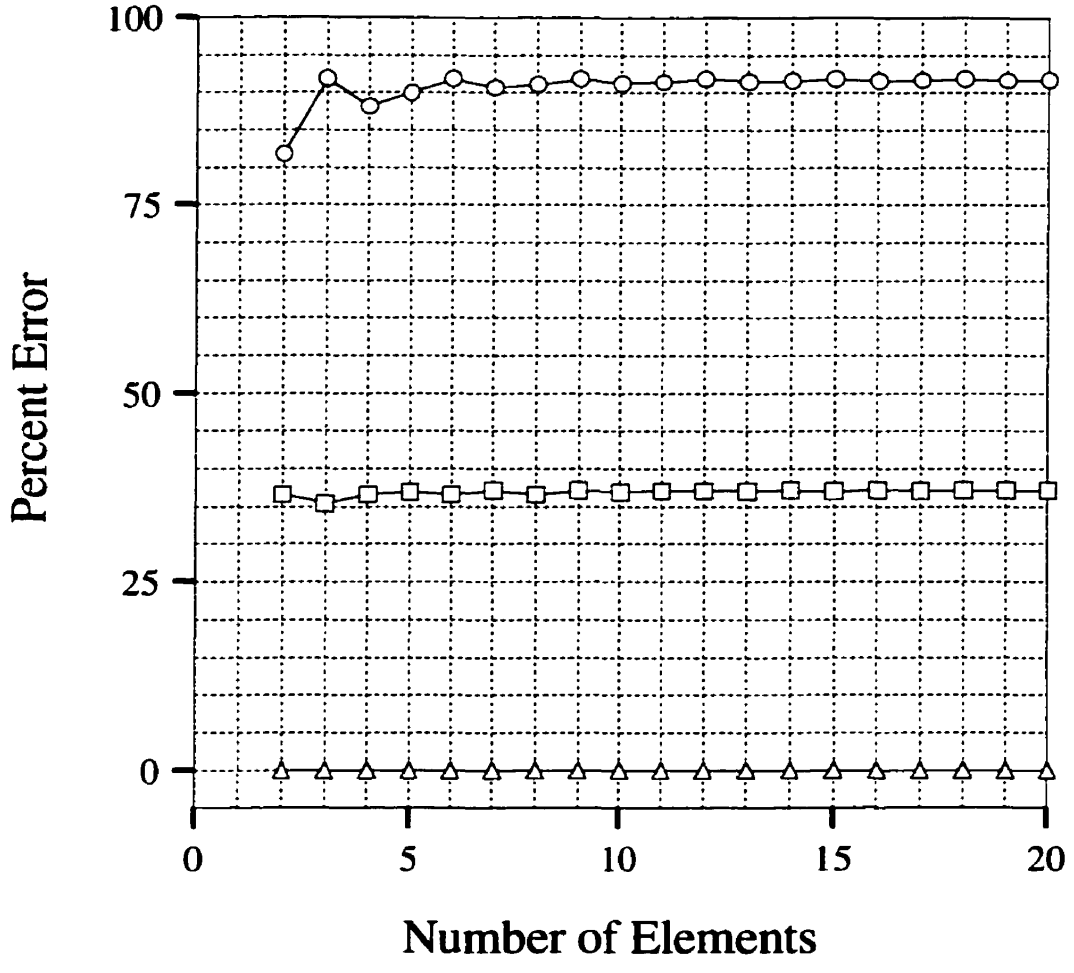

Figure 3.30: Evaluation of optimal discretization properties for optimal first-order discretizations for Benchmark System 2. The plot illustrates the variation of equidistribution error with the number of elements in a mesh. The square knot results correspond to the error in equidistributing the grading function over each element in a mesh. The circle knot results correspond to the error in equidistributing the residual of the partial differential equation over each element in a mesh. The triangle knot results correspond to the error in equidistributing the residual of the partial differential equation scaled by the element size.

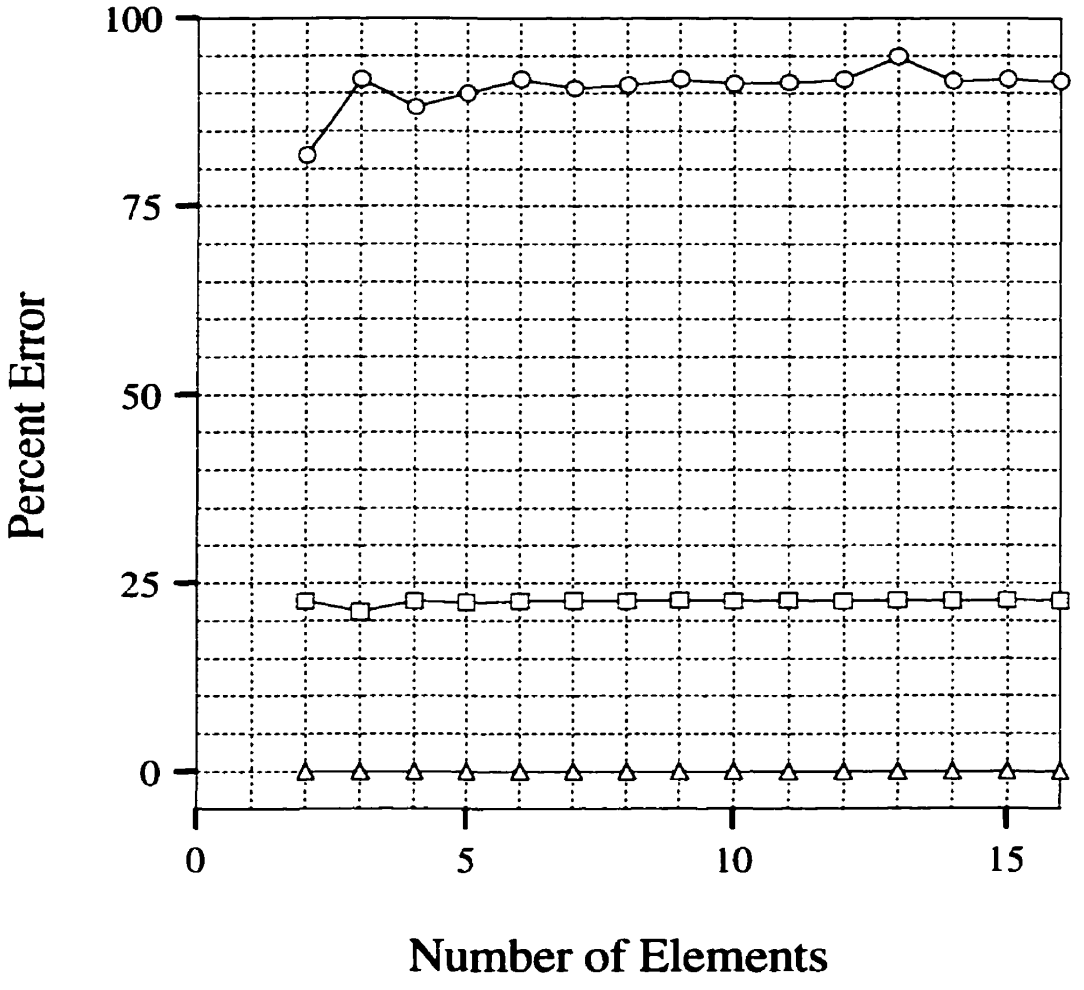

Figure 3.31: Evaluation of optimal discretization properties for optimal second-order discretizations for Benchmark System 2. The plot illustrates the variation of equidistribution error with the number of elements in a mesh. The square knot results correspond to the error in equidistributing the grading function over each element in a mesh. The circle knot results correspond to the error in equidistributing the residual of the partial differential equation over each element in a mesh. The triangle knot results correspond to the error in equidistributing the residual of the partial differential equation scaled by the element size.

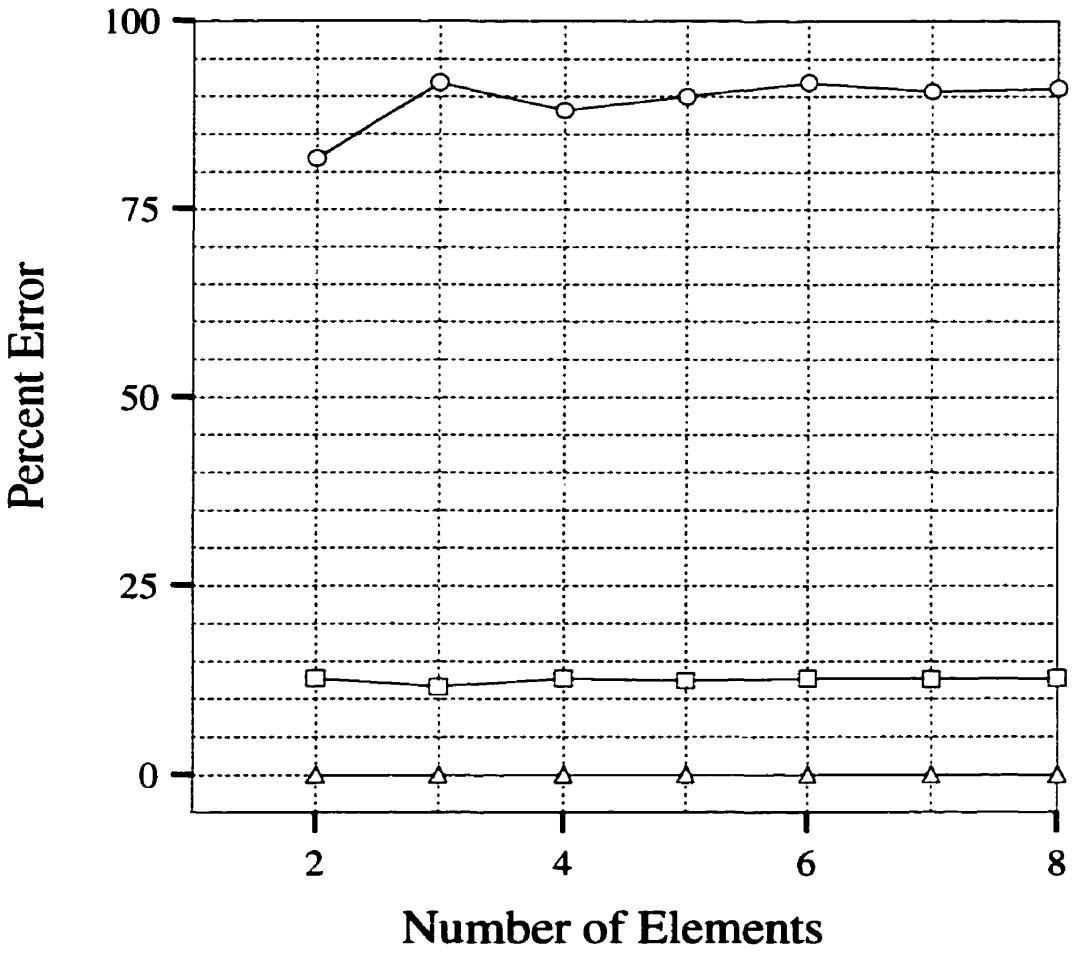

Figure 3.32: Evaluation of optimal discretization properties for optimal fourth-order discretizations for Benchmark System 2. The plot illustrates the variation of equidistribution error with the number of elements in a mesh. The square knot results correspond to the error in equidistributing the grading function over each element in a mesh. The circle knot results correspond to the error in equidistributing the residual of the partial differential equation over each element in a mesh. The triangle knot results correspond to the error in equidistributing the residual of the partial differential equation scaled by the element size.

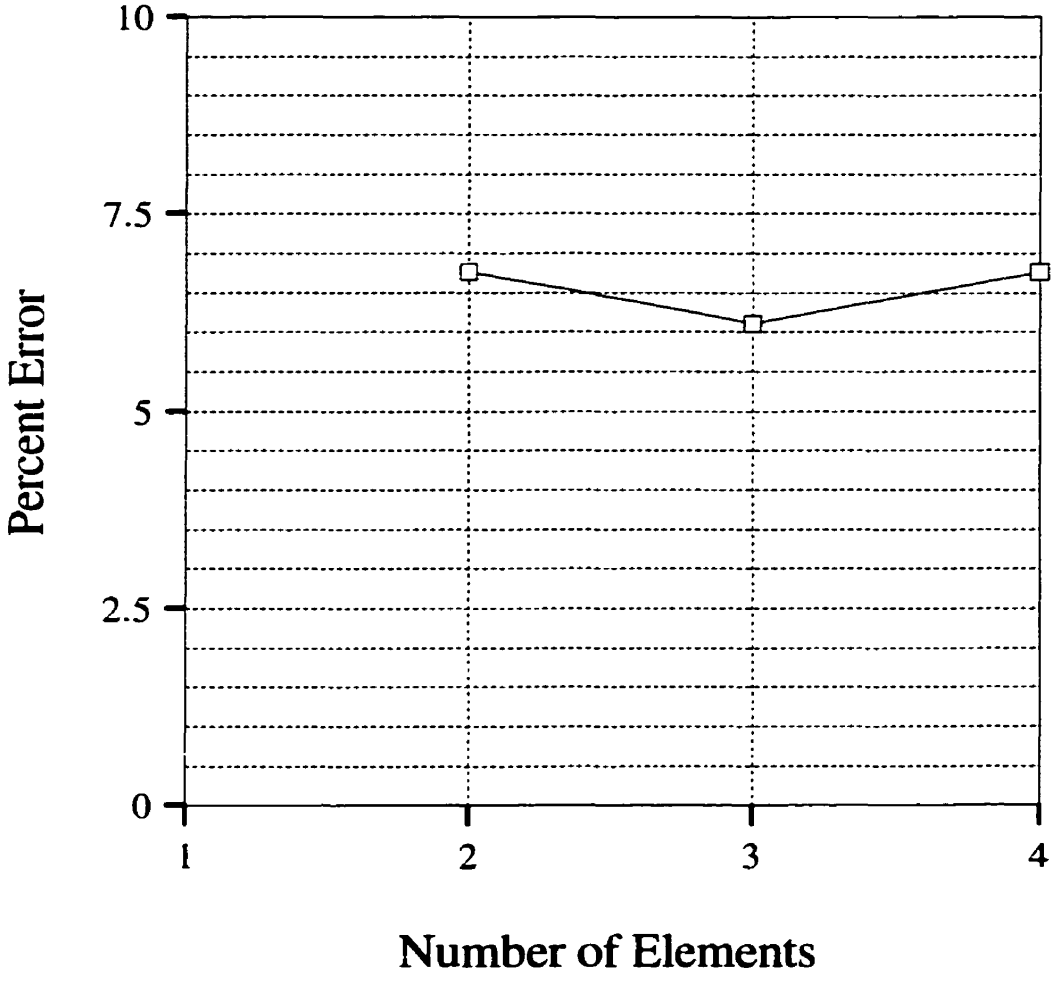

Figure 3.33: Evaluation of optimal discretization properties for optimal eighth-order discretizations for Benchmark System 2. The plot illustrates the variation of equidistribution error with the number of elements in a mesh. The square knot results correspond to the error in equidistributing the grading function over each element in a mesh. Note: only the equidistribution errors for the grading function were computed for the eighth-order optimal discretizations of the line singularity benchmark.

Moreover, some of the most general and powerful optimality criteria, for example, the grading function criteria developed in [127], rely on superconvergence based derivatives of the underlying field solution in order to compute the necessary derivatives from the approximate finite element solutions. Furthermore, other very general optimality criteria are derived primarily from principles that are directly related to derivative superconvergence concepts [131]. In fact, recent theoretical analyses on finite element superconvergence have focused on the development of superconvergent derivatives. Under certain assumptions, a number of these studies have determined that quantities related to first-derivatives of finite element potential solutions should possess superconvergent properties. Further, these studies have concluded that the most accurate derivative values over a given finite element are to be found at the Gauss-Legendre quadrature points of that element [158]. Specifically, it has been argued that when a finite element potential solution computed over first-order elements is interpolatory on the true solution to the continuum problem, the derivatives will be most accurate at the midpoints of the elements [154, 158]. It can be shown, with the mean-value theorem of calculus, that this is not true in general, but may be valid under certain conditions. However, the objective here is to investigate the practical value of superconvergence phenomena in finite element magnetics using computational experiments, in order to better understand the true impact and merit of the concept.

Using the magnetostatic benchmark system, exact derivatives of first-order, potential-based, finite element solutions were examined for properties characteristic of superconvergence. The series of 20 optimal and 20 uniform first-order finite element discretizations were used to compute the results for these investigations. Figure 3.34 illustrates the optimal discretization test results. The triangle knot curve shows the distance between the theoretical derivative superconvergence points (element midpoints) and the actual ones, expressed as a percentage of half the element length. The circle knot curve shows the error in the computed flux density at the theoretical

superconvergence points. Both curves are derived from a series of 20 solutions and are graphed as functions of FEA functional error. These error quantities do not vary from element to element over any optimal mesh. Further, the computed potential values are exact at the element vertices for the optimal discretizations: the first-order FEA solutions are interpolatory on the true solution to the continuum problem. Therefore, according to superconvergence theory, the Gauss-Legendre quadrature points should provide the most accurate derivatives within the elements. However, as described by Figure 3.34, the computed derivatives are exact at other locations within the elements, which vary with global solution accuracy. Also, by superconvergence theory, the error in the computed flux density at these Gauss-Legendre points should converge more rapidly than the global solution error. But, as seen in Figure 3.34, the ratio of these two errors is unity. The results given in Figure 3.35 for the uniform meshes are similar, except the error in the position of the theoretical superconvergence points (triangle knot results) varies from element to element within each mesh: only the minimum value is plotted.

The results of the above experimental studies indicate that superconvergence phenomena, as commonly defined for first-order FEA applications, are not apparent in Benchmark System 2. In particular, these investigations have demonstrated that, for the first-order FEA cases considered, derivatives of potential-based solutions are not generally more accurate at the Guass-Legendre points. Nevertheless, it was observed that, the properties attributed to superconvergence for FEA applications appear to become increasingly evident with increasing solution accuracy. This secondary result suggests that further theoretical and experimental studies may be useful to clearly establish the practical value of superconvergence in engineering FEA applications. However, based on the results from the investigations of the simple magnetostatic system considered here, the following conclusion is inevitable. Optimality criteria which rely on the validity of derivative superconvergence concepts, either for their derivation or for their application, cannot be recommended for practical first-order

FEA of magnetostatic systems with regions of rapid field solution variation. For example, the grading function approach discussed above has been recommended for use with finite element approximate solutions [127]; however, its effectiveness can be contingent on the accuracy of the superconvergence-based derivatives of the finite element field solutions which are required and recommended for its application. Furthermore, it should be noted that the specific grading function optimality criteria in question, were prone to serious reliability problems when evaluated with the first-order optimal discretizations computed for Benchmark System 2. Also, recall that the analytical field solution was used to compute the derivatives required to evaluate the grading functions. However, the superconvergence derivatives computed from the same interpolatory first-order optimal finite element solutions displayed large errors in approximating the true derivative values. Thus, if these erroneous superconvergence derivative values were substituted for the analytically computed derivatives in order to evaluate the grading function optimality criteria, the results of such an evaluation would be unreliable. Moreover, analytical field solutions corresponding to practical systems that are typically analyzed with FEMs, are not usually known; otherwise, there would be no need to use FEMs to analyze the systems! Therefore, on a practical level, the use of field solution superconvergence-based derivatives to evaluate a grading function, which, in turn, is used to determine optimal finite element discretizations, could have serious adverse implications. In particular, the grading functions examined in this work were designed to be most effective when used with analytical derivatives or with derivatives computed from finite element solutions of high accuracy (ideally, interpolatory finite element solutions). However, based on the serious accuracy problems that have been shown to exist with superconvergence-based derivatives computed from interpolatory finite element solutions, it is reasonable to question how effectively grading function and other types of optimality criteria that rely on the accuracy of superconvergent derivatives can be used to compute optimal finite element discretizations for practical systems.

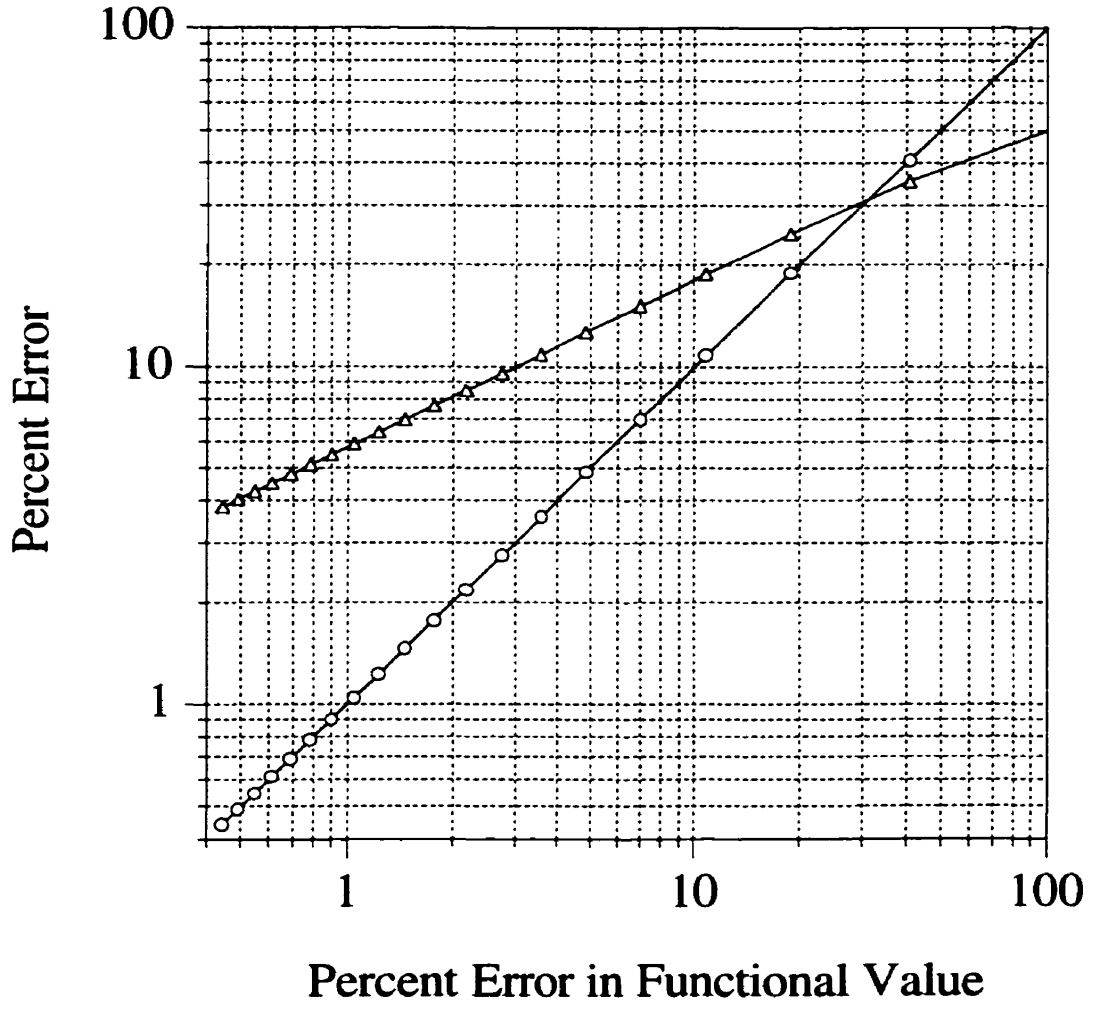

Figure 3.34: Evaluation of derivative superconvergence properties for optimal first-order discretizations for Benchmark System 2. The plot illustrates the variation in error of two superconvergence properties with functional value accuracy. The triangle knot results correspond to the distance between the theoretical derivative superconvergence points (element midpoints) and the actual ones, expressed as a percentage of half the element lengths. The circle knot results correspond to the error in the computed magnetic flux density at the theoretical superconvergence points. Note: both results are derived from a series of 20 solutions computed from the optimal meshes specified by Tables 3.10–3.12. The two error quantities do not vary from element to element over any optimal mesh in this study.

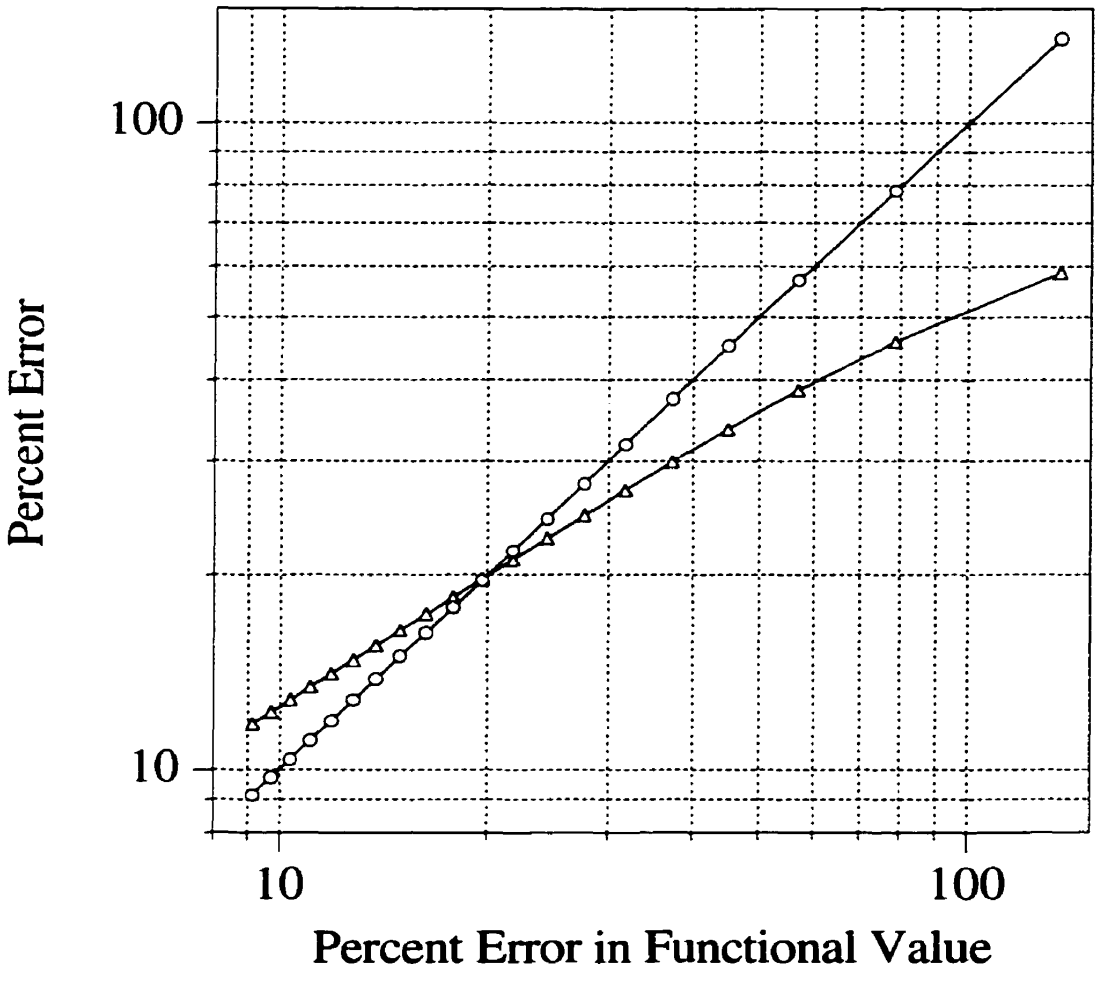

Figure 3.35: Evaluation of derivative superconvergence properties for uniform first-order discretizations for Benchmark System 2. The plot illustrates the variation in error of two superconvergence properties with functional value accuracy. The triangle knot results correspond to the distance between the theoretical derivative superconvergence points (element midpoints) and the actual ones, expressed as a percentage of half the element lengths. The circle knot results correspond to the error in the computed magnetic flux density at the theoretical superconvergence points. Note: both results are derived from a series of 20 solutions computed from uniform meshes ranging from 1 to 20 elements. In cases where the error quantities vary from element to element over any uniform mesh in this study, only the minimum value is plotted.

3.2.3 Discussion

In summary, the validity of commonly used finite element optimality criteria has been evaluated with the optimal discretization benchmark results computed for both the electrostatic and magnetostatic systems considered in section 3.1. In addition, the implications of using optimality criteria that rely on the accuracy of superconvergent derivatives of finite element approximate solutions, have been elucidated based on the numerical results of very simple, yet very revealing, experiments involving the optimal first-order finite element solutions computed for the magnetostatic benchmark system. It should be noted that some of the findings reported for the specific optimality criteria examined in this work, also have implications for other optimality criteria that were not explicitly investigated. For example, a number of optimality criteria which have been reported in the literature [132–136] are based directly on the grading function approach originally developed in [127], and examined comprehensively in this work. Also, the optimality criteria reported in [125, 127] are identical in form to grading functions examined in this work, under certain conditions. Specifically, the grading functions developed in [125, 127] are equivalent to the grading function used in this work to evaluate first-order finite element solutions.

It is worth noting that the optimality criterion based on equidistributing the potential energy of a system over each of the elements in a finite element discretization was also examined for both the electrostatic and the magnetostatic benchmark systems. However, the results from these potential energy investigations were not presented because they do not represent new knowledge: it was confirmed that the optimal solutions for Benchmark System 1 did not have a uniform distribution of potential energy over each of the elements in any of the given meshes corresponding to all of the first-, second-, fourth- and eighth-order series of optimal discretizations; however, the equidistribution of potential energy was indeed apparent in each of the corresponding meshes for Benchmark System 2. Thus, equidistribution of poten-

tial energy is not a universally valid optimality criterion, as previously noted in the literature.

Based on the conclusions reported in this section, it is apparent that the need for optimality criteria appropriate for characterizing optimal finite element discretizations over a sufficiently wide range of problem applications still exists. Moreover, it is also manifest that such optimality criteria should not be developed heuristically, but rather, should be based on well-founded and theoretically justified approaches.

3.3 Benchmark Adaption Studies

The numerical evaluation of currently available optimality criteria presented in sections 3.2.1 and 3.2.2 has revealed that universally valid characterizations of optimal finite element discretizations for electromagnetic systems are needed, which can be used to develop well-founded and theoretically justified refinement criteria for practical AFEA. Moreover, it was shown in sections 3.1.1 and 3.1.2 that the finite element optimization equations of section 2.4.1 can be successfully employed to directly compute optimal discretizations for electromagnetic systems. The purpose of this section is to investigate the potential benefits of using new refinement criteria based on the finite element optimization equations for practical electromagnetic AFEA. The approach used to achieve this objective was to investigate the effectiveness of the primary adaption models, when guided by a new optimal discretization-based refinement criterion, in resolving the two benchmark systems developed above. Hence, in order to evaluate the potential performance advantages of optimal discretization-based practical AFEA, results from a series of adaption studies involving h-, p-, and hp-adaption models are reported for both benchmark systems considered previously. Furthermore, the usefulness of the benchmark adaption studies presented in this section for the analysis and design of optimal hp-adaption strategies will be demonstrated. However, the adaption benchmark results are first preceded by a brief description of how the finite element optimization equations are used to develop an optimal discretization-based refinement criterion for AFEA.

3.3.1 An Optimal Discretization Based Refinement Criterion for AFEA

The perennial challenge for all types of adaption in FEA has been the efficient use of well-defined optimal solution properties as feedback refinement criteria for guiding the solution process towards accurate results [159]. One potential route to successful adaption is to employ local error measures that are closely related to the variational principle used to determine the solution to the finite element problem. The purpose

of the present section is to introduce a new refinement criterion for *h*-, *p*-, and *hp*-adaption, which is based on the variational properties of optimal discretizations for the FEA of electromagnetic systems.

As previously noted, the ideal mesh for a given number of DOF, that is, the mesh that produces the most accurate solution, will exhibit optimal element vertex locations. For such an ideal discretization, the functional corresponding to the variational formulation of the problem, will not only be stationary with respect to the field solution parameters – but also with respect to variations in the geometric discretization parameters, that is, the element vertex positions. Therefore, one possible way to detect and rank regions of inferior discretization in a finite element mesh may be to evaluate the sensitivity of the functional to differential displacements of the element vertices: a small perturbation of the position of an element vertex in a region of adequate discretization should result in a relatively small change in the functional value; however, in a region of relatively poor discretization, a small perturbation in vertex positions may yield a significantly larger change. Thus, by computing the gradients of the functional with respect to element vertex positions, it is possible to determine where to improve the discretization, based on a purely local error indicator that is closely related to the variational principle of the solution. Furthermore, it should be noted that these functional gradients may be computed directly from the finite element optimization equations derived in section 2.4. In fact, the finite element optimization equations corresponding to the geometric discretization parameters are precisely the gradients of the functional, with respect to element vertex positions, equated to zero! Therefore, a refinement criterion for identifying regions of inferior discretization in a finite element mesh may be defined by the degree to which the finite element optimization equations are satisfied when evaluated with fixed, but not necessarily, optimal values of the element vertex positions; that is, based on the magnitudes and directions of the functional gradients with respect to the element vertex positions. Hence, for the one-dimensional discretizations considered in this chapter,

the elements in a mesh can be ranked for refinement based directly on the magnitudes and directions of the functional gradients computed from the two optimization equations corresponding to the two geometric discretization parameters associated with each element which define its vertex positions. The effectiveness of this optimal discretization-based refinement criterion is evaluated in the following two sections, and its implications for practical AFEA are discussed in section 3.3.4.

3.3.2 Benchmark System 1

In order to evaluate the effectiveness of the optimal discretization-based refinement criterion described above, results from a series of studies involving the primary adaption models are reported in this section for Benchmark System 1. Specifically, the convergence of *h*-, *p*- and *hp*-adaption strategies are investigated when the optimal discretization-based refinement criterion is used to guide the adaption. While *h*-adaption has become increasingly popular in electromagnetic FEA research during the past 15 years [85, 160, 161], and more recently, effective *p*-adaption codes have started to emerge [59, 113], practical *hp*-adaption strategies for electromagnetic FEA are more rare. One important reason for this slow progress – aside from the inherent complexity of implementing and controlling *hp*-adaption – is the lack of objective benchmarks by which to measure the merits and flaws of adaptive strategies. As noted earlier, one of the most important challenges for all types of adaption in FEA is the accurate and efficient resolution of the singularities associated with sharp material corners [61, 81, 162]. Thus, a secondary purpose of this section is to illustrate the usefulness of the adaption benchmark studies in the analysis and design of optimal *hp*-adaption strategies. The different types of adaption techniques considered in this section are intended to represent a range of the basic methods most commonly used in practice for electromagnetic AFEA. Finally, it should be noted that in order to obtain the best possible resolution in the rate of convergence for the adaption methods studied in this work, each adaptive iteration was based on increasing the number

of DOF in a discretization by the minimal increments appropriate for the type of adaption being considered.

The convergence of the percent error in functional value for an h-adaption strategy based on element bisection applied to the electrostatic benchmark system is illustrated in Figure 3.36 for first-order elements. The initial mesh consisted of a single element which was bisected, resulting in a uniform mesh of two elements. At each subsequent adaptive iteration, one element in the mesh was selected for refinement by element bisection: the optimal discretization-based refinement criterion described above was used to rank the elements, and the element with the highest ranking was chosen for bisection. It should be noted that the elements were ranked in ascending order of increasing magnitudes of the functional gradients with respect to the element vertex positions. The uniform h-refinement baseline and the optimal first-order discretization functional convergence results are also shown in Figure 3.36 for comparison. The convergence of the h-adaption element bisection scheme guided by the optimal discretization-based refinement criterion has the following interesting feature. Initially, the element bisection h-adaption strategy produces discretizations with functional accuracy levels superior to those of the uniform discretizations with corresponding numbers of elements, but inferior to the optimal first-order discretizations with equivalent numbers of elements. However, after approximately seven adaptive steps the functional accuracy achieved by the optimal discretization-based element bisection scheme is seen to be remarkably close, and almost equivalent, to that of the optimal discretizations. The practical significance of this result is amplified by the relative computational cost of the two approaches used to compute the corresponding finite element solutions. The element bisection h-adaption scheme only entails the evaluation of the nonlinear finite element optimization equations for a given set of fixed element vertex positions in order to compute the functional gradients required for the optimal discretization-based refinement criterion, and is relatively inexpensive compared to solving the same set of nonlinear equations for the optimal values of the

element vertex positions which are necessary to determine the optimal discretizations.

The analogous second-order h-adaption results for Benchmark System 1 are shown in Figure 3.37. The fourth- and eighth-order h-adaption results are shown in Figure 3.38 and Figure 3.39, respectively. For each case, the results were computed using exactly the same procedures as for the first-order h-adaption results described above. It may be noted that for the second- and fourth-order cases, the functional accuracy of the element bisection strategy after approximately seven adaptive steps is almost equivalent to that of the optimal discretizations, which is consistent with the first-order results reported above. The eighth-order h-adaption results were not computed beyond three iterations; however, the element bisection strategy produced discretizations with functional accuracy levels superior to those of the uniform discretizations with corresponding numbers of eighth-order elements. Therefore, based on the complete set of first-, second-, fourth- and eighth-order h-adaption results computed for the electrostatic benchmark system, it is apparent that the new optimal discretization-based refinement criterion is effective for evolving efficient distributions of DOF over the problem domain for Benchmark System 1. Moreover, based on the first-, second- and fourth-order h-adaption results reported for Benchmark System 1, it is suggested that the new optimal discretization-based refinement criterion can be used to efficiently and reliably guide adaptive finite element solvers towards optimal solutions for electrostatic systems with regions of rapid field solution variation.

The convergence of the percent error in functional value for two p-adaption strategies applied to a range of uniform initial meshes for the electrostatic benchmark system is illustrated in Figure 3.40. Specifically, uniform and mixed-order p-adaption schemes were investigated using first-, second-, fourth- and eighth-order elements. The functional convergence based on uniform p-adaption for initial meshes of four, eight and twelve elements is shown by curves A, B and C, respectively. In each case, the uniform meshes were initially comprised of first-order elements. These initial meshes were refined by successively increasing the element orders uniformly to

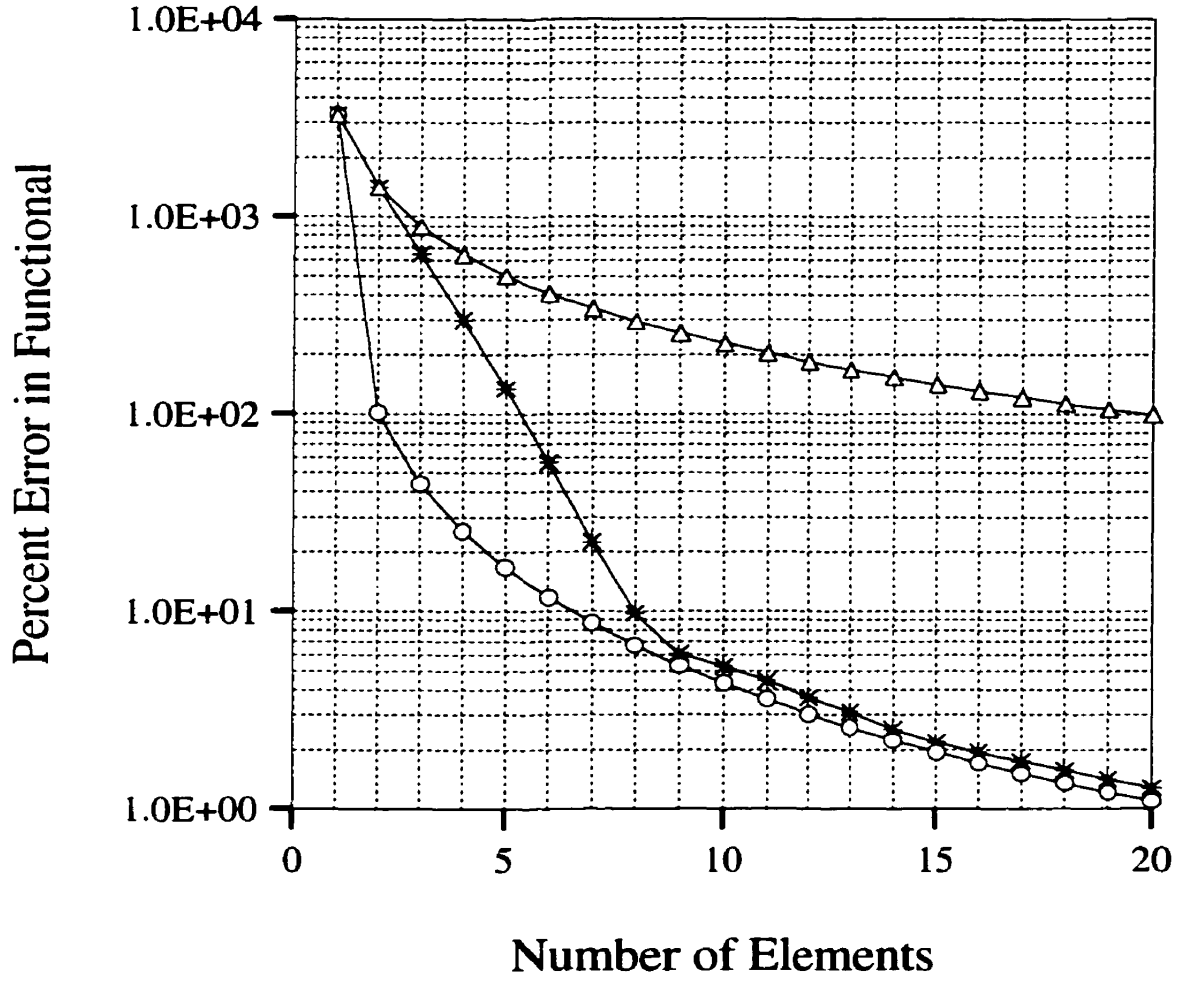

Figure 3.36: The convergence of percent error in functional value with discretization level for first-order h-adaption studies for Benchmark System 1 is illustrated. The triangle knot results correspond to percent error in functional values computed from solutions based on first-order uniform h-refinement discretizations. The asterisk knot results correspond to percent error in functional values computed from solutions based on first-order element bisection h-adaption discretizations evolved using the new optimal discretization-based refinement criterion. The circle knot results correspond to percent error in functional values computed from solutions based on first-order optimal discretizations.

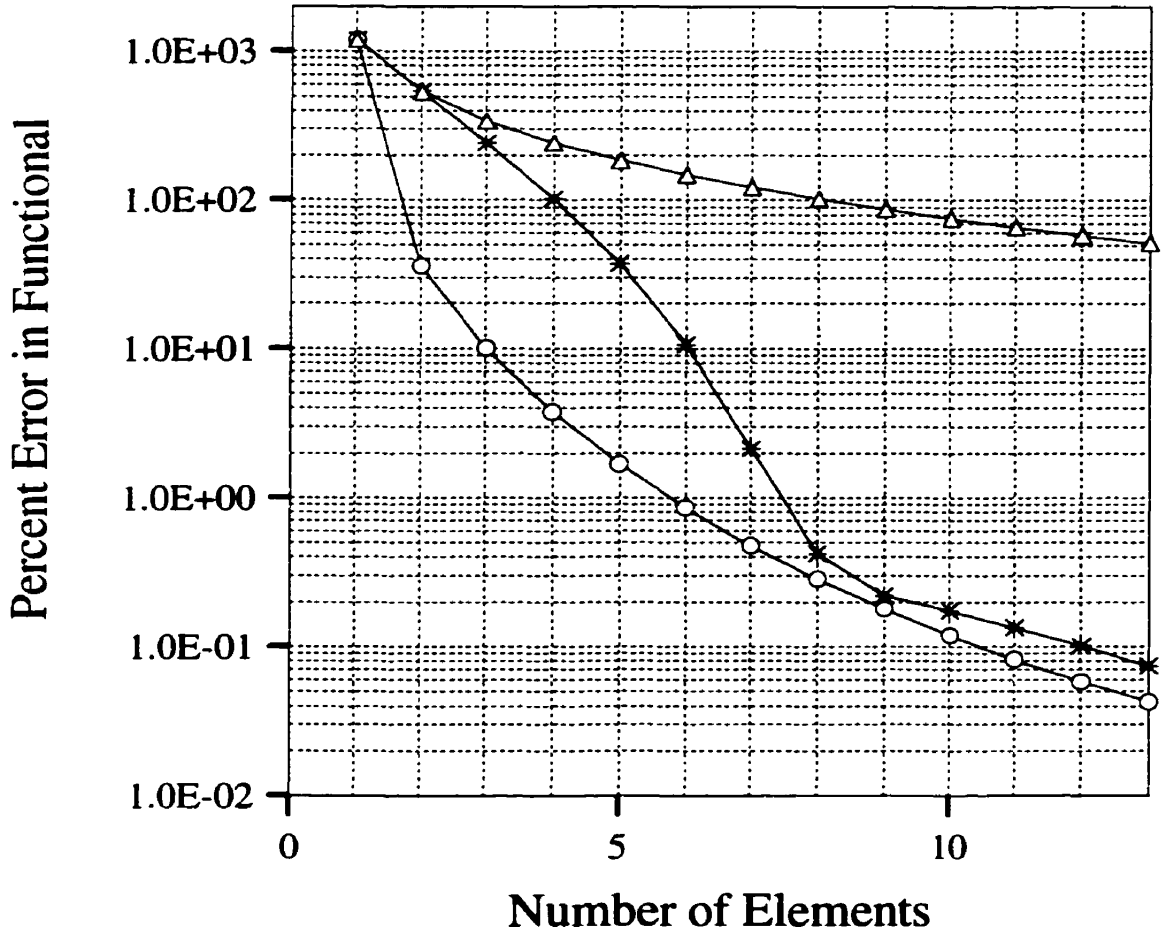

Figure 3.37: The convergence of percent error in functional value with discretization level for second-order h-adaption studies for Benchmark System 1 is illustrated. The triangle knot results correspond to percent error in functional values computed from solutions based on second-order uniform h-refinement discretizations. The asterisk knot results correspond to percent error in functional values computed from solutions based on second-order element bisection h-adaption discretizations evolved using the new optimal discretization-based refinement criterion. The circle knot results correspond to percent error in functional values computed from solutions based on second-order optimal discretizations.

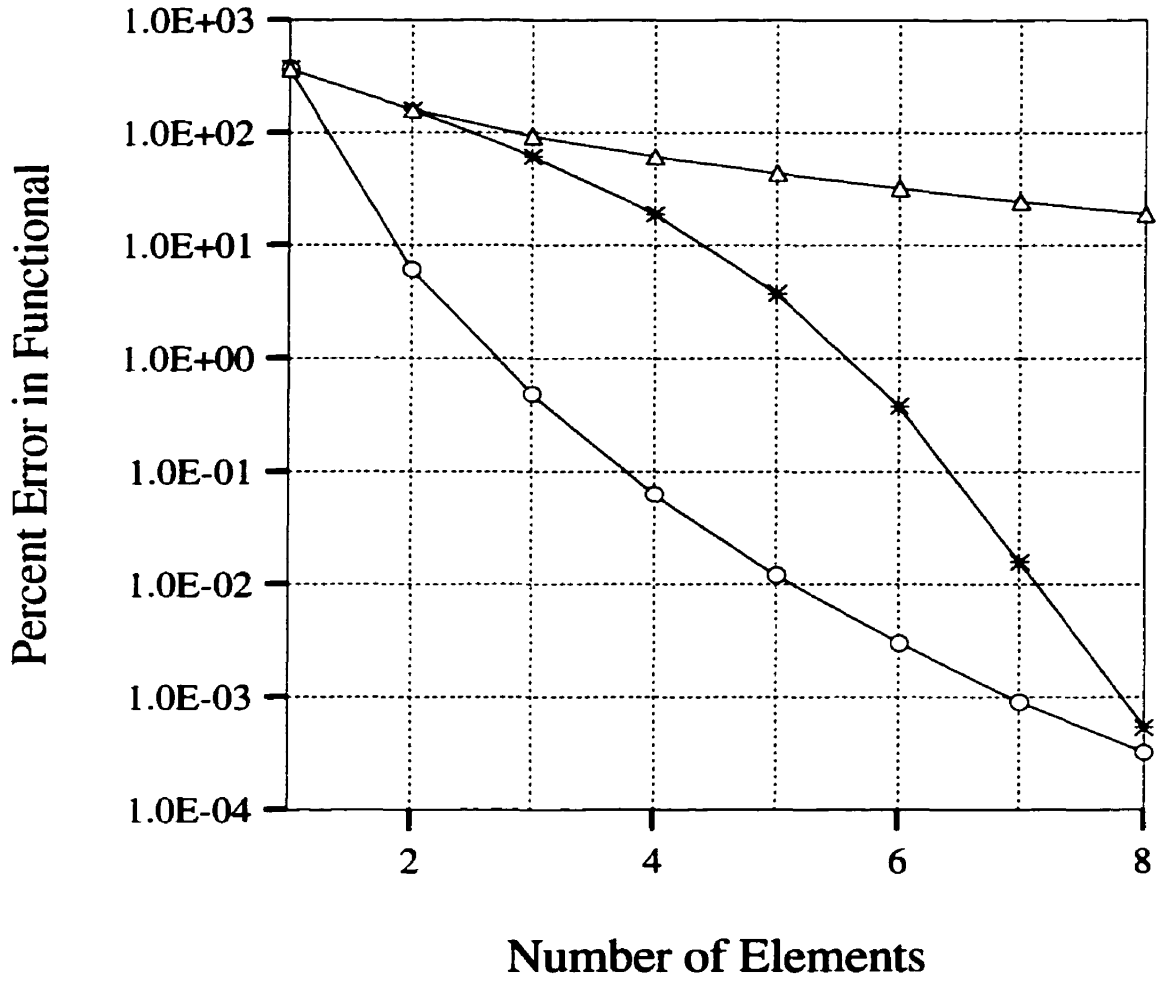

Figure 3.38: The convergence of percent error in functional value with discretization level for fourth-order h-adaption studies for Benchmark System 1 is illustrated. The triangle knot results correspond to percent error in functional values computed from solutions based on fourth-order uniform h-refinement discretizations. The asterisk knot results correspond to percent error in functional values computed from solutions based on fourth-order element bisection h-adaption discretizations evolved using the new optimal discretization-based refinement criterion. The circle knot results correspond to percent error in functional values computed from solutions based on fourth-order optimal discretizations.

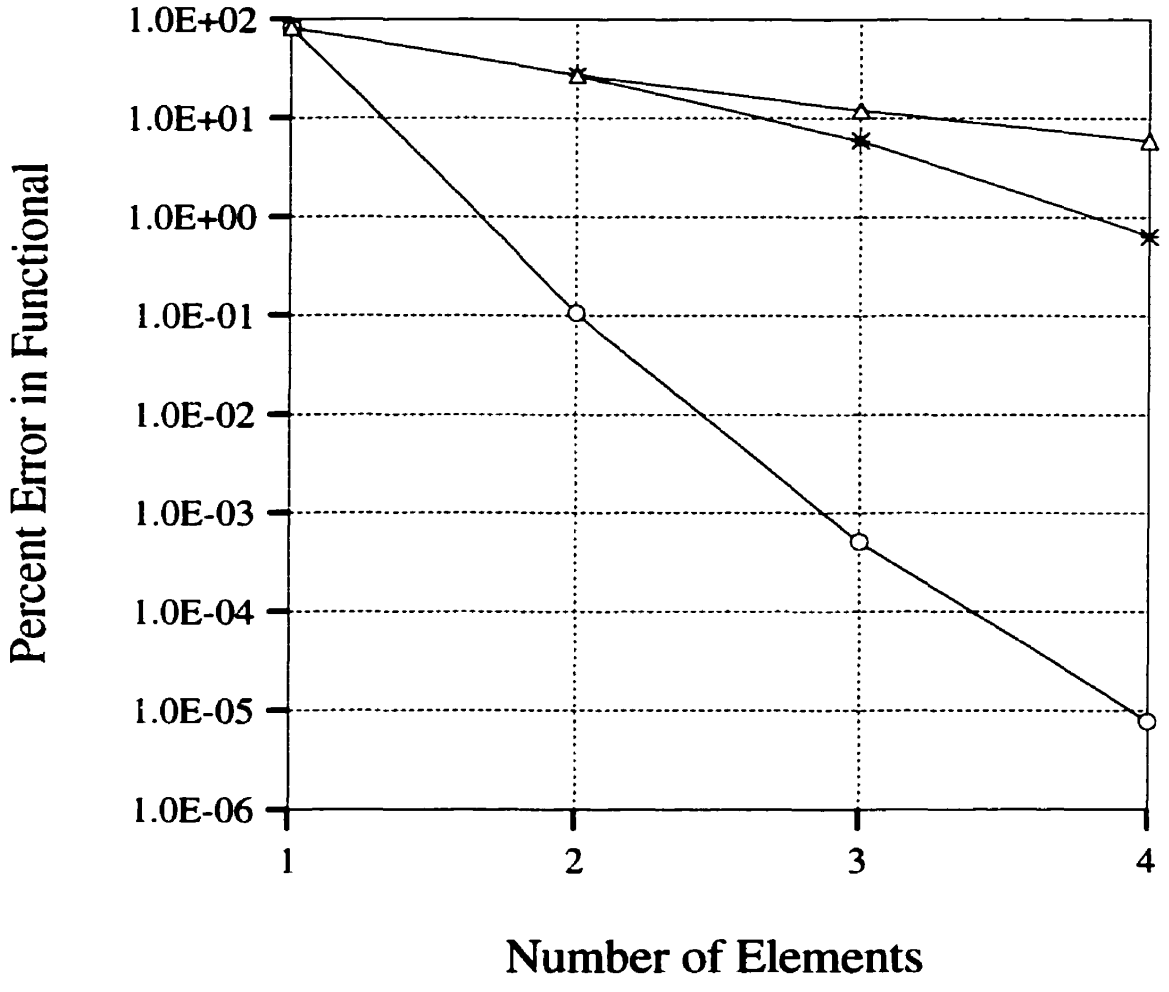

Figure 3.39: The convergence of percent error in functional value with discretization level for eighth-order h-adaption studies for Benchmark System 1 is illustrated. The triangle knot results correspond to percent error in functional values computed from solutions based on eighth-order uniform h-refinement discretizations. The asterisk knot results correspond to percent error in functional values computed from solutions based on eighth-order element bisection h-adaption discretizations evolved using the new optimal discretization-based refinement criterion. The circle knot results correspond to percent error in functional values computed from solutions based on eighth-order optimal discretizations.

second-, fourth- and eighth-order. The functional convergence for the corresponding mixed-order p-adaption scheme is shown by curves D, E and F for the four, eight and twelve element meshes, respectively. For the mixed-order p-adaption scheme, one element in the mesh was selected for refinement at each adaptive iteration: the optimal discretization-based refinement criterion described above was used to rank the elements, and the order of the element with the highest ranking was augmented. It should be noted that the elements were ranked in exactly the same way that was used for the h-adaption studies described above. Moreover, the order of an element selected for refinement was increased successively to second-, fourth- or eighth-order each time the element was selected to be refined; however, if an eighth-order element was chosen for refinement, the highest ranking lower-order element was refined instead. Based on the convergence of the percent errors shown in Figure 3.40 for the two p-adaption schemes considered, it is evident that when starting from uniform initial meshes the mixed-order p-adaption scheme results in a significantly faster rate of convergence relative to the uniform p-adaption strategy for Benchmark System 1. In fact, for the four element case investigated, the same maximal functional accuracy level was achieved with 13 DOF by the mixed-order p-adaption scheme compared with 33 DOF required by the uniform method (a relative savings of approximately 61 percent in the number of DOF). Similarly, for the eight element case a relative reduction of approximately 66 percent in the number of DOF required to achieve maximal functional accuracy was observed when the mixed-order p-adaption scheme was used rather than the uniform method. Analogously, a 68 percent economy in DOF was achieved for the twelve element case. Therefore, it is suggested that the new optimal discretization-based refinement criterion is effective for evolving efficient distributions of DOF by p-adaption over the problem domain for electrostatic systems with regions of rapid field solution variation.

The h- and p-adaption results presented above for Benchmark System 1 have illustrated the effectiveness of the optimal discretization-based refinement criterion for

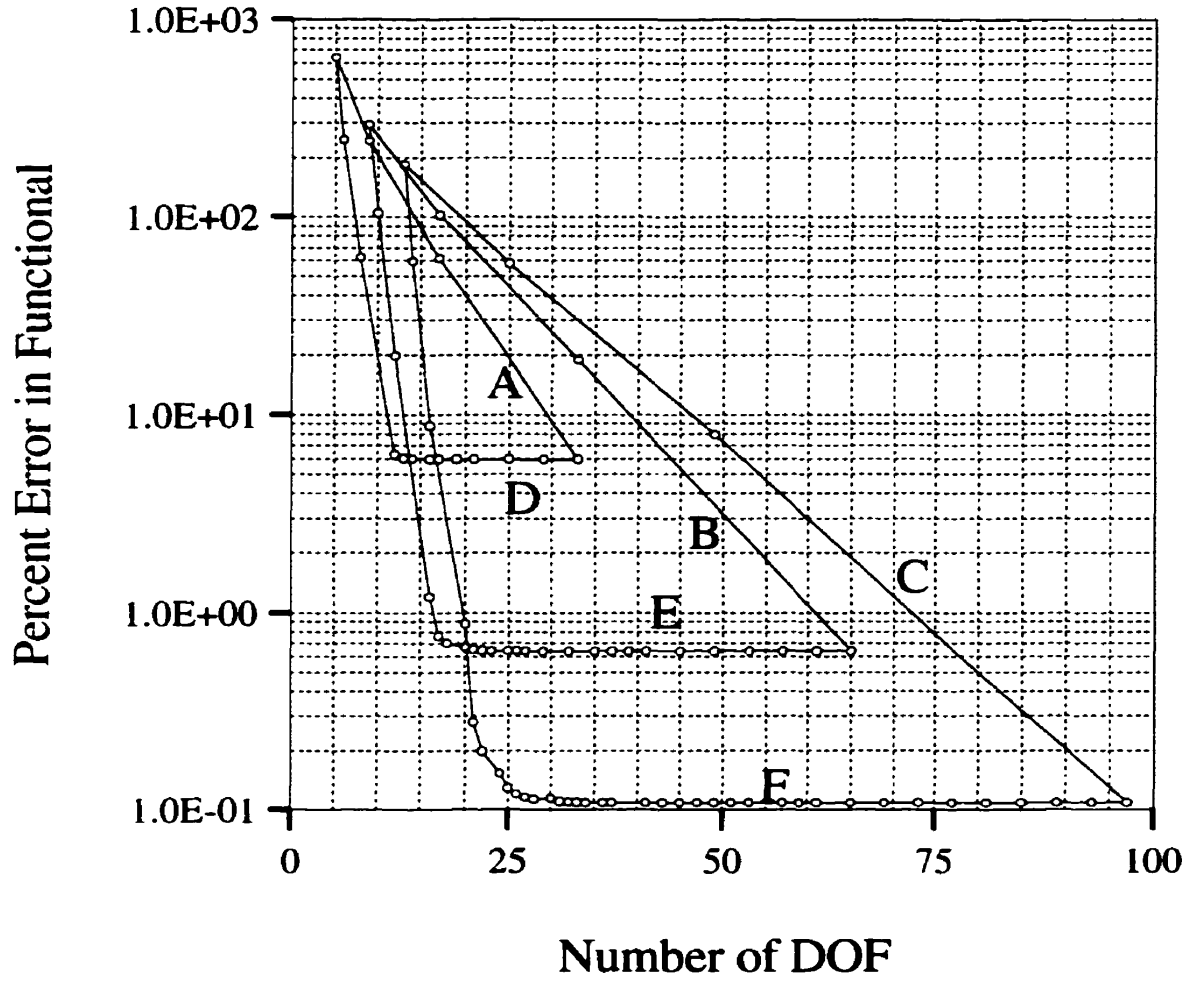

Figure 3.40: The convergence of percent error in functional value with discretization level for the p-adaption studies for Benchmark System 1 is illustrated. Curve A, B, and C results correspond to percent error in functional values computed from solutions based on uniform p-discretizations for initial meshes of four, eight and twelve elements, respectively. Curve D, E, and F results correspond to percent error in functional values computed from solutions based on mixed-order p-discretizations evolved using the new optimal discretization-based refinement criterion for initial meshes of four, eight and twelve elements, respectively.

these two types of adaption models. It is logical to consider the implications of this criterion for *hp*-adaption models next. Specifically, integrated, decoupled and uniform *hp*-adaption models are investigated. The objective for these *hp*-adaption studies is not only to evaluate the effectiveness of the optimal discretization-based refinement criterion for *hp*-adaption, but also to determine which specific type of *hp*-adaption model is more efficient for resolving the singularity associated with Benchmark System 1. At each adaptive step, the integrated *hp*-adaptive strategy improved the discretization by either bisecting an element or increasing the order of an element. The decoupled *hp*-adaptive strategy considered here, first refined the first-order mesh by element bisection for the first six adaptive steps, and then improved the discretization by increasing the order of an element in each subsequent adaptive step (i.e., mixed-order *p*-adaption). For both adaption models, elements were ranked for refinement using the optimal discretization-based refinement criterion in the same way as for the *h*- and *p*-adaption methods described above. Furthermore, the mixed-order *p*-adaption refinements were achieved using exactly the same procedures as described previously for the *p*-adaption studies. The uniform *hp*-adaption results were determined using both an integrated and a decoupled approach. For the integrated approach, all of the elements in a mesh were bisected and their orders augmented alternately at successive iterations of the adaption. For the decoupled approach, the first-order mesh was refined by element bisection for the first three adaptive steps, and the order of the elements was then uniformly increased at each successive adaptive iteration. Finally, all of the *hp*-adaptive studies considered in this section were based on first-, second-, fourth- and eighth-order elements only; the results follow.

The convergence of the percent error in functional value for the the *hp*-adaption strategies described above in resolving the electrostatic benchmark system is illustrated in Figure 3.41. It may be noted that the integrated and decoupled schemes result in superior rates of convergence relative to the uniform *hp*-adaption strategies for Benchmark System 1. Therefore, it may be concluded that the new optimal

discretization-based refinement criterion is effective for evolving efficient distributions of DOF by *hp*-adaption over the problem domain. Furthermore, the decoupled approach is seen to provide a faster rate of convergence relative to the integrated *hp*-adaption. Theoretically, decoupled *hp*-adaption should not produce better convergence performance than fully integrated *hp*-adaption. However, based on the results presented for the analysis of Benchmark System 1, the decoupled approach is more effective for electrostatic systems with regions of rapid field solution variation. The superior *hp*-adaption performance results of the decoupled approach may be explained as follows. The two types of *hp*-adaption produce rather different evolving discretizations which are compared in Figure 3.42. The integrated approach, initially, attempts to resolve the singularity by increasing element order rather than by element bisection. The decoupled approach results in a superior distribution of DOF since it produces meshes with a higher density of DOF near the singularity, compared with the more uniform distribution produced by the integrated approach.

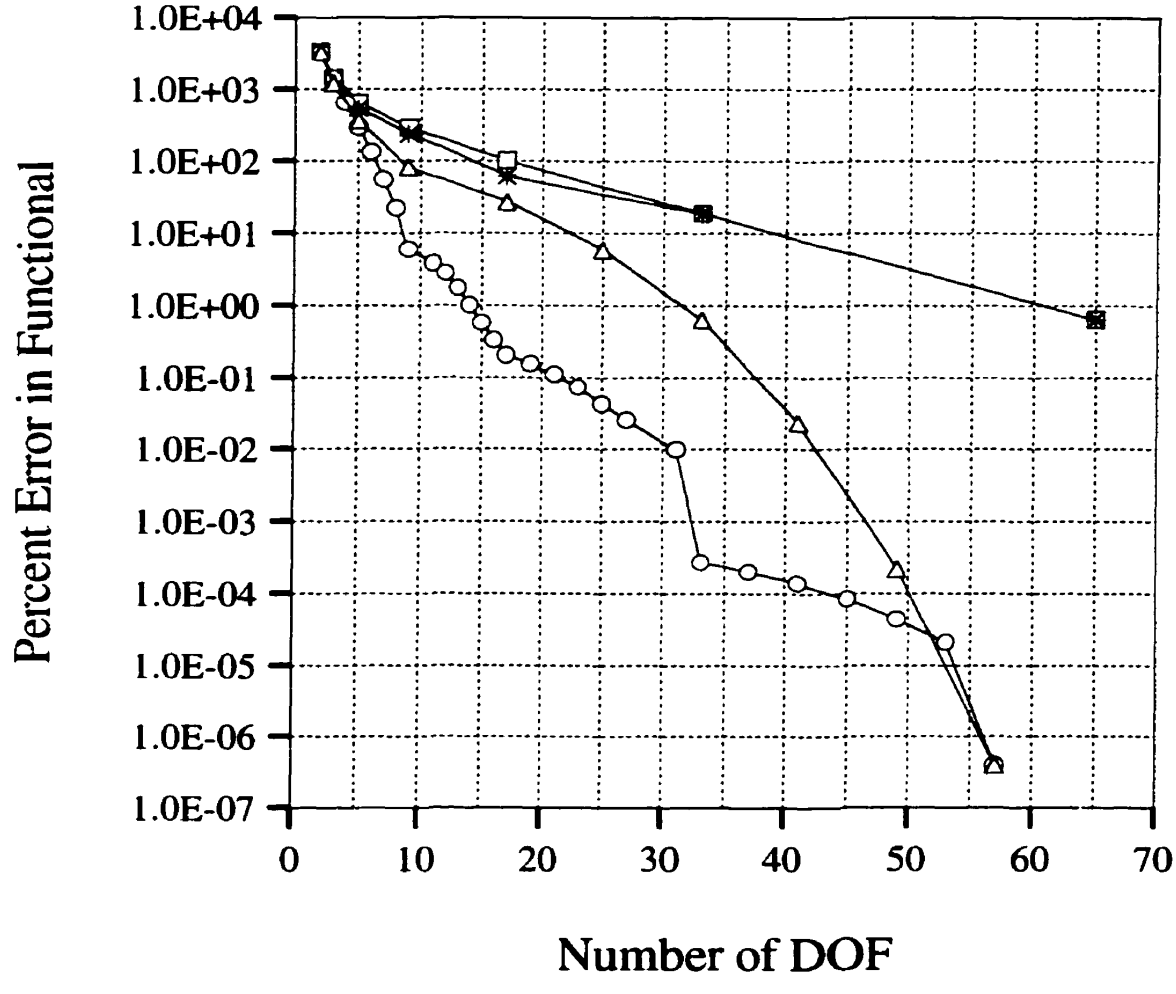

Figure 3.41: The convergence of percent error in functional value with discretization level for *hp*-adaption studies for Benchmark System 1 is illustrated. The triangle knot results correspond to percent error in functional values computed from solutions based on integrated *hp*-discretizations evolved using the new optimal discretization-based refinement criterion. The circle knot results correspond to percent error in functional values computed from solutions based on decoupled *hp*-discretizations evolved using the new optimal discretization-based refinement criterion. The asterisk knot results correspond to percent error in functional values computed from solutions based on uniform integrated *hp*-refinement discretizations. The square knot results correspond to percent error in functional values computed from solutions based on uniform decoupled *hp*-refinement discretizations.

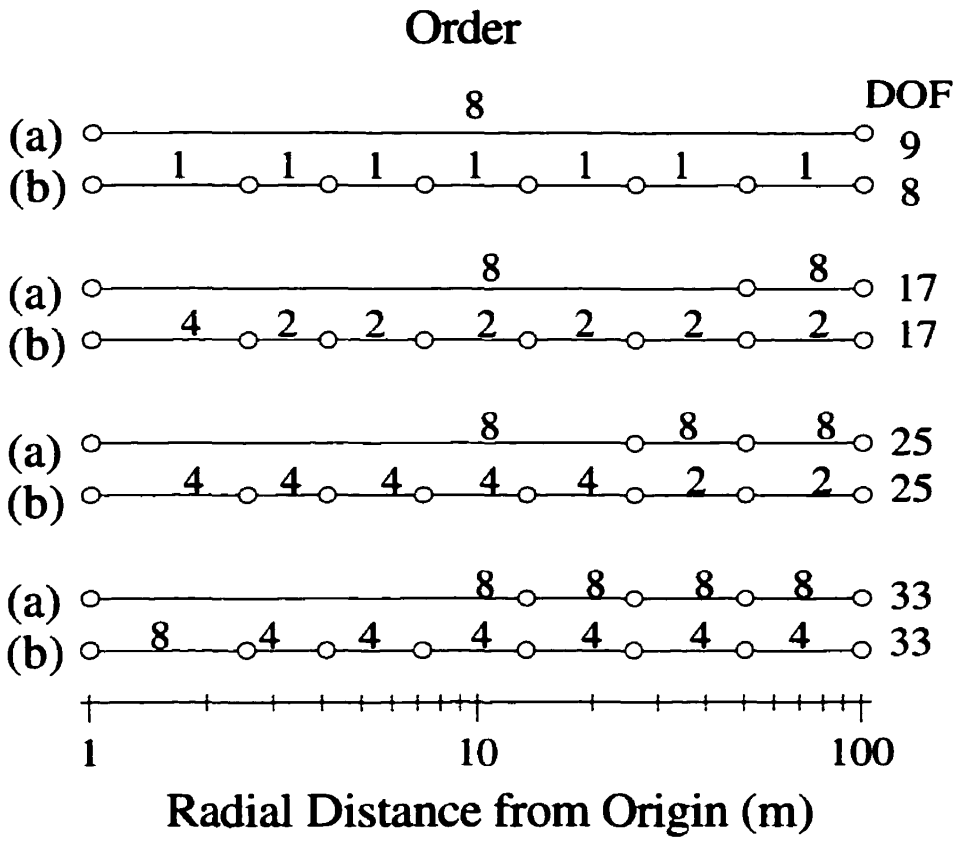

Figure 3.42: Evolving radial discretizations for *hp*-adaption for one-dimensional electrostatic potential analysis of Benchmark System 1 are illustrated: (a) integrated *hp*-adaption discretizations; and (b) decoupled *hp*-adaption discretizations. The radial discretizations are plotted on a logarithmic scale because of the proximity of the element vertices to each other near the singularity. Note: the positions of the element vertices in the meshes are determined by element bisection; the orders of the elements are specified above each element; and the number of DOF in each mesh is shown to the right of each discretization.

3.3.3 Benchmark System 2

The effectiveness of the new optimal discretization-based refinement criterion is evaluated in this section for Benchmark System 2 with a series of studies involving the primary adaption models. Specifically, the convergence of the same range of *h*-, *p*- and *hp*-adaption strategies that were investigated for Benchmark System 1 are also examined for Benchmark System 2 when the optimal discretization-based refinement criterion is used to guide the adaption. As noted earlier, one of the most important challenges for all types of adaption in FEA is the accurate and efficient resolution of the singularities associated with sharp material edges [61, 81, 162]. Moreover, it has been noted that the slow progress in developing practical *hp*-adaption strategies is, partially, due to the lack of objective benchmarks by which to gauge the strengths and weaknesses of adaptive strategies. Therefore, the usefulness of the adaption benchmark results reported in this section for the analysis and design of optimal *hp*-adaption strategies will be illustrated. Finally, it should be noted that the adaption methods employed in this section were implemented using exactly the same procedures that were used for Benchmark System 1.

The convergence of the percent error in functional value for an *h*-adaption strategy based on element bisection applied to the magnetostatic benchmark system is illustrated in Figure 3.43 for first-order elements. The optimal discretization-based refinement criterion was used to rank the elements, and the element bisection refinements were executed in exactly the same way as described for Benchmark System 1. The uniform *h*-refinement baseline and the optimal first-order discretization functional convergence results are also shown in Figure 3.43 for comparison. The convergence of the *h*-adaption element bisection scheme guided by the optimal discretization-based refinement criterion is seen to have the same interesting feature that was noted for Benchmark System 1. Initially, the element bisection *h*-adaption strategy produces discretizations with functional accuracy levels superior to those of the uniform dis-

cretizations with corresponding numbers of elements; moreover, after approximately six adaptive steps the functional accuracy achieved by the optimal discretization-based element bisection scheme is seen to be remarkably close, and approximately equivalent, to that of the optimal discretizations. This similarity in functional accuracy levels for the element bisection h-adaption discretizations and the optimal discretizations is significant for the same important reason discussed in the preceding section: namely, the element bisection scheme is relatively inexpensive compared to solving the the set of nonlinear finite element optimization equations required to compute the optimal discretizations.

The analogous second-order h-adaption results for Benchmark System 2 are shown in Figure 3.44. The fourth- and eighth-order h-adaption results are shown in Figure 3.45 and Figure 3.46, respectively. It may be noted that for the second- and fourth-order cases, the functional accuracy of the element bisection strategy after approximately six adaptive steps is relatively close to that of the optimal discretizations, which is consistent with the first-order results reported above. The eighth-order h-adaption results were not computed beyond three iterations; however, the element bisection strategy produced discretizations with functional accuracy levels superior to those of the uniform discretizations with corresponding numbers of eighth-order elements. Therefore, based on the complete set of h-adaption results computed for the magnetostatic system, the new optimal discretization-based refinement criterion is effective for evolving efficient distributions of DOF over the problem domain for Benchmark System 2. Moreover, based on the first-, second- and fourth-order h-adaption results reported for Benchmark System 2, it is suggested that the new optimal discretization-based refinement criterion can be used to efficiently and reliably guide adaptive finite element solvers towards optimal solutions for magnetostatic systems with regions of rapid field solution variation.

The convergence of the percent error in functional value for two p-adaption strategies applied to a range of uniform initial meshes for the magnetostatic benchmark

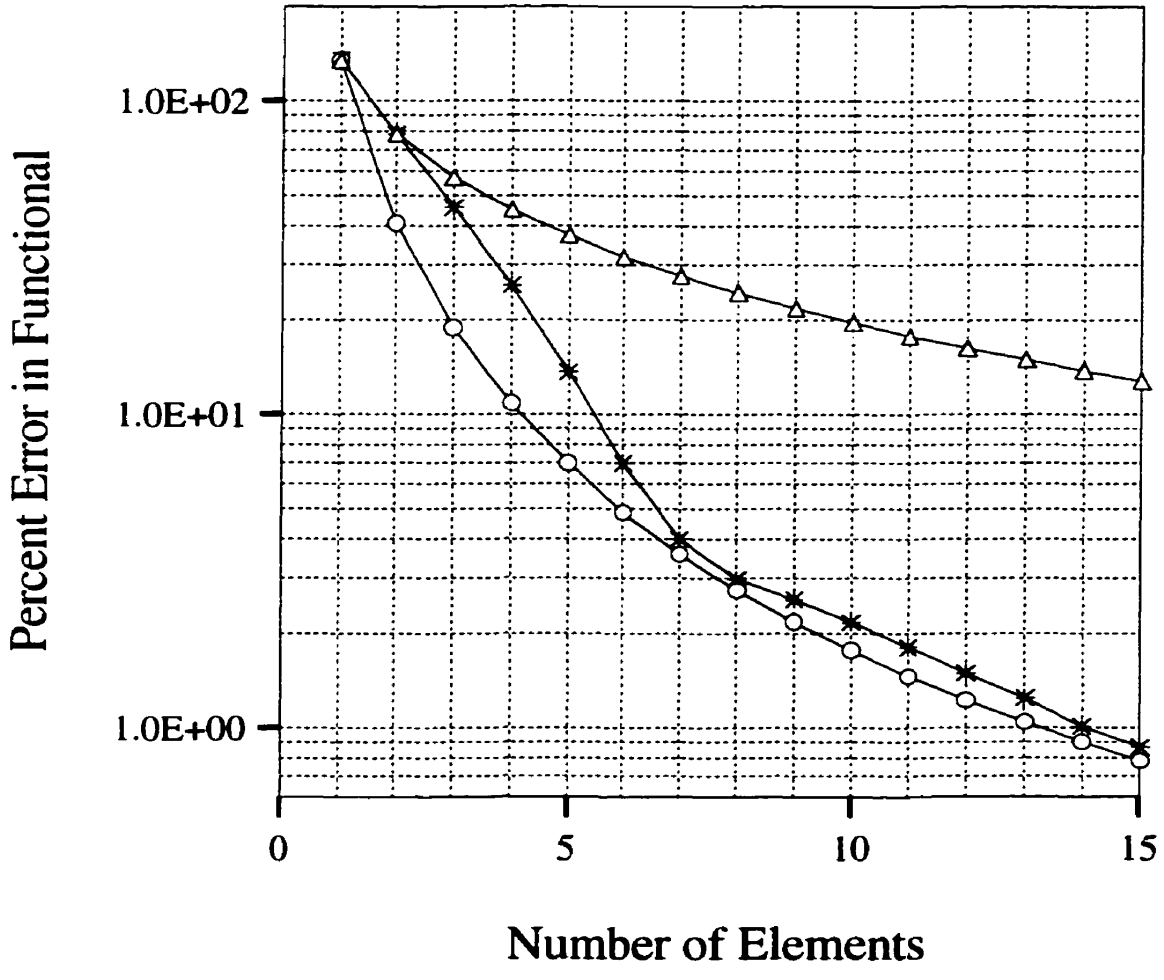

Figure 3.43: The convergence of percent error in functional value with discretization level for first-order h-adaption studies for Benchmark System 2 is illustrated. The triangle knot results correspond to percent error in functional values computed from solutions based on first-order uniform h-refinement discretizations. The asterisk knot results correspond to percent error in functional values computed from solutions based on first-order element bisection h-adaption discretizations evolved using the new optimal discretization-based refinement criterion. The circle knot results correspond to percent error in functional values computed from solutions based on first-order optimal discretizations.

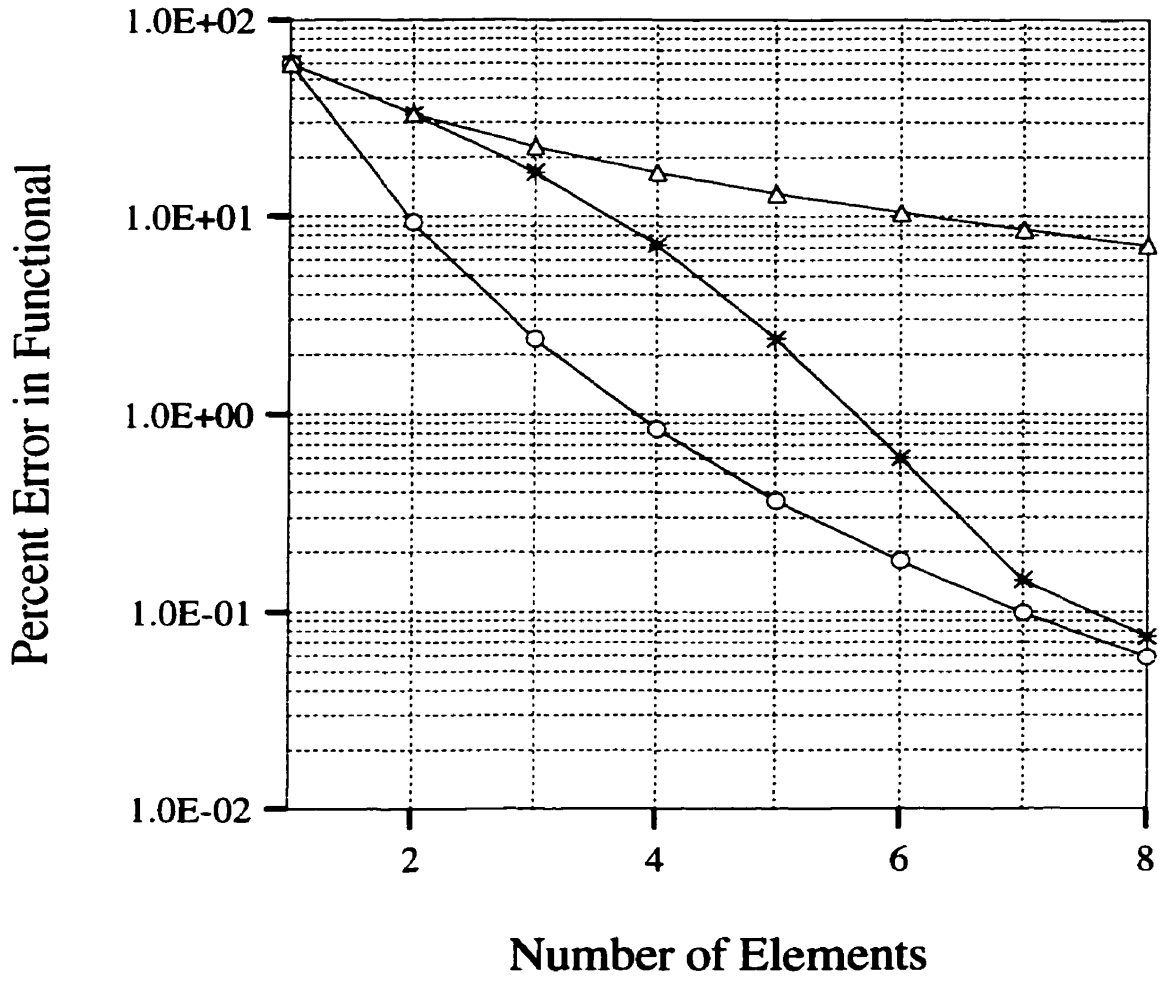

Figure 3.44: The convergence of percent error in functional value with discretization level for second-order h-adaption studies for Benchmark System 2 is illustrated. The triangle knot results correspond to percent error in functional values computed from solutions based on second-order uniform h-refinement discretizations. The asterisk knot results correspond to percent error in functional values computed from solutions based on second-order element bisection h-adaption discretizations evolved using the new optimal discretization-based refinement criterion. The circle knot results correspond to percent error in functional values computed from solutions based on second-order optimal discretizations.

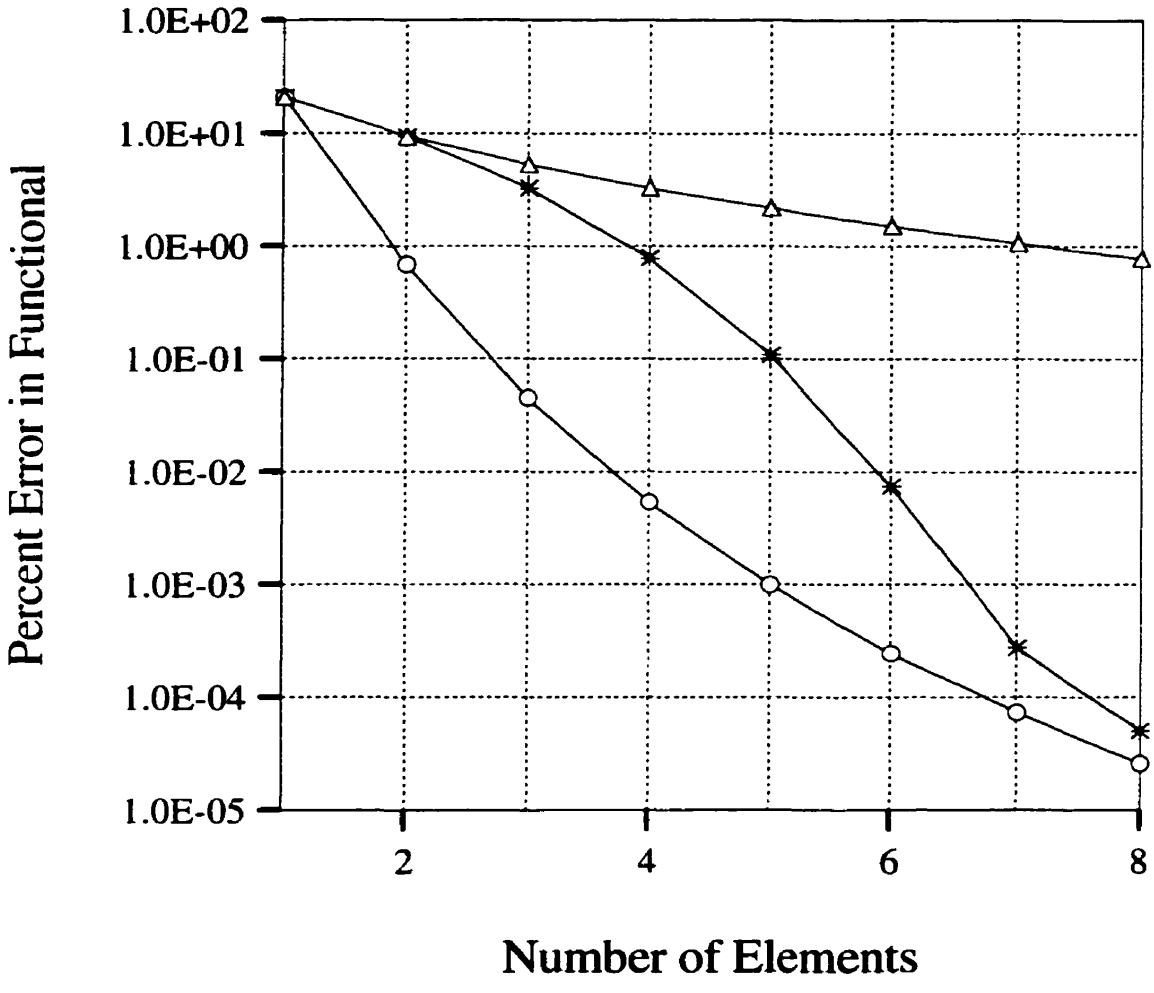

Figure 3.45: The convergence of percent error in functional value with discretization level for fourth-order h-adaption studies for Benchmark System 2 is illustrated. The triangle knot results correspond to percent error in functional values computed from solutions based on fourth-order uniform h-refinement discretizations. The asterisk knot results correspond to percent error in functional values computed from solutions based on fourth-order element bisection h-adaption discretizations evolved using the new optimal discretization-based refinement criterion. The circle knot results correspond to percent error in functional values computed from solutions based on fourth-order optimal discretizations.

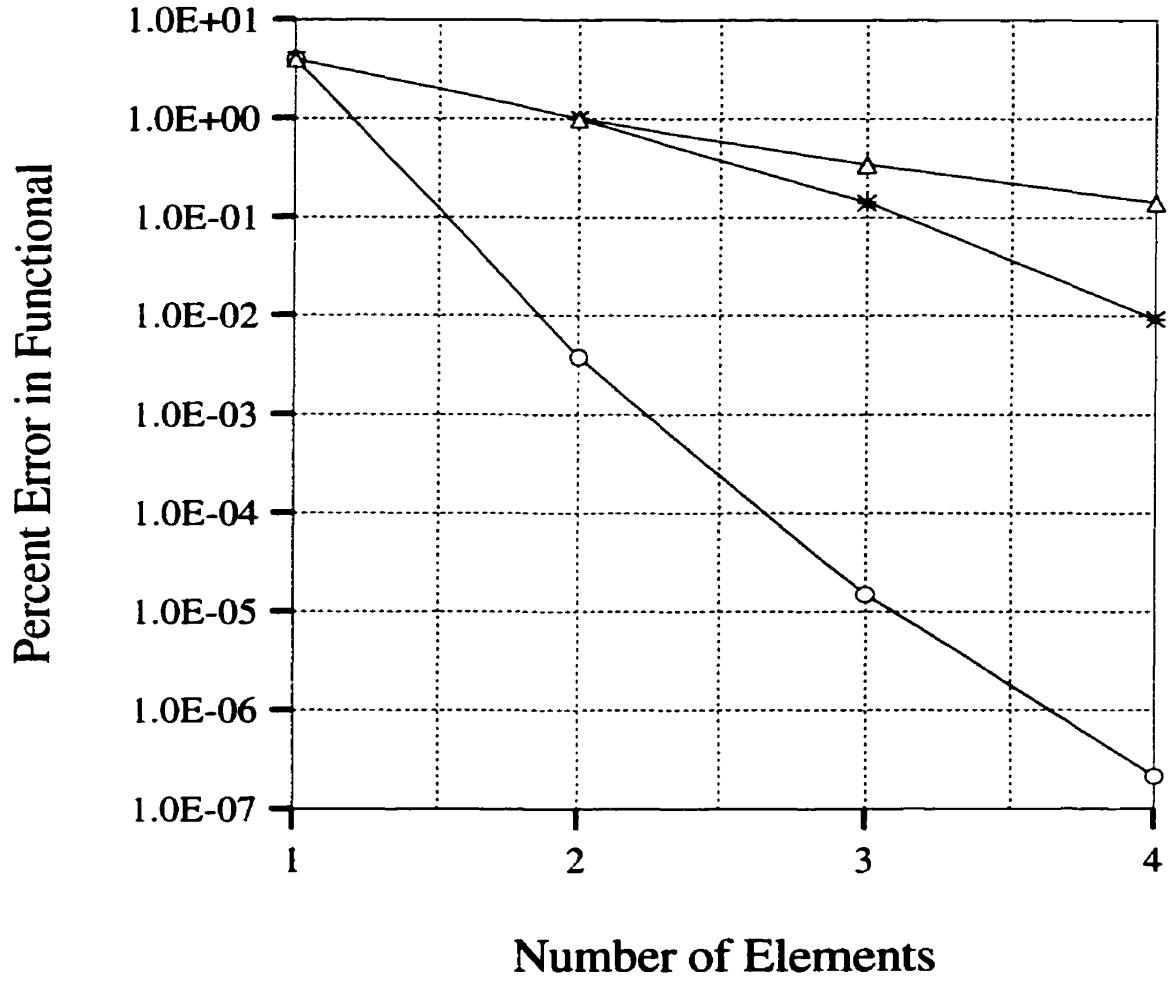

Figure 3.46: The convergence of percent error in functional value with discretization level for eighth-order h-adaption studies for Benchmark System 2 is illustrated. The triangle knot results correspond to percent error in functional values computed from solutions based on eighth-order uniform h-refinement discretizations. The asterisk knot results correspond to percent error in functional values computed from solutions based on eighth-order element bisection h-adaption discretizations evolved using the new optimal discretization-based refinement criterion. The circle knot results correspond to percent error in functional values computed from solutions based on eighth-order optimal discretizations.

system is illustrated in Figure 3.47. Specifically, the same uniform and mixed-order p-adaption schemes that were investigated for Benchmark System 1 were also considered for Benchmark System 2. The functional convergence based on uniform p-adaption for initial meshes of four, eight and twelve elements is shown by curves A, B and C, respectively. The functional convergence for the corresponding mixed-order p-adaption scheme is shown by curves D, E and F for the four, eight and twelve element meshes respectively. In each case, the uniform meshes were initially comprised of first-order elements, which were successively refined using second-, fourth- and eighth-order elements. For the mixed-order p-adaption scheme, the optimal discretization-based refinement criterion was used to guide the adaption using exactly the same procedures that were described for Benchmark System 1. Based on the convergence of the percent errors shown in Figure 3.47 for the two p-adaption schemes considered, it is evident that when starting from uniform initial meshes the mixed-order p-adaption scheme results in a significantly faster rate of convergence relative to the uniform p-adaption strategy for Benchmark System 2. In fact, for the four element case investigated, the same maximal functional accuracy level was achieved with 17 DOF by the mixed-order p-adaption scheme compared with 33 DOF required by the uniform method (a relative savings of approximately 48 percent in the number of DOF). Similarly, for the eight element case a relative reduction of approximately 58 percent in the number of DOF required to achieve maximal functional accuracy was observed when the mixed-order p-adaption scheme was used rather than the uniform method. Analogously, a 64 percent economy in DOF was achieved for the twelve element case. Therefore, it is suggested that the new optimal discretization-based refinement criterion is effective for evolving efficient distributions of DOF by p-adaption over the problem domain for magnetostatic systems with regions of rapid field solution variation.

The same hp-adaption studies that were used to evaluate the effectiveness of the optimal discretization-based refinement criterion for Benchmark System 1, were also

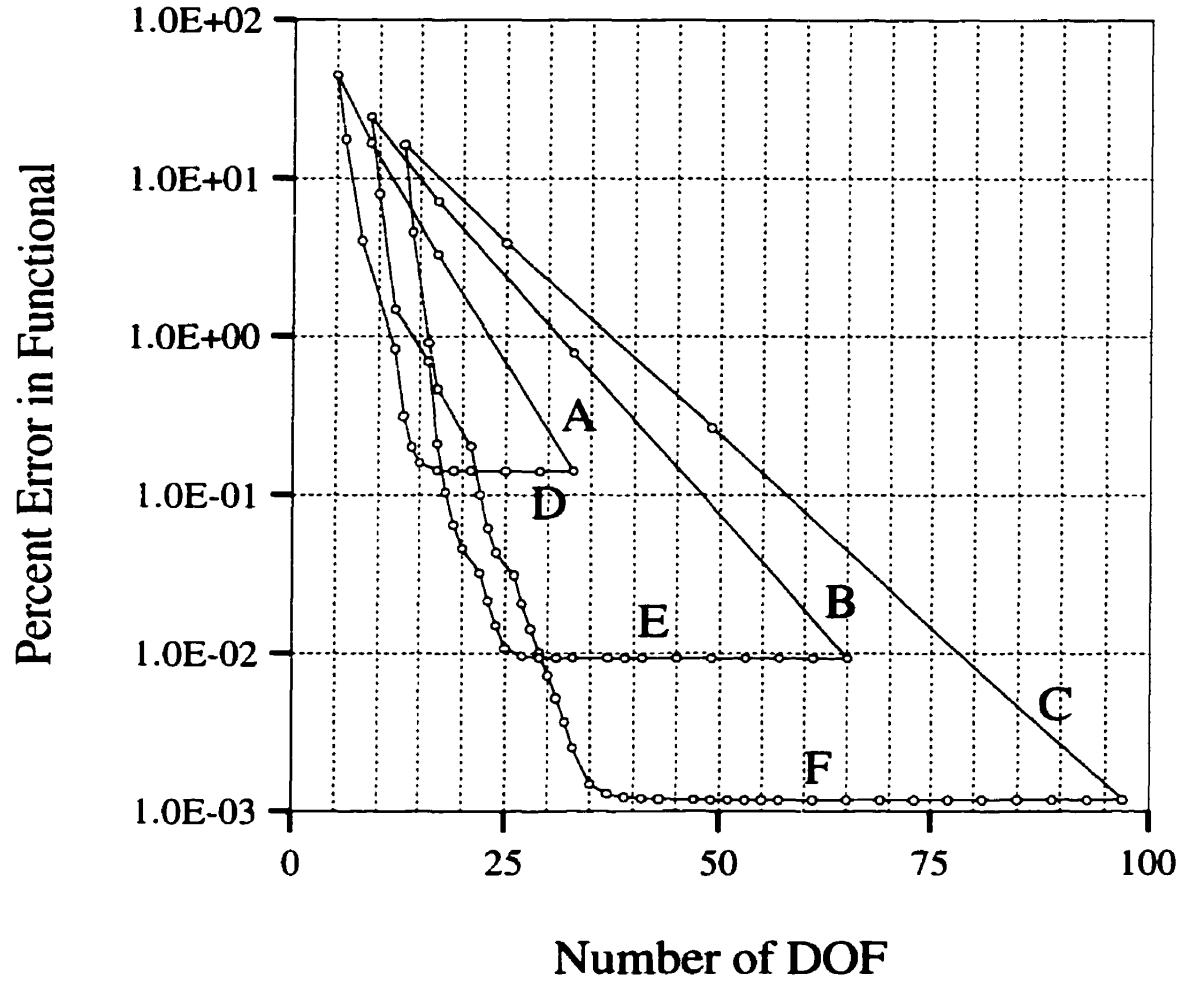

Figure 3.47: The convergence of percent error in functional value with discretization level for the p-adaption studies for Benchmark System 2 is illustrated. Curve A, B, and C results correspond to percent error in functional values computed from solutions based on uniform p-discretizations for initial meshes of four, eight and twelve elements, respectively. Curve D, E, and F results correspond to percent error in functional values computed from solutions based on mixed-order p-discretizations evolved using the new optimal discretization-based refinement criterion for initial meshes of four, eight and twelve elements, respectively.

conducted for Benchmark System 2. The convergence of the percent error in functional value for the *hp*-adaption strategies in resolving the magnetostatic benchmark system is illustrated in Figure 3.48. It may be noted that the integrated and decoupled *hp*-adaption schemes result in superior convergence rates relative to the uniform *hp*-refinements for Benchmark System 2. Therefore, it may be concluded that the new optimal discretization-based refinement criterion is effective for evolving efficient distributions of DOF by *hp*-adaption over the problem domain. Furthermore, the decoupled approach is seen to provide a faster rate of convergence relative to the integrated *hp*-adaption, for the same reasons explained for Benchmark System 1: namely, the decoupled approach produces meshes with a higher density of DOF near the singularity, compared with the more uniform distribution produced by the integrated approach. Therefore, based on the *hp*-adaption results presented for Benchmark System 2, the decoupled approach is more effective for magnetostatic systems with regions of rapid field solution variation.

3.3.4 Discussion

The results presented in the two preceding sections demonstrate the value of employing optimality properties of finite element discretizations to develop effective feedback refinement criteria for guiding adaptive systems efficiently and reliably towards accurate solutions. The significance of this is directly related to the implications that it holds for the development of advanced strategy feedback control systems for AFEA: currently, one of the major research issues in AFEMs for electromagnetics. Essentially, the perennial challenge has been to resolve which error data to feedback after each iteration, and how to use it to initialize the next adaptive step. The hypothesis tested and validated in this section was that the underlying, or fundamental, variational principle on which the finite element method itself is based, could also be used as the basis for deriving new refinement criteria for adaptive finite element solvers. In fact, a new refinement criterion was shown to be quite valuable for both

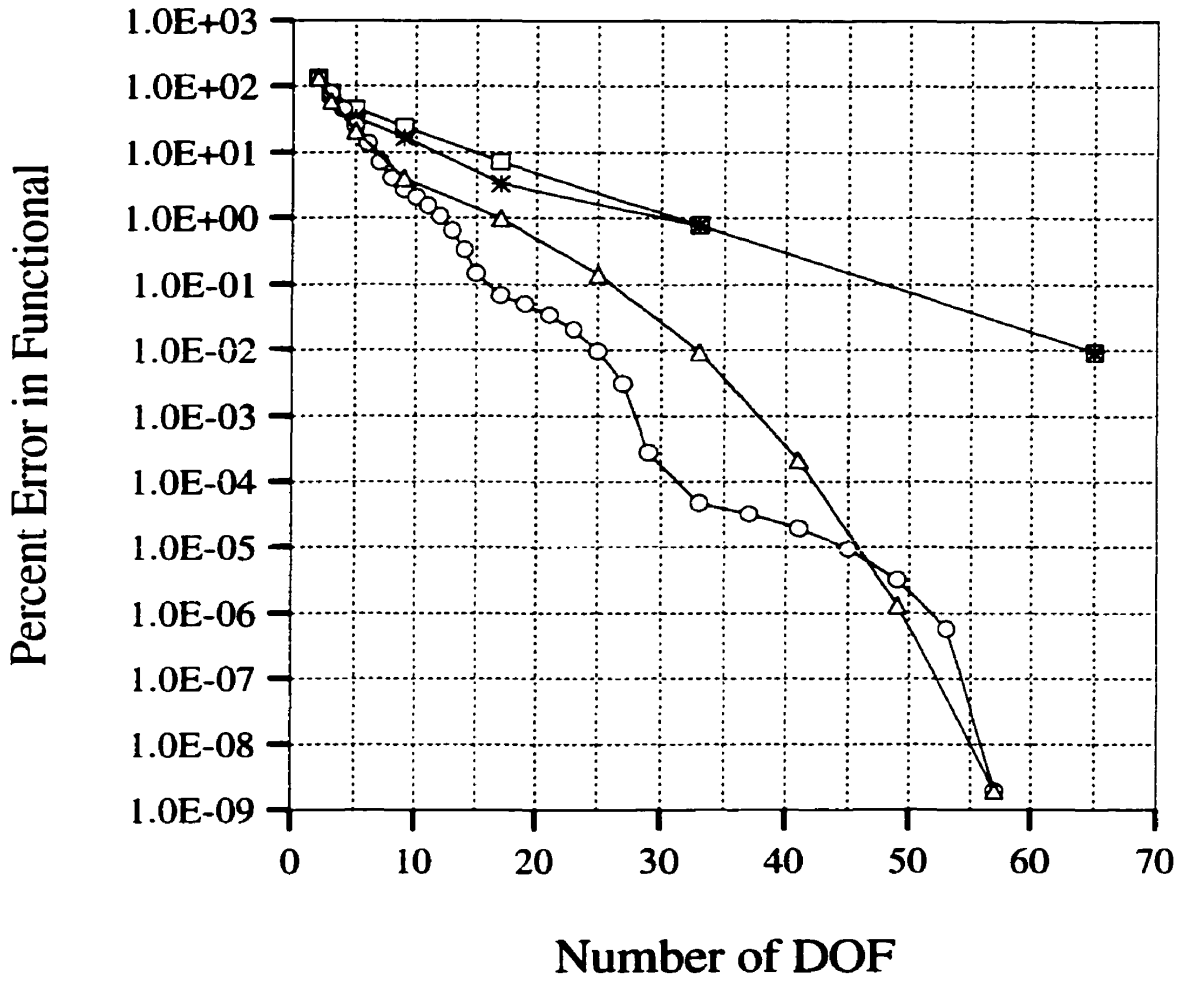

Figure 3.48: The convergence of percent error in functional value with discretization level for *hp*-adaption studies for Benchmark System 2 is illustrated. The triangle knot results correspond to percent error in functional values computed from solutions based on integrated *hp*-discretizations evolved using the new optimal discretization-based refinement criterion. The circle knot results correspond to percent error in functional values computed from solutions based on decoupled *hp*-discretizations evolved using the new optimal discretization-based refinement criterion. The asterisk knot results correspond to percent error in functional values computed from solutions based on uniform integrated *hp*-refinement discretizations. The square knot results correspond to percent error in functional values computed from solutions based on uniform decoupled *hp*-refinement discretizations.

its generality and reliability: it was effective when used with *h*-, *p*- and *hp*-adaption models for the AFEA of both electrostatic and magnetostatic systems.[2] Both of these assets are directly linked to the fundamental and theoretically justified principle used to derive the new refinement criterion. Furthermore, this underlying principle embodies a stationarity property, which is entirely dependent on the optimality of a finite element discretization. Therefore, the refinement criterion developed from this principle possesses the desirable benefit of intrinsically guiding an adaptive process towards optimal finite element solutions. Hence, this new criterion represents an important milestone in developing efficient practical adaptive methods for evolving sufficiently accurate solutions.

The two preceding sections also established a set of primary adaption benchmark results for the two fundamental electromagnetic singularity models, and illustrated their usefulness in the analysis and design of optimal adaption strategies. This is of particular importance, since one of the most challenging problems of AFEA in electromagnetics over the past 15 years has been the accurate and efficient resolution of the singularities associated with sharp material edges and corners. The ability to compute a series of optimal singularity benchmarks has permitted the primary adaption procedures and control schemes to be evaluated and compared on both a relative and an absolute performance scale for two of the most demanding electromagnetic adaption scenarios. This represents a significant advancement over the heuristic assessment approaches that had formerly been relied upon. In fact, prior to this work, it has been recognized that an important reason for the slow development in this research area was the lack of objective standards for judging emerging AFEA methods.

The optimal discretization-based refinement criterion examined in this section, is

[2]The validity of the one-dimensional finite element optimization equations was also confirmed for a Helmholtz system based on the free-space plane-wave model. In addition, optimal discretizations computed for the one-dimensional wave model displayed superior functional accuracy levels relative to corresponding uniform discretizations, suggesting that optimal discretization-based adaption for Helmholtz systems may be advantageous as well. A related two-dimensional Helmholtz system is considered later in this work.

defined by the simple principle of evaluating the finite element optimization equations in order to assess the degree to which they are satisfied by a given set of fixed element vertex positions. This principle, in turn, is based on the optimality criterion that the optimization equations will be satisfied exactly by the ideal mesh for a given number of DOF, that is, the mesh that produces the most accurate solution. This optimality criterion has been confirmed numerically for the one dimensional systems considered, and the one-dimensional results presented above for the optimal discretization-based refinement criterion represent an important contribution to the study and development of feedback control systems for AFEA. The application of similar optimal discretization-based refinement criteria for the AFEA of two- and three-dimensional electromagnetic systems is considered in the next chapter.

Chapter 4

Numerical Evaluation of the Two- and Three-Dimensional Finite Element Optimization Equations

In this chapter, important benchmark electromagnetic problems are introduced in order to achieve a twofold objective. First, the validity of the nonlinear systems of two- and three-dimensional finite element optimization equations, derived in Chapter 2, are confirmed numerically. In order to achieve this objective, the equations are used to compute a series of optimal finite element solutions, that is, solutions with both optimal field solution values and optimal geometric discretization parameters, for the benchmark problems considered. The results are confirmed using techniques which are described in subsequent sections of this chapter. The second objective of this chapter is to develop theoretically justified, efficient, reliable and practical optimal discretization-based refinement criteria for two- and three-dimensional electromagnetic AFEA. Thus, the optimal solutions are used to extend the new concepts developed in the previous chapter to two- and three-dimensional analyses of electromagnetic systems. The performance of the new refinement criteria are evaluated for the primary adaption models and compared with those of some of the best refinement criteria currently available. In addition, two computational analysis and design application examples are presented to help illustrate the practical value of the new optimal discretization-based approach for AFEA.

4.1 Two-Dimensional Systems

The findings from the one-dimensional studies, reported in the previous chapter, suggest that the new optimal discretization-based refinement criterion possesses the required properties to be effective, reliable and efficient for practical AFEA of electromagnetic systems. The purpose of this section is to investigate the potential benefits

of using the finite element optimization equations, derived in section 2.4.2, to develop analogous optimal discretization-based refinement criteria for two-dimensional electromagnetic AFEA. The approach used to achieve this objective is to, first, validate the two-dimensional formulation of section 2.4.2 using a set of numerical tests on translationally symmetric electromagnetic systems. Subsequently, results from a series of studies on Laplace and Helmholtz benchmark systems involving the primary adaption models are analyzed, in order to evaluate the effectiveness of the proposed two-dimensional optimal discretization-based refinement criteria for practical AFEA. For both cases, the performance of the new optimal discretization-based refinement criteria are examined with h-, p- and hp-adaptive solvers. In addition, the practical significance of the new approach is evaluated using performance comparisons with some of the best adaptive solvers currently available. Finally, it should be noted that the hierarchal basis functions developed in [95] are employed to approximate the unknown field solutions over triangular elements for all of the studies reported throughout this section.

4.1.1 Validation of the Optimization Equations

In order to validate the two-dimensional finite element optimization equations derived in section 2.4.2, the x- and y-components of the functional gradients with respect to element vertex positions were tested with a range of numerical benchmark evaluations. Specifically, three translationally symmetrical coaxial transmission line models were used to compute a series of first-, second-, fourth- and eighth-order finite element solutions with both optimal field solution and optimal geometric discretization parameter values. The three models are distinguished by their differently shaped cross-sections and, hence, the corresponding included angles at the sharp reentrant corners of the two-dimensional problem domains used for the finite element analyses. These coaxial transmission line systems will be discussed and described in greater detail subsequently. Although there are several possible choices of two-

dimensional benchmark systems which can be used for the purpose of this section, the coaxial transmission line models were chosen for the following important reason. In two-dimensional electromagnetic systems, the electric field becomes singular at sharp reentrant corners where the included angle exceeds 180 degrees [23]. Consequently, finite element solutions will suffer inaccuracy principally from their inability to model the local field behavior near the reentrant corners: typically, the presence of sharp material edges in three-dimensional physical systems which give rise to such sharp corners in two-dimensional finite element models, can drastically decrease the convergence rate of the finite element method, as noted previously. Therefore, the accurate and efficient resolution of the singularities associated with sharp material corners is an important challenge for all types of finite element analysis. As noted earlier, the finite element method can be made more efficient for problems of this sort by using specialized elements that incorporate basis functions with the right type of field solution singularities [146–148]; however, the reduced convergence rate of the finite element method when field singularities are present may also be improved by using discretizations which have strongly focussed distributions of DOF close to the singularities. Thus, AFEMs which can recognize and refine the regions of rapid solution variation near the singularities will be effective in producing sufficiently accurate solutions efficiently. In order to ensure the effectiveness and reliability of new refinement criteria that are developed, when applied to practical two-dimensional problems in which singular field behavior is a significant factor, it is valuable to first study the characteristics of optimal finite element discretizations of electromagnetic systems where this type of behavior is present and its effects on the convergence of the finite element method can be isolated from other possible contributing factors. To this end, the coaxial transmission line models described and discussed in the following sections represent ideal systems for validation of the two-dimensional finite element

optimization equations.[1]

4.1.1.1 Benchmark System 3(a)

The first benchmark system used to validate the two-dimensional finite element optimization equations derived in section 2.4.2 is defined by Figure 4.1. It consists of an infinitely long, air-filled, uniform, square coaxial line in cross-section. The objective for this benchmark system is to compute the functional value corresponding to the electrostatic potential energy per unit length stored in the air region between the two ideal conductors of the system. The primary feature of this system is the rapid field solution variation close to the sharp reentrant corners with included angles of 270 degrees at the intersections of the edges of the inner conductor. This feature is common to many practical devices that contain sharp material edges, and has been shown to significantly reduce the convergence rate of the finite element method [23].

The electrostatic system used to establish the optimal discretization benchmark results of this section, was analyzed for electric scalar potentials using the two-dimensional finite element formulation given in section 2.4.2, and the corresponding finite element optimization equations were used to test the x- and y-components of the functional gradients with respect to element vertex positions for a series of numerical benchmark evaluations based on the geometry and eight-element mesh defined by Figure 4.2. It is one-quarter of the square coaxial line in cross-section – the standard "L" problem. The conductor boundary conditions (Dirichlet) are $1V$ and $0V$ as indicated; and the symmetry planes are labeled N (Neumann). There are six free geometric discretization parameters corresponding to the x- and y-coordinates of the positions of the element vertices in the mesh labeled 1, 2 and 3. Moreover, it may be noted that the optimal positions of the vertices labeled 1 and 3 are each

[1] It may be noted that the two-dimensional finite element optimization equations for Helmholtz systems are validated equally by the results reported for the coaxial transmission line models. This follows from the fact that the wave and source terms in the two-dimensional optimization equations involve only the same derivatives of the simplex area with respect to the x- and y-coordinates of the element vertices which appear in the Laplacian component of the equations (see Eqs. (2.96) and (2.97), for example).

constrained by the problem geometry to lie along the Neumann boundaries of the problem domain. Furthermore, the optimal position of the vertex labeled 2 must lie, by symmetry, along the diagonal line segment joining the upper right corners of the inner and outer conductor boundaries. Finally, for the first-, second-, fourth- and eighth-order finite element approximations that were computed for this benchmark system, the corresponding functional values were calculated from the computed scalar potentials using exact differentiation and integration.

The basic computational experiment that was performed in order to confirm the validity of the two-dimensional finite element optimization equations used to define the optimal discretization-based refinement criteria later in this section, is described next. This simple numerical experiment was based on resolving the electrostatic benchmark system using the elementary discretization described above and shown in Figure 4.2. Specifically, a series of 127,200 eight-element meshes were used to compute individual functional values corresponding to fixing the element vertices labeled 1 and 3 at 300 regularly spaced positions along the Neumann boundaries and the vertex labeled 2 at 424 regularly spaced positions along the diagonal line joining the upper right corners of the inner and outer conductor boundaries. It should be noted that for each of the meshes defined by this method, the unknown scalar electric potential values for the finite element model were computed using the standard finite element formulation with the geometric discretization held fixed.

Figure 4.3 shows the optimal first-order eight-element mesh for one-quarter of the cross-section of the square coaxial line. The results confirmed those obtained by evaluating the finite element optimization equations directly: the positions of the free vertices which yielded the smallest possible functional value were the same as those which yielded the smallest functional gradients along the permissible directions of optimization described above, with an error tolerance of $\pm 5.0 \times 10^{-5}$ (m). Furthermore, the functional value corresponding to the mesh defined by these optimal vertex positions represents the minimum electrostatic potential energy configuration of the

eight-element first-order finite element model for this benchmark system. This is wholly consistent with the underlying stationarity principle fundamental to the variational finite element formulation used throughout this work. It may be noted that the error tolerance stated above is, simply, one-half of the interval used to define successive vertex positions for computing the range of functional values used to confirm the results obtained by evaluating the finite element optimization equations directly. Similar results were computed for second-, fourth- and eighth-order meshes. In each case, the functional gradients with respect to element vertex positions correctly identified the optimal positions of the free element vertices, to yield the smallest possible functional value. The optimal second-, fourth-, and eighth-order meshes are shown in Figure 4.4, 4.5 and 4.6, respectively. It is interesting to note the increasingly sharp focus of DOF near the reentrant corner with increasing element order. The improved finite element model of the field solution over the outer elements, afforded by the higher-order approximations, allows for this to occur. Finally, the optimal positions of vertices 1, 2 and 3 are specified in Table 4.1 for each of the cases examined.

Table 4.1: Optimal vertex positions for Benchmark System 3(a).

Order / Vertex	1	2	3
1	0.4667	0.3433	0.4667
2	0.3333	0.1700	0.3333
4	0.2167	0.0933	0.2167
8	0.1700	0.0367	0.1700

Note: The table entries represent the ratios of the optimal vertex positions along the length of the line segments in the directions of optimization.

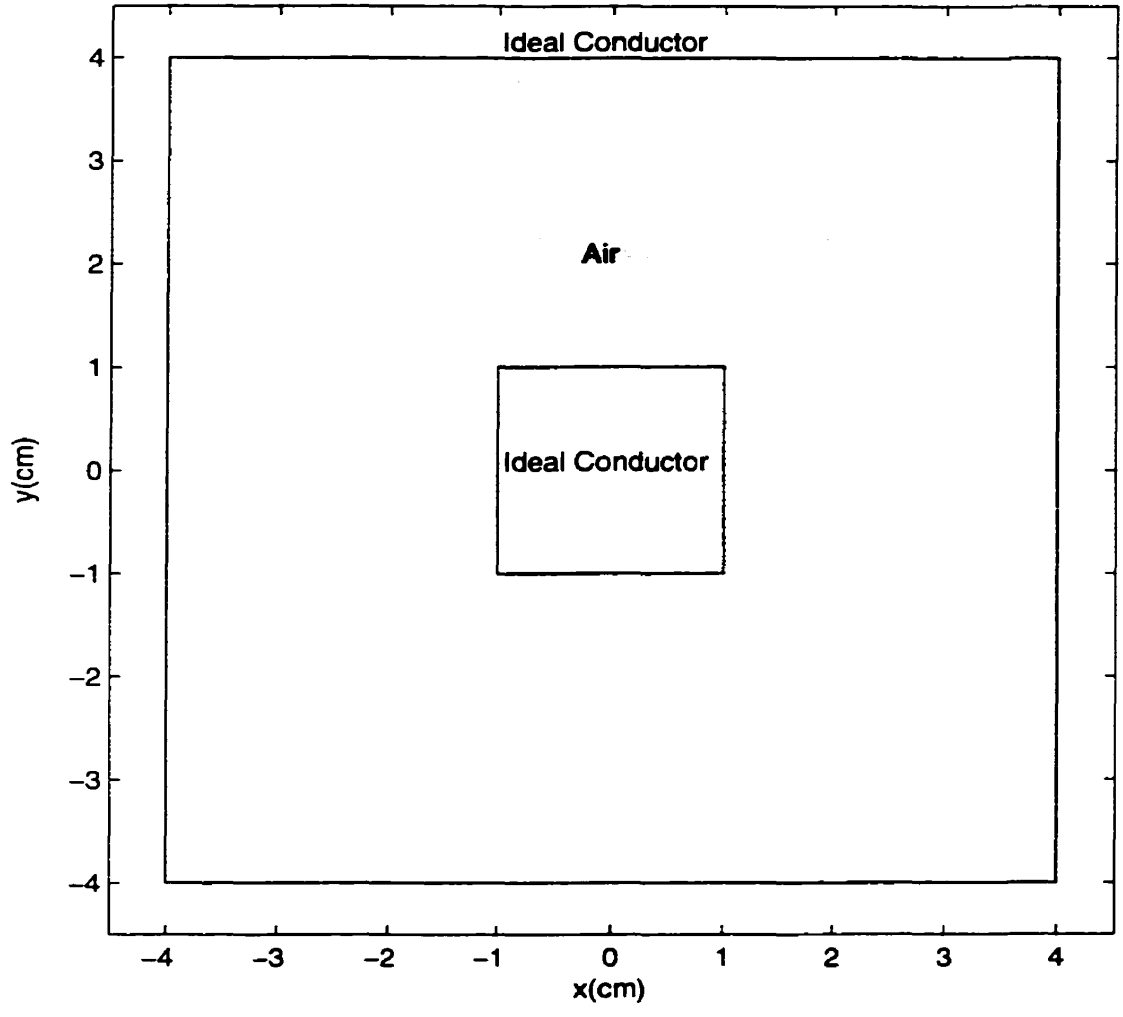

Figure 4.1: A cross-sectional view of Benchmark System 3(a) is illustrated. The two-dimensional view depicts an infinitely long, air-filled, uniform, square coaxial line in cross-section. The shaded annular area represents the air region between the two ideal conductors. The boundary of the inner conductor is prescribed to be a $1V$ equipotential line, and the boundary of the outer conductor is prescribed to be a $0V$ equipotential line.

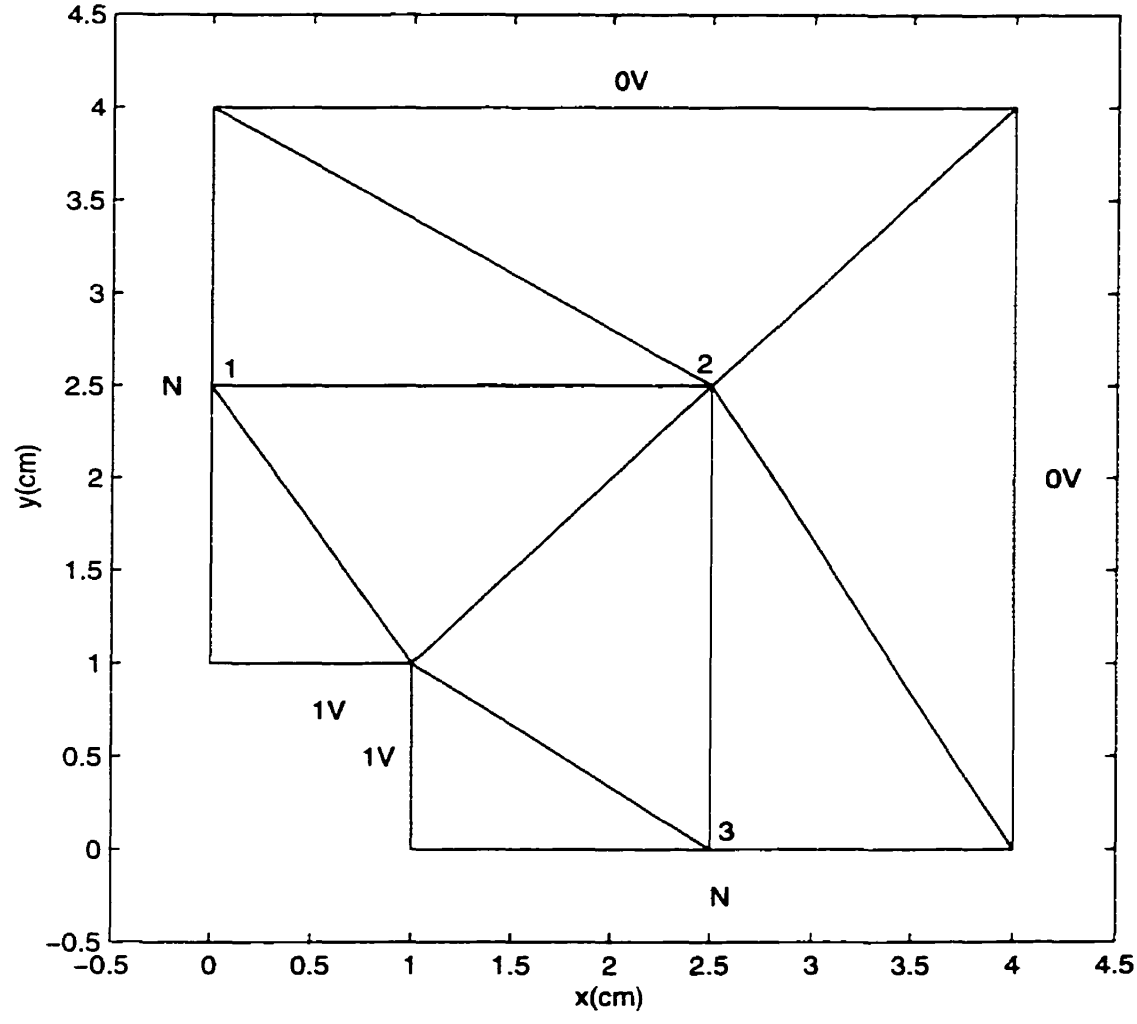

Figure 4.2: The geometry and finite element mesh configuration for the two-dimensional electrostatic potential analysis of Benchmark System 3(a) are illustrated. Eight triangular elements are used to model one-quarter of the square coaxial line in cross-section. The conductor boundary conditions (Dirichlet) are labeled $1V$ and $0V$; the symmetry planes are labeled N (Neumann). The positions of the vertices labeled 1, 2 and 3 correspond to the six free geometric discretization parameters for the finite element model. The sharp reentrant corner at the intersection of the edges of the inner conductor boundary has an included angle of 270 degrees.

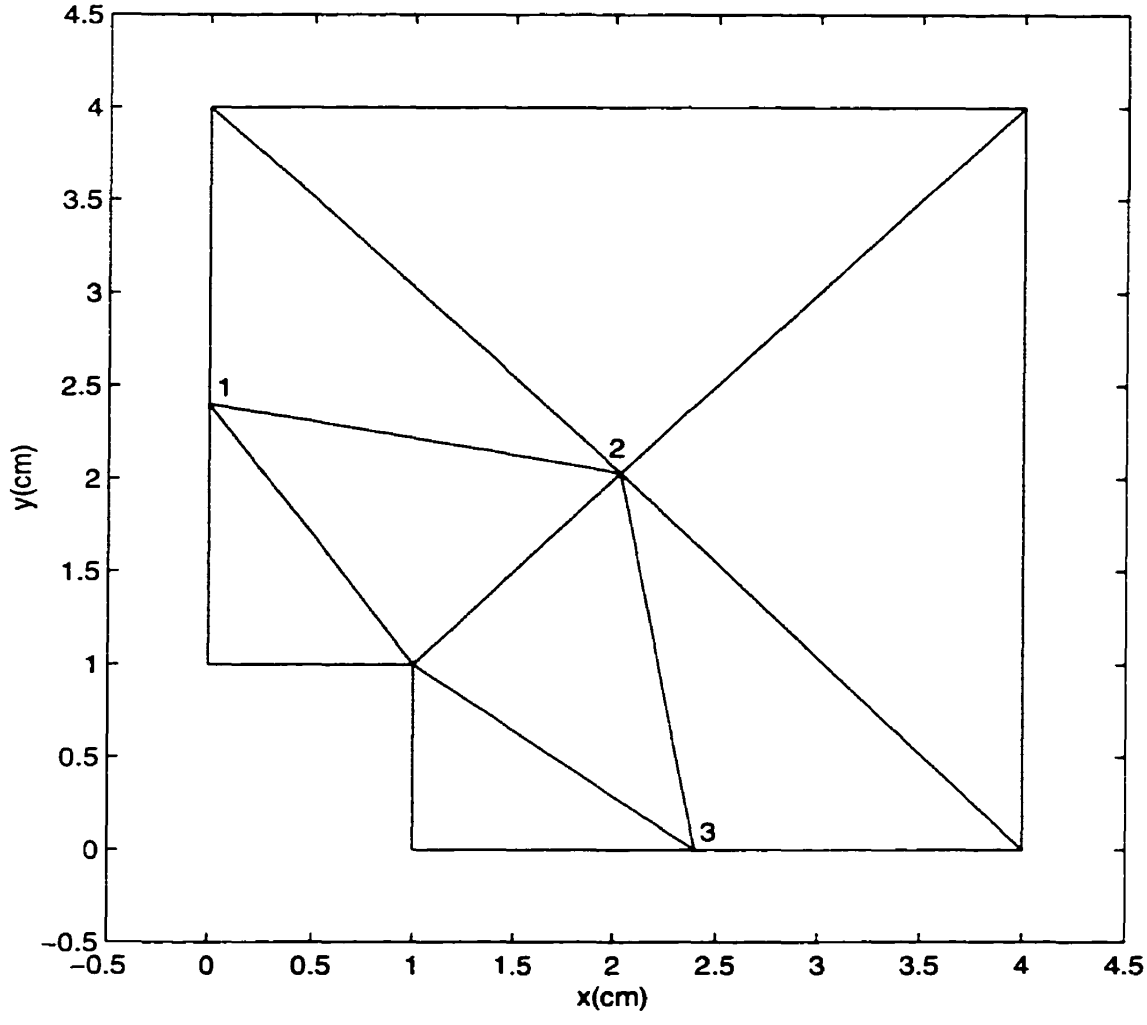

Figure 4.3: The first-order optimal eight-element mesh for the two-dimensional electrostatic potential analysis of Benchmark System 3(a) is illustrated. The vertices labeled 1 and 3 were each constrained, by the problem geometry, to lie along the Neumann boundaries; the vertex labeled 2 was constrained, by symmetry, to lie along the diagonal line segment joining the upper right corners of the inner and outer conductor boundaries. Note: the optimal positions of the element vertices labeled 1, 2 and 3 are specified in Table 4.1.

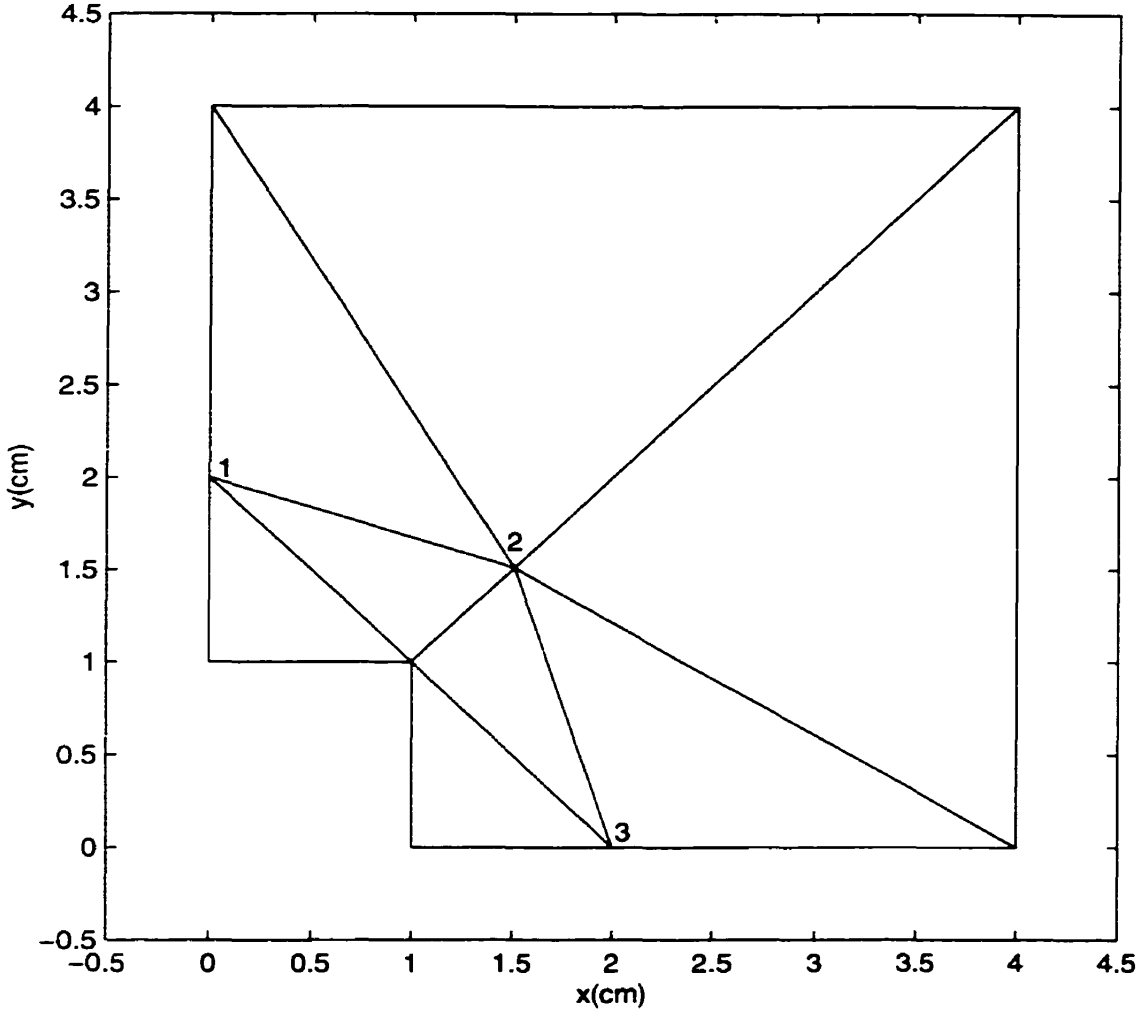

Figure 4.4: The second-order optimal eight-element mesh for the two-dimensional electrostatic potential analysis of Benchmark System 3(a) is illustrated. The vertices labeled 1 and 3 were each constrained, by the problem geometry, to lie along the Neumann boundaries; the vertex labeled 2 was constrained, by symmetry, to lie along the diagonal line segment joining the upper right corners of the inner and outer conductor boundaries. Note: the optimal positions of the element vertices labeled 1, 2 and 3 are specified in Table 4.1.

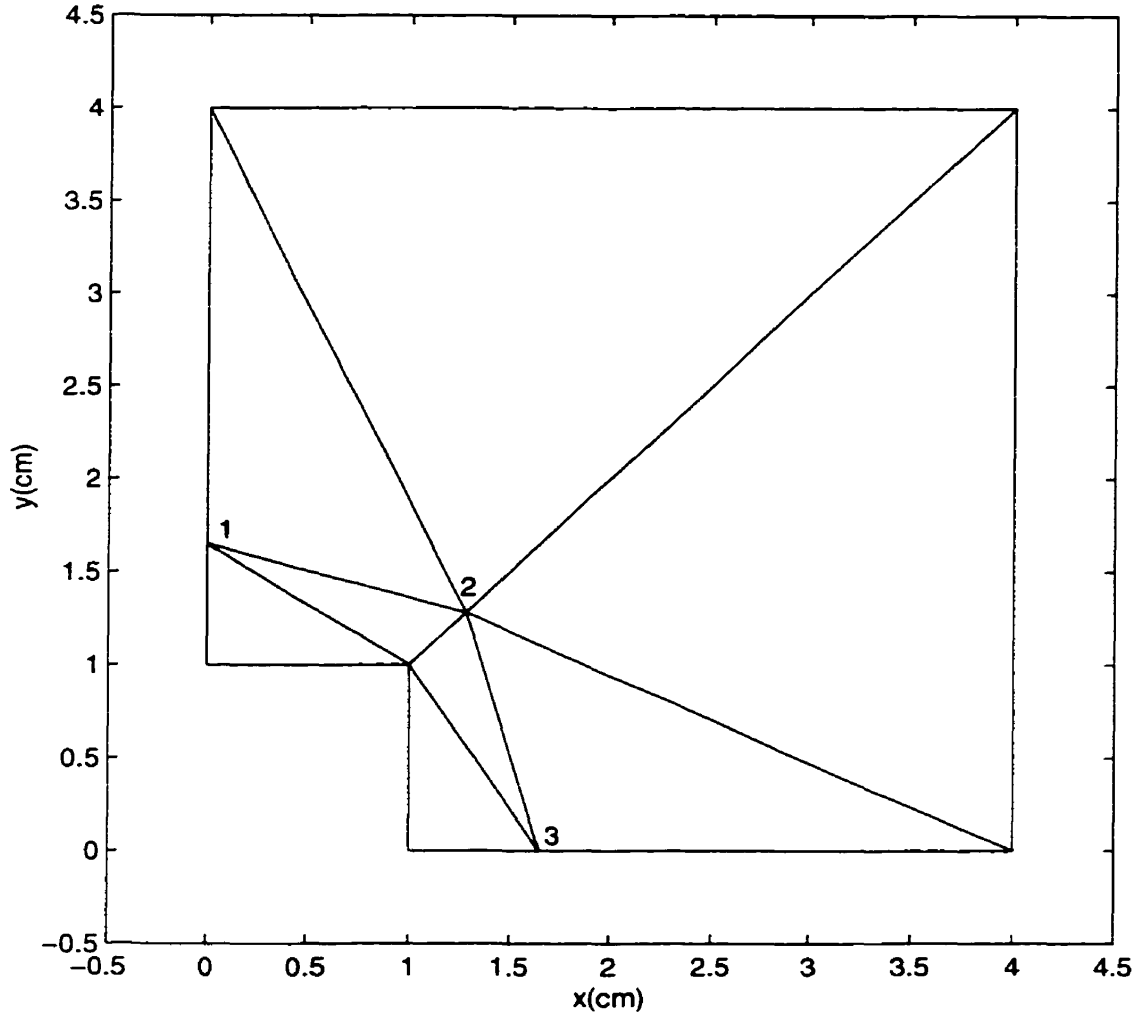

Figure 4.5: The fourth-order optimal eight-element mesh for the two-dimensional electrostatic potential analysis of Benchmark System 3(a) is illustrated. The vertices labeled 1 and 3 were each constrained, by the problem geometry, to lie along the Neumann boundaries; the vertex labeled 2 was constrained, by symmetry, to lie along the diagonal line segment joining the upper right corners of the inner and outer conductor boundaries. Note: the optimal positions of the element vertices labeled 1, 2 and 3 are specified in Table 4.1.

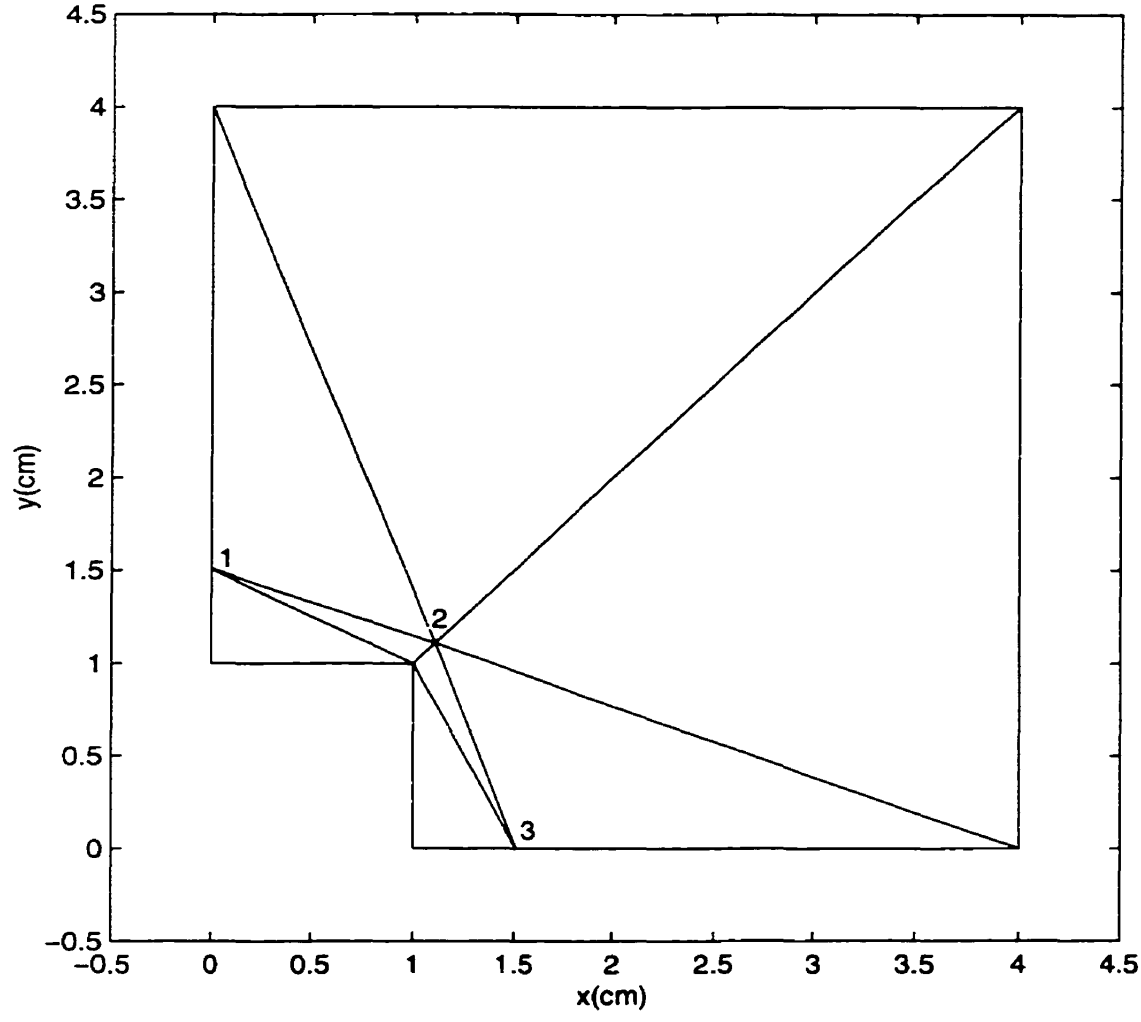

Figure 4.6: The eighth-order optimal eight-element mesh for the two-dimensional electrostatic potential analysis of Benchmark System 3(a) is illustrated. The vertices labeled 1 and 3 were each constrained, by the problem geometry, to lie along the Neumann boundaries; the vertex labeled 2 was constrained, by symmetry, to lie along the diagonal line segment joining the upper right corners of the inner and outer conductor boundaries. Note: the optimal positions of the element vertices labeled 1, 2 and 3 are specified in Table 4.1.

4.1.1.2 Benchmark System 3(b)

The second benchmark system used to validate the two-dimensional finite element optimization equations derived in section 2.4.2 is similar to Benchmark System 3(a), and is defined by Figure 4.7. It also consists of an infinitely long, air-filled, uniform coaxial line, however, having an equilateral triangular cross-section in this case. The objective for this benchmark system is, once again, to compute the functional value corresponding to the electrostatic potential energy per unit length stored in the air region between the two ideal conductors of the system. The primary feature of this system is the rapid field solution variation close to the sharp reentrant corners with included angles of 300 degrees at the intersections of the edges of the inner conductor. It will be interesting to note the effect on the optimal discretization results, if any, of the increased sharpness of the reentrant corner relative to Benchmark System 3(a). The optimal discretization results for this electrostatic system were computed using exactly the same procedures that were used for Benchmark System 3(a). Furthermore, the same range of results were computed, and are discussed next.

The finite element optimization equations of section 2.4.2 for two-dimensional systems were used to test the x- and y-components of the functional gradients with respect to element vertex positions for a series of numerical benchmark evaluations based on the geometry and eight-element mesh defined by Figure 4.8. It is one-third of the equilateral triangular coaxial line in cross-section. The conductor boundary conditions (Dirichlet) are $1V$ and $0V$ as indicated; and the symmetry planes are labeled N (Neumann). There are six free geometric discretization parameters corresponding to the x- and y-coordinates of the positions of the element vertices in the mesh labeled 1, 2, and 3. Moreover, it may be noted that the optimal positions of the vertices labeled 1 and 3 are each constrained by the problem geometry to lie along the Neumann boundaries of the problem domain. Furthermore, the optimal position of the vertex labeled 2 must lie, by symmetry, along the vertical line segment joining the

uppermost corners of the inner and outer conductor boundaries. A series of 180,000 eight-element meshes were used to compute individual functional values corresponding to fixing the element vertices labeled 1 and 3 at 300 regularly spaced positions along the Neumann boundaries and the vertex labeled 2 at 600 regularly spaced positions along the vertical line segment joining the uppermost corners of the inner and outer conductor boundaries. Figure 4.9 shows the optimal first-order eight-element mesh for one-third of the cross-section of the equilateral triangular coaxial line. The corresponding second-, fourth- and eighth-order optimal meshes are shown in Figure 4.10, 4.11 and 4.12, respectively. In each case, the results confirmed those obtained by evaluating the finite element optimization equations directly: the positions of the free vertices which yielded the smallest possible functional value were the same as those which yielded the smallest functional gradients along the permissible directions of optimization described above, with an error tolerance of $\pm 5.0 \times 10^{-5}$ (m). This error tolerance is one-half of the interval used to define successive vertex positions for computing the range of functional values used to confirm the results obtained by evaluating the finite element optimization equations directly. As with Benchmark System 3(a), it is interesting to note the increasingly sharp focus of DOF near the reentrant corner with increasing element order. Once again, the improved finite element model of the field solution over the outer elements, provided by the higher-order approximations, allows for this to occur. In addition, the sharper focus of DOF near the reentrant corner of Benchmark System 3(b) relative to that of Benchmark System 3(a) for corresponding element orders may be noted. The stronger intensity of the field solution singularity associated with the increased sharpness of the reentrant corner relative to Benchmark System 3(a), requires a more focussed distribution of DOF in order to efficiently resolve the more rapid field solution variation for Benchmark System 3(b). Finally, the optimal positions of vertices 1, 2 and 3 are specified in Table 4.2 for each of the cases examined.

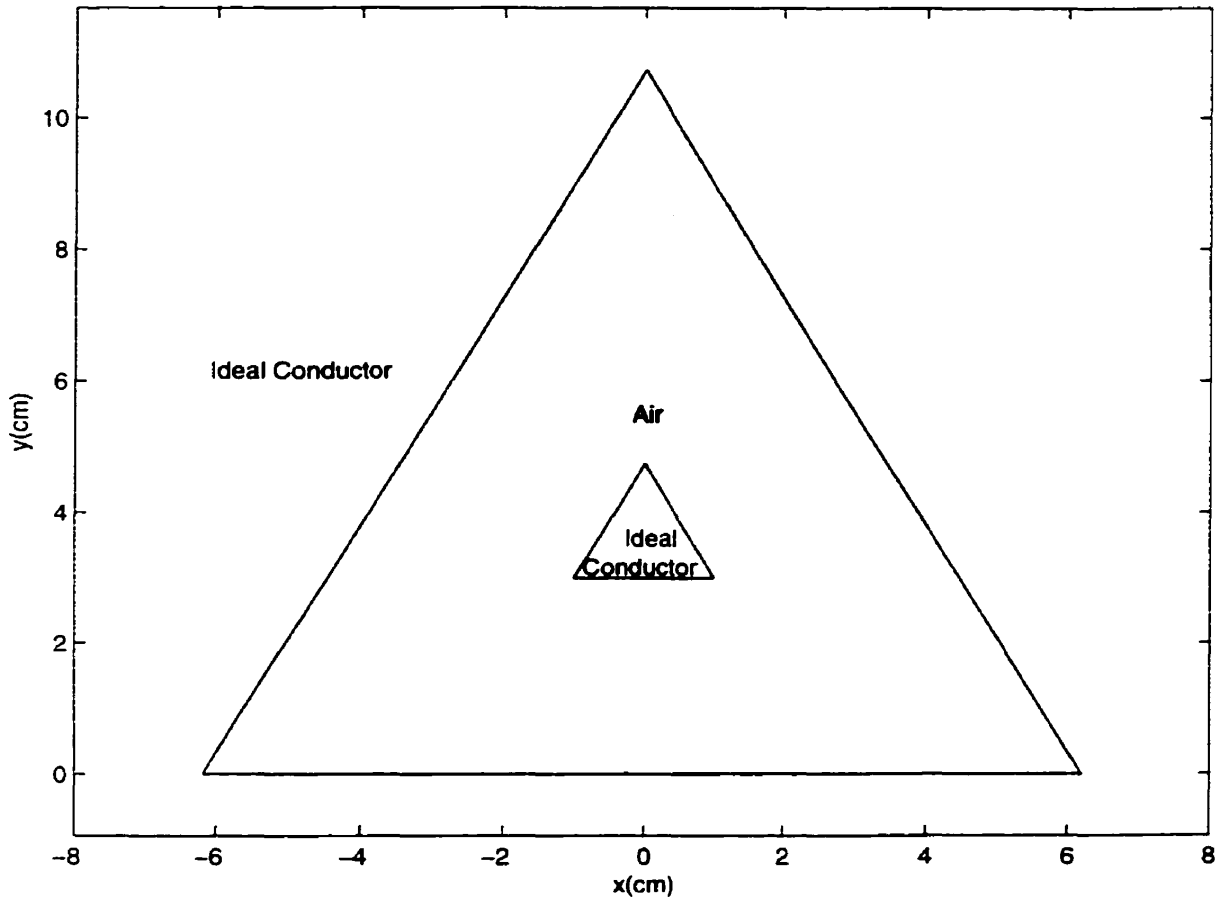

Figure 4.7: A cross-sectional view of Benchmark System 3(b) is illustrated. The two-dimensional view depicts an infinitely long, air-filled, uniform, equilateral triangular coaxial line in cross-section. The shaded annular area represents the air region between the two ideal conductors. The boundary of the inner conductor is prescribed to be a $1V$ equipotential line, and the boundary of the outer conductor is prescribed to be a $0V$ equipotential line.

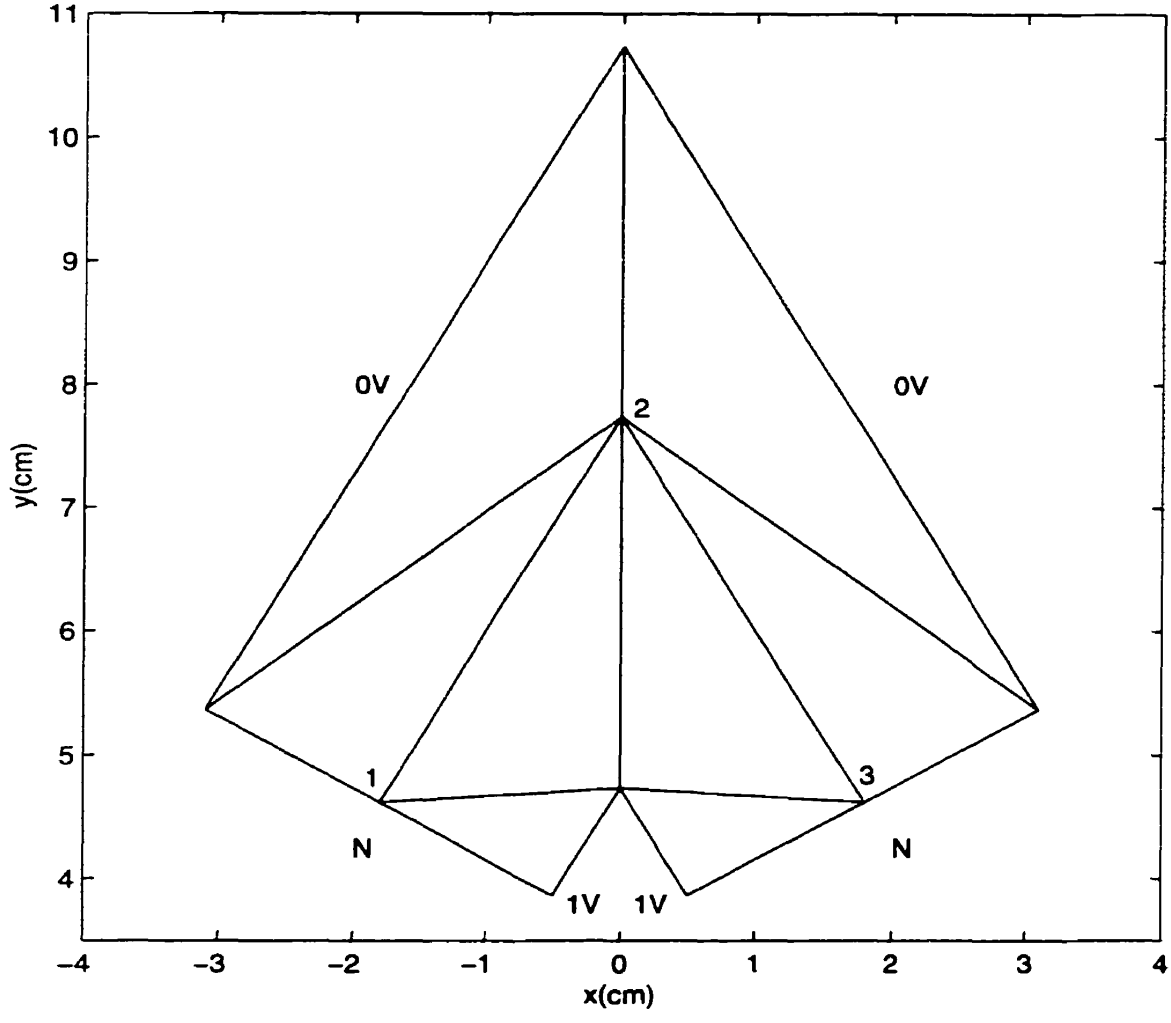

Figure 4.8: The geometry and finite element mesh configuration for the two-dimensional electrostatic potential analysis of Benchmark System 3(b) are illustrated. Eight triangular elements are used to model one-third of the equilateral triangular coaxial line in cross-section. The conductor boundary conditions (Dirichlet) are labeled $1V$ and $0V$; the symmetry planes are labeled N (Neumann). The positions of the vertices labeled 1, 2 and 3 correspond to the six free geometric discretization parameters for the finite element model. The sharp reentrant corner at the intersection of the edges of the inner conductor boundary has an included angle of 300 degrees.

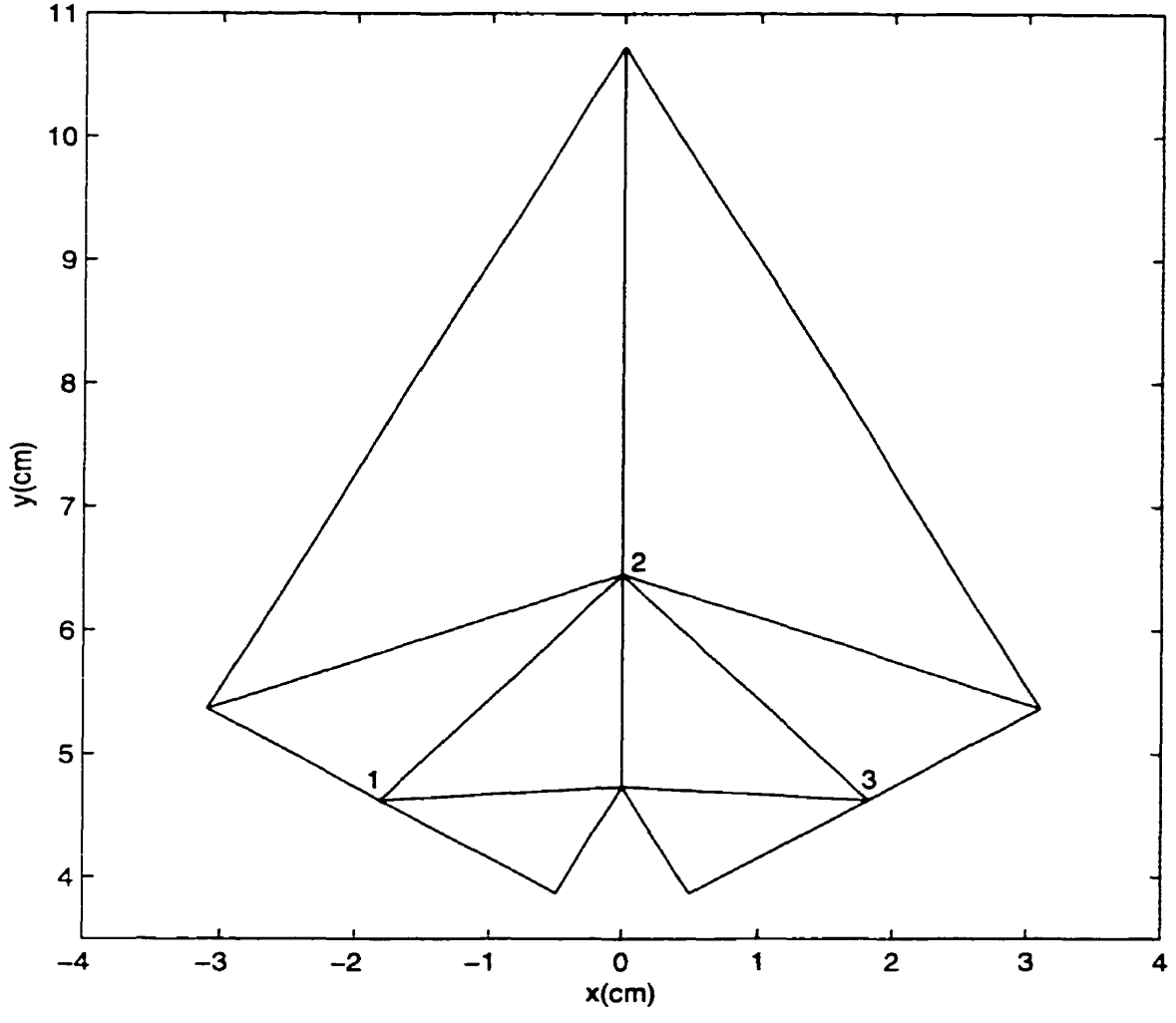

Figure 4.9: The first-order optimal eight-element mesh for the two-dimensional electrostatic potential analysis of Benchmark System 3(b) is illustrated. The vertices labeled 1 and 3 were each constrained, by the problem geometry, to lie along the Neumann boundaries; the vertex labeled 2 was constrained, by symmetry, to lie along the vertical line segment joining the upper corners of the inner and outer conductor boundaries. Note: the optimal positions of the element vertices labeled 1, 2 and 3 are specified in Table 4.2.

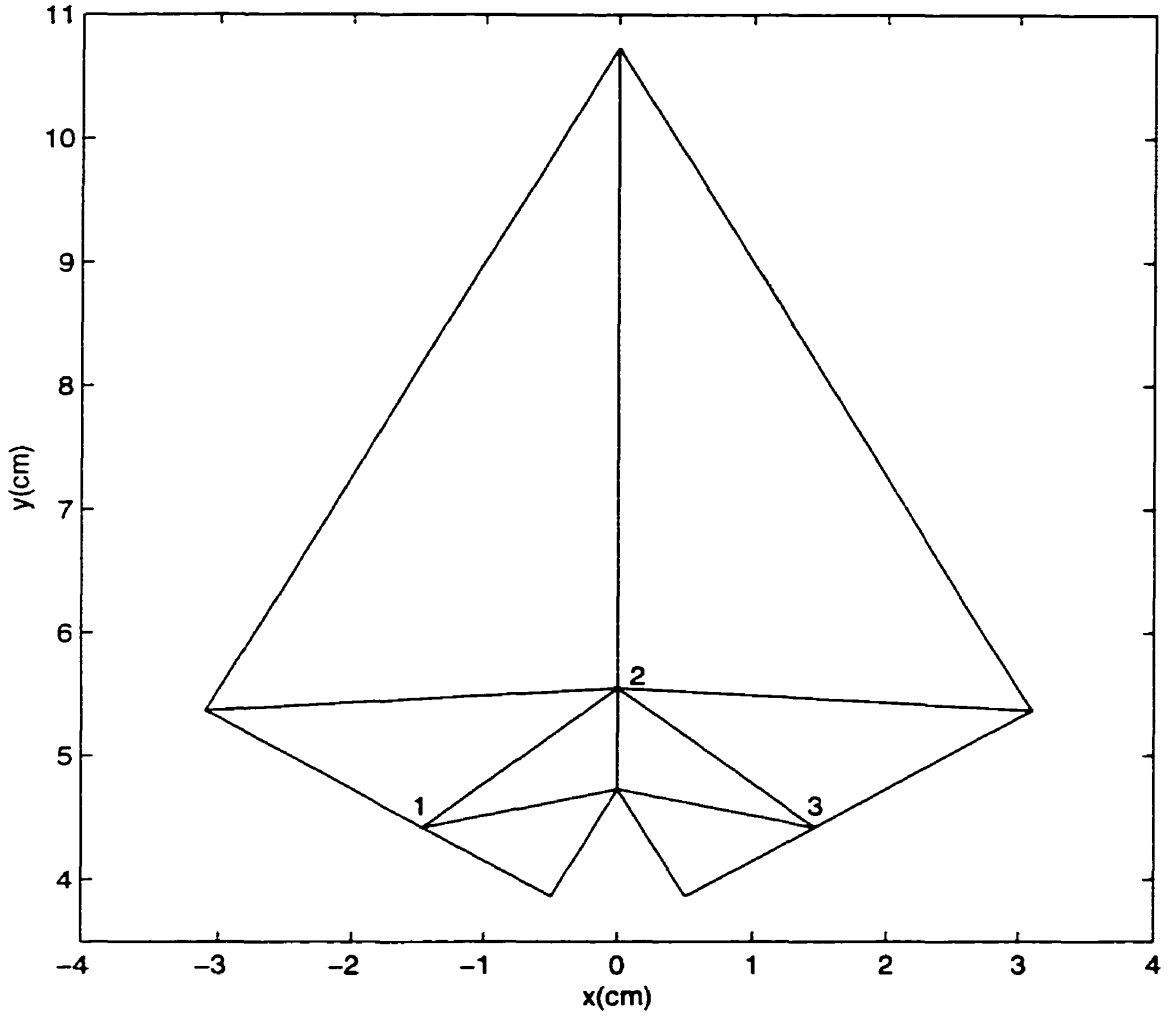

Figure 4.10: The second-order optimal eight-element mesh for the two-dimensional electrostatic potential analysis of Benchmark System 3(b) is illustrated. The vertices labeled 1 and 3 were each constrained, by the problem geometry, to lie along the Neumann boundaries; the vertex labeled 2 was constrained, by symmetry, to lie along the vertical line segment joining the upper corners of the inner and outer conductor boundaries. Note: the optimal positions of the element vertices labeled 1, 2 and 3 are specified in Table 4.2.

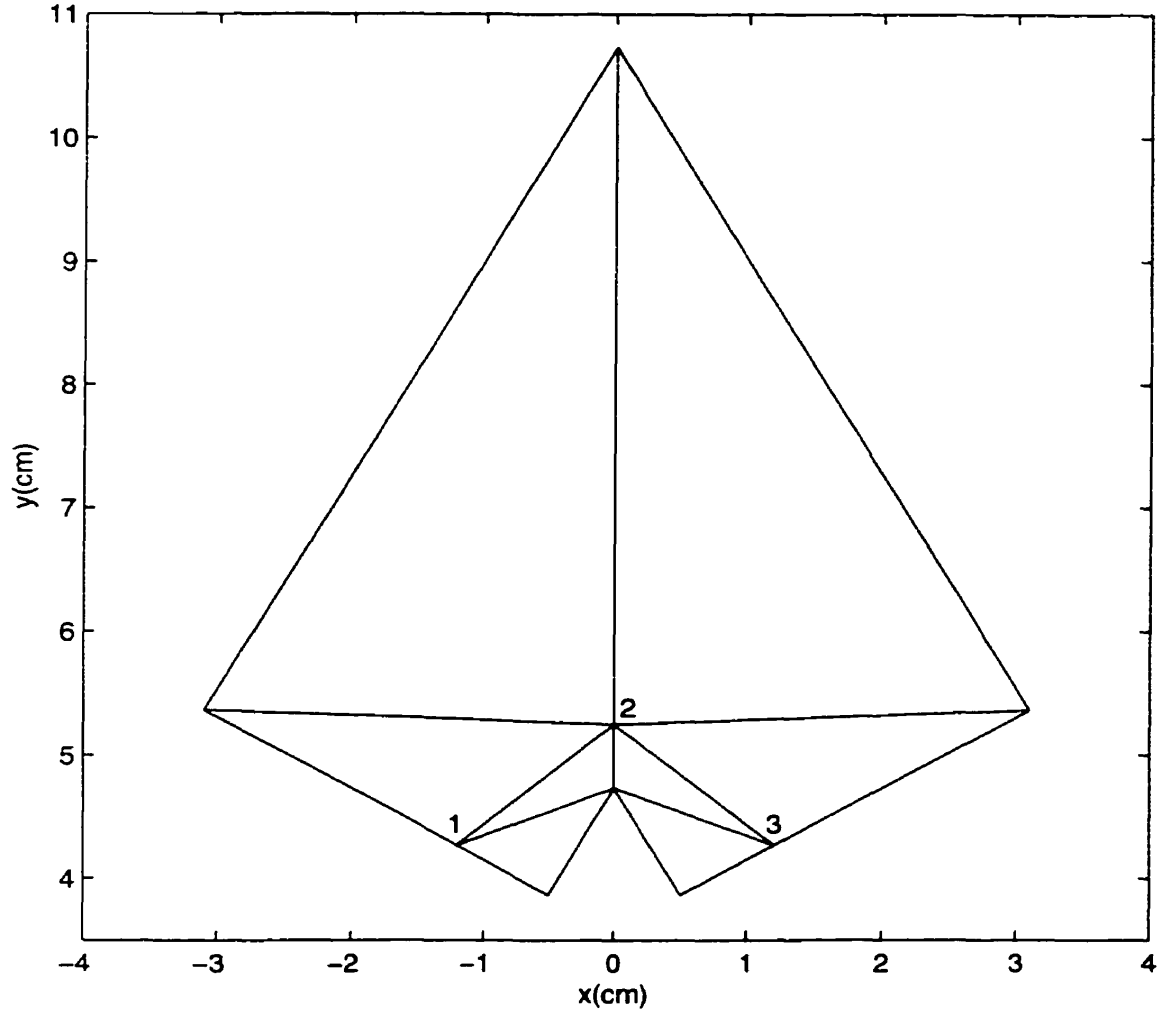

Figure 4.11: The fourth-order optimal eight-element mesh for the two-dimensional electrostatic potential analysis of Benchmark System 3(b) is illustrated. The vertices labeled 1 and 3 were each constrained, by the problem geometry, to lie along the Neumann boundaries; the vertex labeled 2 was constrained, by symmetry, to lie along the vertical line segment joining the upper corners of the inner and outer conductor boundaries. Note: the optimal positions of the element vertices labeled 1, 2 and 3 are specified in Table 4.2.

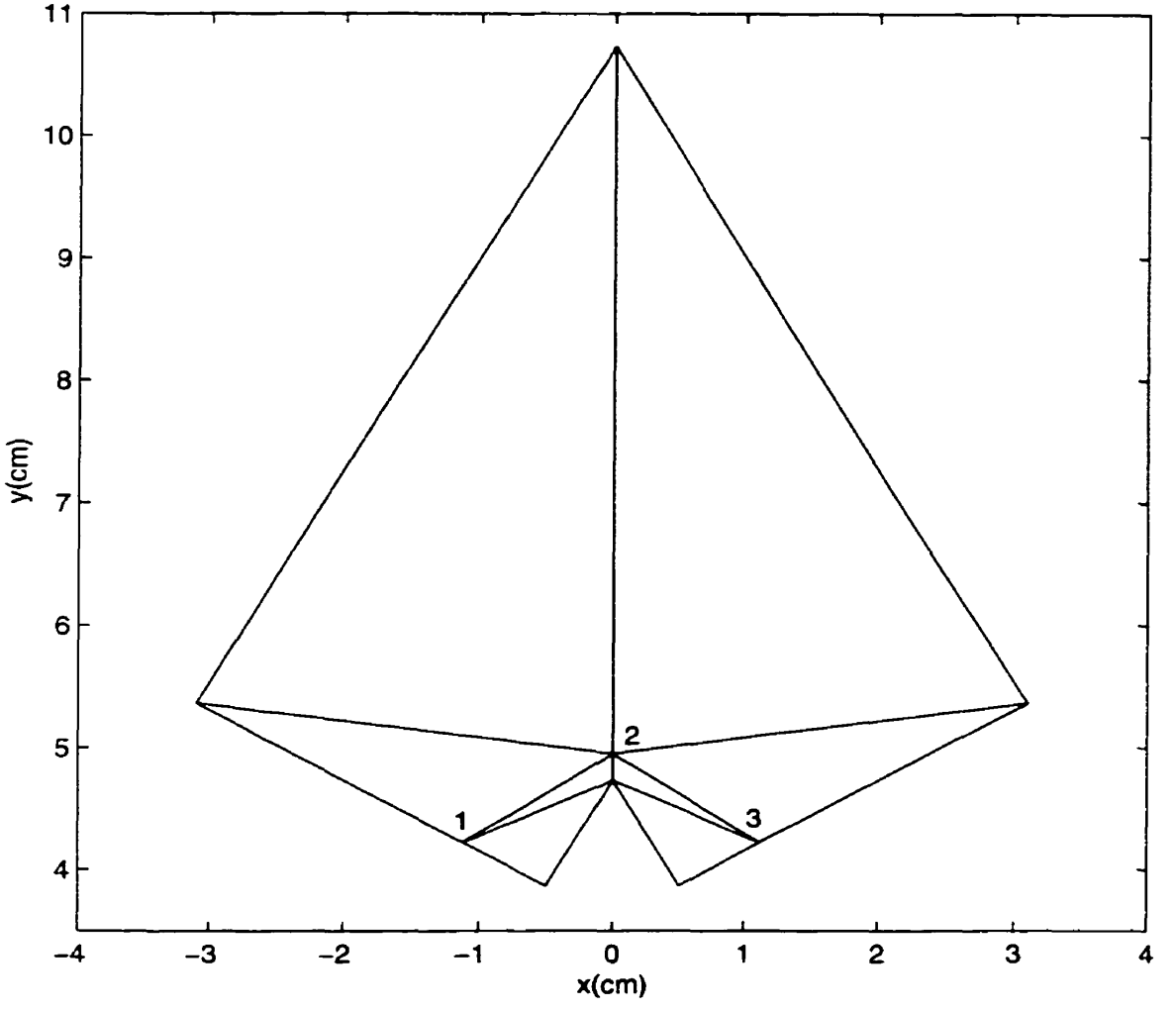

Figure 4.12: The eighth-order optimal eight-element mesh for the two-dimensional electrostatic potential analysis of Benchmark System 3(b) is illustrated. The vertices labeled 1 and 3 were each constrained, by the problem geometry, to lie along the Neumann boundaries; the vertex labeled 2 was constrained, by symmetry, to lie along the vertical line segment joining the upper corners of the inner and outer conductor boundaries. Note: the optimal positions of the element vertices labeled 1, 2 and 3 are specified in Table 4.2.

Table 4.2: Optimal vertex positions for Benchmark System 3(b).

Order / Vertex	1	2	3
1	0.5033	0.2863	0.5033
2	0.3700	0.1363	0.3700
4	0.2700	0.0863	0.2700
8	0.2367	0.0363	0.2367

Note: The table entries represent the ratios of the optimal vertex positions along the length of the line segments in the directions of optimization.

4.1.1.3 Benchmark System 3(c)

The final benchmark system used to validated the two-dimensional finite element optimization equations of section 2.4.2 is similar to Benchmark System 3(a) and 3(b), and is defined by Figure 4.13. It is an infinitely long, air-filled, uniform, hexagonal coaxial line in cross-section. As per the previous two benchmark systems considered, the objective is to compute the functional value corresponding to the electrostatic potential energy per unit length stored in the air region between the two ideal conductors of the system. The primary feature of this system is the rapid field solution variation close to the sharp reentrant corners with included angles of 240 degrees at the intersections of the edges of the inner conductor. For this benchmark system, it will be interesting to note the effect on the optimal discretization results, if any, of the decreased sharpness of the reentrant corner relative to both Benchmark System 3(a) and 3(b). The optimal discretization results for this electrostatic system were computed using exactly the same procedures that were used for Benchmark System 3(a) and 3(b). Furthermore, the same range of results were computed, and are discussed next.

The finite element optimization equations of section 2.4.2 for two-dimensional systems were used to test the x- and y-components of the functional gradients with respect to element vertex positions for a series of numerical benchmark evaluations

based on the geometry and eight-element mesh defined by Figure 4.14. It is one-sixth of the hexagonal coaxial line in cross-section. The conductor boundary conditions (Dirichlet) are $1V$ and $0V$ as indicated; and the symmetry planes are labeled N (Neumann). There are six free geometric discretization parameters corresponding to the x- and y-coordinates of the positions of the element vertices in the mesh labeled 1, 2 and 3. Moreover, it may be noted that the optimal positions of the vertices labeled 1 and 3 are each constrained by the problem geometry to lie along the Neumann boundaries of the problem domain. Furthermore, the optimal position of the vertex labeled 2 must lie, by symmetry, along the diagonal line segment joining the upper right corners of the inner and outer conductor boundaries. A series of 103,800 eight-element meshes were used to compute individual functional values corresponding to fixing the element vertices labeled 1 and 3 at 300 regularly spaced positions along the Neumann boundaries and the vertex labeled 2 at 346 regularly spaced positions along the diagonal line segment joining the upper right corners of the inner and outer conductor boundaries. Figure 4.15 shows the optimal first-order eight-element mesh for one-sixth of the cross-section of the hexagonal coaxial line. The corresponding second-, fourth- and eighth-order optimal meshes are shown in Figure 4.16, 4.17 and 4.18, respectively. In each case, the functional gradients with respect to element vertex positions correctly identified the optimal positions of the free element vertices, to yield the smallest possible functional value, with an error tolerance of $\pm 5.0 \times 10^{-5}$ (m). This error tolerance is one-half of the interval used to define successive vertex positions for computing the range of functional values used to confirm the results obtained by evaluating the finite element optimization equations directly. Once again, it is interesting to note the increasingly sharp focus of DOF near the reentrant corner with increasing element order. As with both Benchmark Systems 3(a) and 3(b), the improved finite element model of the field solution over the outer elements, furnished by the higher-order approximations, allows for this to occur. It may also be noted that the focus of DOF is less sharp near the reentrant corner of Benchmark System

3(c) relative to that of both Benchmark Systems 3(a) and 3(b) for corresponding element orders. This is consistent with the weaker intensity of the field solution singularity associated with the reduced sharpness of the reentrant corner relative to both Benchmark Systems 3(a) and 3(b). Finally, the optimal positions of vertices 1, 2 and 3 are specified in Table 4.3 for each of the cases examined.

Table 4.3: Optimal vertex positions for Benchmark System 3(c).

Order / Vertex	1	2	3
1	0.4367	0.3782	0.4367
2	0.3033	0.2338	0.3033
4	0.1700	0.1184	0.1700
8	0.1367	0.0606	0.1367

Note: The table entries represent the ratios of the optimal vertex positions along the length of the line segments in the directions of optimization.

4.1.2 Benchmark Adaption Studies

The numerical validation of the two-dimensional finite element optimization equations presented in sections 4.1.1.1, 4.1.1.2 and 4.1.1.3 has shown that the functional gradients with respect to element vertex positions can correctly identify the optimal positions of the free element vertices in a finite element discretization to produce the most accurate approximate solution for a given number of DOF. The purpose of this section is to investigate the potential benefits of using new refinement criteria for practical electromagnetic AFEA based on the two-dimensional finite element optimization equations. Hence, the effectiveness of the primary adaption models, when guided by the new optimal discretization-based refinement criteria, in resolving two benchmark systems is investigated. Specifically, the performance of the new criteria are examined with *h*-, *p*- and *hp*-adaption models for Laplace and Helmholtz systems. Furthermore, performance comparisons with some of the best adaptive refinement criteria currently

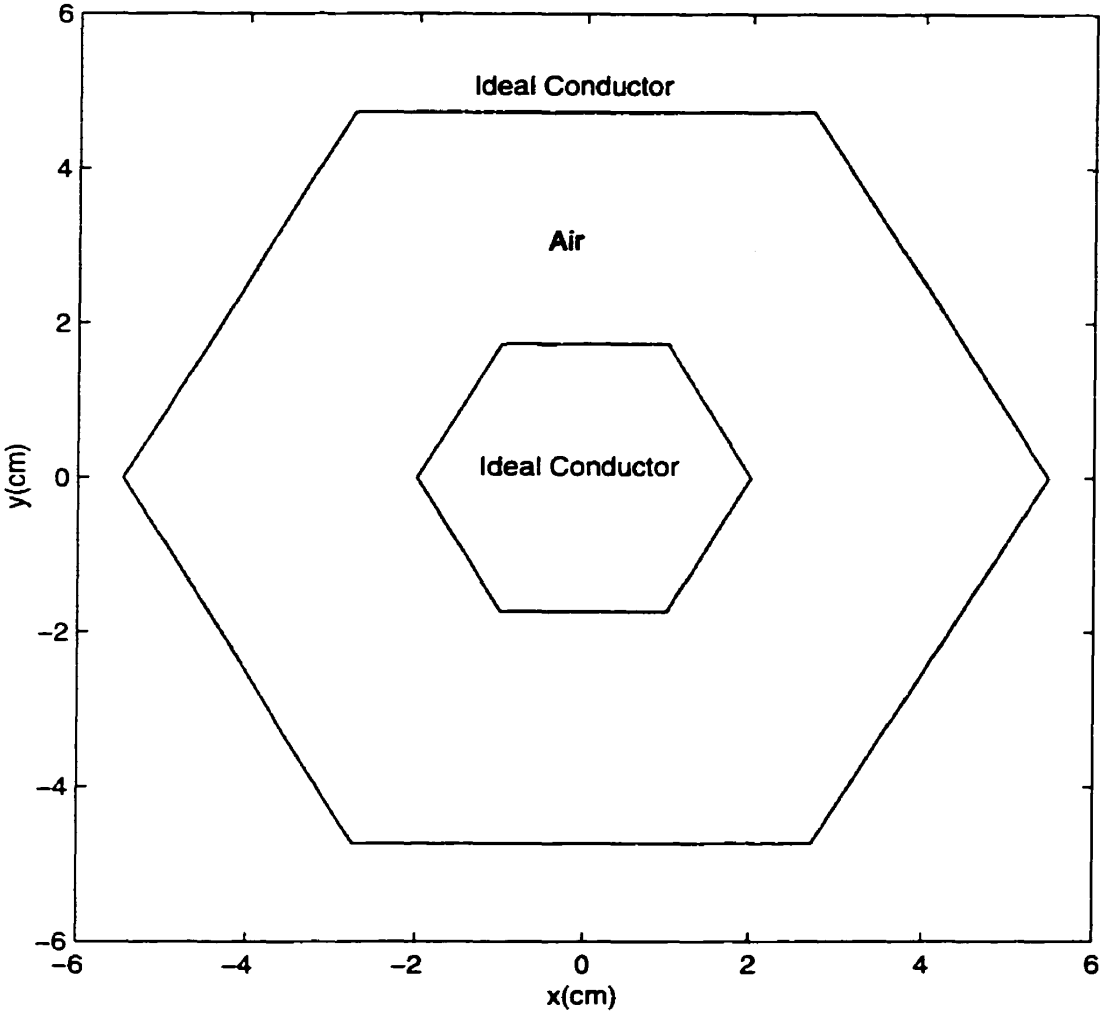

Figure 4.13: A cross-sectional view of Benchmark System 3(c) is illustrated. The two-dimensional view depicts an infinitely long, air-filled, uniform, hexagonal coaxial line in cross-section. The shaded annular area represents the air region between the two ideal conductors. The boundary of the inner conductor is prescribed to be a $1V$ equipotential line, and the boundary of the outer conductor is prescribed to be a $0V$ equipotential line.

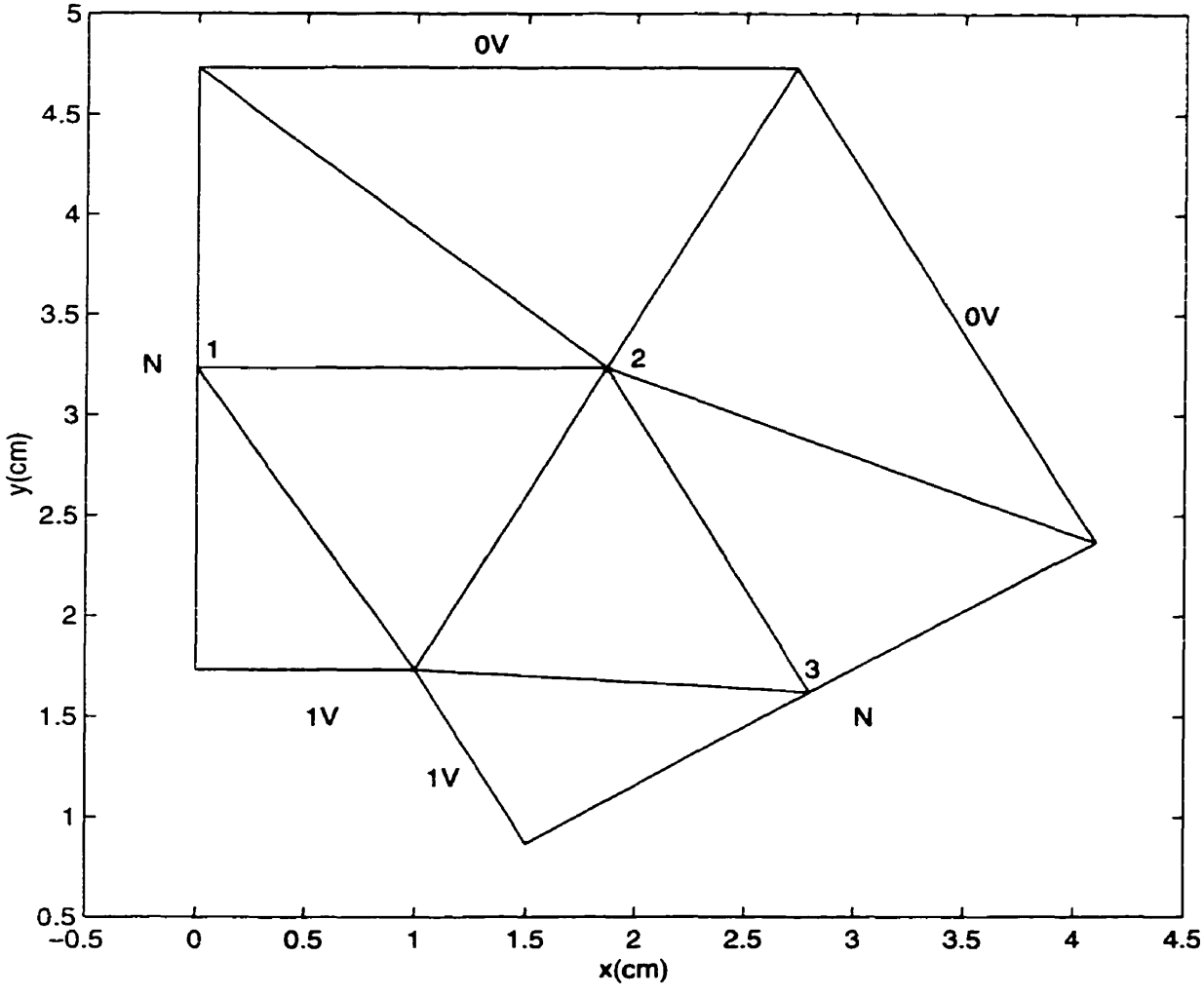

Figure 4.14: The geometry and finite element mesh configuration for the two-dimensional electrostatic potential analysis of Benchmark System 3(c) are illustrated. Eight triangular elements are used to model one-sixth of the hexagonal coaxial line in cross-section. The conductor boundary conditions (Dirichlet) are labeled $1V$ and $0V$; the symmetry planes are labeled N (Neumann). The positions of the vertices labeled 1, 2 and 3 correspond to the six free geometric discretization parameters for the finite element model. The sharp reentrant corner at the intersection of the edges of the inner conductor boundary has an included angle of 240 degrees.

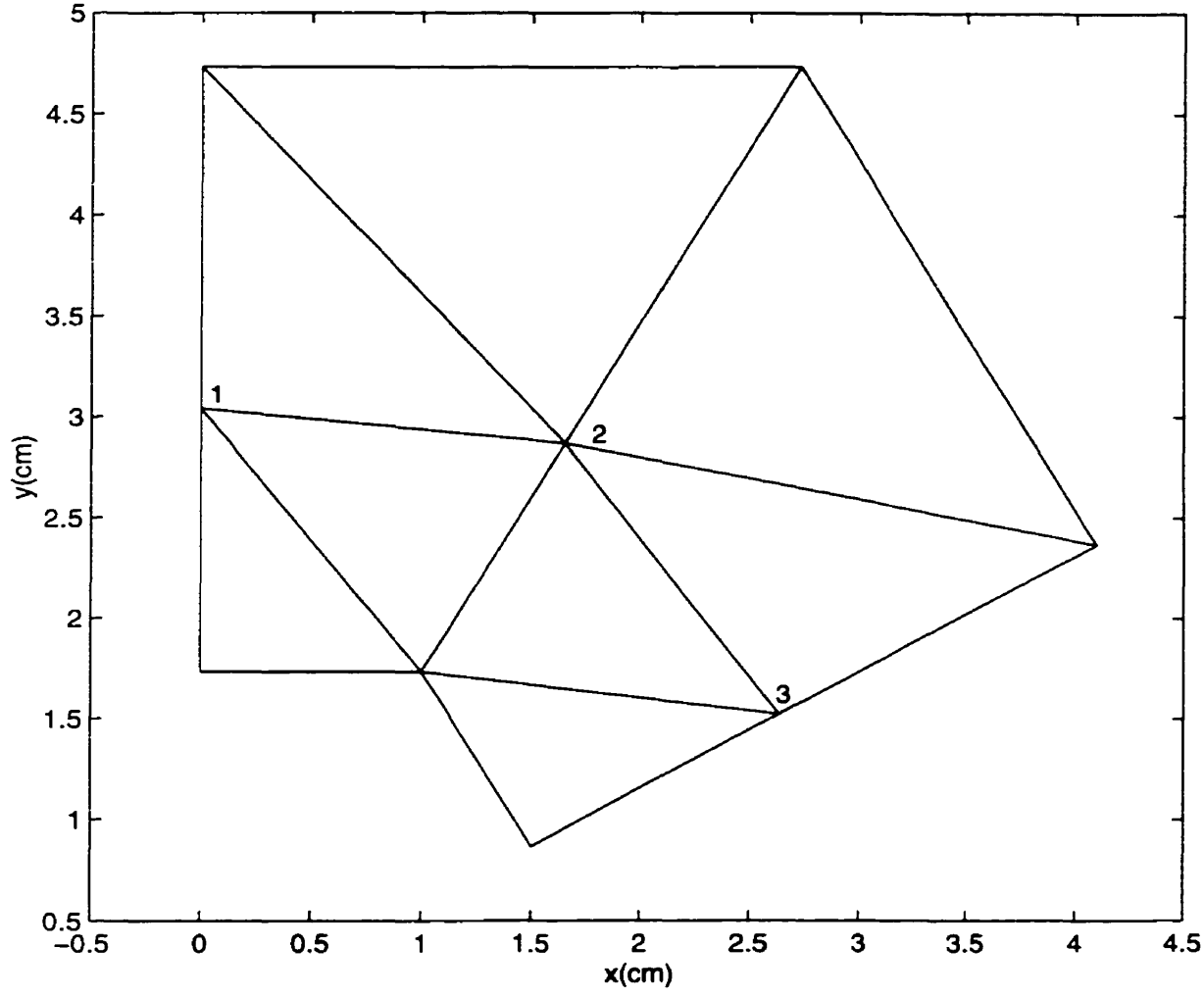

Figure 4.15: The first-order optimal eight-element mesh for the two-dimensional electrostatic potential analysis of Benchmark System 3(c) is illustrated. The vertices labeled 1 and 3 were each constrained, by the problem geometry, to lie along the Neumann boundaries; the vertex labeled 2 was constrained, by symmetry, to lie along the diagonal line segment joining the upper corners of the inner and outer conductor boundaries. Note: the optimal positions of the element vertices labeled 1, 2 and 3 are specified in Table 4.3.

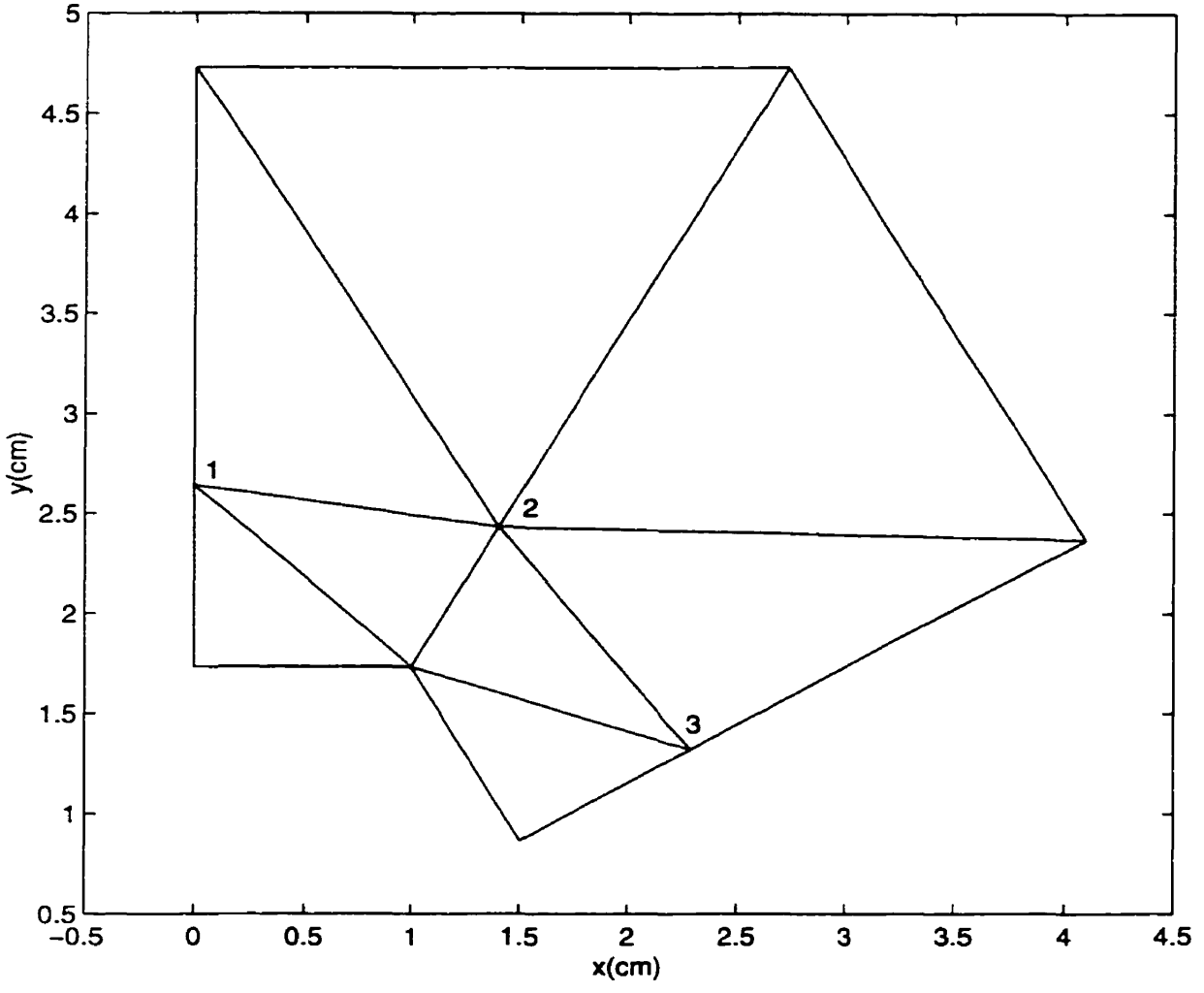

Figure 4.16: The second-order optimal eight-element mesh for the two-dimensional electrostatic potential analysis of Benchmark System 3(c) is illustrated. The vertices labeled 1 and 3 were each constrained, by the problem geometry, to lie along the Neumann boundaries; the vertex labeled 2 was constrained, by symmetry, to lie along the diagonal line segment joining the upper corners of the inner and outer conductor boundaries. Note: the optimal positions of the element vertices labeled 1, 2 and 3 are specified in Table 4.3.

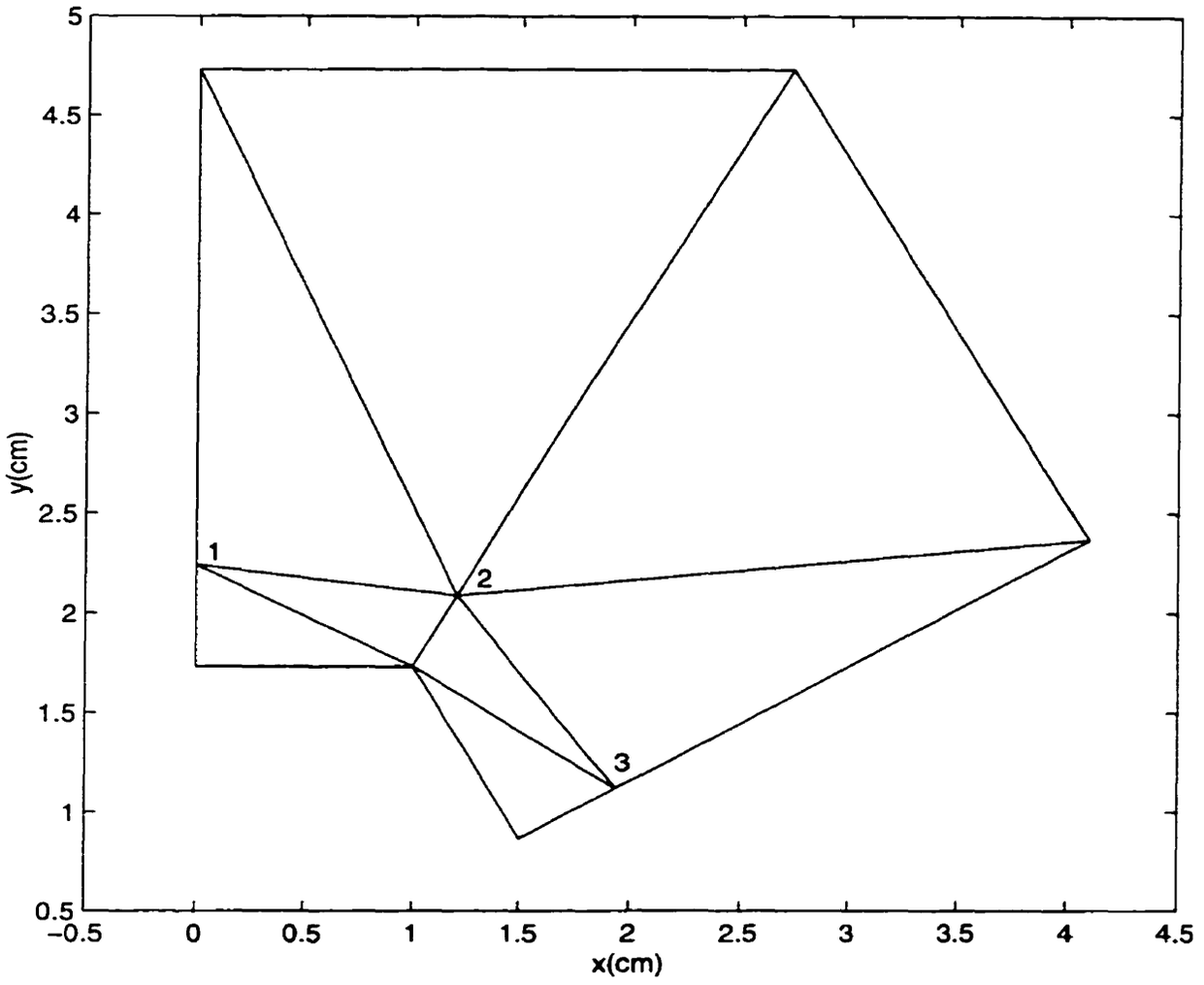

Figure 4.17: The fourth-order optimal eight-element mesh for the two-dimensional electrostatic potential analysis of Benchmark System 3(c) is illustrated. The vertices labeled 1 and 3 were each constrained, by the problem geometry, to lie along the Neumann boundaries; the vertex labeled 2 was constrained, by symmetry, to lie along the diagonal line segment joining the upper corners of the inner and outer conductor boundaries. Note: the optimal positions of the element vertices labeled 1, 2 and 3 are specified in Table 4.3.

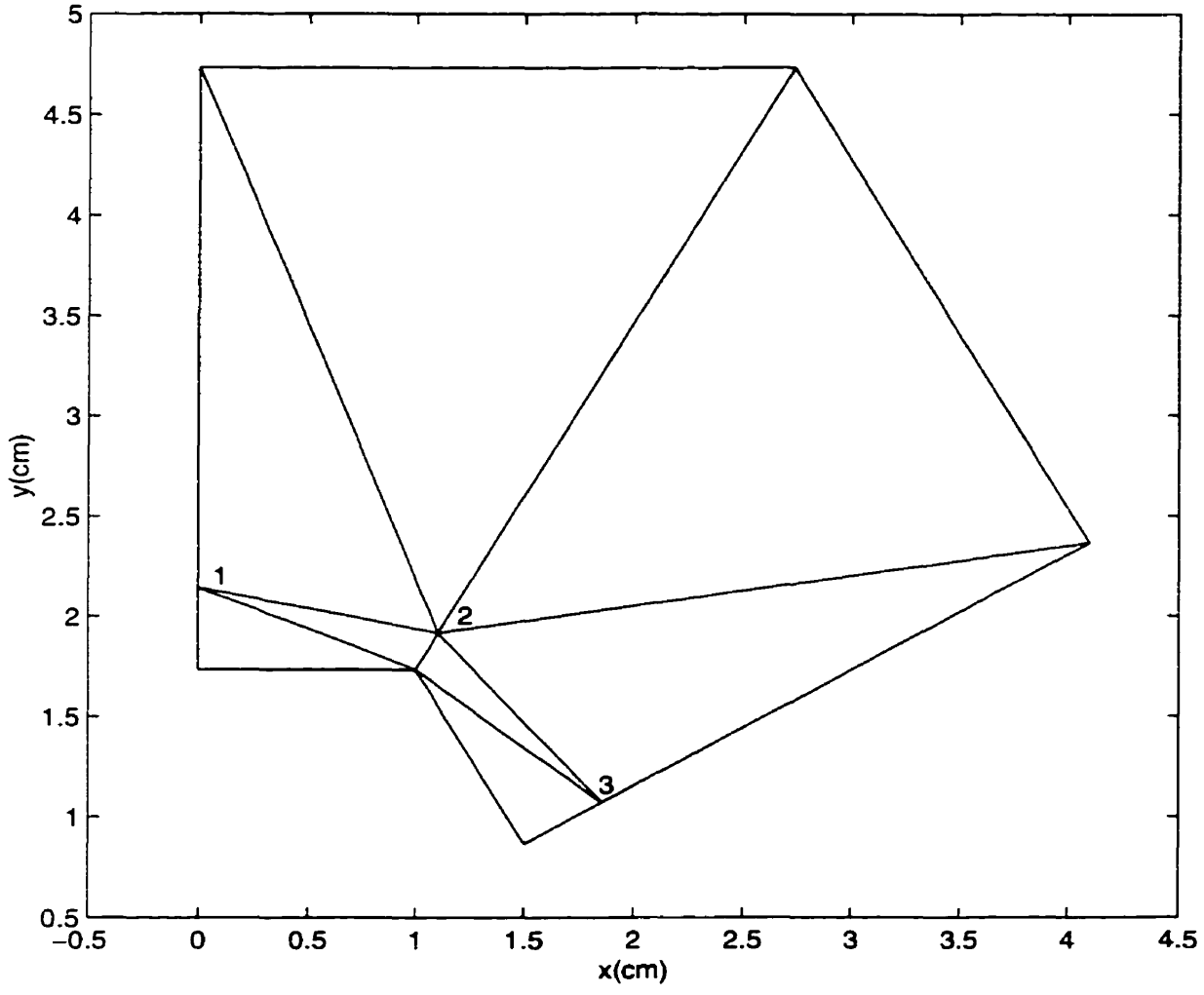

Figure 4.18: The eighth-order optimal eight-element mesh for the two-dimensional electrostatic potential analysis of Benchmark System 3(c) is illustrated. The vertices labeled 1 and 3 were each constrained, by the problem geometry, to lie along the Neumann boundaries; the vertex labeled 2 was constrained, by symmetry, to lie along the diagonal line segment joining the upper corners of the inner and outer conductor boundaries. Note: the optimal positions of the element vertices labeled 1, 2 and 3 are specified in Table 4.3.

available are presented. However, the adaption benchmark results are first preceded by a brief description of how the two-dimensional finite element optimization equations are used to develop optimal discretization-based refinement criteria for AFEA analogous to the one-dimensional criterion developed earlier.

4.1.2.1 Two-Dimensional Optimal Discretization-Based Refinement Criteria

As noted previously, the efficient use of well-defined optimal solution properties as feedback refinement criteria for guiding the solution process towards accurate results has been an important research challenge for all types of adaption in FEA. Furthermore, one route to adaption which was shown to be successful in section 3.3 for one-dimensional systems, is to employ local error measures that are closely related to the variational principle used to determine the solution to the finite element problem. The purpose of the present section is to describe analogous two-dimensional refinement criteria for *h*-, *p*- and *hp*-adaption, which are also based on the variational properties of optimal discretizations for the FEA of electromagnetic systems.

One way to detect and rank regions of inferior discretization in a finite element mesh, as explained in section 3.3.1, is by computing the gradients of the functional with respect to element vertex positions. Furthermore, it has been noted that these functional gradients may be computed directly from the finite element optimization equations derived in section 2.4. Once the gradients of the functional with respect to vertex positions have been computed, they may be used in various ways as error indicators within two-dimensional adaptive solvers. One simple approach is to assess a weighted sum or an average value of the vertex-based functional gradients for each element, then use these values to rank the elements for refinement (Type-*A*). A more directed approach is to employ a weighted sum or an average value of the projections of the vertex-based functional gradients onto vectors directed from the vertices towards the centroids of the elements (Type-*B*). Unlike the first approach, this scheme depends

upon both the directions as well as the magnitudes of the functional gradients. Both of these types of methods are investigated in the following two sections in order to illustrate some of the possible ways to exploit the new two-dimensional refinement criteria proposed for adaptive finite element solvers.

4.1.2.2 Benchmark System 3(a)

In order to evaluate the effectiveness of the optimal discretization-based refinement criteria described above, results from a series of studies involving the primary adaption models are reported in this section for Benchmark System 3(a). Specifically, the convergence of h-, p- and hp-adaption strategies are investigated when optimal discretization-based refinement criteria are used to guide the adaption. The different types of adaption techniques considered in this section are intended to represent a range of the basic methods most commonly used in practice for two-dimensional electromagnetic AFEA. Finally, it should be noted that all of the adaption studies for this Laplace benchmark system were based on the analysis of one-quarter of the square coaxial line in cross-section, shown in Figure 4.2.

The convergence of the percent error in functional value for an h-adaption strategy applied to the Laplace benchmark system is illustrated in Figure 4.19 for first-order elements. The initial mesh used for the h-adaption studies is defined by Figure 4.2. At each subsequent adaptive iteration, the optimal discretization-based refinement criteria described above (Type-A) were used to rank the elements, and the elements with the highest rankings were chosen for refinement. Moreover, a 50 percent increment in the number of DOF per adaptive step was used to update the discretizations. In addition, it may be noted that all of the h-refinements were based on either element bisections or uniform subdivisions of elements into four similar triangles; however, the resulting set of new element vertices were retriangulated at each adaptive step using a Delaunay algorithm [70]. The uniform h-refinement baseline functional convergence result is also shown in Figure 4.19 for comparison. The analogous second-order h-

adaption results for the Laplace benchmark system are shown in Figure 4.20. The fourth- and eighth-order h-adaption results are shown in Figure 4.21 and Figure 4.22, respectively. For each case, the results were computed using exactly the same procedures as for the first-order h-adaption results described above. It may be noted that the h-adaption strategy guided by the optimal discretization-based refinement criteria produced discretizations with functional accuracy levels superior to those of the uniform discretizations with corresponding numbers of DOF, for the first-, second-, fourth- and eighth-order analyses. Finally, an example h-adapted mesh is presented in Figure 4.23 to illustrate the sharp focus of DOF produced by the new refinement criteria near the reentrant corner.

The performance results for a range of p-adaption strategies applied to Benchmark System 3(a) are summarized in Table 4.4. Specifically, uniform and mixed-order p-adaption schemes were investigated using elements which ranged from orders one through ten. The initial mesh of 128 first-order elements defined by Figure 4.24 was used for the p-adaption studies, and is based on uniformly subdividing the eight element mesh shown in Figure 4.2. In addition to the uniform p-refinement baseline, the hierarchal coefficient p-adaption result [59] is presented for comparison. It may be noted that the hierarchal coefficient-based refinement criteria developed in [59] have been shown to be amongst the most effective for p-adaption models [116]. For the new mixed-order p-adaption, the optimal discretization-based refinement criteria described above (Type-A) were used to rank the elements, and the elements with the highest rankings were chosen for refinement. Furthermore, the order of an element selected for refinement was increased successively from first- through to tenth-order each time the element was selected to be refined; however, if a tenth-order element was chosen for refinement the highest ranking lower-order element was refined instead. Moreover, a 50 percent increment in the number of DOF per adaptive step was used to update the discretizations for the p-adaption methods considered for this benchmark problem, excluding the uniform refinement procedure. Based on the

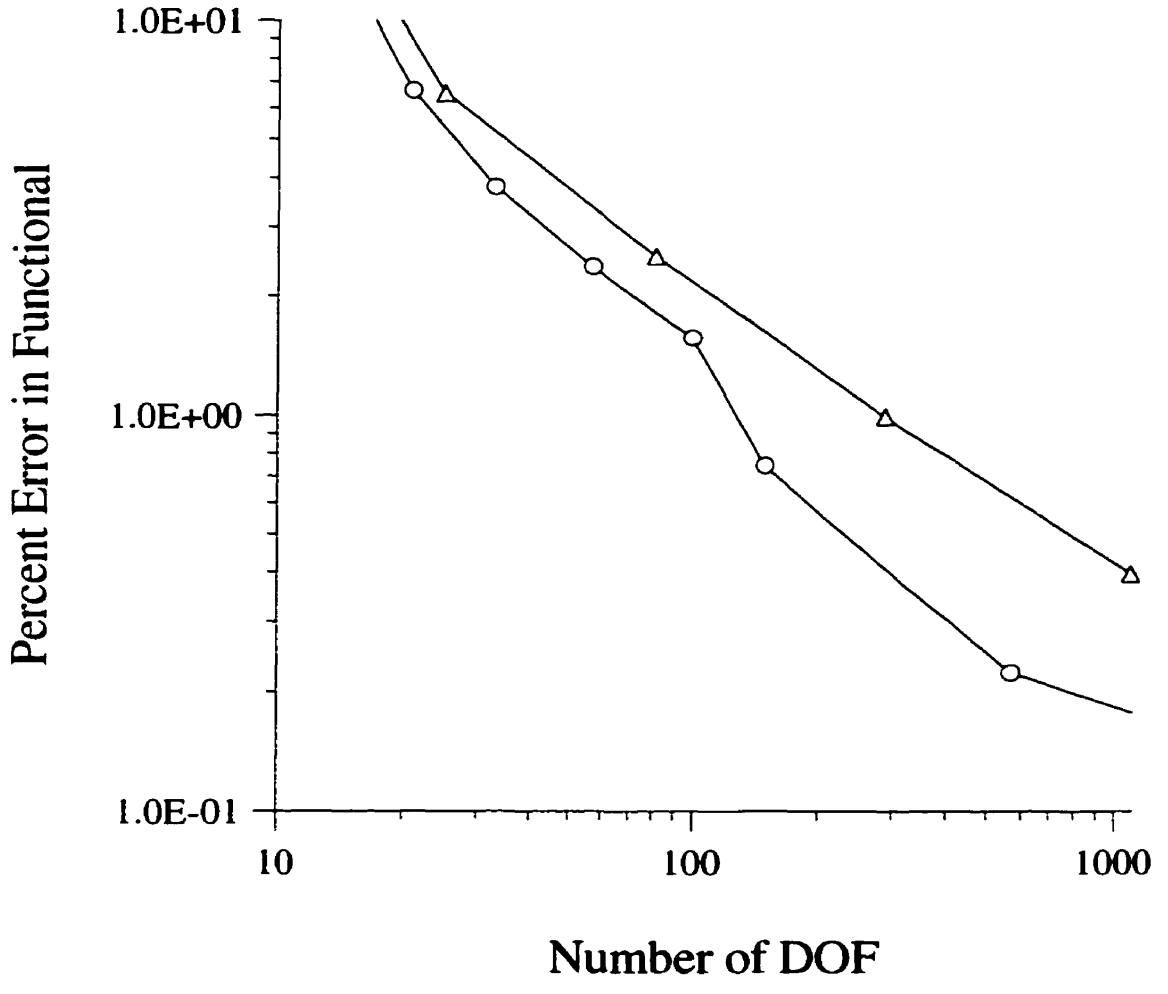

Figure 4.19: The convergence of percent error in functional value with discretization level for first-order h-adaption studies for Benchmark System 3(a) is illustrated. The triangle knot results correspond to percent error in functional values computed from solutions based on first-order uniform discretizations. The circle knot results correspond to percent error in functional values computed from solutions based on first-order h-adaption discretizations evolved using the new optimal discretization-based refinement criteria (Type-A).

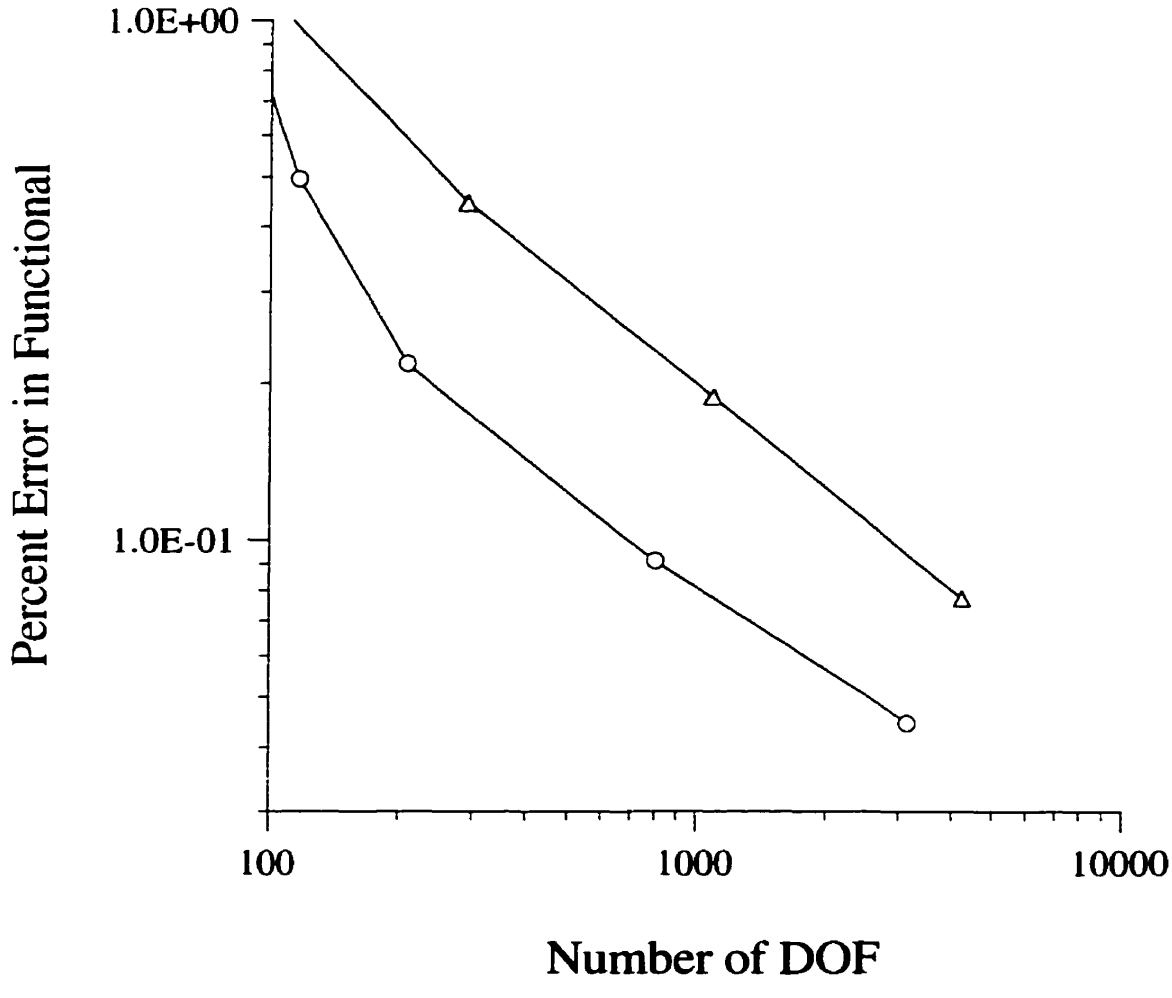

Figure 4.20: The convergence of percent error in functional value with discretization level for second-order h-adaption studies for Benchmark System 3(a) is illustrated. The triangle knot results correspond to percent error in functional values computed from solutions based on second-order uniform discretizations. The circle knot results correspond to percent error in functional values computed from solutions based on second-order h-adaption discretizations evolved using the new optimal discretization-based refinement criteria (Type-A).

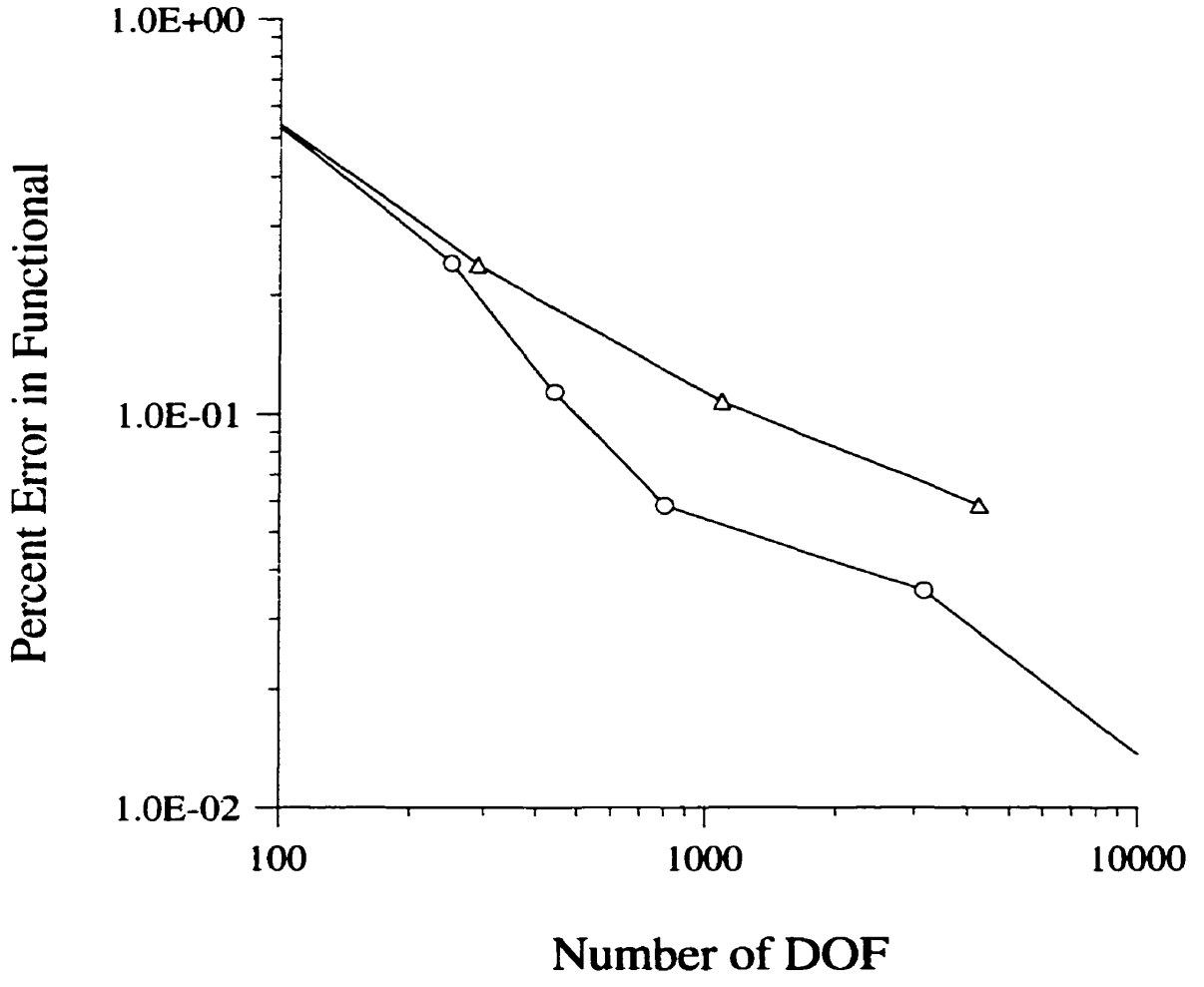

Figure 4.21: The convergence of percent error in functional value with discretization level for fourth-order h-adaption studies for Benchmark System 3(a) is illustrated. The triangle knot results correspond to percent error in functional values computed from solutions based on fourth-order uniform discretizations. The circle knot results correspond to percent error in functional values computed from solutions based on fourth-order h-adaption discretizations evolved using the new optimal discretization-based refinement criteria (Type-A).

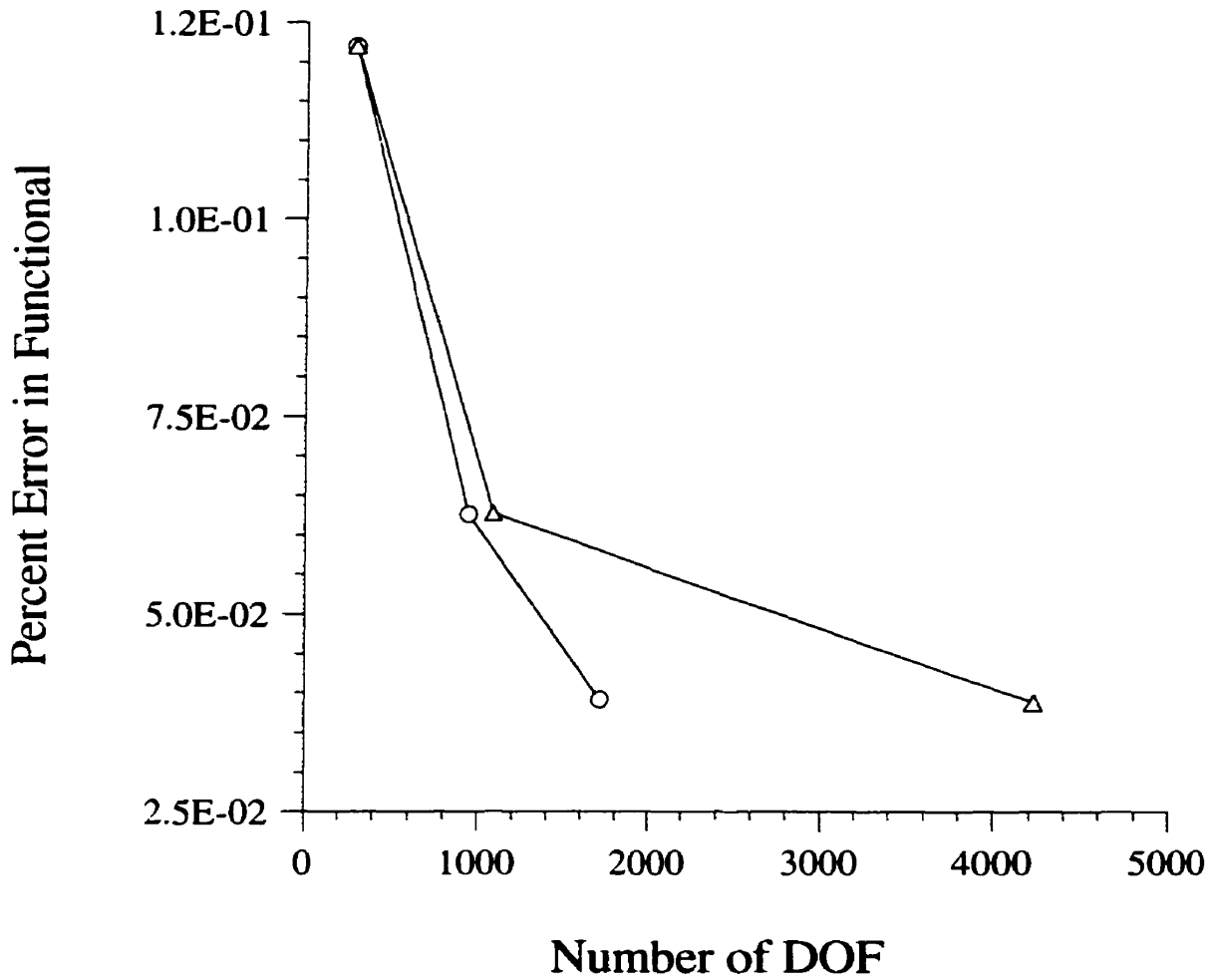

Figure 4.22: The convergence of percent error in functional value with discretization level for eighth-order h-adaption studies for Benchmark System 3(a) is illustrated. The triangle knot results correspond to percent error in functional values computed from solutions based on eighth-order uniform discretizations. The circle knot results correspond to percent error in functional values computed from solutions based on eighth-order h-adaption discretizations evolved using the new optimal discretization-based refinement criteria (Type-A).

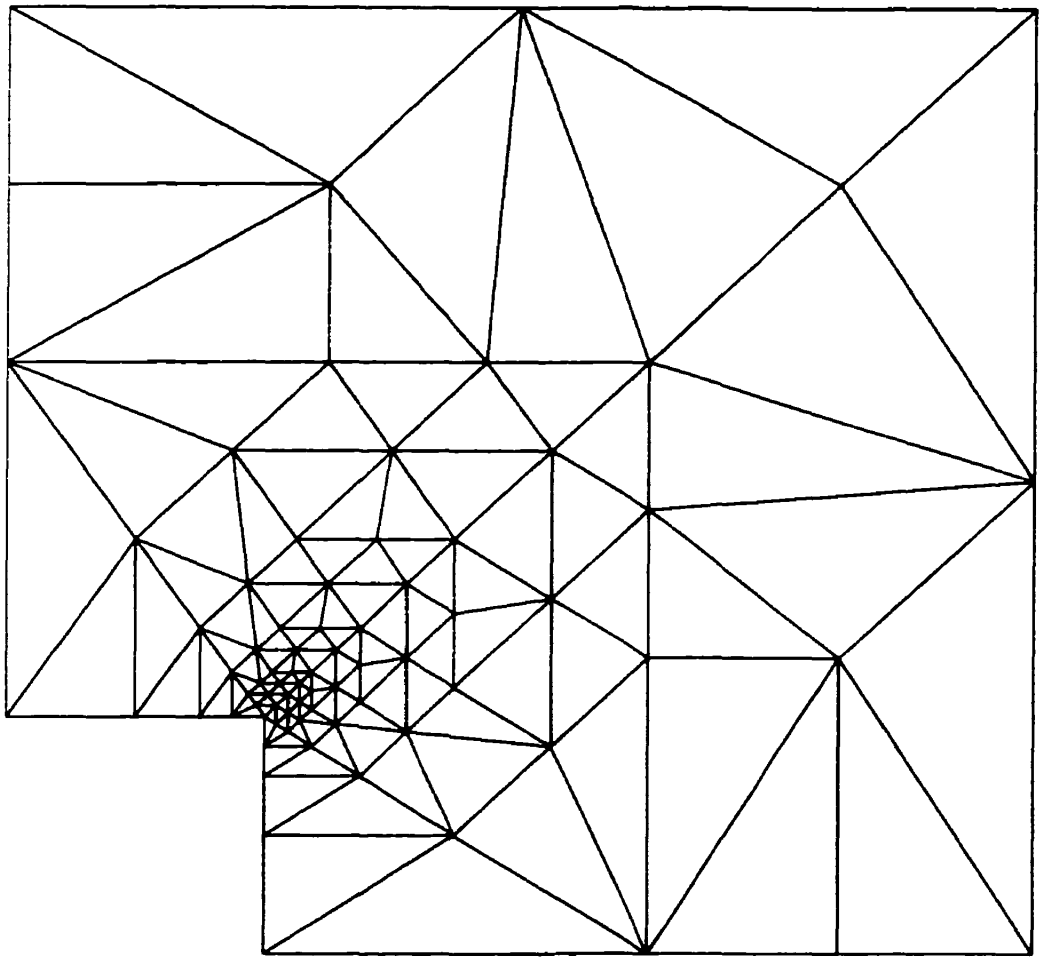

Figure 4.23: An example refinement due to the new h-adaption is illustrated for Benchmark System 3(a). The second-order discretization shown was evolved using the new optimal discretization-based refinement criteria (Type-A). The initial mesh used for the h-adaption is the eight-element discretization defined by Figure 4.2. The h-refinements at each adaptive iteration were based on element bisections and uniform subdivisions of elements into similar triangles. The resulting set of new element vertices were retriangulated using a Delaunay algorithm.

convergence of the percent errors reported in Table 4.4, it is evident that when starting from uniform-order meshes the new mixed-order p-adaption scheme results in a significantly faster rate of convergence relative to the uniform p-adaption strategy for Benchmark System 3(a). In fact, the same maximal functional accuracy level reported for this Laplace benchmark system was achieved with 700 DOF by the optimal discretization-based mixed-order p-adaption scheme compared with 1670 DOF required by the uniform method (a relative savings of approximately 58 percent in the number of DOF). At the same time, it may be noted that the new mixed-order p-adaption performance results reported in Table 4.4 are comparable to the hierarchal coefficient results for Benchmark System 3(a). Therefore, it may be concluded that the new optimal discretization-based refinement criteria are effective for evolving efficient distributions of DOF by p-adaption over the problem domain for electrostatic systems with regions of rapid field solution variation. Finally, an example p-adapted mesh is presented in Figure 4.25 to illustrate the effectiveness of the new optimal discretization-based refinement criteria by the strongly focussed and efficient placement of the higher-order elements near the reentrant corner.

Table 4.4: Discretization level versus percent error in functional for p-adaption strategies applied to Benchmark System 3(a).

Method / #DOF	1.00%	0.50%	0.10%	0.05%
uniform p-adaption	230	290	1050	1670
hierarchal coeff. p-adaption	230	290	530	675
new p-adaption	110	200	550	700
new hp-adaption	100	120	280	375

The performance results for an hp-adaption strategy applied to the Laplace benchmark system are also reported in Table 4.4. The decoupled hp-adaptive strategy considered here, first refined the initial first-order eight-element mesh shown in Figure 4.2 by h-adaption for the first three adaptive steps, and then improved the discretiza-

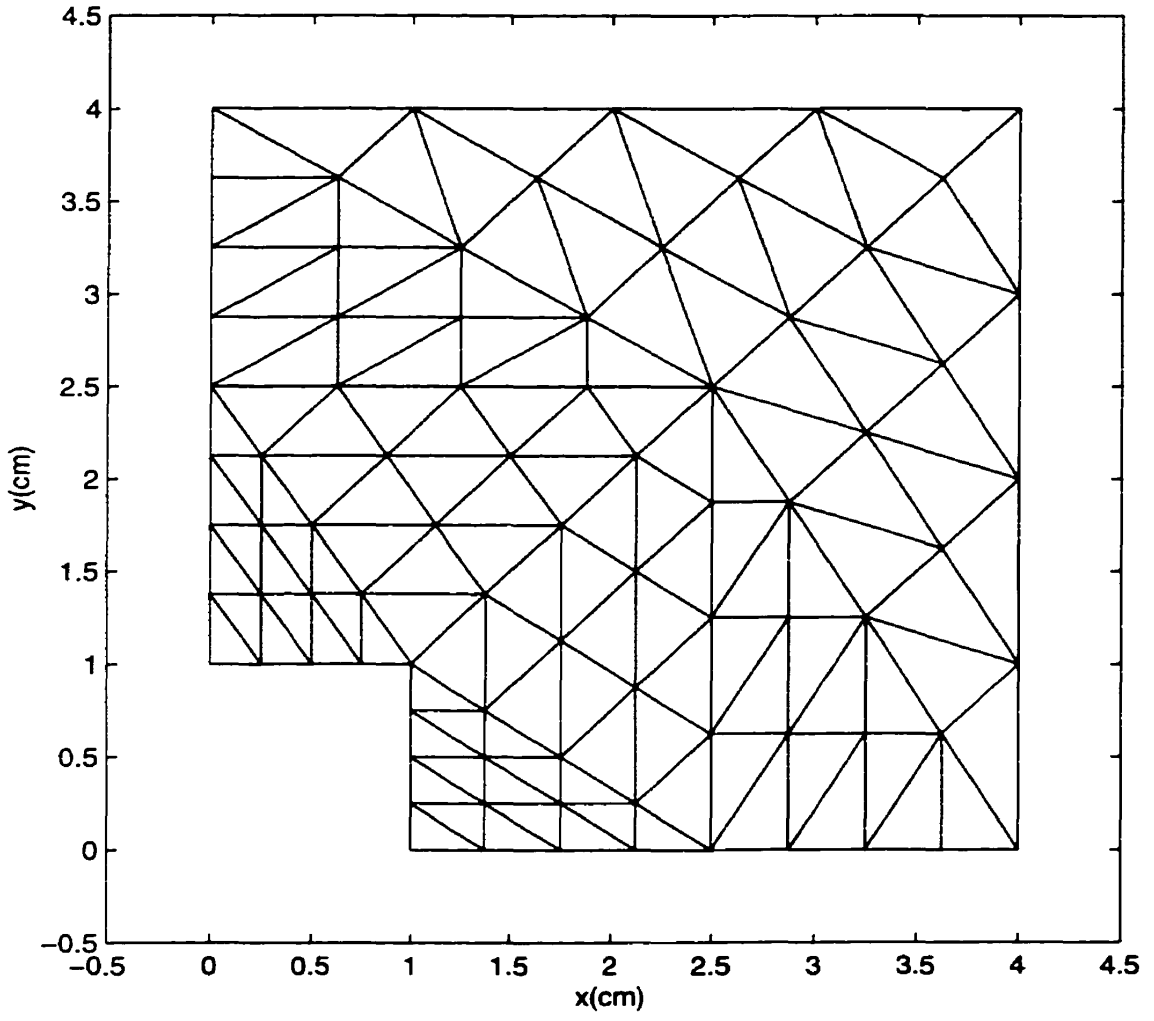

Figure 4.24: The initial mesh used for the p-adaption studies for Benchmark System 3(a) is illustrated. The initial discretization was comprised of 128 first-order elements, and was evolved by uniformly subdividing the eight-element mesh shown in Figure 4.2.

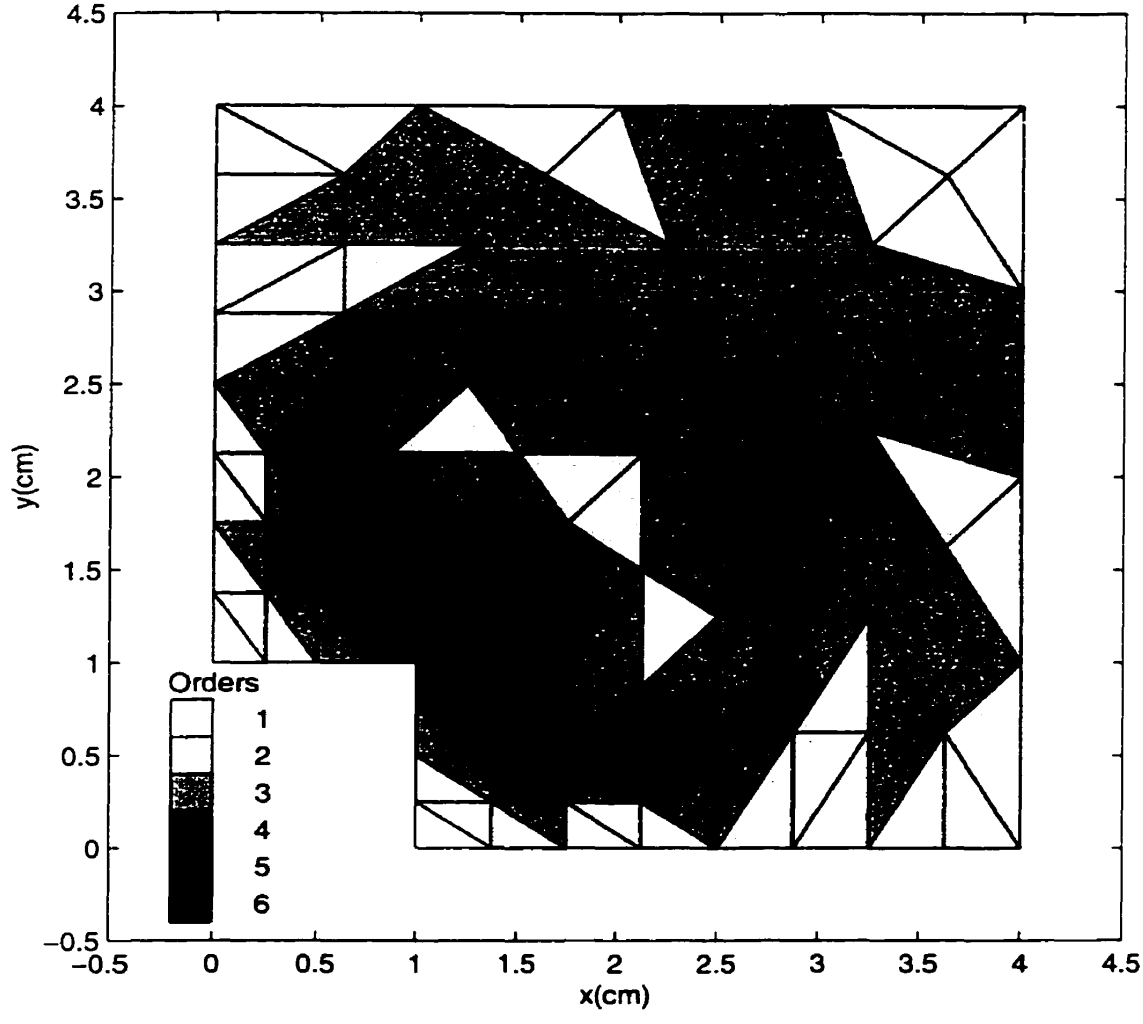

Figure 4.25: An example refinement due to the new p-adaption is illustrated for Benchmark System 3(a). The mixed-order discretization shown was evolved using the new optimal discretization-based refinement criteria (Type-A). The initial discretization used for the p-adaption is the 128 element first-order mesh defined by Figure 4.24. The range of element orders used in the discretization are shown in the legend accompanying the figure.

tion by mixed-order p-adaption in each subsequent adaptive step. For both adaption models, elements were ranked for refinement using the optimal discretization-based refinement criteria (Type-A) in the same way as for the h- and p-adaption methods described above. Furthermore, the h- and p-adaptive refinements were achieved using exactly the same procedures as described previously for the h- and p-adaption studies, respectively. It may be noted that the convergence rate of the percent error in functional value for the decoupled hp-adaption strategy is superior relative to all of the p-adaption strategies investigated for Benchmark System 3(a). Therefore, it may be concluded that the new optimal discretization-based refinement criteria are effective for evolving efficient distributions of DOF by hp-adaption over the problem domain for electrostatic systems with regions of rapid field solution variation.

The comparison of performance results for first-order h- and hp-adaption studies on functional convergence is presented in Figure 4.26. In addition to the uniform h-refinement baseline, a practical field discontinuity h-adaption result is included for comparison [58]. It may be noted that the field discontinuity-based refinement criteria described in [58] have been shown to be amongst the most effective for h-adaption models [116]. For both the new h- and hp-adaption, elements were ranked for refinement using the optimal discretization-based refinement criteria (Type-A) in the same way as for the h- and hp-adaption methods described above. Furthermore, the h- and hp-adaptive refinements were achieved using exactly the same procedures as described previously for the h- and hp-adaption studies, respectively. It may be noted that the new h-adaption performance results shown in Figure 4.26 are comparable to the field discontinuity results for Benchmark System 3(a). Moreover, the convergence rate of the percent error in functional value for the new hp-adaption strategy is superior relative to all of the methods represented in Figure 4.26.

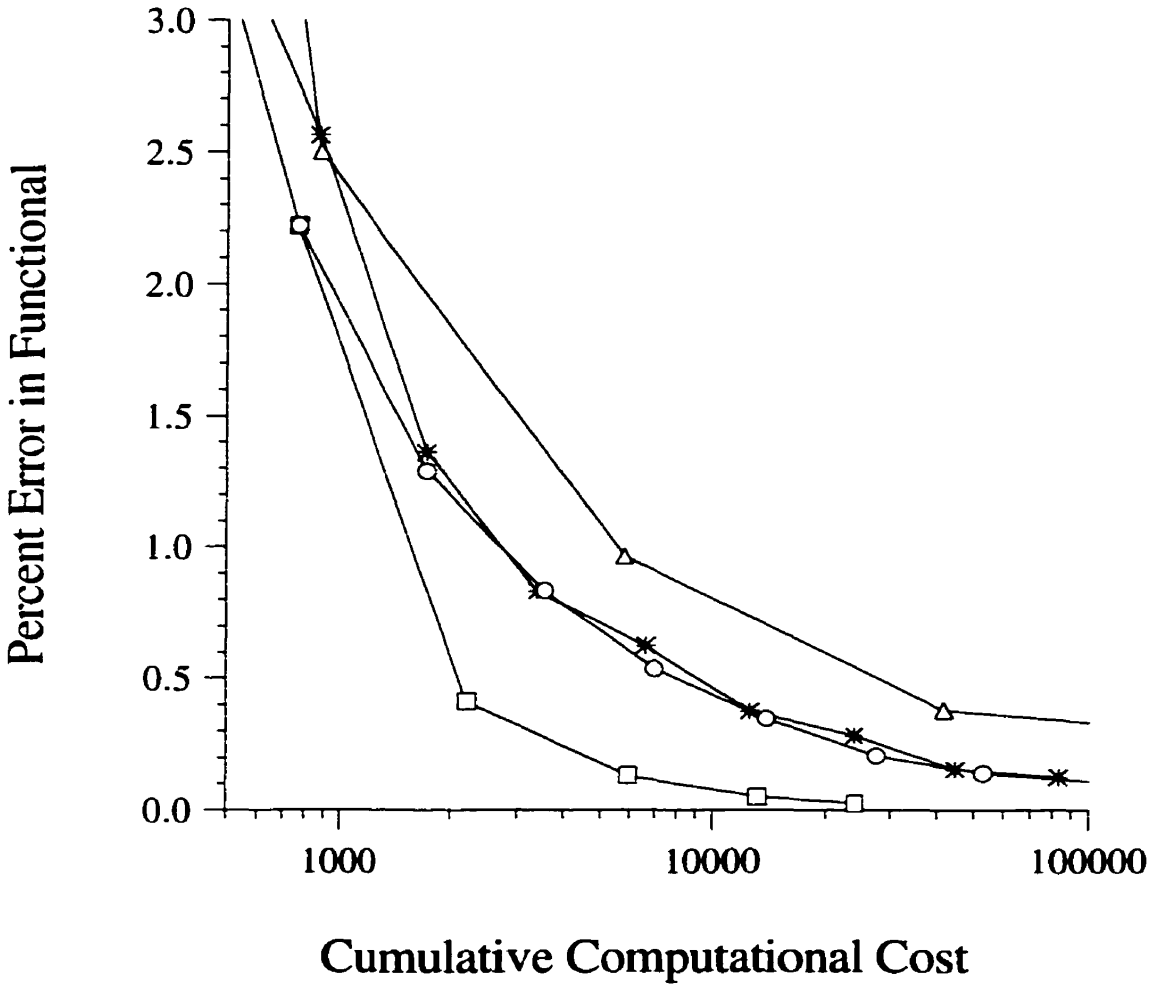

Figure 4.26: The convergence of percent error in functional value with discretization level for first-order h- and hp-adaption studies for Benchmark System 3(a) is illustrated. The triangle knot results correspond to percent error in functional values computed from solutions based on first-order uniform discretizations. The circle knot results correspond to percent error in functional values computed from solutions based on first-order h-adaption discretizations evolved using the new optimal discretization-based refinement criteria (Type-A). The asterisk knot results correspond to percent error in functional values computed from solutions based on first-order h-adaption discretizations evolved using field discontinuity-based refinement criteria. The square-knot results correspond to percent error in functional values computed from solutions based on first-order h- followed by mixed-order p-adaption (i.e., hp-adaption) discretizations evolved using the new optimal discretization-based refinement criteria (Type-A). Note: the cumulative computational cost of adaption was calculated based on using a preconditioned conjugate gradient algorithm to solve the finite element matrix equations.

4.1.2.3 Benchmark System 4

The effectiveness of the new optimal discretization-based refinement criteria are evaluated in this section for a Helmholtz benchmark system with a series of studies involving the primary adaption models. Specifically, the convergence of a range of *h*-, *p*- and *hp*-adaption strategies similar to that investigated for Benchmark System 3(a) are also examined for Benchmark System 4, when optimal discretization-based refinement criteria are used to guide the adaption. Thus, the different types of adaption techniques considered in this section are also intended to represent a range of the methods most often used for practical two-dimensional electromagnetic AFEA. It should be noted that the adaption methods employed in this section were implemented using exactly the same procedures that were used for Benchmark System 3(a), unless otherwise specified.

The Helmholtz benchmark system is described by Figure 4.27. It is an octagonal microstrip patch of size d (34mm), where $\lambda = 0.616d$ (λ is the wavelength in the dielectric substrate below the patch). The device has only one port, at the end of the microstrip transmission line connected to the left hand side of the patch. In this study, the boundaries have been modeled as perfect magnetic walls to yield a two-dimensional electric field system. The objective for this benchmark is to find the phase angle of the reflection coefficient at the input port labeled P. Finally, it may be noted that the initial mesh of 44 elements defined in Figure 4.27 was used for all of the adaption studies considered in this section.

The comparison of performance results for *h*- and *hp*-adaption studies on phase angle convergence for Benchmark System 4 is presented in Figure 4.28. In addition to the uniform *h*-refinement baseline, a practical field discontinuity *h*-adaption result is included for comparison [58], for the same reason given in the previous section. For both the new *h*- and *hp*-adaption, elements were ranked for refinement using the optimal discretization-based refinement criteria (Type-B) in the same way as for the *h*-

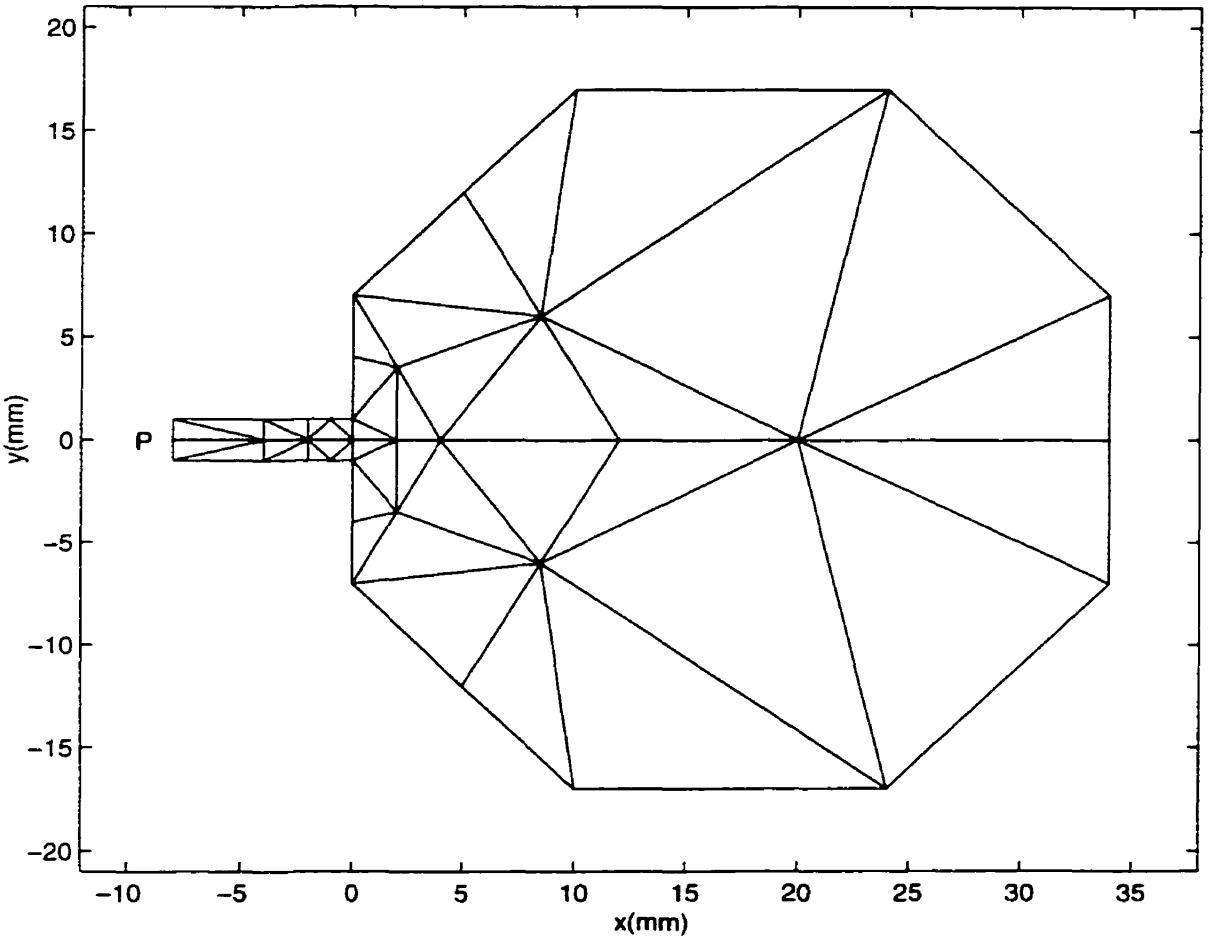

Figure 4.27: The geometry and initial 44 element mesh for the electric field analysis of Benchmark System 4 are illustrated. The two-dimensional view depicts an octagonal microstrip patch. The device has one port labeled P at the end of the microstrip transmission line connected to the left hand side of the patch. The remaining boundaries of the problem domain are modeled as perfect magnetic walls. The electric field wavelength in the dielectric substrate below the patch is $0.616d$, where $d = 34$ (mm).

and *hp*-adaption strategies employed for the analysis of Benchmark System 3(a). Furthermore, the *h*- and *hp*-adaptive refinements for the Helmholtz system were achieved using exactly the same procedures as described for Benchmark System 3(a), with the following exception: a 100 percent increment in the number of DOF per adaptive step was used to update the discretizations, excluding the uniform refinement procedure. For this benchmark system, *h*-adaption results for second-order meshes are reported. However, as per the *hp*-adaption in the Laplace study, only the more efficient decoupled first-order *h*- followed by *p*-adaption performance is presented for the Helmholtz system. It may be noted that the new *h*-adaption performance results shown in Figure 4.28 are comparable to the field discontinuity results for Benchmark System 4. Moreover, the convergence rate of the phase angle error for the new *hp*-adaption strategy is superior relative to all of the methods represented in Figure 4.28, for phase error levels less than two degrees. Therefore, it may be concluded that the new optimal discretization-based refinement criteria are effective for evolving efficient distributions of DOF by *h*- and *hp*-adaption over the problem domain for the Helmholtz system considered.

The performance results for a range of *p*-adaption strategies applied to Benchmark System 4 are summarized in Table 4.5. Specifically, the same uniform and mixed-order *p*-adaption schemes that were investigated for Benchmark System 3(a) were also considered for the Helmholtz system using elements which ranged from order one through ten. In addition to the uniform *p*-refinement baseline, the hierarchal coefficient *p*-adaption result [59] is presented for comparison, for the same reason given in the previous section. For the new mixed-order *p*-adaption, the optimal discretization-based refinement criteria (Type-*B*) were used to rank elements for refinement in exactly the same way as for Benchmark System 3(a). Furthermore, the *p*-adaptive refinements for the Helmholtz system were achieved using exactly the same procedures as described for the analysis of Benchmark System 3(a), with the following exception: a 100 percent increment in the number of DOF per adaptive

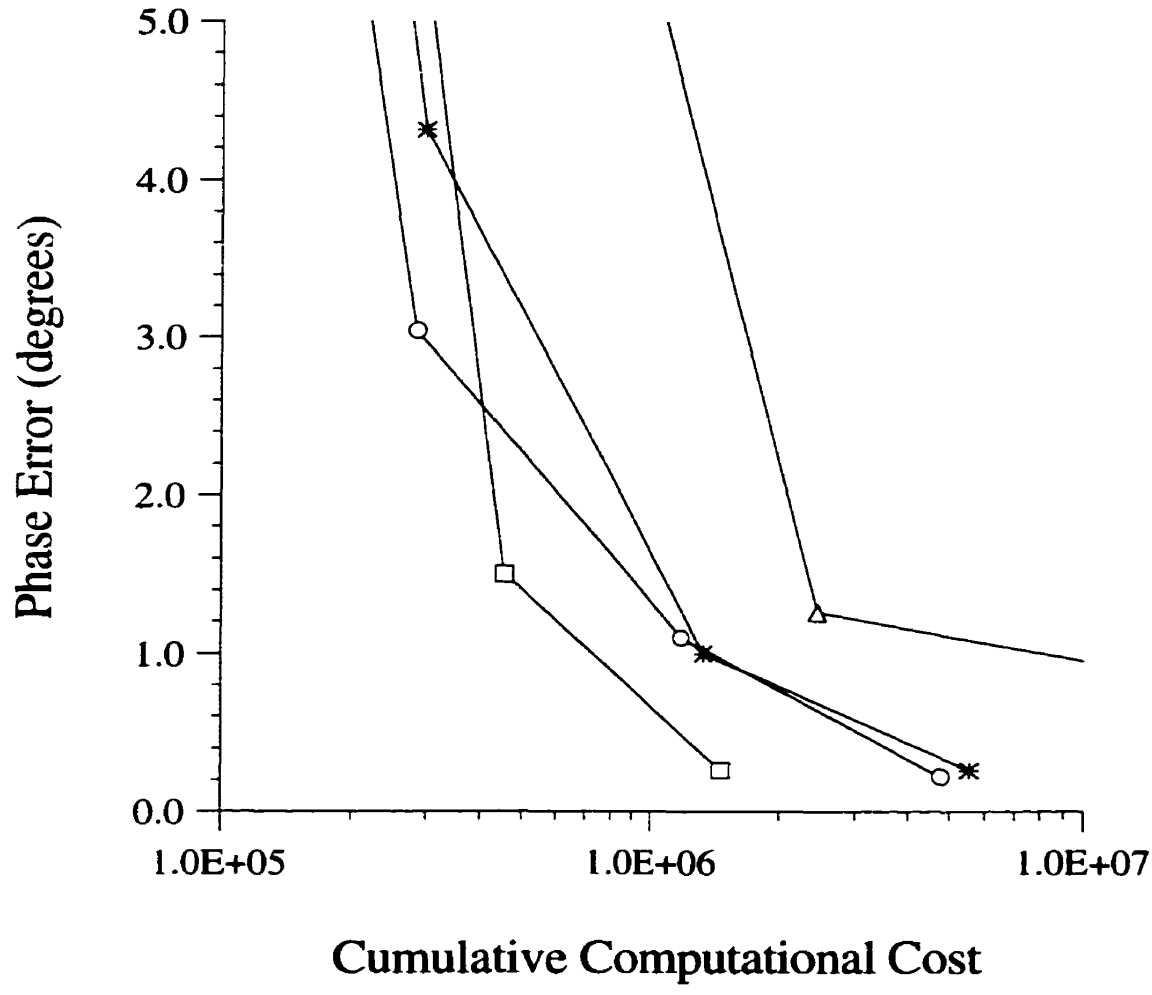

Figure 4.28: The convergence of reflection phase error with discretization level for second-order h- and hp-adaption studies for Benchmark System 4 is illustrated. The triangle knot results correspond to phase error values computed from solutions based on second-order uniform discretizations. The circle knot results correspond to phase error values computed from solutions based on second-order h-adaption discretizations evolved using the new optimal discretization-based refinement criteria (Type-B). The asterisk knot results correspond to phase error values computed from solutions based on second-order h-adaption discretizations evolved using field discontinuity-based refinement criteria. The square-knot results correspond to phase error values computed from solutions based on first-order h- followed by mixed-order p-adaption (i.e., hp-adaption) discretizations evolved using the new optimal discretization-based refinement criteria (Type-B). Note: the cumulative computational cost of adaption was calculated based on using a sparse Gaussian elimination algorithm to solve the finite element matrix equations.

step was used to update the discretizations, excluding the uniform refinement procedure. Based on the convergence of the phase angle errors reported in Table 4.5, it is evident that when starting from uniform-order meshes the new mixed-order *p*-adaption scheme results in a faster rate of convergence relative to both the uniform *p*-adaption strategy and the hierarchal coefficient-based strategy that were considered for Benchmark System 4. Therefore, it may be concluded that the new optimal discretization-based refinement criteria are effective for evolving efficient distributions of DOF by *p*-adaption over the problem domain for this Helmholtz systems. It is interesting to note that the *hp*-adaption result reported in Table 4.5 is inferior to all the *p*-adaptive methods examined for this benchmark system. This result, however, is not inconsistent with the undulating nature of the wave solution to the system: a plot of the electric field over the patch is illustrated in Figure 4.29. Since the spatial variation of the field is not overly rapid anywhere over the device, and it is reasonably compatible with the DOF distribution provided by the initial *p*-mesh, methods which can efficiently evolve a relatively uniform distribution of DOF may be expected to yield the best results. Finally, an example *p*-refined mesh is illustrated in Figure 4.30. The selectivity of the new refinement criteria, and the way it efficiently distributes the DOF over the problem domain, may be observed by comparing the relative field variations to the relative densities of DOF assigned to the finite element analysis.

Table 4.5: Discretization level versus phase error in degrees for *p*-adaption strategies applied to Benchmark System 4.

Method / #DOF	1.5°	1.0°	0.5°	0.1°
uniform p-adaption	400	530	690	865
hierarchal coeff. p-adaption	385	465	550	851
new p-adaption	367	405	445	677
new hp-adaption	587	750	920	1100

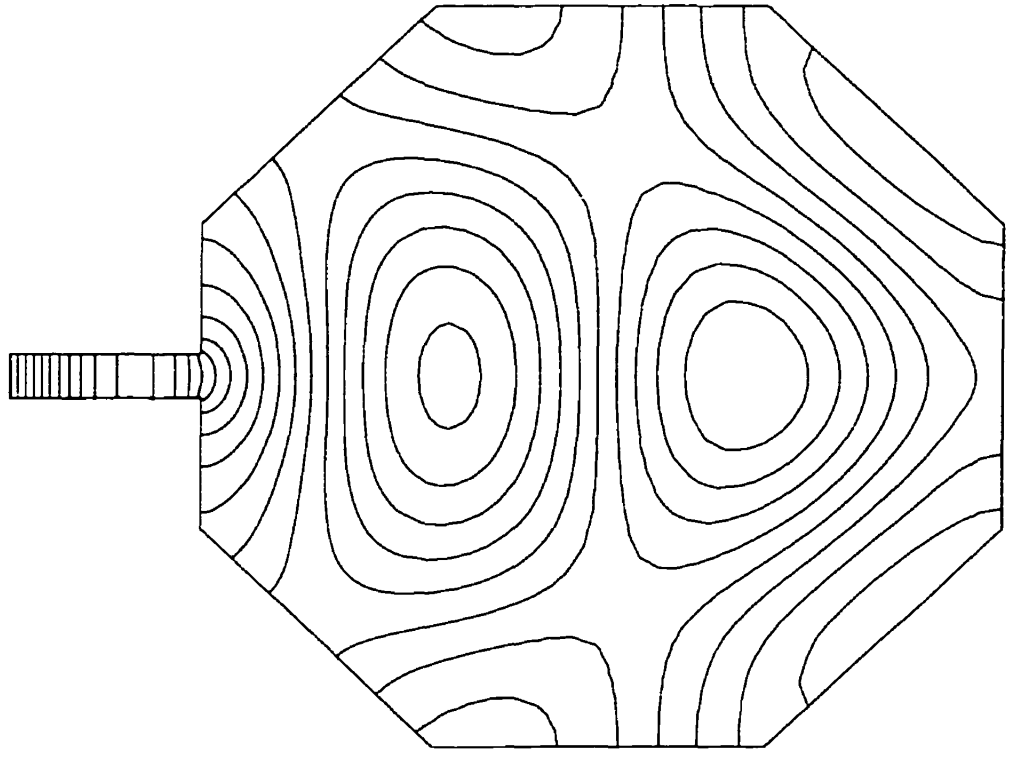

Figure 4.29: An approximate electric field solution for Benchmark System 4 is illustrated. The plot is based on the finite element solution computed using tenth-order elements for the mesh defined by Figure 4.27.

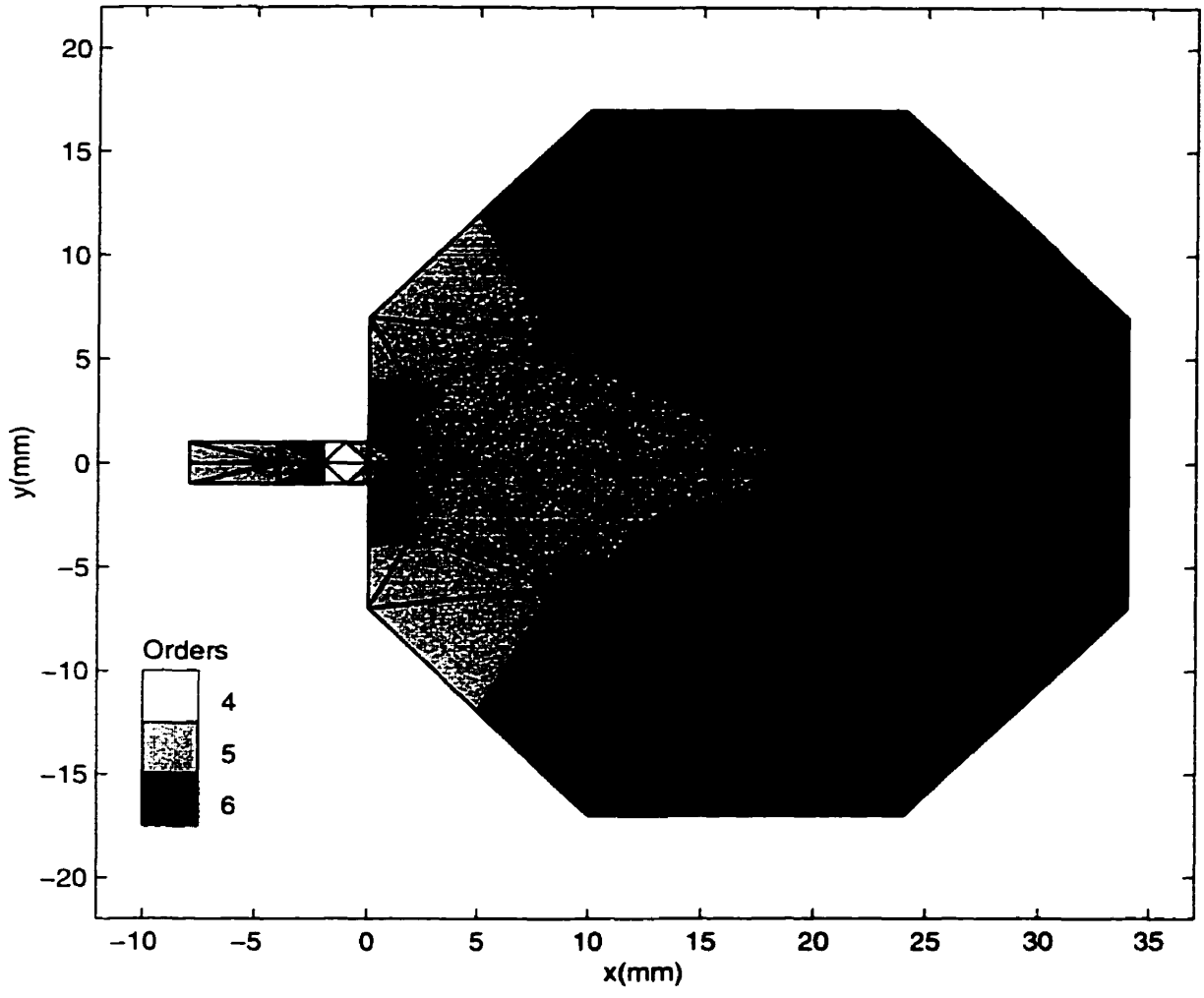

Figure 4.30: An example refinement due to the new p-adaption is illustrated for Benchmark System 4. The mixed-order discretization shown was evolved using the new optimal discretization-based refinement criteria (Type-B). The initial discretization used for the p-adaption is the 44 element first-order mesh defined by Figure 4.27. The range of element orders used in the discretization are shown in the legend accompanying the figure.

4.1.2.4 Discussion

The results presented in the two preceding sections demonstrate the value of employing optimality properties of two-dimensional finite element discretizations to develop effective feedback refinement criteria for efficiently and reliably guiding adaptive systems towards accurate solutions. Briefly stated, new two-dimensional refinement criteria, based on variational aspects of optimal discretizations for scalar Poisson and Helmholtz FEA, have been introduced and evaluated for the primary adaption models. Stationarity of the functional corresponding to the variational formulation is the fundamental principle essential to the development of the new refinement criteria. Specifically, the gradients of the functional with respect to element vertex positions were used to determine the sensitivity of the functional to differential displacements of the element vertices, in order to distinguish and rank regions of insufficient discretization in a finite element mesh.

It is worth noting that the new two-dimensional optimal discretization-based refinement criteria are inexpensive to compute, since they are closely related to the underlying variational principle used to determine the finite element solution. In fact, the only extra terms that are required have been tabulated in Table 2.1 and Table 2.2 of section 2.4.2, and involve quantities which, at any rate, must be evaluated in order to compute the finite element solution to a problem. Moreover, the entries of the matrices in Eqs. (2.104) and (2.105) that are required for the new refinement criteria, are very similar to those of the matrices in Eq. (2.92), the matrix equation that must be solved for the finite element problem. Furthermore, careful examination of Eqs. (2.88), (2.100) and (2.101) reveals that, in effect, the new refinement criteria can be computed extremely efficiently since they involve exactly the same mathematical operations required to determine the entries of standard finite element matrices, modified only by the addition of or multiplication by the extra terms described above.

The performance results for the benchmark systems that were investigated show

that the proposed refinement criteria can be successfully used in adaptive finite element solvers to effectively and economically distribute DOF over the problem domain. In comparison with the state-of-the-art two-dimensional refinement criteria that were evaluated, the new approach produced results that were as good or better, suggesting that further studies involving the application of new optimal discretization-based criteria for the AFEA of three-dimensional electromagnetic systems is warranted. First, two computational analysis and design application examples are presented in the next section to further illustrate the practical value of the new optimal discretization-based approach for AFEA.

4.1.3 Computational Analysis and Design Application Examples

The two-dimensional benchmark problems examined in the previous sections of this chapter are typical electromagnetic systems that AFEA may be applied to. For example, the coaxial transmission line models of section 4.1.1 may be of interest to the microwave engineer who will, no doubt, need to determine the capacitance and inductance per unit length of the lines, or the maximum field strengths occurring between the inner and outer conductors. The correctness of computed values for such quantities is directly dependent on the accuracy of the underlying finite element field solutions for the devices. Similarly, the microstrip patch model examined in section 4.1.2.3 will be of interest to the antenna designer, who may need to determine the radiation field patterns of the device. The radiation fields may be calculated from the current distributions along the antenna structure. Therefore, accurate current distributions must be known in order to precisely evaluate the far fields. However, in order to know the current distributions, the field structure of the patch must be accurately determined. The results of the adaption studies presented in section 4.1.2 have demonstrated the value of the new optimal discretization-based AFEA for efficiently computing accurate solutions to such two-dimensional electromagnetics problems. The purpose of this section is to introduce two additional electromagnetic systems in

order to further illustrate the practical value of the new approach for computational analysis and design. The primary objective is not to provide comprehensive analyses of the systems considered, but rather, to provide simple demonstrations of the effectiveness of the new method.

4.1.3.1 Switched-Reluctance Motor

In this section, the new optimal discretization-based refinement criteria developed earlier are employed for the two-dimensional AFEA of a switched-reluctance motor (SRM) model, in order to provide additional support for their practical value. Specifically, the performance of the new refinement criteria (Type-A) are examined with an h-adaptive solver for the SRM design represented in Figure 4.31. Switched reluctance motors rely on changes in the reluctance of their magnetic circuits with position for torque production, and are commonly found in applications requiring precision movements.

Although standard, non-adaptive, magnetostatic FEMs may be employed for the analysis of the SRM shown in Figure 4.31, there are key features of such devices that render the accurate determination of their field solutions challenging and computationally intensive. For example, the design of SRMs requires the calculation of the magnetic flux linkage of the motor as a function of both rotor position and excitation current [88]. Therefore, to calculate the full behavior of a SRM design reasonably well, in general, at least eight solutions are required at different angular positions of the rotor, and at each of these positions, at least eight different excitation current levels must be considered [88]. Thus, a typical design cycle may involve a minimum of 64 solutions, and for each of the eight different positions, a new adequate finite element discretization must be created. Furthermore, the accurate calculation of the field solutions demands that the complex geometric details of the machine be adequately resolved by the finite element discretizations of the problem domain. For example, the narrow air gap regions and the curved material boundaries of the design must be

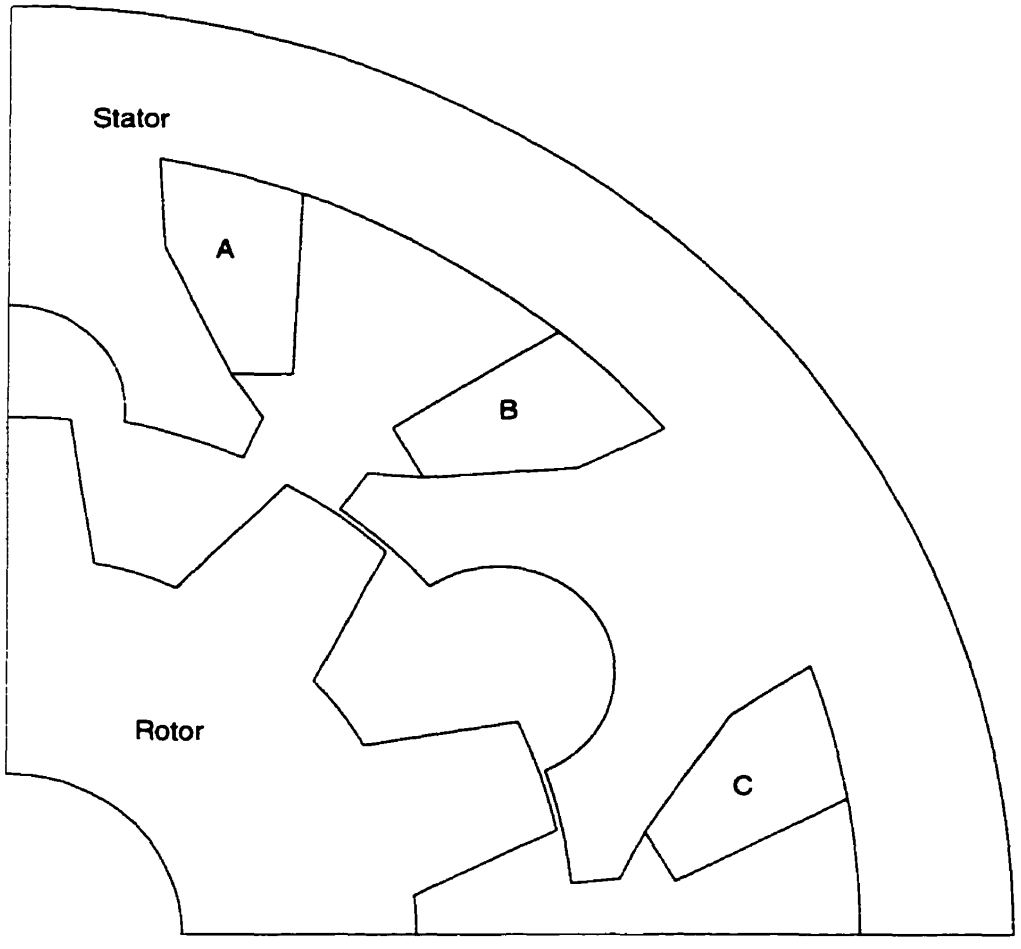

Figure 4.31: The geometry for the magnetic vector potential analysis of a switched reluctance motor is illustrated. The two-dimensional view depicts one-quarter of the cross-section of a 12/10 switched reluctance motor in an unaligned position [70]. The air gap between the stator and rotor is 0.5 (mm), and the total diameter of the motor is 165 (mm). The stator and rotor relative permeabilities are each 1000, and the coil labeled A was excited with a uniform current density of 1.0 (A/m^2) .

sufficiently well-modeled with appropriate numbers and sizes of elements. Moreover, several refinements of an initial discretization may be necessary in order to converge the finite element field solution errors to within pre-specified engineering tolerances. Consequently, a large number of DOF can be required to compute each of the 64 field solutions with sufficient accuracy. For these reasons, AFEMs are essential for an efficient SRM design cycle based on finite element analysis, since the computation of these several fields can consume considerable computer time.

The convergence of the percent error in functional value for an h-adaption strategy applied to the SRM design considered in this section is illustrated in Figure 4.32. The initial mesh used for the h-adaption was comprised of 257 first-order elements. At each subsequent adaptive iteration, the new optimal discretization-based refinement criteria (Type-A) were used to guide 50 percent increments in the number of DOF in order to update the discretizations. The uniform h-refinement baseline functional convergence result based on the same starting mesh is also shown in Figure 4.32 for comparison. For both the new h-adaption and the uniform refinement procedures, a termination criterion of 2.5 percent error in the functional value was used. It may be noted that the new h-adaption performance results indicate a considerable savings in computational cost relative to the uniform refinement approach. For example, a functional accuracy level of approximately 2.8 percent is achieved by the new approach after four adaptive steps and at a relative computational cost of 24,452; whereas, the error in the functional value after three uniform refinements is approximately 3.4 percent and was obtained with a relative computational cost of 109,869. These figures represent approximately a 78 percent reduction in the computational effort required to converge the finite element field solution to a functional accuracy level below 5 percent error, when the new optimal discretization-based adaptive approach is used rather than employing uniform refinements. Similarly, a savings of approximately 94 percent in required computational effort can be achieved by using the new h-adaption in place of uniform refinement for functional accuracy levels of less than 2.5 percent error. The

significance of the computational efficiency of the new optimal-discretization based approach is amplified by the fact that 64 finite element field solutions are, typically, required for the analysis of a SRM design. Therefore, the substantial improvement in the time required to complete the overall design cycle for a SRM, when the new approach is used, can be of great practical benefit to the design engineer. Finally, a plot of the magnetic flux density over the SRM is illustrated in Figure 4.33, where the highly non-uniform variation of the field solution over the problem domain may be noted.

4.1.3.2 Microelectronic System Interconnections

In this section, the new optimal discretization-based refinement criteria developed earlier are employed for the two-dimensional AFEA of a microelectronic system interconnection (MSI) model, in order to further demonstrate their practical value. Specifically, the performance of the new refinement criteria (Type-B) are examined with an h-adaptive solver for the MSI structure represented in Figure 4.34: a cross-sectional view is shown for part of a MSI structure with three rectangular strip-line conductors buried within a dielectric substrate and between two solid conductor planes [163]. This type of MSI structure is common in multi-chip module (MCM) technology used for modern electronic packaging [164].

With today's shrinking feature sizes and increasing clock frequencies, the limiting factor for many high-performance microelectronic systems is now being set by interconnection delays rather than device switching speeds. Further, interconnection effects such as reflection, cross-talk, dispersion and attenuation are now leading sources of signal corruption and a significant cause of system performance degradation at higher operating speeds. Standard circuit analysis techniques are not sufficient for accurately predicting the performance of microelectronic systems when these conditions prevail. Today, the state-of-the-art in MSI research lies in the development of efficient numerical methods capable of accurately and reliably simulating the intercon-

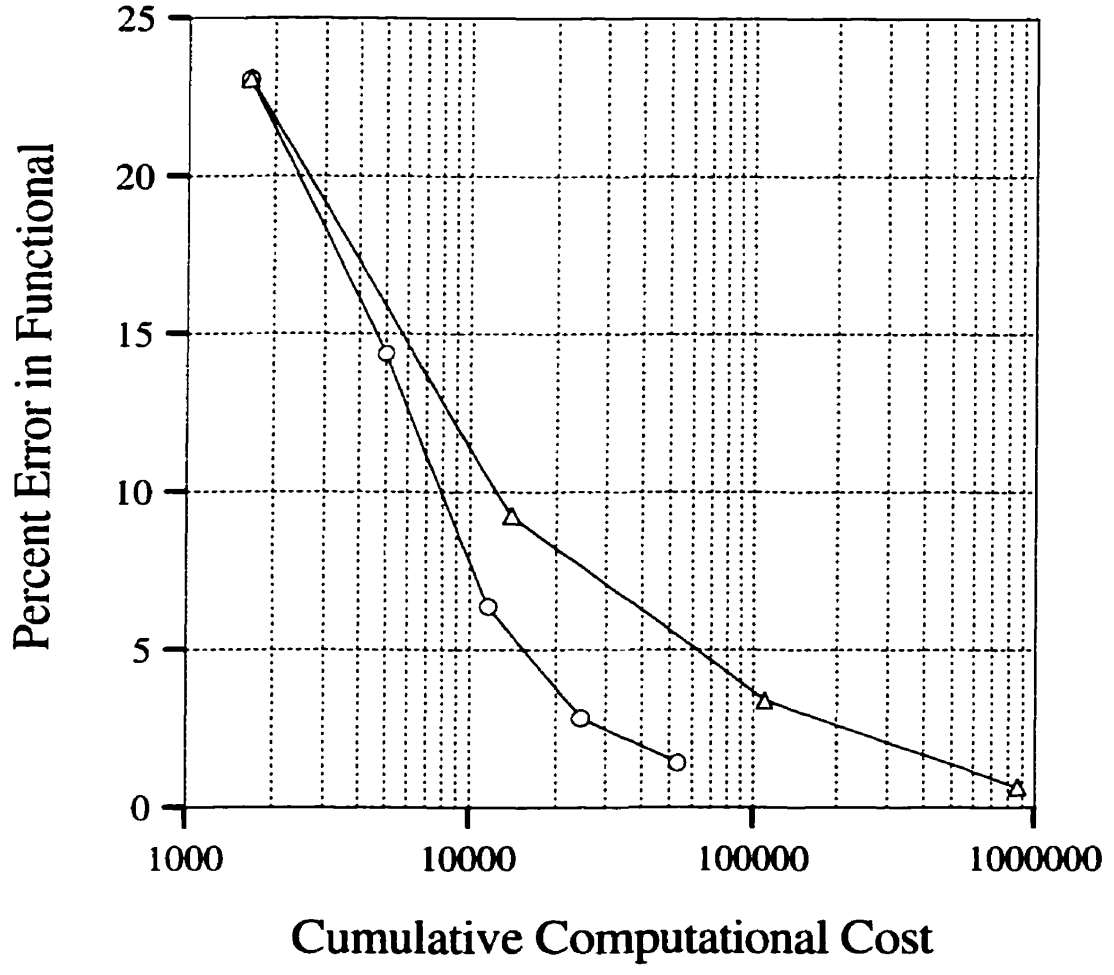

Figure 4.32: The convergence of percent error in functional value with discretization level for first-order h-adaption studies for the switched reluctance motor model of Figure 4.31 is illustrated. The triangle knot results correspond to percent error in functional values computed from solutions based on first-order uniform discretizations. The circle knot results correspond to percent error in functional values computed from solutions based on first-order h-adaption discretizations evolved using the new optimal discretization-based refinement criteria (Type-A). Both results are based on the same initial mesh. Note: the cumulative computational cost of adaption was calculated based on using a preconditioned conjugate gradient algorithm to solve the finite element matrix equations.

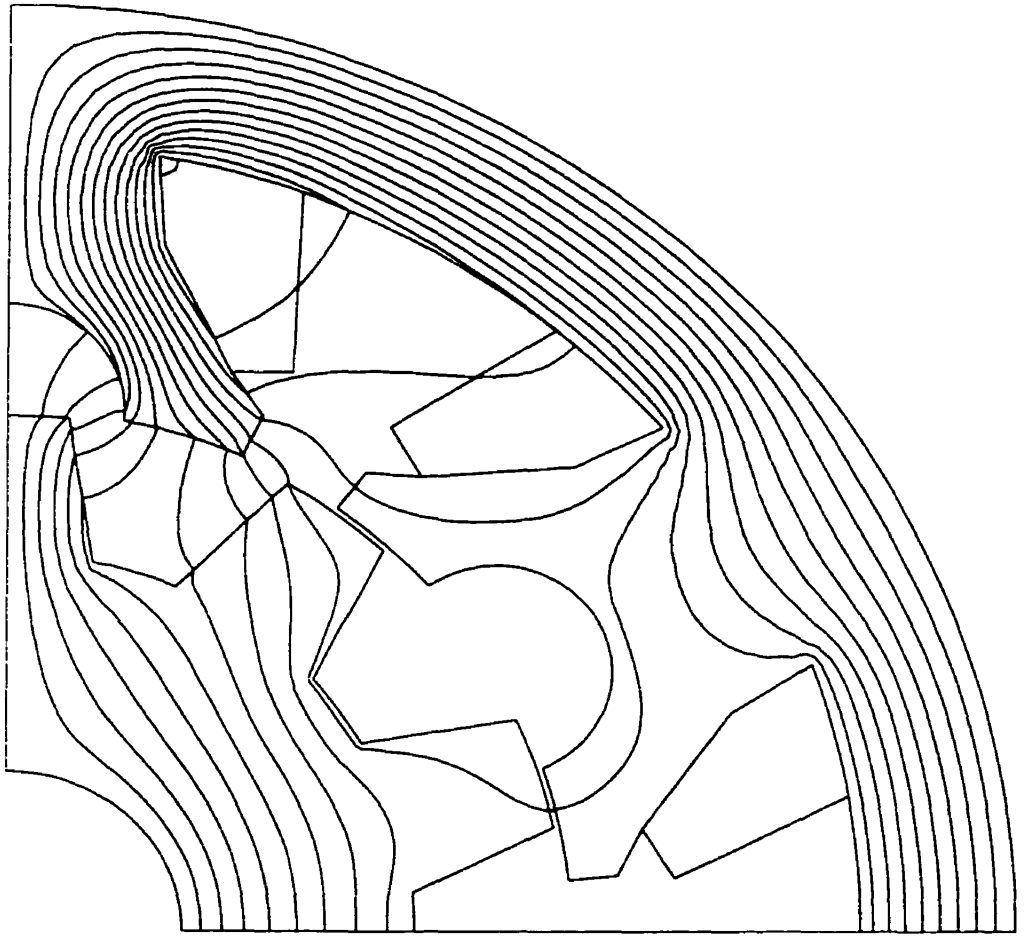

Figure 4.33: An approximate field solution for the switched reluctance motor model of Figure 4.31 is illustrated. The plot is based on the finite element solution computed using an adaptively refined mesh with 1,847 second-order elements.

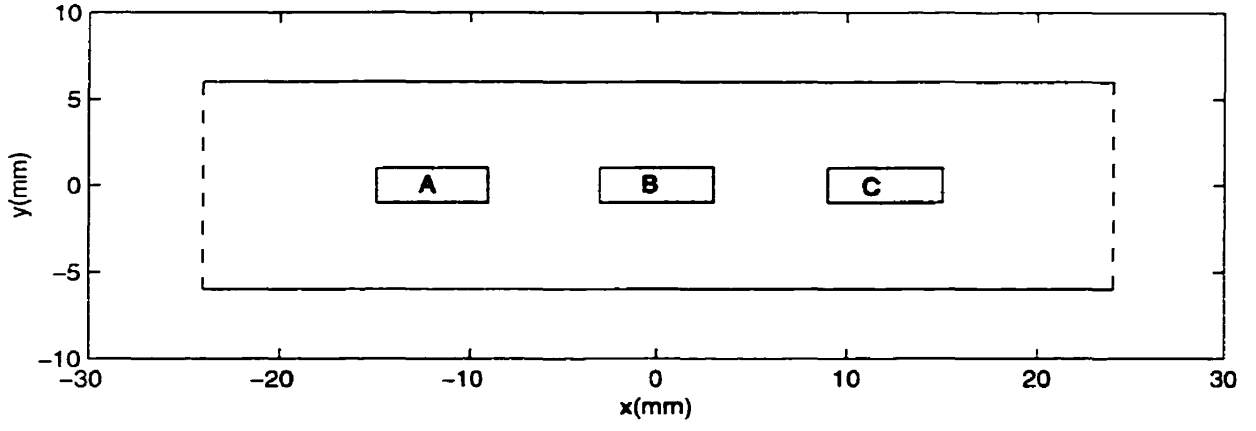

Figure 4.34: The geometry for the electrostatic potential analysis of a microelectronic interconnection structure is illustrated. The two-dimensional view depicts the cross-section of a structure with three rectangular strip-line conductors buried within a dielectric substrate and between two solid conductor reference planes. The strip-lines labeled A and C are each at a potential of 25 (mV) higher than the two reference planes: and the strip-line labeled B is at a potential of 100 (mV) above the reference planes. The dashed vertical lines represent symmetry planes for the MSI structure.

nection electromagnetic fields within the sophisticated microfabricated structures of modern microelectronic systems. The main difficulty with computational MSI analysis is that a very large number of free modeling parameters are needed to compute accurate and reliable simulations for realistic systems. Sufficient mathematical DOF are required to both resolve the geometric and material features of a MSI structure, and represent the fields of the electromagnetic system. The computational effort required for the electromagnetic analysis of the complex, dense, and irregularly routed arrays of high-speed interconnections that comprise modern MSI structures can often be prohibitive. Yet such analysis are critical if MSI system performance is to be simulated with confidence. Currently, the only practical way to overcome this type of computational barrier is by using adaptive solver technologies.

The convergence of the percent error in functional value for an h-adaption strategy applied to the upper one-half of the MSI structure considered in this section is illustrated in Figure 4.35. The initial mesh used for the h-adaption was comprised of 54 first-order elements. At each subsequent adaptive iteration, the new optimal discretization-based refinement criteria (Type-B) were used to guide 50 percent increments in the number of DOF in order to update the discretizations. The uniform h-refinement baseline functional convergence result based on the same starting mesh, is also shown in Figure 4.35 for comparison. For both the new h-adaption and the uniform refinement procedures, a termination criterion of 1.0 percent error in the functional value was used. It may be noted that the new h-adaption performance results indicate a considerable savings in computational cost relative to the uniform refinement approach. For example, a functional accuracy level of approximately 2.4 percent is achieved by the new approach at a relative computational cost of 4,474; whereas, for a similar error in the functional value of approximately 2.2 percent, the relative computational cost of uniform refinement was 13,406. These figures represent approximately a 67 percent reduction in the computational effort required to converge the finite element field solution to a functional accuracy level below 2.5 percent error,

when the new optimal discretization-based adaptive approach is used rather than employing uniform refinements. Similarly, a savings of approximately 81 percent in required computational effort can be achieved by using the new h-adaption in place of uniform refinement for functional accuracy levels of less than 1.0 percent error. Ultimately, this type of approach is intended to benefit the microelectronics engineer by providing effective computer-aided analysis and design tools that can be used with confidence to predict the electromagnetic performance of a newly proposed MSI structure to within the designer's specified tolerances. Finally, an equipotential plot for the MSI structure is illustrated in Figure 4.36, where the non-uniform variation of the field solution over the problem domain may be noted.

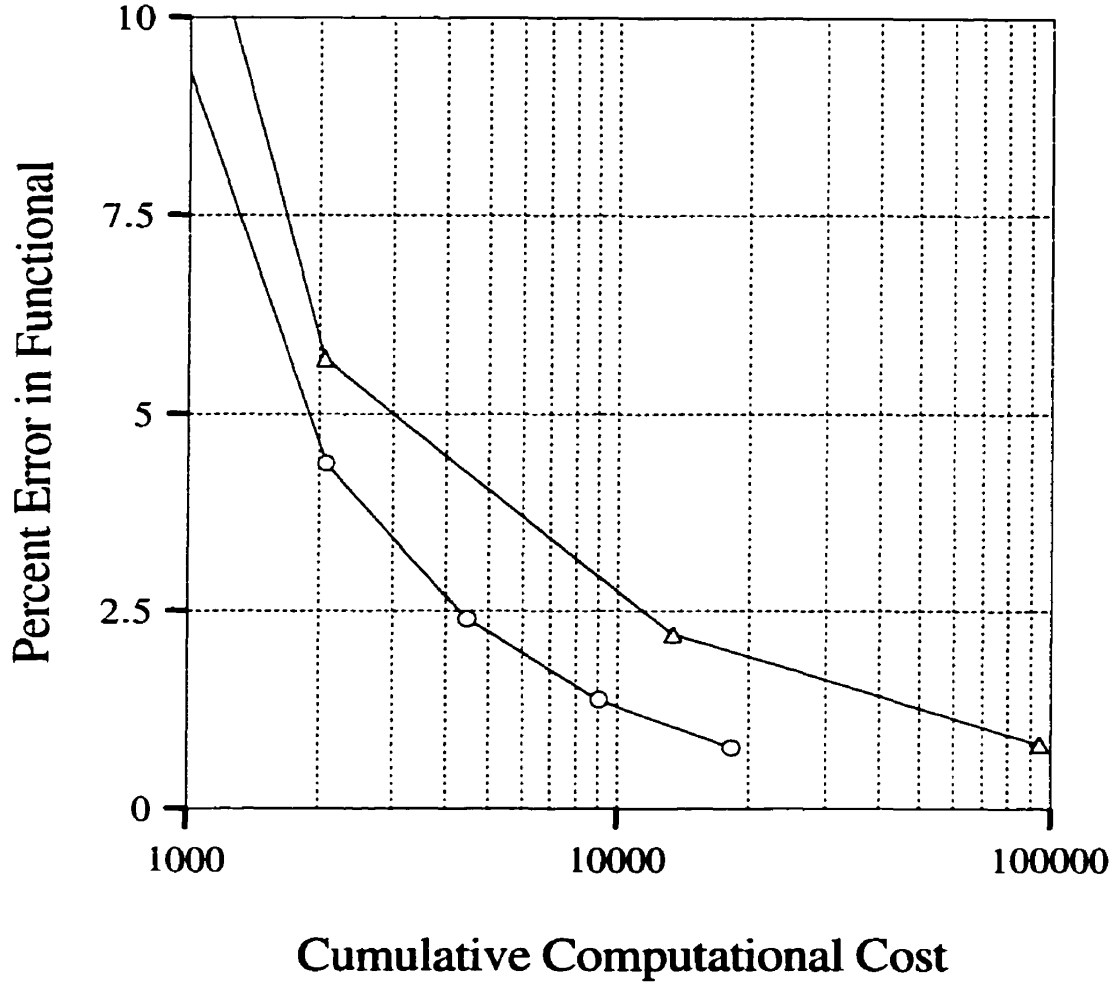

Figure 4.35: The convergence of percent error in functional value with discretization level for first-order h-adaption studies for the upper one-half of the MSI structure shown in Figure 4.34 is illustrated. The triangle knot results correspond to percent error in functional values computed from solutions based on first-order uniform discretizations. The circle knot results correspond to percent error in functional values computed from solutions based on first-order h-adaption discretizations evolved using the new optimal discretization-based refinement criteria (Type-B). Both results are based on the same initial mesh. Note: the cumulative computational cost of adaption was calculated based on using a preconditioned conjugate gradient algorithm to solve the finite element matrix equations.

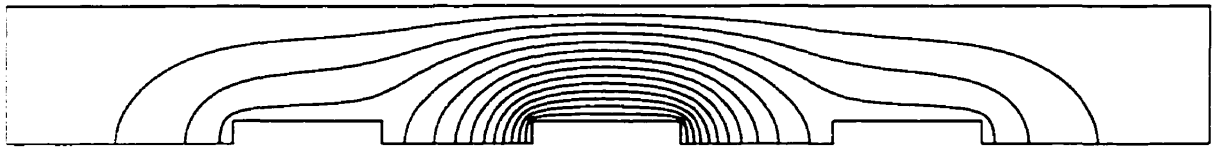

Figure 4.36: An approximate equipotential plot for the upper one-half of the MSI structure represented in Figure 4.34 is illustrated. The plot is based on the finite element solution computed using an adaptively refined mesh with 796 second-order elements.

4.2 Three-Dimensional Systems

The findings from the one- and two-dimensional studies reported in previous sections suggest that the new optimal discretization-based refinement criteria, derived from functional gradient concepts, are well-equipped to be effective, reliable, and economical for practical AFEA of electromagnetic systems. The objective of this section is to investigate the potential benefits and related costs of using the finite element optimization equations, derived in section 2.4.3, to develop analogous optimal discretization-based refinement criteria for three-dimensional electromagnetic AFEA. Hence, the formulation of section 2.4.3 is, first, validated in the next section using a set of numerical tests on three-dimensional electromagnetic benchmark systems. Subsequently, results from studies involving selected finite element analysis refinement models are reported for a three-dimensional benchmark system, in order to evaluate the effectiveness of a proposed three-dimensional optimal discretization-based refinement criterion for practical AFEA.

4.2.1 Validation of the Optimization Equations

In order to validate the three-dimensional finite element optimization equations derived in section 2.4.3, the x-, y- and z-components of the functional gradients with respect to element vertex positions were tested with a range of numerical benchmark evaluations. Specifically, the geometry and mesh defined by Figure 4.37 (Benchmark System 5) were used to compute first-order finite element solutions with both optimal field solution and optimal geometric discretization parameter values for three benchmark evaluations. Each system consisted of a base "bowl" (Figure 4.37) joined to a top "cap" (mirror image of Figure 4.37) across a shared hexagonal plane. For these Laplace tests, all exterior, ideal conductor cap facets were set to $1V$ (Dirichlet); the equilateral triangular, ideal conductor base of the bowl was set to $0V$ (Dirichlet); and all the remaining exterior bowl facets were left unconstrained (Neumann). The three different benchmark evaluations were defined by fixing the bowl base and cap top at

$z = 0$ and $z = 1.6330$ (cm), respectively, and varying the position of the hexagonal plane between them. Specifically, the normalized height of the hexagonal plane between the bowl base and cap top was set to: (A) 0.25, (B) 0.5, and (C) 0.75. The objective for these benchmark evaluations is to compute the functional value corresponding to the electrostatic potential energy stored in the air region of the problem domain.

The electrostatic systems used to establish the optimal discretization benchmark results of this section, were analyzed for electric scalar potentials using the three-dimensional finite-element formulation given in section 2.4.3, and the corresponding finite element optimization equations were used to test the x-, y- and z-components of the functional gradients with respect to element vertex positions. For each of the three benchmark tests described above, there are three free geometric discretization parameters corresponding to the x-, y- and z-coordinates of the interior vertex in the mesh. Moreover, it may be noted that the optimal position of the interior vertex must lie, by symmetry, along the vertical line segment joining the centers the triangular top and base of the systems. Finally, the functional values for the three benchmark evaluations were calculated from the computed scalar potentials using exact differentiation and integration.

The basic computational experiment that was performed in order to confirm the validity of the three-dimensional finite element optimization equations used to define an optimal discretization-based refinement criterion later in this section, is described next. This fundamental numerical experiment was based on resolving Benchmark System 5 using the elementary discretization defined by Figure 4.37. A series of 1,000 20-element meshes were used to compute individual functional values corresponding to fixing the interior vertex at 1,000 regularly spaced positions along the vertical line segment joining the centers of the triangular top and base of the systems. It should be noted that for each of the meshes defined by this method, the unknown scalar electric potential values for the finite element models were computed using the standard finite

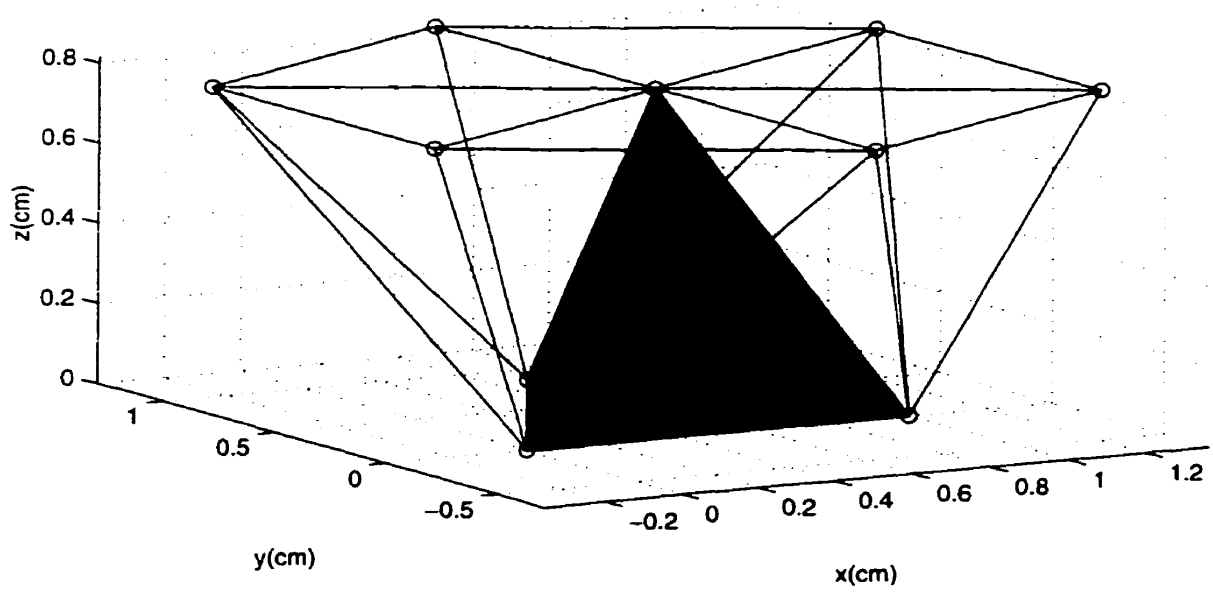

Figure 4.37: The geometry and finite element mesh configuration for the lower half of Benchmark System 5 are illustrated. Ten tetrahedral elements are used to model one-half of the problem domain for three electrostatic systems. Each system consists of a base "bowl" (shown above) joined to a top "cap" (mirror image of the geometry and mesh shown above) across a shared hexagonal plane. Three different systems were defined by fixing the bowl base and cap top at $z = 0$ and $z = 1.6330$ (cm), respectively, and varying the position of the hexagonal plane between them at normalized heights of: (A) 0.25; (B) 0.5; and (C) 0.75. For each of the three electrostatic systems, all exterior, ideal conductor cap facets were set to $1V$ (Dirichlet); the equilateral triangular, ideal conductor base of the bowl was set to $0V$ (Dirichlet); and all remaining exterior bowl facets were left unconstrained (Neumann). The dark tetrahedral region is shaded to aid in visualizing the three-dimensional finite element mesh configuration.

element formulation with the geometric discretizations held fixed.

Figure 4.38 shows the variation of the functional value with the position of the interior vertex along the vertical line segment joining the centers of the triangular top and base of the three systems described above. In each case, the functional gradients with respect to element vertex positions correctly identified the optimal height for the interior vertex, to yield the smallest possible functional value. In particular, the optimal height of the interior vertex which yielded the smallest possible functional value, for each of the three cases examined, was the same as that which yielded the smallest functional gradients along the permissible direction of optimization described above, with an error tolerance of $\pm 8.1650 \times 10^{-6}$ (m). Furthermore, the x- and y-components of the functional gradients were confirmed to evaluate numerically to zero for all three benchmark evaluations, as expected from the symmetry inherent in the xy-plane of these test problems. Finally, it may be noted that the error tolerance stated above is, simply, one-half of the interval used to define successive vertex positions for computing the range of functional values used to confirm the results obtained by evaluating the finite element optimization equations directly.

4.2.2 Benchmark Adaption Studies

The numerical validation of the three-dimensional finite element optimization equations presented in section 4.2.1 has shown that the functional gradients with respect to element vertex positions can correctly identify the optimal positions of the free element vertices in a finite element discretization to produce the most accurate approximate solution for a given number of DOF. The objective of this section is to investigate the potential benefits and related costs of using a new refinement criterion for practical electromagnetic AFEA based on the three-dimensional finite element optimization equations. Hence, the effectiveness of an h-adaption model, when guided by the new optimal discretization-based refinement criterion, in resolving a Laplace benchmark system is investigated.

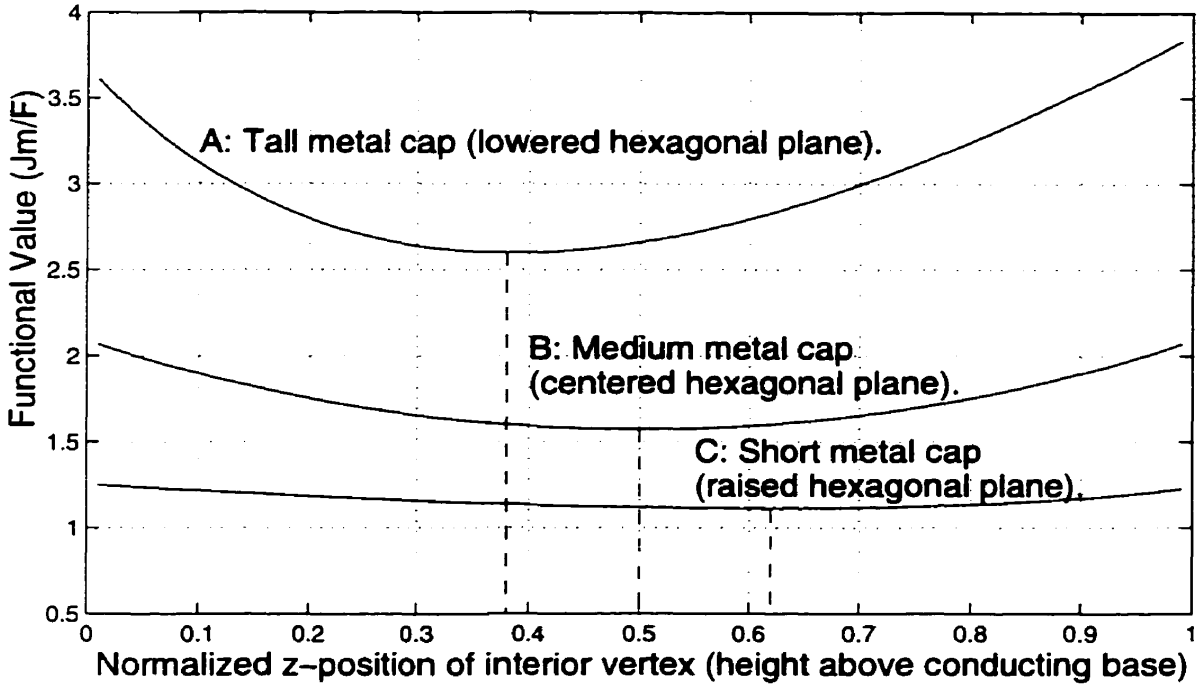

Figure 4.38: The variation in functional value with vertical position of the interior vertex is illustrated for the three electrostatic evaluations based on Benchmark System 5. Each of the three plots is based on 1,000 functional values computed by fixing the interior vertex at 1,000 regularly spaced positions along the vertical line segment joining the centers of the triangular top and base of the systems. Note: the functional value is scaled by ε_o.

By computing the gradients of the functional with respect to element vertex positions, it has been demonstrated for one- and two-dimensional systems that it is possible to detect and rank regions of inferior discretization in a finite element mesh. Functional gradient error indicators associated with three-dimensional optimal discretization-based refinement criteria are also defined in terms of derivatives with respect to tetrahedral vertex positions. Furthermore, these derivatives may be computed directly from the finite element optimization equations derived in section 2.4.3. As in the two-dimensional case, once the gradients of the functional with respect to vertex positions have been computed, they may be used in various ways as error indicators. One simple approach is to assess a weighted sum of vertex-based functional gradients for each element, then use these values to rank the elements for refinement. In this section, this method is investigated to illustrate one possible way to exploit the new three-dimensional optimal discretization-based refinement criteria proposed for scalar adaptive finite element solvers.

The proposed three-dimensional optimal discretization-based refinement criterion was evaluated using a second electrostatic problem (Benchmark System 6), which is described by Figure 4.39. One-eighth of an air-filled, concentric, cuboidal capacitor is shown– the 3-D analog to the standard 2-D "L"problem. The conductor boundary conditions are $1V$ on the smaller, inner, ideal conductor cube and $0V$ on the outer, ideal conductor cube. The symmetry planes defined by $x = 0$, $y = 0$, and $z = 0$ were left unconstrained (Neumann) between the two ideal conductors. The objective for this benchmark system is to compute the functional value corresponding to the electrostatic potential energy stored in the air region between the two ideal conductors. The primary feature of this system is the rapid field solution variation close to the sharp reentrant edges and corners at the intersections of the boundaries of the inner conductor. This feature is common to many practical devices that contain sharp material edges and corners, and has been shown to significantly reduce the convergence rate of the finite element method [76, 165].

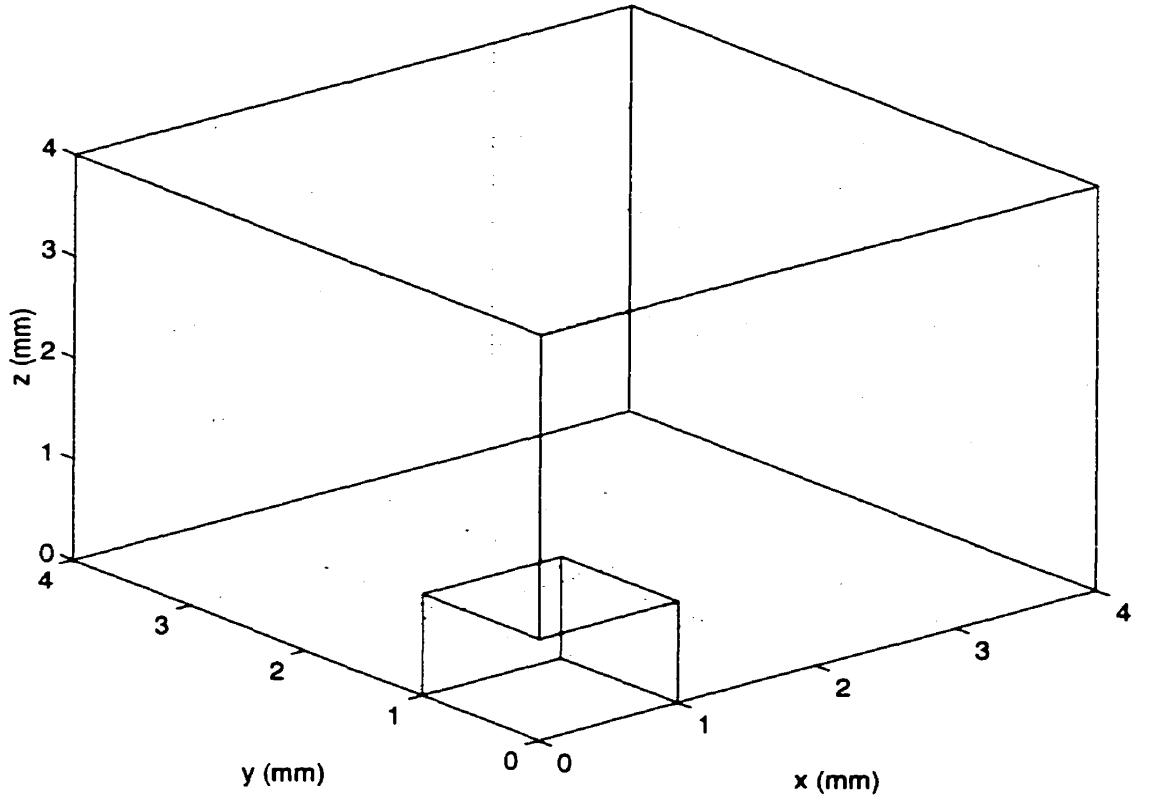

Figure 4.39: The geometry used for the three-dimensional electrostatic potential analysis of Benchmark System 6 is illustrated. The figure depicts one-eighth of an air-filled, concentric, cuboidal capacitor. The conductor boundary conditions are $1V$ (Dirichlet) on the smaller, inner, ideal conductor cube and $0V$ (Dirichlet) on the outer, ideal conductor cube. The symmetry planes defined by $x = 0$, $y = 0$, and $z = 0$ were left unconstrained (Neumann) between the two ideal conductors.

The convergence of the percent error in functional value for an h-adaption strategy applied to Benchmark System 6 is illustrated in Figure 4.40 for first-order elements. The initial mesh used for the h-adaption studies was comprised of 144 tetrahedra. At each subsequent adaptive iteration, the optimal discretization-based refinement criterion described above was used to rank the elements, and the elements with the highest rankings were chosen for refinement. Moreover, a 100 percent increment in the number of DOF per adaptive step was used to update the discretizations. In addition, the h-refinements were achieved using the tetrahedral mesh refinement algorithms described in [166]. The uniform h-refinement baseline functional convergence result is also included in Figure 4.40 for comparison. It may be noted that the h-adaption strategy guided by the optimal discretization-based refinement criterion produced discretizations with functional accuracy levels superior to those of the uniform discretizations for corresponding computational costs. For example, for a level of solution accuracy close to one percent, more than a ten-fold savings in computational cost is achieved by the h-adaption based on the new three-dimensional refinement criterion relative to the uniform h-refinement scheme. Therefore, it may be concluded that the new optimal discretization-based refinement criterion is effective for evolving efficient distributions of DOF by h-adaption over the problem domain for electrostatic systems with regions of rapid field solution variation. Finally, an example h-adapted mesh is represented in Figure 4.41, in terms of the distribution of tetrahedra vertices, to illustrate the sharp focus of DOF produced by the new refinement criterion near the reentrant edges and corners of the inner conducting cube.

4.2.3 Discussion

The results of the preceding section illustrate the usefulness of employing the three-dimensional finite element optimization equations of section 2.4.3 to develop effective and reliable feedback refinement criteria for efficiently guiding adaptive systems towards accurate solutions. Furthermore, it is worth noting that the new three-

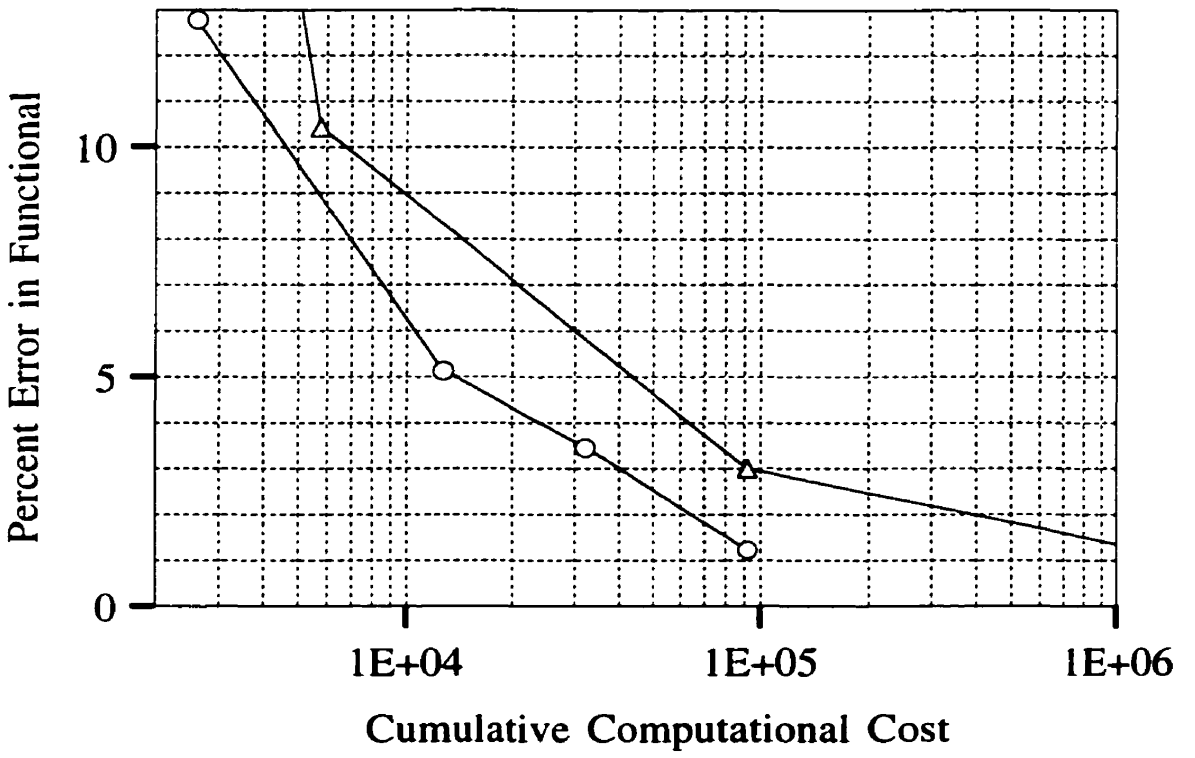

Figure 4.40: The convergence of percent error in functional value with discretization level for first-order h-adaption studies for Benchmark System 6 are illustrated. The triangle knot results correspond to percent error in functional values computed from solutions based on first-order discretizations evolved using uniform h-refinements. The circle knot results correspond to percent error in functional values computed from solutions based on first-order h-adaption discretizations evolved using the new optimal discretization-based refinement criterion. Note: the cumulative computational cost of adaption was calculated based on using a preconditioned conjugate gradient algorithm to solve the finite element matrix equations.

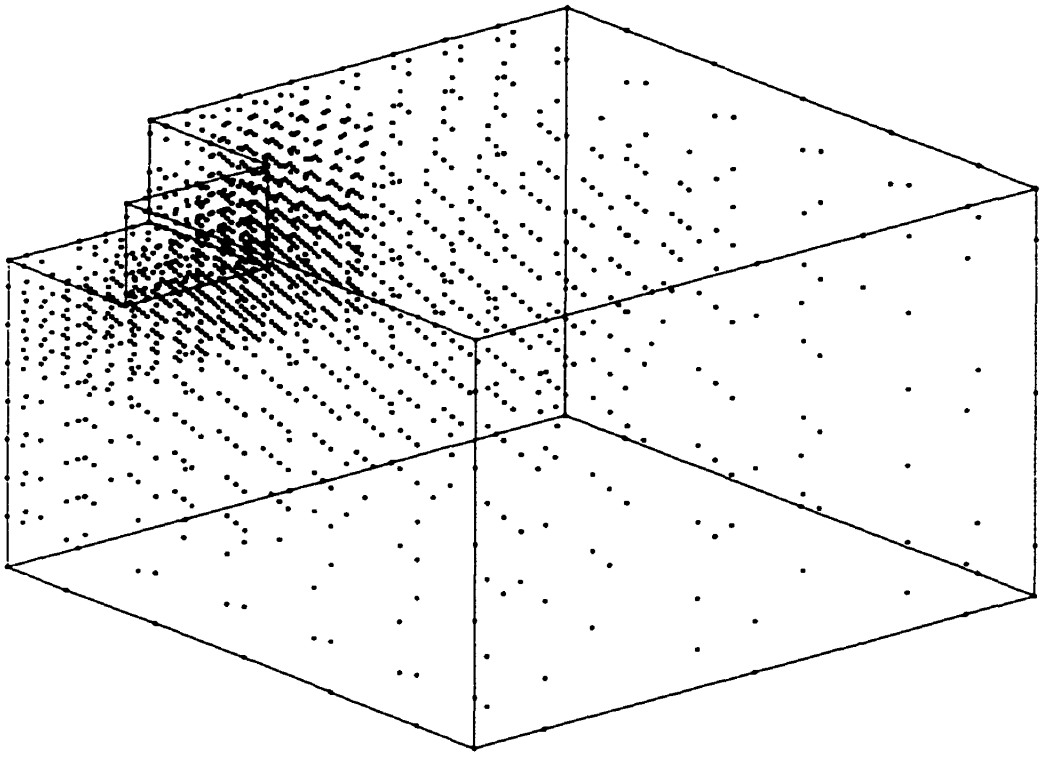

Figure 4.41: An example refinement achieved using the new h-adaption is illustrated, in terms of the distribution of tetrahedra vertices, for Benchmark System 6. The first-order discretization represented above was evolved using the new optimal discretization-based refinement criterion. The initial mesh used for the h-adaption was comprised of 144 elements.

dimensional optimal discretization-based refinement criterion is inexpensive to compute, since it is closely related to the underlying variational principle used to determine the finite element solution. In fact, the only extra terms that are required have been given in Tables 2.3–2.8 of section 2.4.3. Moreover, the entries of the matrices in Eqs. (2.142), (2.143) and (2.144) that are required for the new refinement criterion, are very similar to those of the matrices in Eq. (2.121), the matrix equation that must be solved for the finite element problem. In addition, careful examination of Eqs. (2.122), (2.135), (2.136) and (2.139) reveals that, in effect, the new refinement criterion can be computed extremely efficiently since it involves exactly the same mathematical operations required to determine the entries of standard finite element matrices, modified only by the addition of or multiplication by the extra terms described above.

In summary, the three-dimensional finite element optimization equations were validated by tests based on a simple three-dimensional electrostatic system.[2] Furthermore, the h-adaption performance results for the benchmark system that was investigated, show that the new optimal discretization-based refinement criterion can be successfully used in three-dimensional adaptive finite element solvers to effectively and economically distribute DOF over the problem domain.

[2]It may be noted that the three-dimensional finite element optimization equations for Helmholtz systems are validated equally by the results reported for the electrostatic system. This follows from the fact that the wave and source terms in the three-dimensional optimization equations involve only the same derivatives of the simplex volume with respect to the x-, y- and z-coordinates of the element vertices which appear in the Laplacian component of the equations (see Eqs. (2.131) and (2.132), for example).

Chapter 5

Second-Order Functional Derivatives in Optimal Discretization Based AFEA for Electromagnetics

As noted previously, the study of error estimation for finite element adaption in electromagnetics has been the focus of a great amount of work over the past ten years, and now represents a well-established research area [57, 84]. Today, a variety of error indicators are used, and many of the most effective ones are based on local derivatives of the approximated fields [56, 167]. Common examples include field discontinuity, PDE residual and local energy error indicators, as well as the functional gradient measures introduced in this work. As with all local error estimation methods, derivative-based approaches can yield misleading results when used with insufficient or unbalanced discretizations [144, 159]. It is not uncommon for evolving, unconverged finite element models to give rise to locally smooth regions of high relative error, which yield well-behaved first-order derivatives. The difficulty with error estimation is that well-behaved first-order derivatives are primarily correlated with indicators of stability and low error. The purpose of this chapter is to introduce and investigate the use of second-order functional derivative indicators, which are largely unaffected by such problematic error distributions. Hence, the potential advantages and related costs of using second-order functional mesh discretization derivatives for error estimation in AFEA for electromagnetics are considered. In particular, second-order functional derivative-based refinement criteria for two-dimensional AFEA are proposed to identify and stabilize erroneous first-order error distributions that arise in insufficient or unbalanced discretization regions. Finally, effective combined first- and second-order derivative estimators are introduced and evaluated in practical two-dimensional applications.

5.1 Two-Dimensional Second-Order Functional Derivatives

In previous chapters, functional gradient error indicators associated with optimal discretization based refinement criteria, have been employed successfully in AFEMs for electromagnetics. Despite their demonstrated effectiveness, these first-order functional derivative based indicators are not immune to the problems associated with guiding adaptive methods reliably and efficiently when used with insufficient or unbalanced discretizations. Under such conditions, ineffective discretizations may evolve during the course of the adaption. Consequently, poor adaption performance results may be observed over part, or throughout the entire adaptive process, if problematic error distributions due to unstable first-order functional derivative error indicators are not detected and corrected.

The hypothesis tested in this chapter is that second-order functional derivatives can be used to analyze the stability and estimate the reliability of first-order derivative-based local error assessments. More specifically, it is proposed that locally smooth regions of high relative error in finite element models are usually unstable, and therefore, easy to detect with second-order derivative tests. Electromagnetic systems that possess translational or rotational symmetries may be analyzed using two-dimensional finite element formulations, and second-order functional derivative based error indicators are defined in terms of derivatives with respect to element vertex positions for such two-dimensional systems in this section. For example, in Cartesian problems where the field solution variation is independent of the coordinate variable z, i.e., $u = u(x, y)$, the second-order functional derivatives may be computed directly from the finite element optimization equations derived in section 2.4.2. Consider a scalar triangular element with vertex positions (x_l, y_l), $l = 1, 2, 3$. For Helmholtz systems the x- and y-components, of the second-order functional derivatives may be readily determined from the matrix forms:

$$\frac{1}{2}\mathbf{u}^T\mathbf{P}\mathbf{u}, \tag{5.1}$$

and

$$\frac{1}{2}\mathbf{u}^T\mathbf{Q}\mathbf{u}, \tag{5.2}$$

respectively, evaluated over the elements that share the vertex in question. Here, $\mathbf{u}$ is the field solution vector. The square matrices $\mathbf{P}$ and $\mathbf{Q}$ contain the x and y second-order derivative information, respectively, that corresponds to the Laplacian part of the functional for vertex $l(l = 1, 2, 3)$ of the triangular element. The entries of the matrices $\mathbf{P}$ and $\mathbf{Q}$ are defined by:

$$\begin{aligned} P_{ij} &= \frac{1}{4A^2}\sum_{m=1}^{3}\sum_{n=1}^{3}\left[c_l\frac{\partial(c_m c_n)}{\partial x_l} - b_l\frac{\partial(b_m b_n)}{\partial y_l} + 2A\,\frac{\partial^2(c_m c_n)}{\partial x_l^2}\right] I_{ijmn} \\ &\quad - \frac{1}{A}(b_l + c_l)S_{ij}, \end{aligned} \tag{5.3}$$

and

$$\begin{aligned} Q_{ij} &= \frac{1}{4A^2}\sum_{m=1}^{3}\sum_{n=1}^{3}\left[b_l\frac{\partial(b_m b_n)}{\partial y_l} - c_l\frac{\partial(c_m c_n)}{\partial x_l} + 2A\,\frac{\partial^2(b_m b_n)}{\partial y_l^2}\right] I_{ijmn} \\ &\quad - \frac{1}{A}(b_l + c_l)T_{ij}, \end{aligned} \tag{5.4}$$

where A is the element area: and b_i and c_i are geometric parameters related to an element's vertex positions, previously defined in section 2.4.2. I_{ijmn} is the elemental integral (in homogeneous coordinates) of the product of the derivatives of the ith and jth basis functions, with respect to the mth and nth simplex coordinates, also previously defined in section 2.4.2. It should be noted that the "mixed" second-order functional derivative terms with respect to both the x and y element vertex positions are incorporated into the definitions of matrices $\mathbf{P}$ and $\mathbf{Q}$ in (5.3) and (5.4) above. Furthermore, S_{ij} and T_{ij} are the ij-entries of the first-order functional derivative matrices, with respect to element vertex positions, as defined in Eq. (2.106) in section 2.4.2. It may also be noted that the second-order partial derivatives of $(b_m b_n)$ and $(c_m c_n)$ with respect to the element vertex positions, which appear in (5.3) and (5.4) may be readily determined from Eq. (2.82), Table 2.1 and Table 2.2 of section 2.4.2, and evaluate to simple numerical constants (1, -1 and 0).

It has been shown in Chapter 4 that first-order functional derivative quantities are efficient to compute because they are closely related to the variational principle used to determine the solution to the finite element problem. Similarly, the new second-order quantities are inexpensive to compute since the only extra terms required are numerical constants which can be tabulated once and for all. As in the first-derivative case, the second-order functional derivative formulas derived above are valid for any choice of legitimate finite element basis functions. Furthermore, the functional derivatives may be computed for uniform- or mixed-order meshes as may be required by specific refinement models such as *h*-, *p*-, or *hp*-adaptive methods. Although the above formulation has been derived for scalar Helmholtz systems, it is interesting to note that the second-order derivatives of the wave and source terms of the functional, with respect to the vertex positions, are zero. This suggests that two-dimensional Laplace systems may benefit most from error estimation based on using both first- and second-order functional derivatives.

5.2 Numerical Evaluation of Second-Order Functional Derivative Indicators

Two benchmark systems are examined in this section to illustrate the error estimation pitfalls that can occur with insufficient or unbalanced discretizations, and the potential value of using second-order derivative methods to avoid them. Specifically, a two-dimensional Laplace system and a two-dimensional Helmholtz system are examined in order to investigate the practical significance of the new approach.

5.2.1 Benchmark System 3(a)

The two-dimensional Laplace benchmark system examined in this section, and the initial mesh used for the *h*-adaption studies were defined by Figure 4.2 in section 4.1.1.1. It is one-quarter of a square coaxial line in cross-section – the standard "L" problem previously considered in section 4.1. Performance results for second-order *h*-adaption studies on functional convergence are presented in Figure 5.1. The uniform

h-refinement baseline (A) is included for comparison with h-refinement based on a first-order derivative error estimator (B) and a combined first- and second-order error estimator (C). A 50 percent increment in the number of DOF per adaptive step was used to update the discretizations for these studies, excluding the uniform refinement procedure. For the specific type of error estimator examined here (Type-A), and for the given amount of DOF update used per adaptive step, these results demonstrate a marginal improvement in performance for functional accuracy levels between 1 and 0.1 percent when the combined error estimator is used (C) versus the first-derivative estimator (B), and a more significant improvement for functional accuracy levels beyond 0.1 percent.

The performance results for second-order h-adaption studies based on a second type of error estimator (Type-B) are presented in Figure 5.2. In this case, a 20 percent increment in the number of DOF per adaptive step was used. These results clearly demonstrate the practical value of the new approach and support the hypothesis that second-order functional derivatives can be used to analyze the stability and estimate the reliability of first-order derivative based local error assessments: curve (A) shows the uniform h-refinement baseline for comparison; curves (B) and (C) show the relative h-adaption performance for the first-order and the combined first- and second-order based error estimation methods, respectively. In addition, two example h-refined meshes corresponding to curve (B) and curve (C) are presented in Figure 5.3 and Figure 5.4, respectively, to further illustrate the potential benefits of using the combined-derivative approach.

5.2.2 Benchmark System 4

The two-dimensional Helmholtz benchmark system examined in this section, and the initial mesh used for the p-adaption studies were defined by Figure 4.27 in section 4.1.2.3. It is the octagonal microstrip patch of size d (34mm), where $\lambda = 0.616d$ (λ is the wavelength in the dielectric substrate below the patch), previously considered

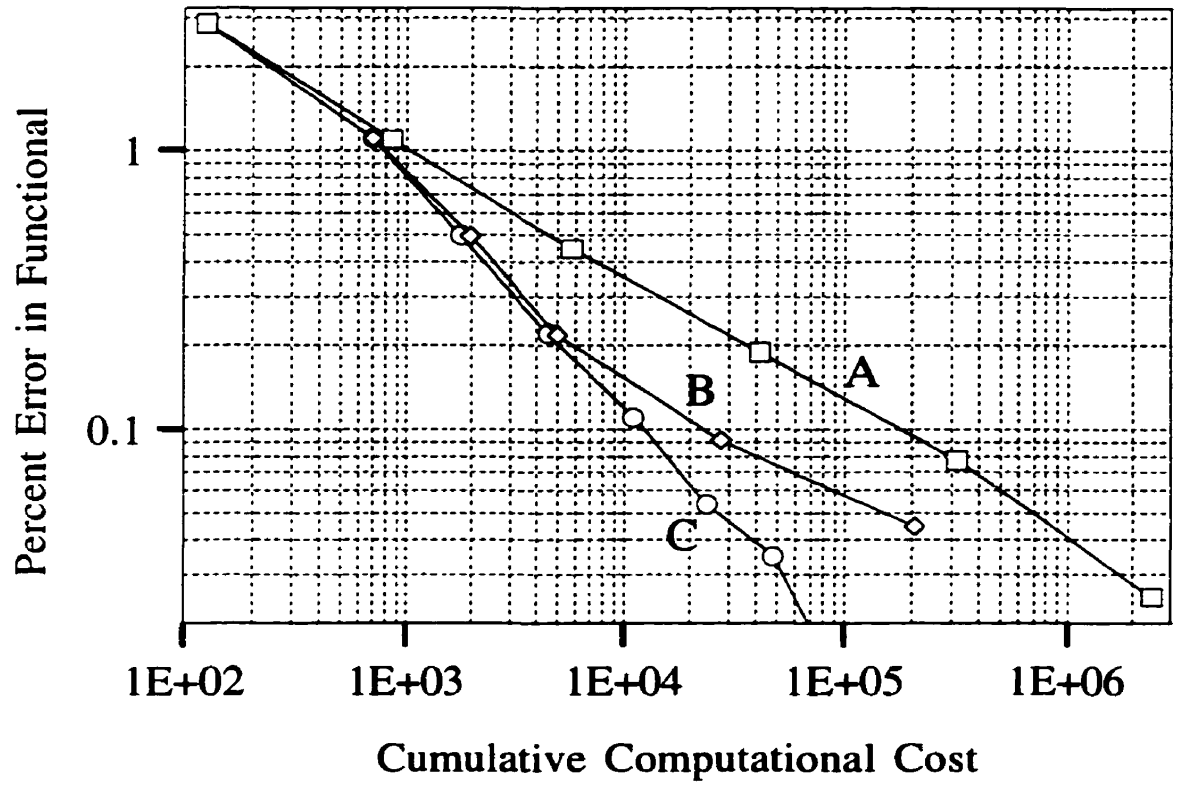

Figure 5.1: The convergence of percent error in functional value with discretization level for second-order h-adaption studies with 50 percent DOF updates for Benchmark System 3(a) is illustrated. The curve (A) results correspond to percent error in functional values computed from solutions based on second-order uniform discretizations. The curve (B) results correspond to percent error in functional values computed from solutions based on second-order h-adaption discretizations evolved using a first-order derivative error estimator (Type-A). The curve (C) results correspond to percent error in functional values computed from solutions based on second-order h-adaption discretizations evolved using a combined first- and second-order error estimator (Type-A). Note: The cumulative computational cost of adaption was calculated based on using a preconditioned conjugate gradient algorithm to solve the finite element matrix equations.

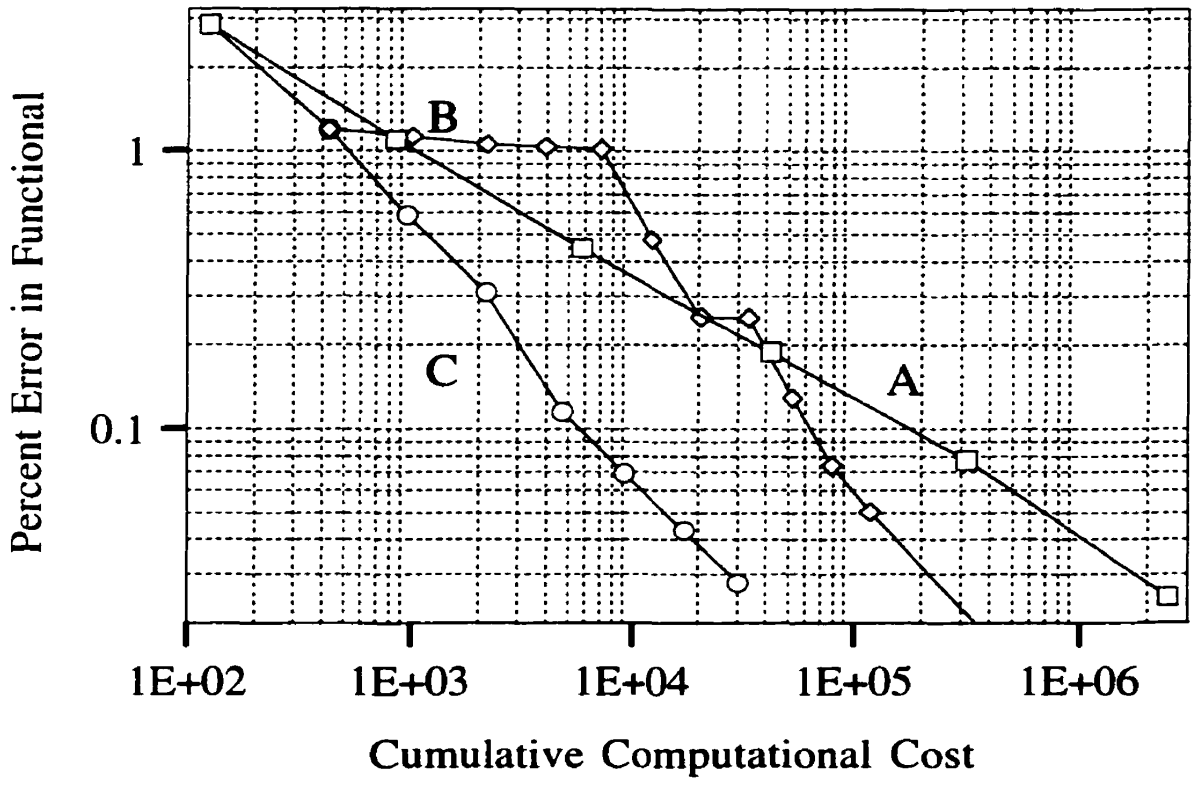

Figure 5.2: The convergence of percent error in functional value with discretization level for second-order h-adaption studies with 20 percent DOF updates for Benchmark System 3(a) is illustrated. The curve (A) results correspond to percent error in functional values computed from solutions based on second-order uniform discretizations. The curve (B) results correspond to percent error in functional values computed from solutions based on second-order h-adaption discretizations evolved using a first-order derivative error estimator (Type-B). The curve (C) results correspond to percent error in functional values computed from solutions based on second-order h-adaption discretizations evolved using a combined first- and second-order error estimator (Type-B). Note: The cumulative computational cost of adaption was calculated based on using a preconditioned conjugate gradient algorithm to solve the finite element matrix equations.

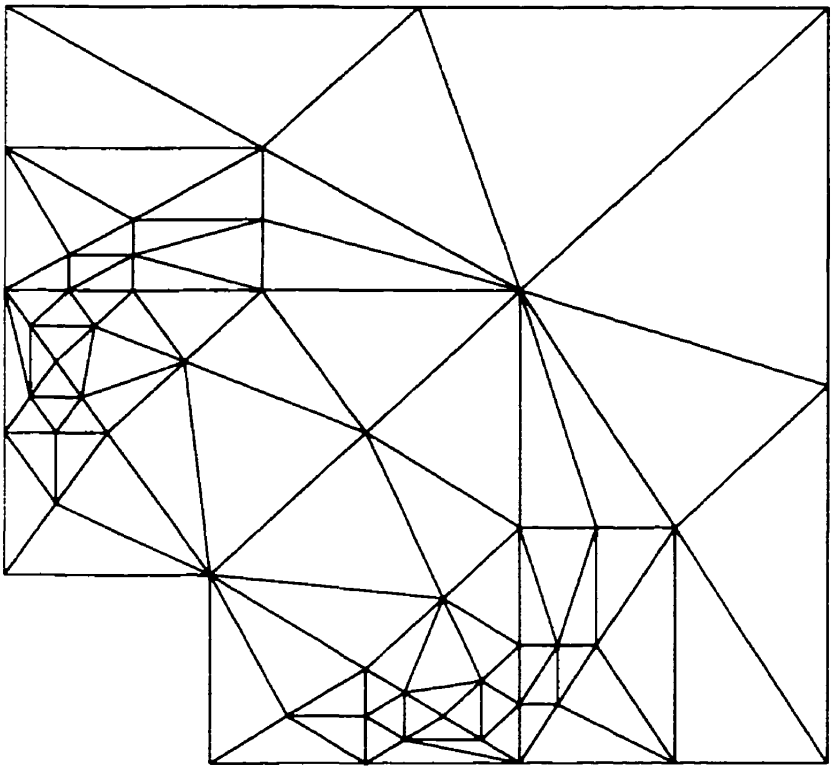

Figure 5.3: An example of an ineffective h-refinement discretization due to unstable first-order derivative-based error estimation for Benchmark System 3(a) is illustrated. The mesh shown above corresponds to the adaption performance results represented by curve (B) of Figure 5.2. Note: the discretization is comprised of 84 second-order elements.

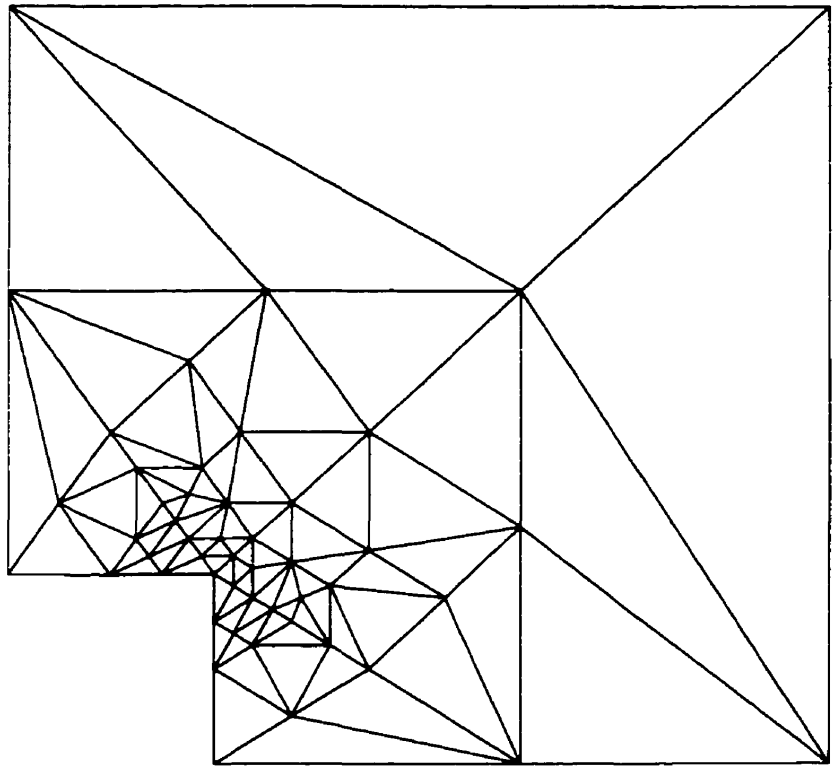

Figure 5.4: An example of an effective h-refinement discretization due to combined first- and second-order derivative-based error estimation for Benchmark System 3(a) is illustrated. The mesh shown above corresponds to the adaption performance results represented by curve (C) of Figure 5.2. Note: the discretization is comprised of 84 second-order elements.

in section 4.1. Performance results for p-adaption studies on phase angle convergence are reported in Table 5.1. The uniform p-refinement baseline result is presented for comparison. The p-discretizations ranged from orders 1 through 10, and a 20 percent increment in the number of DOF per adaptive step was used to improve the discretizations for the methods considered, excluding the uniform refinement procedure. For the type of error estimator investigated (Type-B), an average savings of approximately 20 percent in the number of DOF required to achieve phase error levels between 5.0 and 0.5 degrees was observed for the combined-derivative approach, relative to the first-order derivative method.

Table 5.1: Discretization level versus phase error in degrees for Benchmark System 4.

Method / #DOF	5.0°	2.5°	1.25°	1.0°	0.75°	0.5°
Uniform	360	385	440	490	530	580
First-order	320	390	450	490	540	600
Combined	265	322	400	420	435	450

This data corresponds to the p-adaption results for the 2-D mesh described in Fig.4.27. Uniform indicates uniform p-adaption. First-order indicates first-order functional derivative based error indicators were used to guide the p-adaption. Combined indicates both first- and second-order functional derivative based error indicators were used.

5.3 Discussion

New error estimators, based on combined first- and second-order functional derivatives for scalar 2-D Poisson and Helmholtz FEA, have been introduced and evaluated for adaption. The performance results for the benchmark systems investigated demonstrate that second-order derivative indicators can identify and stabilize erroneous first-order error distributions, and that combined derivative error estimation methods can be successfully used in adaptive finite element solvers to more reliably and economically distribute DOF over a problem domain.

Chapter 6

Conclusions

The objective of this work has been to develop effective refinement criteria based on optimal solution properties for efficiently and reliably guiding electromagnetic adaptive finite element solvers towards accurate solutions. To achieve this goal, a new theoretical formulation for optimal finite element solutions to partial differential equations of macroscopic electromagnetics has been derived. The theory was validated with a set of comprehensive numerical benchmark evaluations, and the increased solution accuracy furnished by the formulation was judged to be quite valuable. The optimal characteristics of approximate finite element solutions, as predicted by the theory, and observed numerically, were employed to develop new optimal discretization-based feedback refinement criteria for use with advanced strategy adaption models in finite-element-based electromagnetics. Specifically, variational aspects of optimal discretizations for Helmholtz systems, that are closely related to the underlying stationarity principle used in computing finite element solutions to continuum problems, were essential to the development of the new refinement criteria. In comparison with the state-of-the-art refinement criteria that were evaluated, performance results from benchmark adaption studies show that the new refinement criteria are effective and economical for efficiently and reliably guiding practical *h*-, *p*- and *hp*-adaption models towards accurate solutions. Ultimately, the proposed refinement criteria represent a vital solution to the practical engineering problem of effectively discretizing a system with adaptive methods for efficiently computing sufficiently accurate fields in finite-element-based electromagnetic analysis and design.

The original contributions of this work are summarized in the next section, followed by suggestions for possible future work.

6.1 Original Contributions

The theory developed in this work on optimal discretization-based refinement criteria is an important contribution to the study and development of feedback control systems for AFEA. Specifically, this work clearly demonstrated the value of employing optimality properties of finite element discretizations to develop effective practical feedback refinement criteria for guiding adaptive systems efficiently and reliably towards accurate solutions. The new practical refinement criteria presented in this work are quite valuable for both their generality and reliability. Both of these assets are directly linked to the fundamental and theoretically justified principle used to derive them. Furthermore, this underlying principle embodies a stationarity property, which is entirely dependent on the optimality of a finite element discretization; therefore, the refinement criteria computed from this principle possess the desirable benefit of intrinsically guiding an adaptive processes towards optimal finite element solutions. Hence, these new criteria represent an important milestone in developing efficient practical adaptive methods for evolving sufficiently accurate solutions in a cost-effective manner.

This work also represents a valuable contribution to the research and development of adaptive finite element analysis theory and practice for the following reason. The inception of the theoretical and numerical study of optimality in electromagnetic AFEA by this work is of principal importance to the research area. Specifically, this research established a set of primary adaption benchmarks for the fundamental electromagnetic singularity models, and illustrated their usefulness in the analysis and design of optimal adaption strategies. This is of particular importance, since one of the most challenging problems of AFEA in electromagnetics over the past decade has been the accurate and efficient resolution of the singularities associated with sharp material edges and corners. The ability to compute a series of optimal singularity benchmarks permitted the primary adaption procedures and control schemes to be

evaluated and compared, for the first time, on both a relative and an absolute performance scale for some of the most demanding electromagnetic adaption scenarios. This represents a significant advancement over the heuristic assessment approaches that had formerly been relied upon. In fact, prior to this work, it has been recognized that an important reason for the slow development in this research area was the lack of objective standards for judging emerging AFEA methods. Hence, one of the key obstacles that had previously hindered progress in realizing practical advanced-strategy AFEA has now been overcome.

Also in this work, many of the theoretical and computational difficulties inherent to the currently available characterizations of optimal finite element discretizations were explained and illustrated with numerical results. In particular, the validity of commonly used finite element optimality criteria have been evaluated with optimal discretization benchmark results computed for the fundamental electromagnetic singularity models. In addition, the implications of using optimality criteria that rely on the accuracy of superconvergent derivatives of finite element approximate solutions, have been elucidated. In recent years, the development and application of superconvergence concepts for AFEA error estimation and control has attracted a good deal of interest from the research community. The implications of the findings presented in this work are especially significant for finite element adaption, since many feedback control systems used in AFEA are currently based on refinement criteria derived from superconvergence theory [152, 153]. Moreover, it should be noted that some of the most convincing experimental evidence supporting the conclusions presented in this work were based on error data computed from optimal finite element discretizations. This is particularly important, since the specific optimal discretizations that were examined possessed the key interpolatory property fundamental to superconvergence theory. Thus, the results computed under these conditions could not be refuted. Furthermore, this key property is not, in general, evident in finite element approximations, and can only be achieved asymptotically with increasing

numbers of degrees of freedom for non-optimized discretizations. Therefore, previous studies published on typical, or arbitrary, test systems had failed to provide the rigorous experimental evidence required to examine the fundamental claims of superconvergence theory. The use of optimally discretized systems in this work was a critical element in obtaining the necessary evidence. Furthermore, the implications for other optimality criteria that were not explicitly investigated, were explained by showing the connections amongst the different techniques reported in the literature for characterizing optimal finite element discretizations. In essence, the defining characteristics of the fundamental techniques examined were used to gauge the relative merits and disadvantages of the theoretical concepts and practical techniques related to the development of finite element optimality criteria, and to clarify their usefulness for practical adaptive finite element analysis. Based on the conclusions reported in this work, it was apparent that criteria appropriate for characterizing optimal finite element discretizations over a sufficiently wide range of problem applications were needed. Moreover, it was also manifest that such optimality criteria should not be developed heuristically, but rather, should be based on well-founded and theoretically justified approaches.

Finally, new error indicators, based on combined first- and second-order functional derivatives for scalar two-dimensional Poisson and Helmholtz FEA, have been introduced and evaluated for adaption. Second-order derivative indicators were shown to be important because they can identify and stabilize erroneous first-order error distributions due to unbalanced or insufficient discretizations, and combined derivative error estimation methods can be successfully used in adaptive finite element solvers to more reliably and economically distribute DOF over a problem domain.

6.2 Future Work

Three interesting research directions for future work which may have significant implications for AFEMs are discussed in this section. First, the development of

algorithms suitable for implementing the new refinement criteria in parallel processing architectures are recommended in order to investigate the potential benefits and related costs for parallel adaptive finite-element-based electromagnetic analysis and design. Second, the development of analogous theoretical formulations for the numerical study of optimal vector finite element solutions are recommended to further explore the performance of the new optimal discretization-based refinement criteria approach. Finally, research towards the development of convergence criteria for adaptive finite element methods based on functional derivative concepts is recommended. This third line of investigation is, perhaps, the most ambitious and will probably require substantial effort; however, the potential benefits of an effective, efficient and reliable method for assessing the accuracy of finite-element-based field solutions are very valuable for AFEMs.

References

[1] Park Benjamin. *A History of Electricity.* Arno Press, New York, 1975. Reprint of the 1898 edition published by Wiley, New York.

[2] Bertrand Russell. *A History of Western Philosophy: And its connection with political and social circumstances from the earliest times to the present day.* Simon and Schuster, New York, 1945.

[3] Sir Edmund Whittaker. *A History of the Theories of Aether and Electricity,* volume 1: The Classical Theories. Thomas Nelson and Sons Ltd, London, 1951. First published 1910.

[4] Robert S. Elliot. *Electromagnetics: History, Theory, and Applications.* IEEE Press, Piscataway, NJ, 1993.

[5] Benjamin Franklin. *Benjamin Franklin's Experiments: A New Edition of Franklin's Experiments and Observations on Electricity.* Harvard University Press, Cambridge, Mass., 1941. Edited, with a critical and historical introduction by I. B. Cohen.

[6] James Clerk Maxwell. *A Treatise on Electricity and Magnetism,* volume 1 and 2. Dover Publications, New York, third edition, 1954. Unaltered republication of the third edition, 1891.

[7] Daniel M. Siegel. *Innovation in Maxwell's Electromagnetic Theory: Molecular Vortices, Displacement Current, and Light.* Cambridge University Press, New York, 1991.

[8] Thomas S. Kuhn. *The Structure of Scientific Revolutions.* The University of Chicago Press, Chicago, second, enlarged edition, 1970.

[9] Kenneth S. Krane. *Modern Physics.* John Wiley and Sons, Inc., New York, 1983.

[10] R. Plonsey and R. Collin. *Principles and Applications of Electromagnetic Fields.* McGraw-Hill Book Company, New York, 1961.

[11] Lian Chi Shen and Jin Au Kong. *Applied Electromagnetism.* PWS Publishers, Boston, MA, second edition, 1987.

[12] Simon Ramo, John. R. Whinnery, and Theodore Van Duzer. *Fields and Waves in Communication Electronics.* John Wiley and Sons, Inc., New York, third edition, 1993.

[13] O. P. Gandhi, editor. *Biological Effects and Medical Applications of Electromagnetic Energy.* Prentice-Hall, Englewood Cliffs, NJ, 1990.

[14] R. Reitz and F. J. Milford. *Foundations of Electromagnetic Theory.* Addison-Wesley, Reading, MA, 1960.

[15] David K. Cheng. *Field and Wave Electromagnetics.* Addison-Wesley Publishing Company, Reading, MA, 1983.

[16] Carl T. A. Johnk. *Engineering Electromagnetic Fields and Waves.* John Wiley and Sons, New York, second edition, 1988.

[17] Herman A. Haus and James R. Melcher. *Electromagnetic Fields and Energy.* Prentice-Hall, Englewood Cliffs, NJ, 1988.

[18] J. Van Bladel. *Electromagnetic Fields.* McGraw-Hill Book Company, New York, 1964.

[19] P.P. Silvester. Finite element solution of homogeneous waveguide problems. *Alta Frequenza*, 38:313–317, 1969.

[20] P. P. Silvester. High-order polynomial triangular finite elements for potential problems. *International Journal of Engineering Science*, 7:849–861, 1969.

[21] P. P. Silvester. A general high-order finite-element waveguide analysis program. *IEEE Transactions on Microwave Theory and Techniques*, 17:204–210, April 1969.

[22] S. Ahmed and P. Daly. Waveguide solutions by the finite element method. *Radio and Electronic Engineer*, 38:217–223, 1969.

[23] P. P. Silvester and R. L. Ferrari. *Finite Elements for Electrical Engineers.* Cambridge University Press, Cambridge, second edition, 1990.

[24] Nathan Ida and Joao P. A. Bastos. *Electromagnetics and Calculation of Fields.* Springer-Verlag, New York, 1992.

[25] Jianming Jin. *The Finite Element Method in Electromagnetics.* John Wiley and Sons, Inc., New York, 1993.

[26] M. Calamia, G. Pelosi, and P. P. Silvester, editors. *Second International Workshop on Finite Element Methods for Electromagnetic Wave Problems: Siena, Italy, May 1994*. James and James, London, UK, 1994.

[27] J. P. Webb. Application of the finite-element method to electromagnetic and electrical topics. *Reports on Progress in Physics*, 58:1673–1712, December 1995.

[28] R. F. Harrington. *Field Computation by Moment Methods*. The Macmillan Company, New York, 1968.

[29] R. Mittra, editor. *Computer Techniques for Electromagnetics*. Pergamon Press, New York, 1973.

[30] R. Sorrentino, editor. *Numerical Methods for Passive Microwave and Millimeter Wave Structures*. IEEE Press, Piscataway, NJ, 1989.

[31] Christan Hafner. *The Generalized Multipole Technique for Computational Electromagnetics*. Artech House, Norwood, MA, 1990.

[32] Matthew N. O. Sadiku. *Numerical Techniques in Electromagnetics*. CRC Press, Boca Raton, 1992.

[33] Richard C. Booton. *Computational Methods for Electromagnetics and Microwaves*. John Wiley and Sons, Inc., New York, 1992.

[34] E. K. Miller, L. Medgyesi-Mitschang, and E. H. Newman, editors. *Computational Electromagnetics*. IEEE Press, Piscataway, NJ, 1992.

[35] K. S. Kung and R. J. Leubbers. *The Finite-Difference Time Domain Method for Electromagnetics*. CRC Press, Boca Raton, 1993.

[36] P. M. Morse and H. Feshbach. *Methods of Theoretical Physics*. McGraw-Hill Book Company, New York, 1953.

[37] R. Courant and D. Hilbert. *Methods of Mathematical Physics*, volume II: Partial Differential Equations. Interscience, New York, 1962.

[38] S. G. Mikhlin. *Variational Methods in Mathematical Physics*. Pergamon Press, New York, 1964.

[39] K. F. Riley. *Mathematical Methods for the Physical Sciences*. Cambridge University Press, Cambridge, 1974.

[40] J. T. Oden. *Applied Functional Analysis: A First Course for Students of Mechanics and Engineering Science.* Prentice-Hall. Englewood Cliffs. New Jersey. 1979.

[41] J. N. Reddy. *Applied Functional Analysis and Variational Methods in Engineering.* McGraw-Hill. New York. 1986.

[42] C. Johnson. *Numerical solution of partial differential equations by the finite element method.* Cambridge University Press. Cambridge. U.K.. 1987.

[43] P. G. Ciarlet. *The Finite Element Method for Elliptic Problems.* North-Holland Publishing Company. New York. 1978.

[44] G. Strang an G. J. Fix. *An Analysis of the Finite Element Method.* Prentice-Hall. Englewood Cliffs. NJ. 1973.

[45] A. K. Aziz. editor. *The Mathematical Foundations of the Finite Element Method with Applications to Partial Differential Equations.* Academic Press. New York. 1972.

[46] S. C. Brenner and L. Ridgway Scott. *The Mathematical Theory of Finite Element Methods.* Springer-Verlag, New York, 1994.

[47] C. Patterson. Sufficient conditions for convergence in the finite element method for any solution of finite energy. In J. R. Whiteman. editor. *The Mathematics of Finite Elements and Applications: Proceedings of the Brunel University Conference of the Institute of Mathematics and its Applications held in 1972.* pages 213–224. New York. 1973. Academic Press.

[48] D. A. Lowther and P. P. Silvester. *Computer-Aided Design in Magnetics.* Springer-Verlag, New York, 1986.

[49] J. C. Sabonnadiere and J. L. Coulomb. *Finite Element Methods in CAD: Electric and Magnetic Fields.* Springer-Verlag, New York. 1987.

[50] S. R. H. Hoole. *Computer-Aided Analysis and Design of Electromagnetic Devices.* Elsevier Science Publishing Company. New York. 1989.

[51] I. Wickelgren. The strange senses of other species. *IEEE Spectrum*, 33(3):32–37. March 1996.

[52] Zoltan J. Cendes. Em simulators: Cae tools. *IEEE Spectrum*, 27(11):73–77. November 1990.

[53] Jean-Claude Sabonnadiere and Adalbert Konrad. Computing em fields. *IEEE Spectrum*, 29(11):52–56, November 1992.

[54] J. Mackerle. Error analysis, adaptive techniques and finite and boundary elements — A bibliograpphy (1991 - 1993). *Finite Elements in Analysis and Design*, 17:231–246, 1994.

[55] O. C. Zienkiewicz and R. L. Taylor. *The Finite Element Method*, volume 1: Basic Formulation and Linear Problems. McGraw-Hill Book Company, London, fourth edition, 1989.

[56] S. McFee and D. Giannacopoulos. Optimal discretization based refinement criteria for finite element adaption. *IEEE Transactions on Magnetics*, 32(3):1357–1360, 1996.

[57] D. Giannacopoulos and S. McFee. Towards optimal *h-p* adaption near singularities in finite element electromagnetics. *IEEE Transactions on Magnetics*, 30(5):3523–3526, 1994.

[58] J. P. Webb and B. Forghani. Adaptive improvement of magnetic fields using hierarchal tetrahedral finite elements. *IEEE Transactions on Magnetics*, 30(5):3511–3514, 1994.

[59] S. McFee and J.P. Webb. Adaptive finite element analysis of microwave and optical devices using hierarchal triangles. *IEEE Transactions on Magnetics*, 28(2):1708–1711, 1992.

[60] P. Daly. Singularities in transmission lines. In J. R. Whiteman, editor, *The Mathematics of Finite Elements and Applications: Proceedings of the Brunel University Conference of the Institute of Mathematics and its Applications held in 1972*, pages 337–350, New York, 1973. Academic Press.

[61] W. Rachowicz, J. T. Oden, and L. Demkowicz. Toward a universal *h-p* adaptive finite element strategy. Part 3: Design of *h-p* meshes. *Computer Methods in Applied Mechanics and Engineering*, 77:181–212, 1989.

[62] J. T. Oden and A. Patra. A parallel adaptive strategy for *hp*- finite element computaions. Technical report, Texas Institute for Computational and Applied Mathematics, University of Texas at Austin, Austin, Texas, May 1994. Published electronically.

[63] B. A. Szabo. Estimation and control of error based on p-convergence. In I. Babuska, O. C. Zienkiewicz, J. Gago, and E. R. de Oliveira, editors, *Accuracy estimates and adaptive refinements in finite element computations*, chapter 3. Wiley, New York, 1986.

[64] J. Van Bladel. *Singular Electromagnetic Fields and Sources*. Oxford University Press, New York, 1991.

[65] P. G. Ciarlet. Orders of convergence in finite element methods. In J. R. Whiteman, editor, *The Mathematics of Finite Elements and Applications: Proceedings of the Brunel University Conference of the Institute of Mathematics and its Applications held in 1972*, pages 113–129, New York, 1973. Academic Press.

[66] P. J. Davies. *Interpolation and Approximation*. Blaisdell Publishing Company, Waltham, Massachusetts, 1963.

[67] D. N. Shenton and Z. J. Cendes. Three-dimensional finite element mesh generation using delaunay tesselation. *IEEE Transactions on Magnetics*, 21(6):2535–2538, 1985.

[68] J. Z. Zhu, O. C. Zienkiewicz, E. Hinton, and J. Wu. A new approach to the development of automatic quadrilateral mesh generation. *International Journal for Numerical Methods in Engineering*, 32:849–866, 1991.

[69] P. Fernandes, P. Girdinio, M. Repetto, and G. Secondo. Refinement strategies in adaptive meshing. *IEEE Transactions on Magnetics*, 28(2):1739–1742, 1992.

[70] S. McFee and J. P. Webb. Automatic mesh generation for h-p adaption. *IEEE Transactions on Magnetics*, 29(3):1896–1897, 1993.

[71] R. V. Nambiar et al. An algorithm for adaptive refinement of triangular element meshes. *International Journal for Numerical Methods in Engineering*, 36:499–509, 1993.

[72] K. C. Chellamuthu and N. Ida. Algorithms and data structures for 2D and 3D adaptive finite element mesh refinement. *Finite Elements in Analysis and Design*, 17:205–229, 1994.

[73] K. Forsman and L. Kettunen. Tetraheldral mesh generation in convex primitives by maximizing solid angles. *IEEE Transactions on Magnetics*, 30(5):3535–3538, 1994.

[74] J. Bey. Tetrahedral grid refinement. *Computing*, 55:355–378, 1995.

[75] R. W. Lewis, Y. Zheng, and A. S. Usmani. Aspects of adaptive mesh generation based on domain decomposition and Delaunay triangulation. *Finite Elements in Analysis and Design*, 20:47–70, 1995.

[76] L. Janicke and A. Kost. Error estimation and adaptive mesh generation in the 2D and 3D finite element method. *IEEE Transactions on Magnetics*, 32(3):1334–1337, 1996.

[77] P. J. Green and R. Sibson. Computing dirichlet tesselations in the plane. *The Computer Journal*, 21(2):168–173, 1979.

[78] B. Joe. Delaunay triangular meshes in convex polygons. *SIAM Journal on Scientific Computing*, 7(2):514–539, 1986.

[79] B. Joe. Construction of three-dimensional improved-quality triangulations using local transformations. *SIAM Journal on Scientific Computing*, 16:1292–1307, 1995.

[80] G. H. Golub and C. F. Van Loan. *Matrix Computations*. The Johns Hopkins University Press, Baltimore, MD, second edition, 1989.

[81] L. Demkowicz, J. T. Oden, W. Rachowicz, and O. Hardy. Toward a universal *h-p* adaptive finite element strategy. Part 1: Constrained approximation and data structure. *Computer Methods in Applied Mechanics and Engineering*, 77:79–112, 1989.

[82] A. R. Pinchuck and P. P. Silvester. Error estimation for automatic adaptive finite element mesh generation. *IEEE Transactions on Magnetics*, 21(6):2551–2554, 1985.

[83] C. S. Biddlecombe, J. Simkin, and C. W. Trowbridge. Error analysis in finite element models of electromagnetic fields. *IEEE Transactions on Magnetics*, 22(5):811–813, 1986.

[84] P. Fernandes, P. Girdinio, P. Molfino, and M. Repetto. Local error estimates for adaptive mesh refinement. *IEEE Transactions on Magnetics*, 24(1):299–302, 1988.

[85] P. Fernandes, P. Girdinio, P. Molfino, G. Molinari, and M. Repetto. A comparison of adaptive strategies for mesh refinement based on *a-posteriori* local error estimation procedures. *IEEE Transactions on Magnetics*, 26(2):795–798, 1990.

[86] P. Fernandes, P. Girdinio, P. Molfino, and M. Repetto. An enhanced error estimation procedure for finite element field computation with adaptive mesh refinement. *IEEE Transactions on Magnetics*, 26(5):2187–2189, 1990.

[87] G. Drago, P. Molfino, M. Nervi, and M. Repetto. A local field error problem approach for error estimation in finite element analysis. *IEEE Transactions on Magnetics*, 28(2):1743–1746, 1992.

[88] A. G. Jack, J. W. Finch, and J. P. Wright. Adaptive mesh generation applied to switched-reluctance motor design. *IEEE Transactions on Industry Applications*, 28(2):370–375, 1992.

[89] B. Baccus, D. Collard, and E. Dubois. Adaptive mesh refinement for multilayer process simulation using the finite element method. *IEEE Transactions on Computer-Aided Design*, 11(3):396–403, 1992.

[90] K. C. Chellamuthu and N. Ida. *A-posteriori* element by element local error estimation technique and 2D and 3D adaptive finite element mesh refinement. *IEEE Transactions on Magnetics*, 30(5):3527–3530, 1994.

[91] P. Alotto et al. Mesh adaptation in finite element analysis of 2D steady state time harmonic eddy current problems. *IEEE Transactions on Magnetics*, 32(3):1361–1364, 1996.

[92] P. Girdinio et al. Non-linear magnetostatic adaption using a local field error approach. *IEEE Transactions on Magnetics*, 32(3):1365–13668, 1996.

[93] J. F. Remacle et al. A posteriori error estimation and adaptive meshing using error in constitutive relation. *IEEE Transactions on Magnetics*, 32(3):1369–1372, 1996.

[94] W. Gui and I. Babuska. The *h*, *p* and *h-p* versions of the finite element method in 1 dimension. Part 2: The error analysis of the *h*- and *h-p* versions. *Numerische Mathematik*, 49:613–657, 1986.

[95] J.P. Webb and S. McFee. The use of hierarchal triangles in finite-element analysis of microwave and optical devices. *IEEE Transactions on Magnetics*, 27(5):4040–4043, 1991.

[96] O. C. Zienkiewicz, J. P. De S. R. Gago, and D. W. Kelly. The hierarchical concept in finite element analysis. *Computers and Structures*, 16(1-4):53–65, 1983.

[97] D. Rodger. Experience with hierarchical finite elements in 2D electromagnetics. *IEEE Transactions on Magnetics*, 23(5):3560–3562, 1987.

[98] J. P. Webb and R. Abouchacra. Hierarchal triangular elements using orthogonal polynomials. *International Journal for Numerical Methods in Engineering*, 38:245–257, 1995.

[99] F. G. Uler and O. A. Mohammed. A 3-D finite element mesh generator for complex volumes. *IEEE Transactions on Magnetics*, 30(5):3539–3542, 1994.

[100] A. Raizer. A 3D autoadaptive mesh generator for magnetostatic and magnetodynamic problems. *IEEE Transactions on Magnetics*, 30(5):3531–3534, 1994.

[101] J. T. Oden and L. Demkowicz. Advances in adaptive improvements: A survey of adaptive finite element methods in computational mechanics. In A. K. Noor and J. T. Oden, editors, *State-of-the-Art Surveys on Computational Mechanics*, chapter 13, pages 441–467. The American Society of Mechanical Engineers, New York, 1989.

[102] J. T. Oden and L. Demkowicz. *h-p* adaptive finite element methods in computational fluid dynamics. *Computer Methods in Applied Mechanics and Engineering*, 89:11–40, 1991.

[103] M. K. Georges and M. S. Shephard. Automated adaptive two-dimensional system for the *hp*-version of the finite element method. *International Journal for Numerical Methods in Engineering*, 32:867–893, 1991.

[104] A. W. Craig, M. Ainsworth, J. Z. Zhu, and O. C. Zienkiewicz. *h* and *h-p* version error estimation and adaptive procedures from theory to practice. *Engineering with Computers*, 5:221–234, 1989.

[105] P. Leinen. Data structures and concepts for adaptive finite element methods. *Computing*, 55(4):325–354, 1995.

[106] D. A. Field and Y. Pressburger. An *h-p* multigrid method for finite element analysis. *International Journal for Numerical Methods in Engineering*, 36:893–908, 1993.

[107] W. Gui and I. Babuska. The *h*, *p* and *h-p* versions of the finite element method in 1 dimension. Part 3: The adaptive *h-p* version. *Numerische Mathematik*, 49:659–683, 1986.

[108] O. C. Zienkiewicz, J. Z. Zhu, and N. G. Gong. Effective and practical *h-p* version adaptive analysis procedures for the finite element method. *International Journal for Numerical Methods in Engineering*, 28:879–891, 1989.

[109] L. F. Zeng and N. E. Wiberg. Adaptive *h-p* procedures for high accuracy finite element analysis of two-dimensional linear elastic problems. *Computers and Structures*, 42(6):869–886, 1992.

[110] Y. Q. Tang, Y. P. Liang, H. R. Wu, X. L. Meng, S. C. Xu, and G. X. Fan. An adaptive finite element computation of *h-p* version for magnetic field problems. *IEEE Transactions on Magnetics*, 30(5):3519–3522, 1994.

[111] P. R. Kotiuga. Arithmetic for evaluating three-dimensional *h* vs. *p* finite-element refinement strategies. *Journal of Applied Physics*, 73(10):1–4, 1993.

[112] I. Babuska. The *p* and *h-p* versions of the finite element method: The state of the art. In D. L. Dwoyer, M. Y. Hussaini, and R. G. Voigt, editors, *Finite Elements: Theory and Applications*, chapter 10. Springer-Verlag, New York, 1986.

[113] A. Raizer, S. R. H. Hoole, G. Meunier, and J. L. Coulomb. *p* and *h*-type adaptive mesh generation. *Journal of Applied Physics*, 67(9):5803–5805, 1990.

[114] E. Rank and I. Babuska. An expert system for the optimal mesh design in *hp*-version of the finite element method. *International Journal for Numerical Methods in Engineering*, 24:2087–2106, 1987.

[115] K. S. Bey. *An HP-Adaptive Discontinuous Galerkin Method for Hyperbolic Conservation Laws*. PhD thesis, The University of Texas at Austin, Austin, USA, 1994.

[116] S. McFee and D. Giannacopoulos. The implications of parallel processing on *h-p* adaptive finite element analysis for electromagnetics. *IEEE Transactions on Magnetics*, 34(5):3284–3287, 1998.

[117] J. T. Oden, T. Strouboulis, and P. Devloo. Adaptive finite element methods for the analysis of inviscid compressible flow. Part 1: Fast refinement/unrefinement and moving mesh methods for unstructured meshes. *Computer Methods in Applied Mechanics and Engineering*, 59:327–362, 1986.

[118] S. Jensen. A posteriori error estimates, feedback, adaptivity. Electronically, October 1989.

[119] O. C. Zienkiewicz and J. Z. Zhu. Adaptivity and mesh generation. *International Journal for Numerical Methods in Engineering*, 32:783–810, 1991.

[120] V. E. Denny and R. B. Landis. A new method for solving two-point boundary value problems using optimal node distribution. *Journal of Computational Physics*, 9:120–137, 1972.

[121] W. E. Carroll and R. M. Barker. A theorem for optimum finite-element idealizations. *International Journal of Solids and Structures*, 9:883–895, 1973.

[122] W. Prager. A note on the optimal choice of finite element grids. *Computer Methods in Applied Mechanics and Engineering*, 6:363–366, 1975.

[123] J. W. Tang and D. J. Turcke. Characteristics of optimal grids. *Computer Methods in Applied Mechanics and Engineering*, 11:31–37, 1977.

[124] E. F. Masur. Some remarks on the optimal choice of finite element grids. *Computer Methods in Applied Mechanics and Engineering*, 14:237–248, 1978.

[125] I. Babuska and W. C. Rheinboldt. Analysis of optimal finite element meshes in R_1. *Mathematics of Computation*, 33(146):435–463, 1979.

[126] K. Miller and R.N. Miller. Moving finite elements: Parts 1 and 2. *SIAM Journal on Numerical Analysis*, 18(6):1019–1057, 1981.

[127] G. F. Carey and H. T. Dinh. Grading functions and mesh redistribution. *SIAM Journal on Numerical Analysis*, 22(5):1028–1040, October 1985.

[128] M. Delfour, G. Payre, and J. P. Zolesio. An optimal triangulation for second-order elliptic problems. *Computer Methods in Applied Mechanics and Engineering*, 50:231–261, 1985.

[129] D. F. Hawken, J. J. Gottlieb, and J. S. Hansen. Review of some adaptive node-movement techniques in finite-element and finite-difference solutions of partial differential equations. *Journal of Computational Physics*, 95:254–302, 1991.

[130] E. Onate and G. Bugeda. A study of mesh optimality criteria in adaptive finite element analysis. *Engineering Computations*, 10:307–321, 1993.

[131] K. Viswanadham and S. R. Koneru. Finite element method for one-dimensional and two-dimensional time dependent problems with B-splines. *Computer Methods in Applied-Mechanics and Engineering*, 108:201–222, 1993.

[132] M. J. Baines. Algorithms for optimal discontinuous piecewise linear and constant L_2 fits to continuous functions with adjustable nodes in one and two dimensions. *Mathematics of Computation*. 62(206):645–669. 1994.

[133] M. J. Baines. On the relationship between the moving finite-element procedure and best piecewise L_2 fits with adjustable nodes. *Numerical Methods for Partial Differential Equations*. 10:191–203. 1994.

[134] K. E. Chen. Error equidistribution and mesh adaptation. *SIAM Journal on Scientific Computing*. 15(4):798–818. 1994.

[135] W. Huang. Y. Ren. and R. D. Russel. Moving mesh partial differential equations (MMPDEs) based on the equidistribution principle. *SIAM Journal on Numerical Analysis*. 31(3):709–730. 1994.

[136] W. Huang and D. M. Sloan. A simple adaptive grid method in two dimensions. *SIAM Journal on Scientific Computing*. 15(4):776–797. 1994.

[137] L. Y. Li and P. Bettess. Notes on mesh optimal criteria in adaptive finite element computations. *Communications in Numerical Methods in Engineering*. 11:911–915. 1995.

[138] P. P. Silvester and R. L. Ferrari. *Finite Elements for Electrical Engineers*. Cambridge University Press. Cambridge. third edition. 1996.

[139] L. V. Kantorovitch. *Bulletin of the Acadamey of Sciences of U.S.S.R.*. No. 5. 1903.

[140] L. V. Kantorovitch. *Applied Mathematics and Mechanics*. 6:31–40. 1942.

[141] Charles Fox. *An Introduction to the Calculus of Variations*. Oxford University Press. Oxford. England. 1963.

[142] R. Courant. Variational methods for the solution of problems of equilibrium and vibration. *Bulletin of the American Mathematical Society*. 49:1–23. 1943.

[143] R. J. Melosh. *Development of the Stiffness Method to Define Bounds on Elastic Behaviour of Structures*. PhD thesis. University of Washington. Seattle. 1962.

[144] D. Giannacopoulos and S. McFee. An experimental study of superconvergence phenomena in finite element magnetics. *IEEE Transactions on Magnetics*. 33(5):4137–4139. 1997.

[145] P. Silvester. Tetrahedral polynomial finite elements for the Helmholtz equations. *International Journal for Numerical Methods in Engineering*, 4:405–413, 1972.

[146] J.P. Webb. Finite element analysis of dispersion in waveguides with sharp metal edges. *IEEE Transactions on Microwave Theory and Techniques*, 36(12):1819–1824, 1988.

[147] J.M. Gill and J. Zapata. Efficient singular element for finite element analysis of quasi-TEM transmission lines and waveguides with sharp metal edges. *IEEE Transactions on Microwave Theory and Techniques*, 42(1):92–98, 1994.

[148] Z. Pantic-Tanner, J.S. Savage, D.R. Tanner, and A.F. Peterson. Two-dimensional singular vector elements for finite element analysis. *IEEE Transactions on Microwave Theory and Techniques*, 46(2):178–184, 1998.

[149] J.E. Dennis Jr. and R.B. Schnabel. *Numerical Methods for Unconstrained Optimization and Nonlinear Equations*. Prentice-Hall, Englewood Cliffs, NJ, 1983.

[150] Symbolic Math Toolbox. The MathWorks, Inc., 1994. Computer Software.

[151] T. Strouboulis and K. A. Haque. Recent experiences with error estimation and adaptivity. Part 1: Review of error estimators for scalar elliptic problems. *Computer Methods in Applied Mechanics and Engineering*, 97:399–436, 1992.

[152] J.Z. Zhu and O.C. Zienkiewicz. Superconvergence recovery techniques and *a posteriori* error estimators. *International Journal for Numerical Methods in Enginerring*, 30:1321–1339, 1990.

[153] O.C. Zienkiewicz and J.Z. Zhu. The superconvergent patch recovery (spr) and adaptive finite element refinement. *Computer Methods in Applied Mechanics and Engineering*, 101:207–224, 1992.

[154] M. Krizek. Superconvergence phenomena in the finite element method. *Computer Methods in Applied Mechanics and Engineering*, 16:157–163, 1994.

[155] P.P. Silvester and D. Omeragić. A two-dimensional Zhu-Zienkiewicz method for gradient recovery from finite-element solutions. *COMPEL*, 12(3):191–204, 1993.

[156] S.X. Chen et al. Superconvergence theory and its application to precision force calculations. *IEEE Transactions on Magnetics*, 32(5):4275–4277, 1996.

[157] P.P. Silvester and D. Omeragić. A comparative experimental study of differentiation methods on finite elements. *International Journal of Applied Electromagnetics in Materials*, 4:123–136, 1993.

[158] R.J. Mackinnon and G.F. Carey. Superconvergent derivatives: A Taylor series analysis. *International Journal for Numerical Methods in Engineering*, 28:489–509, 1989.

[159] I. M. Babuska and R. Rodriguez. The problem of the selection of an *a posteriori* error indicator based on smoothening techniques. *International Journal for Numerical Methods in Engineering*, 36:539–567, 1993.

[160] Z. J. Cendes and D. N. Shenton. Adaptive mesh refinement in the finite element computation of magnetic fields. *IEEE Transactions on Magnetics*, 21(5):1811–1816, 1985.

[161] T. Tarnhuvud, K. Reichert, and J. Skoczylas. Problem-oriented adaptive mesh-generation for accurate finite-element calculation. *IEEE Transactions on Magnetics*, 26(2):779–782, 1990.

[162] J. T. Oden, L. Demkowicz, W. Rachowicz, and T. A. Westermann. Toward a universal *h-p* adaptive finite element strategy. Part 2: *A-posteriori* error estimation. *Computer Methods in Applied Mechanics and Engineering*, 77:113–180, 1989.

[163] B.K. Gilbert and G.W. Pan. MCM packaging for present- and next-generation high clock-rate digital- and mixed-signal electronic systems: areas for development. *IEEE Transactions on Microwave Theory and Techniques*, 45(10):1819–1835, 1997.

[164] A. Deutsch. Electrical characteristics of interconnections for high-performance systems. *Proceedings of the IEEE*, 86(2):315–355, 1998.

[165] N.A. Golias and T.D. Tsiboukis. Adaptive refinement strategies in 3D. *IEEE Transactions on Magnetics*, 29(2):1886–1889, 1993.

[166] Y. Kallinderis and P. Vijayan. Adaptive refinement-coarsening scheme for three-dimensional unstructured meshes. *American Institute of Aeronautics and Astronautics Journal*, 31(8):1441–1447, 1993.

[167] N.A. Golias and T.D. Tsiboukis. Adaptive methods in computational magnetics. *International Journal of Numerical Modelling: Electronic Networks, Devices, and Fields*. 9:71–80. 1996.